Theoretical Chemistry and Computational Modelling

Maurizio Persico · Giovanni Granucci

Photochemistry

A Modern Theoretical Perspective

EXTRAS ONLINE

Springer

Theoretical Chemistry and Computational Modelling

Modern Chemistry is unthinkable without the achievements of Theoretical and Computational Chemistry. As a matter of fact, these disciplines are now a mandatory tool for the molecular sciences and they will undoubtedly mark the new era that lies ahead of us. To this end, in 2005, experts from several European universities joined forces under the coordination of the Universidad Autónoma de Madrid, to launch the *European Masters Course on Theoretical Chemistry and Computational Modeling* (TCCM). The aim of this course is to develop scientists who are able to address a wide range of problems in modern chemical, physical, and biological sciences via a combination of theoretical and computational tools. The book series, *Theoretical Chemistry and Computational Modeling*, has been designed by the editorial board to further facilitate the training and formation of new generations of computational and theoretical chemists.

Prof. Manuel Alcami
Departamento de Química
Facultad de Ciencias, Módulo 13
Universidad Autónoma de Madrid
28049 Madrid, Spain

Prof. Ria Broer
Theoretical Chemistry
Zernike Institute for Advanced Materials
Rijksuniversiteit Groningen
Nijenborgh 4
9747 AG Groningen, The Netherlands

Dr. Monica Calatayud
Laboratoire de Chimie Théorique
Université Pierre et Marie Curie, Paris 06
4 place Jussieu
75252 Paris Cedex 05, France

Prof. Arnout Ceulemans
Departement Scheikunde
Katholieke Universiteit Leuven
Celestijnenlaan 200F
3001 Leuven, Belgium

Prof. Antonio Laganà
Dipartimento di Chimica
Università degli Studi di Perugia
via Elce di Sotto 8
06123 Perugia, Italy

Prof. Colin Marsden
Laboratoire de Chimie
et Physique Quantiques
Université Paul Sabatier, Toulouse 3
118 route de Narbonne
31062 Toulouse Cedex 09, France

Prof. Otilia Mo
Departamento de Química
Facultad de Ciencias, Módulo 13
Universidad Autónoma de Madrid
28049 Madrid, Spain

Prof. Ignacio Nebot
Institut de Ciència Molecular
Parc Científic de la Universitat de València
Catedrático José Beltrán Martínez, no. 2
46980 Paterna (Valencia), Spain

Prof. Minh Tho Nguyen
Departement Scheikunde
Katholieke Universiteit Leuven
Celestijnenlaan 200F
3001 Leuven, Belgium

Prof. Maurizio Persico
Dipartimento di Chimica e Chimica
Industriale
Università di Pisa
Via Moruzzi 13
56124 Pisa, Italy

Prof. Maria Joao Ramos
Chemistry Department
Universidade do Porto
Rua do Campo Alegre, 687
4169-007 Porto, Portugal

Prof. Manuel Yáñez
Departamento de Química
Facultad de Ciencias, Módulo 13
Universidad Autónoma de Madrid
28049 Madrid, Spain

More information about this series at http://www.springer.com/series/10635

Maurizio Persico · Giovanni Granucci

Photochemistry

A Modern Theoretical Perspective

Springer

Maurizio Persico
Department of Chemistry and Industrial Chemistry
University of Pisa
Pisa
Italy

Giovanni Granucci
Department of Chemistry and Industrial Chemistry
University of Pisa
Pisa
Italy

Additional material to this book can be downloaded from http://extras.springer.com.

ISSN 2214-4714 ISSN 2214-4722 (electronic)
Theoretical Chemistry and Computational Modelling
ISBN 978-3-319-89971-8 ISBN 978-3-319-89972-5 (eBook)
https://doi.org/10.1007/978-3-319-89972-5

Library of Congress Control Number: 2018939009

Printed on acid-free paper

This Springer imprint is published by the registered company Springer International Publishing AG part of Springer Nature
The registered company address is: Gewerbestrasse 11, 6330 Cham, Switzerland

To Lida and Silvia,
our loved and patient wives.

Preface

This book aims to offer an introduction to photochemistry for students with a minimal background in physical chemistry and molecular quantum mechanics. The focus is on the theoretical side and particularly on excited state dynamics. We describe the main conceptual models of the photochemical and photophysical processes that are the basis to interpret both the classical steady-state experimental results (essentially product branching ratios and quantum yields) and the wealth of information about excited state dynamics revealed in the last decades by time-resolved spectroscopies. A significant but not major space will be devoted to the computational techniques offered by quantum chemistry and molecular dynamics.

The expected readers are students of master and of last year of bachelor courses in Chemistry or researchers at their first approach to this field. This book differs from most introductory textbooks in photochemistry in being more theoretically oriented. The famous textbook by Klessinger and Michl (*Excited States and Photochemistry of Organic Molecules*, Wiley, 1995) provides theoretical explanations for many photochemical reactions, focussing on the potential energy surfaces and properties of the excited states. Our book will concentrate more on the modeling of dynamical aspects, as can be seen from the contents.

Finally, we would like to thank Davide Accomasso, Neus Aguilera Porta, and Meilani Wibowo who carefully read the manuscript, providing corrections and very valuable comments.

Pisa, Italy
January 2018

Maurizio Persico
Giovanni Granucci

Contents

Chapter 1
Introduction to Photochemistry

Abstract This chapter summarizes some general concepts in photochemistry, with two aims: to provide an overview of phenomena and empirical rules that will be discussed on theoretical grounds in the next chapters, and to present a language and some physical laws concerning light and its interaction with matter. We shall introduce the main differences between thermal chemistry that takes place in the ground electronic state, and photochemistry, that involves optical excitation. The first overview of elementary photoinduced events will highlight the different ways the excitation energy can be disposed of. We shall distinguish primary and secondary processes and define their quantum yields. Excitation rates will be introduced in connection with the Lambert and Beer law. Some elementary examples of photochemical kinetics will be discussed. Much more extended introductions to photochemistry can be found in well-renowned textbooks by Wayne (Principles and Applications of Photochemistry. Oxford University Press, Oxford, 1988 [1]), Wardle (Principles and Applications of Photochemistry. Wiley, Chichester, 2009 [2]), Turro (Modern Molecular Photochemistry of Organic Molecules. University Science Books, Sausalito, 2010 [3]), Balzani (Photochemistry and Photophysics: Concepts Research, Applications. Wiley, Chichester, 2014 [4]), Rohatgi-Muckerjee (Fundamentals of Photochemistry. New Age International, New Delhi, 2017 [5]), and others.

Keywords Light · Photon · Primary and Secondary processes · Quantum yeild Photochemical kinetics

1.1 What Is Photochemistry?

Photochemistry deals with the chemical reactions and other physicochemical phenomena induced by the absorption of light. This definition stems from a basic rule formulated by Grotthuss in 1917 and independently by Draper in 1842. The Grotthuss–Draper law states that only the light absorbed by a material sample can induce chemical transformations. In fact, if the sample is transparent light goes through it without being attenuated, i.e., no light is absorbed (see Sect. 1.6.1). Then, the sample can be temporarily affected; for instance, it can experience periodic oscillations of its charge distribution in response to the electric field of light, but no

M. Persico and G. Granucci, *Photochemistry*, Theoretical Chemistry and Computational Modelling, https://doi.org/10.1007/978-3-319-89972-5_1

chemical reactions occur. If instead a fraction of the impinging radiation is absorbed by the sample, chemical change can result and the amount of chemically transformed substrate will be proportional to the absorbed radiation. How much radiation is adsorbed depends on experimental conditions such as the irradiation time, the radiation intensity, and the concentration of the absorbing compound. As we shall see, pure proportionality is observed only for simple reactions or when the outcome of an elementary photochemical event can be singled out in a more complex mechanism. The exact meaning of the proportionality between absorbed radiation and photochemical change requires the definition of some basic physical quantities, as we shall see in the next sections.

During the nineteenth century the concept of molecule was progressively precised and at the beginning of the next century the quantum of light, later called photon, was introduced. This opened the way to a new formulation of the relationship between light absorption and photochemical reaction. Stark and Einstein suggested, in close analogy with the photoelectric effect, that an isolated molecule (in gas phase) can absorb one photon and then undergo an elementary photoreaction act. Actually, after photon absorption, a molecule can react in different ways or else undergo processes that do not involve chemical transformations and are therefore labeled as "photophysical." A given photochemical or photophysical elementary event will follow photon absorption with a predictable probability (the "quantum yield," see Sect. 1.5), which is in the first place determined by quantum dynamics. Exciting a molecule is then very close to "playing dice," quite at variance with the good habits of Einstein's God. We can therefore reformulate the Stark and Einstein law as: "every photochemical or photophysical process is triggered by the absorption of one photon by one molecule." Much later, with the introduction of lasers, it was demonstrated that two or more photons can be absorbed at once by one molecule when the radiation intensity is high enough. However, in usual conditions with solar light or laboratory lamps, the Stark–Einstein law remains valid.

1.2 Light and Photons

The previous section makes clear that we need to characterize and quantify the "amount of light" that is absorbed by molecules in a medium. In this book we shall use both the classical description of radiation in terms of oscillating electric and magnetic fields, and the quantum one, based on the concept of photon, depending on which allows for the simpler explanation of photophysical phenomena. For a comprehensive treatment of this subject see, for instance, Cohen-Tannoudji et al [6].

1.2.1 Monochromatic Light

A linearly polarized plane wave in vacuo is made of two related electric and magnetic fields **E** and **B**:

$$\mathbf{E}(\mathbf{r}, t) = \mathbf{E}_0 \ \cos(\omega t - \mathbf{k} \cdot \mathbf{r} - \varphi) \tag{1.1}$$

$$\mathbf{B}(\mathbf{r}, t) = \mathbf{B}_0 \ \cos(\omega t - \mathbf{k} \cdot \mathbf{r} - \varphi) \tag{1.2}$$

Here ω is the angular frequency, measured in rad/s and related to the frequency ν (s^{-1}) by $\omega = 2\pi\nu$; c is the speed of light and the module of **k**, the vector that identifies the direction of propagation, is $k = \omega/c$; φ is a phase constant. The wavelength is $\lambda = c/\nu = 2\pi c/\omega$. The **E** and **B** vectors are orthogonal to each other and to the propagation vector **k**. According to the classical theory, embodied in Maxwell's equations, E_0 and B_0 can assume any value but are related by $B_0 = E_0/c$.

In the above formulas $\mathbf{E}_0$ is a constant vector, i.e., both its direction and its amplitude are fixed: these two assumptions correspond, respectively, to linear polarization and to a continuous wave of infinite duration. We shall consider in Sect. 3.8 the case of a radiation pulse of finite duration, in which the amplitude E_0 depends on time. Also the orthogonal directions of the **E** and **B** fields can change in time. For instance, assuming **k** lies along the $\hat{z}$-axis, we may have:

$$\begin{aligned} E_x(z, t) &= \quad E_{0,x} \ \cos[\omega(t - z/c) - \varphi] \\ E_y(z, t) &= \pm E_{0,y} \ \sin[\omega(t - z/c) - \varphi] \end{aligned} \tag{1.3}$$

Depending on whether E_x and E_y are equal or not, we have circular or elliptic polarization. The $\pm$ sign in the second equation determines the right- or left-handedness of the polarization.

The energy density (energy per unit volume) of the electromagnetic field is

$$\rho_{energy} = \frac{\varepsilon_0}{2} \left(E^2 + c^2 B^2\right) = \varepsilon_0 \ E^2 \tag{1.4}$$

where ε_0 is the vacuum permittivity; see Appendix A. The average density over an optical cycle, i.e., a time interval of $2\pi/\omega$ or a space interval of one wavelength, is then

$$U \equiv \left\langle \rho_{energy} \right\rangle = \frac{\varepsilon_0}{2} \ E_0^2 \ . \tag{1.5}$$

The energy going through a surface perpendicular to the propagation vector **k** per time and surface unit (flux density) is called irradiance or light intensity and can be measured in W/m^2:

$$I = c \ U = \frac{c\varepsilon_0}{2} \ E_0^2 \ . \tag{1.6}$$

Light also carries a linear momentum **P** directed along the propagation vector **k**. The average density of its norm P over an optical cycle is

$$\langle \rho_P \rangle = \frac{\varepsilon_0}{2c} E_0^2 \,. \tag{1.7}$$

Finally, circularly polarized light carries angular momentum, which is also directed along the propagation vector, with + sign for the left-handed polarization and − sign for the right-handed. The J average density over an optical cycle is

$$\langle \rho_J \rangle = \frac{\varepsilon_0}{2\omega} E_0^2 \,. \tag{1.8}$$

Linearly polarized light, which can be thought as the superposition of two right and left circularly polarized waves with the same amplitude, frequency, and phase, owns no net angular momentum.

1.2.2 Nonmonochromatic Light: The Radiation Spectrum

So far we have dealt with monochromatic light, characterized by one frequency ν and one wavelength λ. Approximately monochromatic light can only be produced in special conditions, for instance, by atomic spontaneous emission or by lasers. In normal conditions, light is a superposition of waves like those of Eqs. (1.1), (1.2) or (1.3), with different frequencies, polarizations, propagation directions, and phases. Because of the linearity of Maxwell's equations, such waves evolve independently of each other and do not exchange energy or momentum, unless through their interactions with matter. Unpolarized light is a superposition of linearly (or circularly) polarized waves differing (at least) because of their random phases.

If we restrict ourselves to linearly polarized light traveling in a given direction (say $\hat{z}$), the electric field can be represented as:

$$\mathbf{E}(z,t) = \int_0^\infty \mathbf{E}_\omega(\omega)\ \cos[\omega(t - z/c) - \varphi(\omega)]\ \mathrm{d}\omega \tag{1.9}$$

where $\mathbf{E}_\omega$ is a vector of constant direction (only its norm depends on ω). This expression can be generalized to the case of nonpolarized light by adding an electric field orthogonal to the one of Eq. (1.9), with independent $\mathbf{E}_\omega(\omega)$ and $\varphi(\omega)$ functions. As we shall see in Sect. 3.8, waves of different frequencies can be combined coherently to yield a light pulse peaking at a given value of $t - z/c$ and dying off at previous or later times. Here we shall assume that the combination of different frequency components is not coherent (no light pulse), so that the amplitude of the electric field fluctuates but averages to a constant value over long-time intervals. The time-averaged energy density is

$$U_{tot} = \frac{\varepsilon_0}{2} \int_0^\infty E_\omega^2(\omega)\ \mathrm{d}\omega \tag{1.10}$$

and the corresponding irradiance is of course

$$I_{tot} = \frac{c\ \varepsilon_0}{2} \int_0^\infty E_\omega^2(\omega)\ \mathrm{d}\omega\ . \tag{1.11}$$

We can then define a spectral energy density

$$U_\omega(\omega) = \frac{\varepsilon_0\ E_\omega^2(\omega)}{2} \tag{1.12}$$

and a spectral irradiance

$$I_\omega(\omega) = \frac{c\ \varepsilon_0\ E_\omega^2(\omega)}{2} \tag{1.13}$$

meaning that $U_\omega(\omega)\mathrm{d}\omega$ and $I_\omega(\omega)\mathrm{d}\omega$ are the energy density and irradiance contained in the frequency interval $[\omega, \omega + \mathrm{d}\omega]$. U_ω and I_ω are then expressions of the light spectrum. Notice that the spectral quantities are often formulated as functions of ν or λ with analogous meanings, which implies, for instance,

$$I_\nu(\nu) = 2\pi\ I_\omega(2\pi\nu) \tag{1.14}$$

and

$$I_\lambda(\lambda) = \frac{c}{\lambda^2} I_\nu(c/\lambda) = \frac{2\pi c}{\lambda^2}\ I_\omega(2\pi c/\lambda)\ . \tag{1.15}$$

In this context, the irradiance or the energy density of a monochromatic wave of frequency ω_0 can be represented by means of a δ function (see Appendix C):

$$I_\omega(\omega) = I_{tot}\ \delta(\omega - \omega_0)\ . \tag{1.16}$$

1.2.3 Photons

We switch now to an elementary quantum description of radiation, which is based on light particles or quanta, called photons. A photon is a massless particle, traveling at the speed of light. The vector **k** now indicates the direction of the photon motion. In a monochromatic light beam each photon carries an energy

$$E_{ph} = h\nu = \frac{hc}{\lambda} \tag{1.17}$$

where h is Planck's constant. Given the energy density (1.5), the number of photons per unit volume is

$$\rho_{ph} = \frac{U}{h\nu} = \frac{\varepsilon_0 E_0^2}{2h\nu} \tag{1.18}$$

and their flux density or photon irradiance is

$$I_{ph} = \frac{I}{h\nu} = \frac{c\varepsilon_0 E_0^2}{2h\nu} \,. \tag{1.19}$$

When necessary to avoid ambiguity, the previously defined energy flux density is tagged as "energy" irradiance.

By dividing the average momentum density (1.7) by ρ_{ph}, we obtain the momentum of one photon, $P_{ph} = h\nu/c$. In the same way, we get the component of its angular momentum along the **k**-axis, $J_{ph} = \pm h/2\pi = \pm\hbar$. The photon is a boson, since its angular momentum is an integer in $\hbar$ units, with the peculiarity that the projection of $\mathbf{J}_{ph}$ on the **k**-axis cannot be null. A beam of linearly polarized or unpolarized light is made of equal numbers of photons with opposite angular momenta.

Turning to nonmonochromatic light, we can define the spectral photon irradiance as:

$$I_{ph,\omega}(\omega) = \frac{I_\omega(\omega)}{\hbar\omega} = \frac{c\varepsilon_0 E_\omega^2(\omega)}{2\hbar\omega} \,. \tag{1.20}$$

For the equivalent quantities $I_{ph,\nu}(\nu)$ and $I_{ph,\lambda}(\lambda)$ Eqs. (1.14) and (1.15) are valid. The total photon flux density or total irradiance is obtained by integrating the spectral quantities:

$$I_{ph,tot} = \int_0^\infty I_{ph,\omega}(\omega)\, \mathrm{d}\omega = \int_0^\infty I_{ph,\nu}(\nu)\, \mathrm{d}\nu = \int_0^\infty I_{ph,\lambda}(\lambda)\, \mathrm{d}\lambda \,. \tag{1.21}$$

Notice that there is no direct relationship between $I_{ph,tot}$ and I_{tot}, except in the case of monochromatic light.

1.3 Photochemistry Versus Thermal Chemistry

The electronic excitations that trigger photochemical and photophysical events require energies roughly in the interval 100–1000 kJ/mol (1–10 eV, or 24–240 kcal/mol). These energies are of the right order of magnitude to break bonds or cause other major molecular rearrangements: in fact, the excitation often consists in bringing an electron from a bonding or nonbonding orbital to an antibonding one. The corresponding wavelengths go from 1200 to 120 nm, encompassing all the visible spectrum ($\lambda \in [400, 750]$ nm), a large part of the ultraviolet (UV, $\lambda \in [10, 400]$ nm) and the near-infrared (NIR, $\lambda \in [750, 1500]$ nm).

The flux of light (or any other form of energy) going through a material system puts it in a state of nonequilibrium. A (normally small) fraction of molecules will populate excited states with energies much higher than the average. To quantify such a departure from equilibrium we must take into account the average time spent by a molecule in one of the excited states normally accessed through light absorption. A reasonable value for such "lifetime" is $\tau = 10^{-9}$ s. Suppose we irradiate compound A during a given time, say one hour, in order to convert it to B. If nearly all molecules

of A must be excited at least once during one hour, a fraction $\tau/3600$ of them will be in the excited state at every instant during the experiment. With $\tau = 10^{-9}$ s, the excited fraction would be about $3 \cdot 10^{-13}$. The population of an excited state at thermal equilibrium is proportional to the factor $\exp(-\Delta E/K_B T)$, where K_B is Boltzmann's constant and ΔE is the energy difference with respect to the ground state (lowest energy level). With $\Delta E = 400$ kJ/mol, again a reasonable value, in order to reach the same population of excited molecules as in the photochemical experiment we must raise the temperature to $T = 1670$ K. This would destroy most molecular samples.

Where is the difference? Heating the whole sample pours energy in all the translational, rotational, and vibrational modes of all molecules, many of which will certainly react in unwanted ways. On the contrary, the optical excitation puts energy only in the few happy molecules that absorb a photon and get electronically excited. This allows to promote reactions that would not occur in thermal chemistry, in the first place endothermic reactions that would be thermodynamically nonviable. Of course, the excited molecules dispose of the excess energy by transferring it to the surrounding molecules, by emitting radiation or by storing it as chemical energy in the reaction products: every single molecule can channel its surplus energy in a different way.

Besides the energetic aspects, we shall see that excitation of molecules with photons in the above energy range changes the electronic wavefunction. This means that some bonds are weakened, others may be strengthened, and the molecular equilibrium geometry and the charge distribution are altered as well as the interactions with surrounding molecules. All these changes contribute to differentiate the photoreactivity from the ground state thermal chemistry.

1.4 An Overview of Photochemical and Photophysical Processes

In this section we shall list the main photochemical and photophysical phenomena that can occur after photoexcitation, with some comments about energy disposal which is one of the main differences between thermal and photochemical reactivity. We shall also anticipate some data about typical timescales, since they determine the competition between the energetically viable primary processes.

The usual ways to indicate the excitation of molecule A are

$$\mathrm{A} + h\nu \rightarrow \mathrm{A}^* \tag{1.22}$$

or

$$\mathrm{A} \xrightarrow{h\nu} \mathrm{A}^* \tag{1.23}$$

The star suffix indicates an electronically excited species. The photon absorption event is often described as extremely fast, although the real meaning of this simplified view will be made clear in Chap. 3. Just after excitation, the molecule can be thought of as keeping the same geometry it had in the ground state, which is a classical view of the Franck–Condon principle. Then, in the new electronic state, the nuclei experience different forces and will start moving, which can give place to a small rearrangement of the molecular geometry or to more important changes, including chemical reactions. The processes undergone directly by the excited species A* are labeled as "primary." The competition among all the possible primary processes is basically determined by their relative rates. The primary products may give place to further "secondary" reactions or photophysical events. Here is a list of primary processes:

- Ionization:

$$A^* \rightarrow A^+ + e^- \tag{1.24}$$

  Ionization normally requires high energies, needed to extract an electron from the neutral molecule, and is an extremely fast process. The ionization energy or ionization potential is at least 8–10 eV for molecules in gas phase not containing metal atoms. The corresponding wavelengths are about 120–150 nm. The excess energy is mostly converted into kinetic energy of the emitted electron. In fact, when a molecule produces two fragments of any nature the conservation of both energy and momentum requires that their translational energies E_1 and E_2 in a common center of mass reference frame are

$$E_1 = \frac{m_2}{m_1 + m_2} E_{tot} \qquad E_2 = \frac{m_1}{m_1 + m_2} E_{tot} \tag{1.25}$$

  where m_i is the mass of fragment i and $E_{tot} = E_1 + E_2$ is the total kinetic energy.
- Luminescence:

$$A^* \rightarrow A + h\nu' \tag{1.26}$$

  Luminescence is the spontaneous emission of a photon of frequency ν', associated with a transition of the excited molecule to a lower state, usually the ground state. ν' can be different from the exciting frequency ν and usually $\nu' < \nu$, because other processes convert part of the excitation energy into heat (i.e., mostly into vibrational energy) before and after photon emission. Rates of emission can vary over a very wide range, depending on whether the transition is spin- and symmetry-allowed or forbidden. When luminescence is due to a spin-allowed transition then it is called fluorescence, otherwise, phosphorescence. Large rate constants are only found for fluorescence and can be of the order of 1 ns^{-1}.
- Radiationless decay:

$$A^* \rightarrow A \tag{1.27}$$

  In this case the electronic transition is not accompanied by photon emission, nor by a chemical reaction. While the molecule switches to the ground state or to a lower

excited state, its energy must be conserved, so a certain amount of electronic energy will be converted into vibrational energy. The latter will be transferred to the environment, within times of the order of 10 ps in condensed phase and much more slowly in gas phase. Ultrafast decays occur in less than 100 fs, but spin-changing radiationless transitions can be much slower, in the μs range or even more. Radiationless transitions between states belonging to the same spin manifold are called "internal conversion" (IC). When the initial and final state are of different spin the process is called "intersystem crossing" (ISC).

- Quenching:

$$A^* + B \rightarrow A + B \tag{1.28}$$

The excited molecule A^* interacts with the quencher B and transfers to it part of the excitation energy. When they move apart, none of them is electronically excited and the excess energy has been transferred to the nuclear degrees of freedom (vibrational, rotational, and translational) of both molecules, much in the same way as in the case of unimolecular radiationless decay. In all bimolecular processes of course the rate depends on the concentrations of both species, $[A^*]$ and [B]. However, in order to compare with the rates of unimolecular processes the common factor $[A^*]$ is irrelevant and one can adopt the point of view of a single A^* molecule. With an efficient quencher B at reasonable concentrations (or partial pressures in gas phase), quenching can compete with unimolecular processes if the lifetime of A^* is 1 ns or longer. These considerations apply also to excitation transfer, charge transfer, and bimolecular reactions (see below).

- Excitation transfer or sensitization:

$$A^* + B \rightarrow A + B^* \tag{1.29}$$

As in quenching, the excited sensitizer A^* donates energy to B, but the transferred energy is sufficient to electronically excite the acceptor. As a consequence, a minor fraction of the excitation energy goes into the nuclear degrees of freedom.

- Photoisomerization:

$$A^* \rightarrow B \tag{1.30}$$

The excited molecule A isomerizes to B and reverts to the ground state by radiationless decay. The photon energy is used to overcome the activation barrier of the reaction by performing part of the structural change in the excited state. A detailed analysis of the dynamics, performed by experimental or theoretical means, may reveal the temporal relationship of the two events, isomerization and radiationless transition: in fact, they may turn out to be essentially simultaneous. If the $A \rightarrow B$ isomerization is endothermic, a usually minor fraction of the photon energy is stored as chemical energy while the rest is dissipated in the environment.

- Photodissociation:

$$A^* \rightarrow B + C \tag{1.31}$$

In a photodissociation reaction a substantial part of the photon energy is used to break a chemical bond, possibly producing two radicals. Moreover, one of the two fragments or both can be in an excited state. The remaining energy will be found as vibrational, rotational, and translational energy of both fragments. In gas phase, the relative translational energy will be partitioned according to Eq. (1.25). As we shall see, A^* can be metastable with respect to bond breaking, in which case a preemptive radiationless decay to the ground state or other slow events may be required before dissociation can take place: the whole phenomenon is then called predissociation. The alternative case, of a molecule that dissociates while remaining in the excited state, is qualified as "direct" dissociation.

- Electron transfer:

$$A^* + B \rightarrow A^+ + B^- \tag{1.32}$$

or

$$A^* + B \rightarrow A^- + B^+ \tag{1.33}$$

An excited molecule is at once a better electron donor and electron acceptor than in its ground state. Once the ion pair has been created, much energy can be needed to separate the two charged partners against the Coulomb potential. Polar solvents can greatly facilitate the separation by specific solvation and bulk dielectric effects.

- Bimolecular reaction:

$$A^* + B \rightarrow C + D \tag{1.34}$$

There are many kinds of bimolecular reactions in which one of the reagents is an excited species and two products are formed. Most of them consist in the transfer of atoms or groups, for instance, hydrogen abstraction and proton transfer. The available energy, which is a function of the exo- or endothermicity of the reaction, will be found in the nuclear degrees of freedom of the products.

- Addition reaction:

$$A^* + B + M \rightarrow AB + M \tag{1.35}$$

Here M is a "third body" that does not react but is necessary to withdraw part of the available energy from the product AB, that would otherwise be unstable. In fact, even starting from the ground state reactants A+B, a reaction yielding AB would be fully reversible without energy dissipation and even more so by adding the photon energy. In a gas mixture, M can be any molecule and a three-body collision is needed. Actually the last requirement can be relaxed for sufficiently large molecules, because many vibrational modes can share the excess energy making extremely unlikely for enough energy to be channeled into a reaction coordinate. Then, two-body collisions with other molecules can take place at later times and cool down the "hot" reaction product AB. In condensed phase, the role of M is played by the nuclear degrees of freedom of the medium (solvent, pure liquid or solid or other matrices) and can be taken for granted.

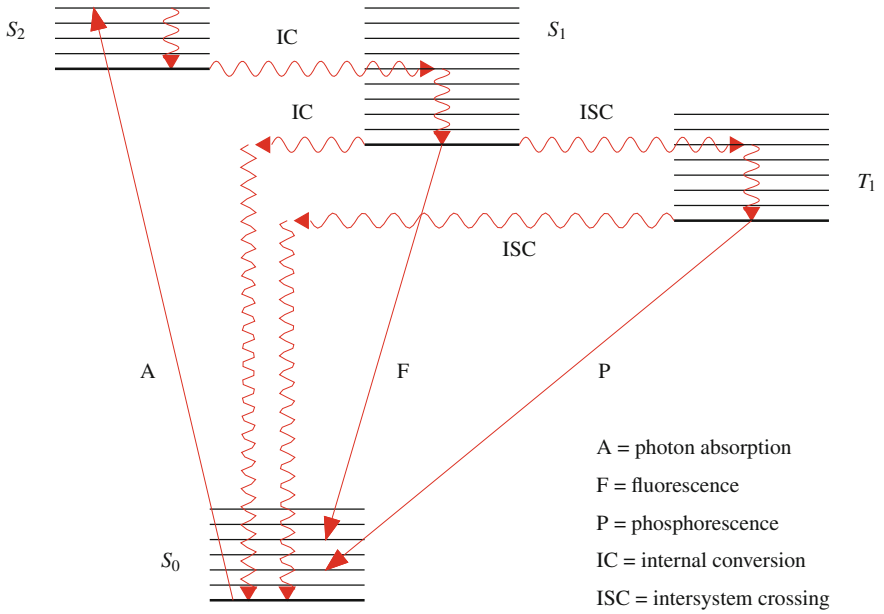

Fig. 1.1 Example of Jablonski diagram. Symbols: A, photon absorption; F, fluorescence; IC, internal conversion; ISC, intersystem crossing; P, phosphorescence

The energetic relationships of states and photophysical processes can be graphically represented by the Jablonski diagrams, as shown in Fig. 1.1. According to the photochemical nomenclature, the electronic states are named after their spin multiplicity: S_n for singlets and T_n for triplets, the two most important spin manifolds for most molecules with an even number of electrons. The suffix n is 0 for the ground state and numbers the excited states starting from S_1 and T_1 according to their energy ordering. In the diagram, every electronic state is represented by a schematic ladder of vibrational states. The radiative processes (absorption and luminescence) are indicated by straight arrows and the nonradiative ones by undulating arrows.

In Fig. 1.1 we have represented the nonradiative processes by a horizontal wavy line plus a vertical one, to distinguish two conceptually different events: the first is the electronic transition by which energy is conserved, at least in isolated molecules; the second is the vibrational energy loss to the environment, leading to "thermalization" or "vibrational relaxation," i.e., to the population of the lowest vibrational and rotational levels according to Boltzmann's statistics. For simplicity, the Jablonski diagrams often feature slanted wavy arrows to represent both processes at once. In the example of Fig. 1.1 a hypothetical molecule is excited to the S_2 state with a certain amount of vibrational energy, which is determined by the exciting wavelength. The vibrational energy excess is readily lost (typical times are of the order of 10 ps in condensed phase), then IC to S_1 follows with subsequent thermalization. At this point three kinds of transitions are in competition: IC or fluorescence emission can

lead to the ground state, while ISC populates T_1. From the triplet state the decay to S_0 can take place by phosphorescence emission or ISC. Actually in many cases the vibrational relaxation and the electronic transitions (especially IC between excited states) occur in the same timescale and considerably affect each other, so the slanted arrows can be a closer representation of the physical reality.

Many of the products of primary events are reactive species that readily undergo "secondary" chemical or photophysical transformations. For instance, starting from neutral molecules with even numbers of electrons, neutral radicals are produced by homolytic photodissociation and hydrogen abstraction, oppositely charged ion pairs by proton transfer; radical cations by photoionization and electron transfer; and radical anions too by the last process. All these species are likely to react in different ways and times, depending on the environment. The photosensitization produces excited species that can undergo substantially the same processes listed above as "primary." The ground state products of several primary events, radiationless decay in the first place, are endowed with a large amount of energy in the nuclear degrees of freedom and can give place to "hot ground state" reactions that would not occur at normal temperatures.

1.5 Quantum Yields

To any well-identified photochemical or photophysical process X we can associate a quantum yield Φ, which is by definition the ratio between the number of molecules undergoing that process and the number of absorbed photons:

$$\Phi_X \equiv \frac{number\ of\ molecules\ undergoing\ process\ X}{number\ of\ absorbed\ photons} . \tag{1.36}$$

If more than one light absorbing compound is present, we only count the photons absorbed by the species originating the chain of events to which process X belongs. The process X, however complex and not known in detail, can be univocally identified on the basis of a chemical product it generates or a molecular state it populates: for instance, we can talk about the triplet quantum yield of a given compound, without knowing through which sequence of radiationless transitions its triplet states are populated. If, as usual, one absorbed photon corresponds to one excited molecule, the denominator of Eq. (1.36) is equal to the number of excited molecules. The quantum yield is measured over a given interval of time, which is assumed to encompass all possible occurrences of X: for instance, if X is an excited state process, the measurement time must be much longer than the lifetime. Alternatively, in a steady-state situation as to the (fast) process X, the quantum yield can be evaluated as a rate ratio:

$$\Phi_X = \frac{rate\ of\ process\ X}{rate\ of\ photon\ absorption} . \tag{1.37}$$

Here the rates can be expressed as molecules or moles per unit time ($\mathrm{mol \cdot s^{-1}}$), or, as usual in chemistry, also per unit volume ($\mathrm{mol \cdot s^{-1} L^{-1}}$). In the latter case we have instantaneous and local rates and quantum yields, which can change in time and space as functions of the sample conditions (concentrations, temperature, etc).

Since all the excited molecules A^* will eventually undergo one of the events that transform or deactivate the excited state, the sum of the quantum yields of the primary processes must equal one:

$$\sum_{X \in primary\ processes} \Phi_X = 1 \tag{1.38}$$

Of course none of the yields Φ_X can be larger than one. This rule can help distinguishing primary and secondary processes.

As an example, consider the four reactions of Chapman's cycle that maintain the (almost) steady concentration of ozone in the stratosphere [7]:

$$O_2 \xrightarrow{h\nu} 2\,O \tag{1.39}$$

$$O_2 + O + M \rightarrow O_3 + M \tag{1.40}$$

$$O_3 + O \rightarrow 2\,O_2 \tag{1.41}$$

$$O_3 \xrightarrow{h\nu} O_2 + O \tag{1.42}$$

The primary step in the production of ozone is the photodissociation of molecular oxygen, reaction (1.39), which requires excitation wavelengths below 240 nm, corresponding to the O_2 dissociation energy of 498 kJ/mol. At these wavelengths, the photodissociation quantum yield in rarefied air is practically 1: it is the only primary process observed, because bond breaking is the fastest way to get rid of the surplus energy. Being absorbed by O_2 itself and also by O_3, solar UV light with such wavelengths becomes progressively less intense by decreasing altitude. At the base of the stratosphere (about 15 km), practically no O_2 photodissociation occurs. This limits the ozone production at low altitudes.

The association reaction (1.40) requires a three-body collision. The rate at which an oxygen atom experiences such an event is proportional to $P_{O_2} \cdot P_{tot}$ (partial pressure of O_2 times total pressure), therefore it decreases very fast with altitude. This is why the ozone production also vanishes progressively beyond 40 km. De facto, the ozone concentration peaks between 20 and 28 km. The quantum yield for the production of ozone due to the secondary reaction (1.40) can be as high as 2 in the lower stratosphere, because two O atoms are produced per absorbed photon and both have a high probability to undergo the three-body collision before being involved in other reactions. Instead, at mid-altitudes in the stratosphere reaction (1.41) becomes competitive because of the increase of O_3 concentration and decrease of total pressure. Therefore, the quantum yield for the production of ozone from the photodissociation

of O_2 declines. The photodissociation of O_3, reaction (1.42), contributes to stabilize the O_3 concentration at low levels.

Reaction (1.41) presents a small activation barrier and therefore can be speeded up by catalyzers. The most important catalytic cycle is:

$$O_3 + Cl \rightarrow O_2 + ClO \tag{1.43}$$

$$O + ClO \rightarrow O_2 + Cl \tag{1.44}$$

Chlorine atoms are mainly supplied by chlorofluorocarbons, very stable synthetic compounds that are not destroyed until they reach the stratosphere. Here the C-Cl bonds are photodissociated by UV light, as in

$$CF_3Cl \xrightarrow{h\nu} CF_3 \cdot + Cl \tag{1.45}$$

This is the source of Cl atoms that catalyze the conversion of O_3 to O_2. Reaction (1.44) restores the Cl atom used by reaction (1.43). If a single Cl atom goes through the cycle n times, the quantum yield of ozone destruction following the photodissociation of CH_3Cl is n, which can be of the order of thousands. Since the cycle (1.43)–(1.44) also converts an oxygen atom to O_2, thus eliminating a precursor of ozone, the real loss of ozone molecules per absorbed photon is $2n$.

1.6 Photochemical Kinetics

In the previous sections we provided some data about typical timescales of photochemical and photophysical phenomena. Actually it is useful to distinguish two categories of time-dependent regimes, dynamics and kinetics. We can define dynamics as the time evolution of the molecular properties that are all connected to the time-dependent wavefunction. Then, in principle, all photoinduced processes, such as structural changes or electronic transitions, belong to the realm of dynamics. However, in many cases a single molecule or molecular aggregate does not undergo any important change, apart from small thermal fluctuations, for long-time intervals. This occurs, for instance, in gas phase, where a molecule can remain in a time-independent state until a collision triggers a reaction event or a transition to another state. Moreover, when slow and gradual transitions between two stationary states take place, the probabilistic nature of quantum mechanics allows us to treat a large sample as composed of molecules that still occupy the initial state and molecules that already populate the final one. If the reactive collisions or the population changes occur according to well-defined rates, we can switch to kinetics and describe the macroscopic phenomena by rate equations. Still, at molecular level, we shall need dynamics for a detailed understanding of the processes and to compute their rates.

This book is mainly devoted to dynamics, but we shall also present some basics of photochemical kinetics in order to bridge the gap with the macroscopic description.

1.6.1 Excitation Rate

The molecular excitation by light absorption, if the irradiance is not too high, consists of relatively rare transitions to an excited state, the interval between two events being much longer than the time needed for the molecule to get back to the ground state. Let us consider a thin layer of any homogeneous material, crossed perpendicularly by a beam of light. Each molecule in the layer has got a probability $P(\nu)\mathrm{d}\nu\mathrm{d}t$ of absorbing a photon of frequency within the frequency interval $[\nu, \nu + \mathrm{d}\nu]$ during the time $\mathrm{d}t$. P is proportional to the number of photons that happen to be close to the molecule during a time unit, i.e., to the spectral photon irradiance:

$$P(\nu)\ \mathrm{d}\nu\ \mathrm{d}t = \sigma(\nu)\ I_{ph,\nu}(\nu)\ \mathrm{d}\nu\ \mathrm{d}t\ . \tag{1.46}$$

Since both sides of this equation are pure numbers, σ is a surface area, called the "absorption cross section" of the molecule. The cross section is not directly related to any geometric section of the molecule and is usually much smaller, but it is an extensive quantity (a protein molecule absorbs much more than a single amino acid). For small molecules σ can be of the order of 10^{-20} m^2 or much less, depending on the frequency. In going through a layer of thickness $\mathrm{d}l$, the rate of photon absorption in the interval $[\nu, \nu + \mathrm{d}\nu]$ will be

$$N\ S\ \mathrm{d}l\ P(\nu)\ \mathrm{d}\nu = N\ S\ \mathrm{d}l\ \sigma(\nu)\ I_{ph,\nu}(\nu)\ \mathrm{d}\nu \tag{1.47}$$

where N is the number density of molecules, S is the considered layer surface, and then $NS\mathrm{d}l$ is the number of molecules in that portion of the layer. Since this is a fraction of the photons within the frequency interval $\mathrm{d}\nu$ that are going through the surface S, we see that the irradiance decreases by

$$dI_{ph,\nu} = -N\ \sigma(\nu)\ I_{ph,\nu}(\nu)\ \mathrm{d}l\ . \tag{1.48}$$

This differential equation can be integrated to yield the expression of the irradiance as a function of the length l of the pathway covered by the light in the absorbing medium, called the "optical pathway":

$$I_{ph,\nu}(\nu, l) = I_{ph,\nu}(\nu, 0)\ \mathrm{e}^{-N\,\sigma(\nu)\,l} \tag{1.49}$$

where $I_{ph,\nu}(\nu, 0)$ is the irradiance of the incident light. This is the Lambert–Beer law, most often written in terms of molarity and energy irradiance, and with a base 10 exponential (instead of number density, photon irradiance, and base e, respectively):

$$I_\nu(\nu, l) = I_\nu(\nu, 0)\ 10^{-M\ \varepsilon(\nu)\ l}\ . \tag{1.50}$$

The units commonly used for l are cm, so the molar extinction coefficient $\varepsilon(\nu)$ is expressed in $\text{mol}^{-1}\text{L cm}^{-1}$ and its relationship to σ is:

$$\sigma\ /\ \text{m}^2 = C_{\varepsilon,\sigma}\ \varepsilon\ /\ \text{mol}^{-1}\text{L cm}^{-1} \tag{1.51}$$

where the conversion factor is

$$C_{\varepsilon,\sigma} = \frac{\ln(10)}{10 N_A} = 3.8235 \cdot 10^{-25}\ . \tag{1.52}$$

The absolute value of the exponent in the RHS of Eq. (1.50) is called absorbance (A or sometimes A_{10} to specify that we are using a base 10 exponential):

$$A(\nu) \equiv \log_{10}\left(\frac{I_\nu(\nu, 0)}{I_\nu(\nu, l)}\right) = M\ \varepsilon(\nu)\ l\ . \tag{1.53}$$

If more than one species absorbs at frequency ν, the expression of the absorbance modifies to

$$A(\nu) = \sum_K M_K\ \varepsilon_K(\nu)\ l \tag{1.54}$$

where M_K and ε_K are the molarity and the extinction coefficient of the molecular species K.

From Eq. (1.48) we obtain the rate at which molecules of the species K are excited by photons in the range $[\nu, \nu + \text{d}\nu]$, in a unit volume:

$$[R_{exc,K}(\nu)\ \text{d}\nu]\ /\ \text{m}^{-3}\text{s}^{-1} = N_K\ \sigma_K(\nu)\ I_{ph,\nu}(\nu)\text{d}\nu\ . \tag{1.55}$$

From here onward we drop the dependence of $I_{ph,\nu}$ on the position in space that can vary according to the irradiation conditions. Notice that the value of $I_{ph,\nu}(\nu)\text{d}\nu$ is invariant versus the choice of units for ν: actually one can also replace ν with λ, using $I_{ph,\lambda}(\lambda)\text{d}\lambda$, as already discussed in Sect. 1.2.2. In the usual chemical units

$$[R_{exc,K}(\nu)\ \text{d}\nu]\ /\ \text{mol L}^{-1}\text{s}^{-1} = C_{\varepsilon,\sigma}\ M_K\ \varepsilon_K(\nu)\ I_{ph,\nu}(\nu)\text{d}\nu \tag{1.56}$$

or

$$[R_{exc,K}(\lambda)\ \text{d}\lambda]\ /\ \text{mol L}^{-1}\text{s}^{-1} = C_{\varepsilon,\sigma}\ M_K\ \varepsilon_K(\lambda)\ I_{ph,\lambda}(\lambda)\ \text{d}\lambda\ . \tag{1.57}$$

In order to obtain the total rate for a finite frequency interval we must integrate:

$$R_{exc,K}^{(\nu_a,\nu_b)} = \int_{\nu_a}^{\nu_b} R_{exc,K}(\nu)\ \text{d}\nu = \int_{\lambda_b}^{\lambda_a} R_{exc,K}(\lambda)\ \text{d}\lambda \tag{1.58}$$

where of course $\lambda_{a,b} = c/\nu_{a,b}$. In this expression the excitation rate $R_{exc,K}$ contains the factor M_K (or N_K if we use the molecular cross section). By dropping the concentration factor we get a "rate constant"

$$J_{exc,K}^{(\nu_a,\nu_b)} \;/\; \mathrm{s}^{-1} = C_{\varepsilon,\sigma} \int_{\nu_a}^{\nu_b} \varepsilon_K(\nu)\; I_{ph,\nu}(\nu)\; \mathrm{d}\nu \;. \tag{1.59}$$

The excitation rate is then expressed like in thermal chemistry, as $J_{exc,K}^{(\nu_a,\nu_b)}\; N_K$ or $J_{exc,K}^{(\nu_a,\nu_b)}\; M_K$. If the radiation spectrum is limited to a sufficiently narrow bandwidth $[\nu_a, \nu_b]$, it is reasonable to define the weighted average of the extinction coefficient

$$\overline{\varepsilon}_K = \frac{\int_{\nu_a}^{\nu_b} \varepsilon_K(\nu)\; I_{ph,\nu}(\nu)\; \mathrm{d}\nu}{I_{ph,tot}} \tag{1.60}$$

and analogously for the cross section $\overline{\sigma}_K$. Then, formally, the excitation rate constant is simply the product of a molecular quantity times the total irradiance:

$$J_{exc,K}^{(\nu_a,\nu_b)} \;/\; \mathrm{s}^{-1} = \overline{\sigma}_K\; I_{ph,tot} = C_{\varepsilon,\sigma}\; \overline{\varepsilon}_K\; I_{ph,tot} \;. \tag{1.61}$$

1.6.2 Rates of Photochemical Reactions and Photophysical Processes

To formulate the rate of a process triggered by photon absorption, we must decide whether the excited state decay is fast or slow. In this context, fast means much shorter than the time resolution afforded by the experimental equipment. If so, we can resort to the approximation that after photon absorption the unimolecular primary processes occur (almost) instantaneously. If fast transitions between different excited states take place, in the kinetic treatment they can be overlooked too. The rate of a fast process X is then simply determined by an integral of the absorption factor $\sigma_K(\nu)\; I_{ph,\nu}(\nu)$ times the quantum yield $\Phi_{X,K}(\nu)$. As in the case of the excitation rates, we define a photochemical rate constant as

$$J_{X,K} \;/\; \mathrm{s}^{-1} = C_{\varepsilon,\sigma} \int_0^{\infty} \varepsilon_K(\nu)\; I_{ph,\nu}(\nu)\; \Phi_{X,K}(\nu)\; \mathrm{d}\nu \tag{1.62}$$

and the rate is obtained by multiplying $J_{X,K}$ by the concentration:

$$R_{X,K} \;/\; \mathrm{m}^{-3}\mathrm{s}^{-1} = J_{X,K}\; N_K \tag{1.63}$$

$$R_{X,K} \;/\; \mathrm{mol\,L}^{-1}\mathrm{s}^{-1} = J_{X,K}\; M_K \tag{1.64}$$

We see that, once the spectrum of the exciting light is fixed, the photochemical rate constant is proportional to the total irradiance.

Equation (1.62) can be simplified if the quantum yield is approximately constant in the frequency interval $[\nu_a, \nu_b]$ and vanishes elsewhere. This is rather common: for instance, in gas phase the photodissociation quantum yield of a small molecule with dissociation energy E_{diss} is almost one for $\nu > E_{diss}/h$ and drops to zero below this threshold (see also the last part of Sect. 3.11). In such cases, we can write

$$J_{X,K} \simeq J_{exc,K}^{(\nu_a,\nu_b)} \, \Phi_{X,K} \; . \tag{1.65}$$

When using monochromatic light of frequency ν_{exc} these relationships simplify without approximations:

$$J_{X,K} = J_{exc,K}^{(\nu_{exc})} \, \Phi_{X,K}(\nu_{exc}) = C_{\varepsilon,\sigma} \, \varepsilon_K(\nu_{exc}) \, I_{ph,tot} \, \Phi_{X,K}(\nu_{exc}) \; . \tag{1.66}$$

For this reason, and for a better reproducibility, many experiments are performed with monochromatic light.

The case in which the decay of the excited state(s) of molecule K is slow enough as to be monitored with the available techniques calls for a kinetic treatment that takes into account their transient populations. However, it is not always possible to define a set of rate constants for the primary processes, because the excited state dynamics may depend on a complex interplay of structural changes, energy transfer to the environment and radiationless electronic transitions, as will be discussed in Chaps. 4 and 5. A typical case in which the definition of rate constants for a kinetic treatment is viable occurs when the electronically excited molecules can become thermally equilibrated as to their nuclear degrees of freedom by interaction with the environment. In condensed phase, this requires lifetimes much longer than 10 ps, which are not uncommon.

As an example, it has became clear thanks to experimental and theoretical work that the excited state dynamics of benzophenone is a rather complicated sequence of fast transitions of IC and ISC type, involving S_2 (the state connected with S_0 by the strongest optical transition), S_1, T_2, and higher triplets (see [5, 8, 9] and refs. therein). Almost 100% of the benzophenone molecules end up in the lowest triplet state, T_1. Then, a slow ISC to the ground state takes place, in competition with phosphorescence emission. Given its high triplet quantum yield and the long lifetime of its T_1 state, benzophenone is a good triplet sensitizer. Triplet sensitization is used to populate the triplet states of other molecules in which the ISC from singlet to triplet states is not efficient. A further advantage is the possibility to irradiate with longer wavelengths than those needed to directly excite the energy acceptor, when the absorbing singlet states of the latter absorb at short wavelengths. Moreover, in certain cases it may be convenient to bypass the singlet states of the acceptor, when they would undergo undesired reactions. In Fig. 1.2 we show the Jablonski diagrams of benzophenone and of naphthalene. The triplet quantum yield of the latter, in benzene at 29 °C, is $\Phi_T = 0.39$ and that of phosphorescence is $\Phi_P = 0.03$. That means that 39% of the excited naphthalene molecules populate T_1, while the others decay to

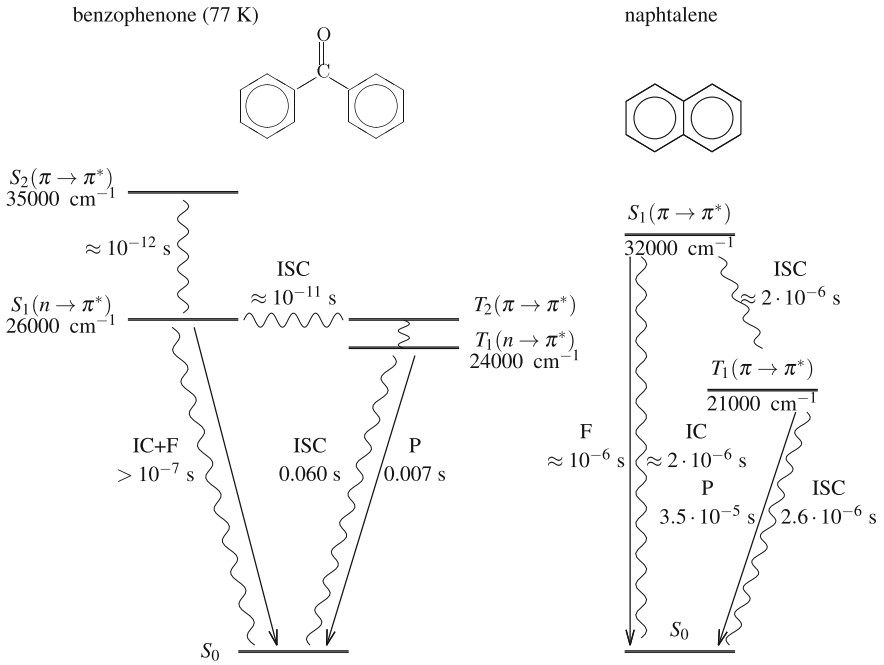

Fig. 1.2 Jablonski diagrams: benzophenone and naphthalene

the ground state by IC and fluorescence emission. Moreover, only about 7% of the molecules that populate T_1 emit a photon instead of decaying to the ground state by ISC. When adding benzophenone to the solution, the phosphorescence emission of naphthalene becomes more intense and its Φ_P increases. In optimal conditions, i.e., by irradiating at $\lambda = 366$ nm, where only benzophenone absorbs, and with a sufficiently high concentration of naphthalene, Φ_P goes up to 0.07. In a series of classical experiments, Lamola et al [9] showed that by linking in one molecule the two chromophores, the sensitization becomes very efficient. The alkyl chain connecting benzophenone and naphthalene in the compound of Fig. 1.3 does not affect the optical spectra of the chromophores. By irradiating at $\lambda = 366$ nm, benzophenone is excited in the $n \to \pi^*$ band but the phosphorescence spectrum is almost identical to that of naphthalene. With $\lambda = 313$ nm, naphthalene is excited and the phosphorescence spectrum is the same as before, but its quantum yield is higher than in naphthalene. What happens is that the excitation is transferred first from S_1 of naphthalene to S_1 of benzophenone, and then from T_1 of benzophenone to T_1 of naphthalene. Since the ISC of benzophenone is much more efficient than that of naphthalene, this alternative pathway adds a significant contribution to the triplet quantum yield of naphthalene.

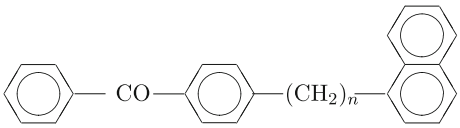

Fig. 1.3 Benzophenone and naphthalene chromophores in one compound

1.6.3 Photoisomerization with Thermal Direct and Reverse Reaction

Many compounds can exist in different isomeric forms that can be interconverted by photochemical and/or thermal reactions. In the absence of light the thermal isomerizations produce a mixture of isomers at equilibrium. Here we shall consider two isomers, A and B, of which A is the more stable. The photoisomerization

$$\mathrm{A} \xrightarrow{h\nu} \mathrm{B} \tag{1.67}$$

occurs with quantum yield $\Phi_{A\to B}$ and the thermal reactions

$$\mathrm{A} \longrightarrow \mathrm{B} \tag{1.68}$$

and

$$\mathrm{B} \longrightarrow \mathrm{A} \tag{1.69}$$

have rate constants $K_{A\to B}$ and $K_{B\to A}$. Spiropyrans and spiroxazines are classes of compounds which, in suitable conditions, only undergo these three reactions. The less stable isomer B is an open ring form that absorbs visible light, whereas isomer A only absorbs UV light. As a consequence, by exposure to a source of UV light, including sunlight, a material containing such dyes becomes colored, while in the dark it reverts to transparency. Because of this property they are used to manufacture photochromic sunglasses (Fig. 1.4).

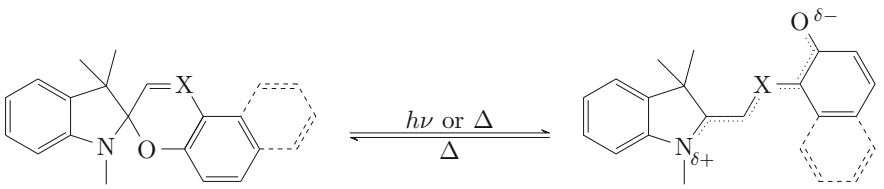

colorless form colored form

X = CH: spiropyran
X = N: spiroxazine

Fig. 1.4 Examples of spiropyran and spiroxazine photochromic compounds

The concentrations of A and B obey the kinetic law

$$-\frac{\mathrm{d}\,[\mathrm{A}]}{\mathrm{d}t} = \frac{\mathrm{d}\,[\mathrm{B}]}{\mathrm{d}t} = (J_{A\to B} + K_{A\to B})\ [\mathrm{A}] - K_{B\to A}\,[\mathrm{B}] = \\ = (J_{A\to B} + K_{A\to B} + K_{B\to A})\ [\mathrm{A}] - K_{B\to A}\ C_{tot} \tag{1.70}$$

where C_{tot} indicates the sum of the A and B molarities, constant in time. As noted in Sect. 1.6.2, the photochemical rate constant $J_{A\to B}$ is proportional to $I_{ph,tot}$. With monochromatic light, $J_{A\to B} = C_{\varepsilon,\sigma}\ \varepsilon_A(\nu_{exc})\ I_{ph,tot}\ \Phi_{A\to B}(\nu_{exc})$. The general solution of this equation is

$$[\mathrm{A}] = P\ \mathrm{e}^{-t/\tau} + Q\ . \tag{1.71}$$

By replacing [A] with this expression in Eq. (1.70) one finds

$$\tau^{-1} = J_{A\to B} + K_{A\to B} + K_{B\to A} \tag{1.72}$$

and

$$Q = K_{B\to A}\ C_{tot}\ \tau = \frac{K_{B\to A}}{J_{A\to B} + K_{A\to B} + K_{B\to A}}\ C_{tot}\ . \tag{1.73}$$

While τ and Q are determined by the constants contained in Eq. (1.70), P depends instead on the initial conditions, namely on the A concentration at $t = 0$, $[\mathrm{A}]_0$:

$$P = [\mathrm{A}]_0 - Q\ . \tag{1.74}$$

For instance, if at $t = 0$ we have an equilibrium mixture, $[\mathrm{A}]_0 = C_{tot} K_{B\to A}/(K_{A\to B} + K_{B\to A})$. Q is the asymptotic concentration of A that is approached when $t \gg \tau$ in what is called the "photostationary state." The asymptotic concentration ratio is

$$\frac{[\mathrm{B}]_\infty}{[\mathrm{A}]_\infty} = \frac{J_{A\to B} + K_{A\to B}}{K_{B\to A}}\ . \tag{1.75}$$

$J_{A\to B}$ can be increased either by using a higher irradiance, or a wavelength at which the product $\varepsilon_A \Phi_{A\to B}$ is larger. As a result, the conversion of A to B at any time is more complete and the photostationary state is approached faster, i.e., τ is smaller (see Fig. 1.5). In the photostationary state, which can be very far from the thermodynamic equilibrium, the photochemical and thermal rates compensate each other: $(J_{A\to B} + K_{A\to B})\,[\mathrm{A}] = K_{B\to A}\,[\mathrm{B}]$. When the light is switched off the system reverts to equilibrium with a similar first-order kinetics, but more slowly ($\tau_{therm}^{-1} = K_{A\to B} + K_{B\to A}$).

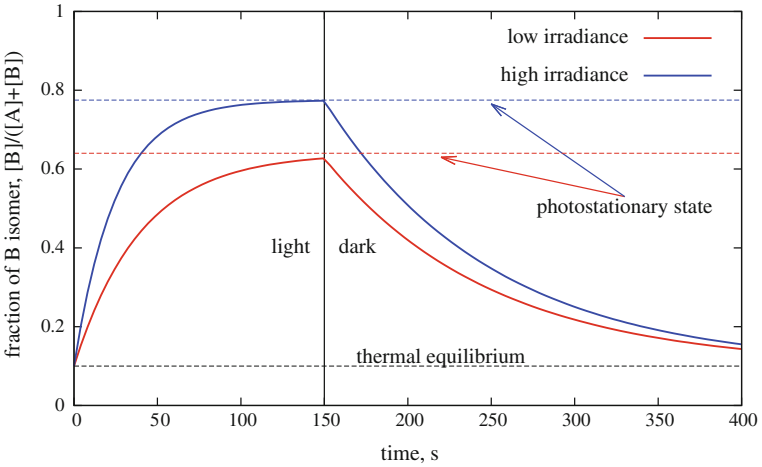

Fig. 1.5 Photoisomerization kinetics with thermal direct and reverse reaction. The time dependence of the ratio [B]/ ([A] + [B]) is plotted for two values of the irradiance, the higher one double than the lower one. The irradiation is switched off after 150 s. The dashed lines show the photostationary value of the ratio that would be reached after a long irradiation

1.6.4 Reversible Photoisomerization

When the photoisomerization does not change substantially the electronic structure, as in the *cis–trans* isomerization, usually both isomers absorb light and react photochemically in similar ways. If the thermal reaction rates can be neglected, the kinetic equation is

$$-\frac{\mathrm{d}\,[\mathrm{A}]}{\mathrm{d}t} = \frac{\mathrm{d}\,[\mathrm{B}]}{\mathrm{d}t} = J_{A\to B}\ [\mathrm{A}] - J_{B\to A}\ [\mathrm{B}] = (J_{A\to B} + J_{B\to A})\,[\mathrm{A}] - J_{B\to A}\ C_{tot}\ . \tag{1.76}$$

This equation has the same structure as (1.5): the main difference consists in the physical meaning of the $J_{B\to A}$ constant. The general solution is still given by Eq. (1.71), with $P = [\mathrm{A}]_0 - Q$, but

$$\tau^{-1} = J_{A\to B} + J_{B\to A} \tag{1.77}$$

and

$$Q = \frac{J_{B\to A}}{J_{A\to B} + J_{B\to A}}\ C_{tot}\ . \tag{1.78}$$

The reaction lifetime τ is now inversely proportional to the irradiance, while the asymptotic concentration ratio is independent on the irradiance:

$$\frac{[\mathrm{B}]_\infty}{[\mathrm{A}]_\infty} = \frac{J_{A\to B}}{J_{B\to A}} = \frac{\varepsilon_A \Phi_{A\to B}}{\varepsilon_B \Phi_{B\to A}}\ . \tag{1.79}$$

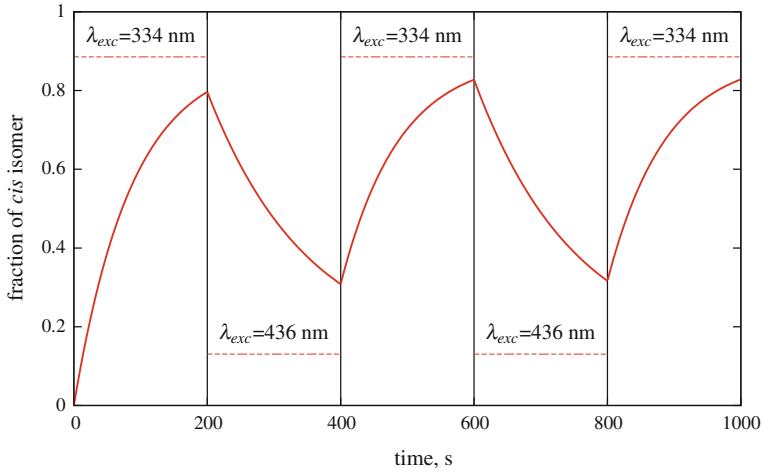

Fig. 1.6 Kinetics of $trans \rightarrow cis$ and $cis \rightarrow trans$ azobenzene photoisomerization in methanol. The solution is irradiated alternatively with $\lambda = 334$ nm and $\lambda = 436$ nm for periods of 200 s. The irradiance at $\lambda = 436$ nm is twice that at $\lambda = 334$ nm, to compensate for the lower absorption. The concentrations are computed from the following data: at $\lambda = 334$ nm, ε_{trans}=16980 M^{-1} cm^{-1}, ε_{cis}=1100 M^{-1} cm^{-1}, $\Phi_{trans \rightarrow cis}$=0.15, $\Phi_{cis \rightarrow trans}$=0.30; at $\lambda = 436$ nm, ε_{trans}=490 M^{-1} cm^{-1}, ε_{cis}=1140 M^{-1} cm^{-1}; $\Phi_{trans \rightarrow cis}$=0.22, $\Phi_{cis \rightarrow trans}$=0.63 (from Gauglitz et al [10]). The dashed lines indicate the asymptotic fraction of the cis isomer that would be obtained for the given λ_{exc}

Therefore, the only way to change the asymptotic composition of the isomeric mixture is to change the excitation wavelength, i.e., the extinction coefficients ε_A and ε_B. Notice that also the quantum yields depend on λ, but normally to a lesser extent. In Fig. 1.6 we show how $trans$- and cis-azobenzene can be reversibly interconverted by using UV and visible light.

Problems

1.1 Compute the energy, in kJ/mol, of an infrared photon with frequency 1500 cm^{-1} and of a visible photon with wavelength 500 nm.

1.2 Compare the irradiance of sunlight in the visible part of the spectrum (about 500 W/m^2 in a clear day) with: (1), the irradiance of a 1 mW He–Ne laser with a beam diameter of 1 mm and, (2) the irradiance of a 100 W tungsten lamp at a distance of 2 meters, assuming that 2% of its power is converted into visible light.

1.3 A molecule is exposed to monochromatic light with $\lambda = 500$ nm and irradiance 100 W/m^2. How frequently does it absorb a photon, if its molar absorption coefficient at 500 nm is $\varepsilon = 1000$ mol^{-1} L cm^{-1}?

1.4 The chlorofluorocarbons are photodissociated in the stratosphere only when they reach an altitude where UV light with sufficiently short wavelengths is present. CCl_3CF_3 does not absorb significantly at $\lambda > 220$ nm. The C-Cl dissociation energy is about 330 kJ/mol. Are short wavelengths needed for the photodissociation because of the absorption spectrum of CCl_3CF_3 or because of the C-Cl bond strength?

1.5 Compute the lifetimes of T_1 and S_1 of benzophenone and its phosphorescence quantum yield. The same for naphthalene, with the addition of its fluorescence quantum yield. Use the lifetime of each process indicated in Fig. 1.2 (remember that the inverse of a lifetime is the rate constant of the process).

1.6 In the example of photochromic reaction kinetics discussed in Sect. 1.6.3, suppose the experiment with high irradiance is repeated at a higher temperature, so that $K_{A\to B}$ increases by 80% and $K_{B\to A}$ by 50%. Based on the data that can be inferred from Fig. 1.5, which fraction of B is expected at 150 s?

References

1. Wayne, R.P.: Principles and Applications of Photochemistry. Oxford University Press, Oxford (1988)
2. Wardle, B.: Principles and Applications of Photochemistry. Wiley, Chichester (2009)
3. Turro, N.J., Ramamurthy, V., Scaiano, J.C.: Modern Molecular Photochemistry of Organic Molecules. University Science Books, Sausalito (2010)
4. Balzani, V., Ceroni, P., Juris, A.: Photochemistry and Photophysics: Concepts, Research, Applications. Wiley, Chichester (2014)
5. Rohatgi-Mukherjee, K.K.: Fundamentals of Photochemistry. New Age International, New Delhi (2017)
6. Cohen-Tannoudji, C., Dupont-Roc, J., Grynberg, G.: Atom-Photon Interactions: Basic Processes and Applications. Wiley-VCH, Weinheim (2004)
7. Wayne, R.P.: Chemistry of the Atmospheres. Oxford University Press, Oxford (2000)
8. Favero, L., Granucci, G., Persico, M.: Surface hopping investigation of benzophenone excited state dynamics. Phys. Chem. Chem. Phys. **18**, 10499–10506 (2016)
9. Lamola, A.A., Leermakers, P.A., Beyers, G.W., Hammond, G.S.: Intramolecular electronic energy transfer between nonconjugated chromophores in some model compounds. J. Am. Chem. Soc. **87**, 2322–2332 (1965)
10. Gauglitz, G., Hubig, S.: Chemical actinometry in the UV by azobenzene in concentrated solution: a convenient method. J. Photochem. **30**, 121–125 (1985)

Chapter 2
Molecular States

Abstract This chapter will introduce the quantum mechanical equation of motion, i.e., the time-dependent Schrödinger equation. We will show how the separation of variables can be exploited to partition the molecular wavefunction in translational, rotational, vibrational, and electronic components, with special emphasis on the Born–Oppenheimer approximation and its breakdown. We shall then provide an overview of the electronic structure and reactivity of excited states commonly found in organic molecules.

Keywords Molecular states · Born · Oppenheimer approximation
Electric excited states · Photochemical reactions

2.1 The Time-Dependent Schrödinger Equation

In the first sections of this chapter we develop the quantum mechanical theory of molecular states. The basic physical principles can be found in any textbook of quantum mechanics, for instance in Merzbacher [1] or Sakurai and Napolitano [2]. For more chemical approaches, see Atkins and Friedman [3] or Levine [4] among others. Good introductions to excited states and the theory of photochemistry are Michl and Bonačić-Koutecký [5] and Klessinger and Michl [6].

In nonrelativistic quantum mechanics the time evolution of a physical system is given by the time-dependent Schrödinger equation (TDSE):

$$\mathrm{i}\hbar\frac{\mathrm{d}\Psi(\mathbf{x},t)}{\mathrm{d}t} = \hat{H}\Psi(\mathbf{x},t) \tag{2.1}$$

where $\hat{H}$ is the Hamiltonian operator. The physical state of the system is described by the wavefunction Ψ, which depends on time t and on the collection of spatial and spin coordinates $\mathbf{x}$ of all the particles belonging to the system.

M. Persico and G. Granucci, *Photochemistry*, Theoretical Chemistry
and Computational Modelling, https://doi.org/10.1007/978-3-319-89972-5_2

The Hamiltonian operator is linear, as most of the other operators that appear in this book. That is: $\hat{H}(c_1\Psi_1 + c_2\Psi_2) = c_1\hat{H}\Psi_1 + c_2\hat{H}\Psi_2$, where c_1 and c_2 are complex coefficients. Therefore, the TDSE is also linear, which has a very important consequence: a linear combination of distinct solutions of the TDSE is still a solution. This is the *superposition principle*.

The quantity $|\Psi(\mathbf{x}, t)|^2\,\mathrm{d}\mathbf{x}$ is proportional to the probability of finding the system in the interval of coordinates $\mathrm{d}\mathbf{x}$. More precisely, for each particle i we consider an infinitesimal volume $\mathrm{d}r_i^3$ and a given value of the z spin component s_i. We can integrate $|\Psi(\mathbf{x}, t)|^2$ over the whole range of each space coordinate and sum over all the allowed spin values. This operation can be for simplicity indicated as an integral over the vector $\mathbf{x}$ or, in Dirac's notation (see Appendix B), as the scalar product of state $|\Psi\rangle$ with itself:

$$I = \int_{all\ space} |\Psi(\mathbf{x}, t)|^2\,\mathrm{d}\mathbf{x} \equiv \langle\Psi\,|\Psi\,\rangle \tag{2.2}$$

If I is a finite quantity, $\Psi(\mathbf{x}, t)$ can be divided by the factor $\sqrt{I}$ (thanks to the linearity of the TDSE), obtaining a *normalized* wavefunction $\Psi' = I^{-1/2}\,\Psi$. In that case,

$$\left\langle\Psi'\,\middle|\,\Psi'\right\rangle = I^{-1}\ \langle\Psi\,|\Psi\,\rangle = 1 \tag{2.3}$$

and $\rho(\mathbf{x}, t) = \left|\Psi'(\mathbf{x}, t)\right|^2$ exactly corresponds to the probability density of finding the system in $\mathbf{x}$.

Contrary to what happens in classical mechanics, the TDSE is first order in the time derivative. Therefore, once the wavefunction has been specified at some time t_0, the physical state of the system is univocally determined at any t. In particular, $\Psi(\mathbf{x}, t_0)$ is easily propagated to an infinitesimally close time $t_0 + \mathrm{d}t$

$$\begin{aligned}\Psi(\mathbf{x}, t_0 + \mathrm{d}t) &= \Psi(\mathbf{x}, t_0) + \frac{\mathrm{d}\Psi(\mathbf{x}, t_0)}{\mathrm{d}t}\mathrm{d}t \\ &= \Psi(\mathbf{x}, t_0) - \frac{\mathrm{i}\mathrm{d}t}{\hbar}\hat{H}(t_0)\Psi(\mathbf{x}, t_0) \\ &= \hat{U}(t_0, t_0 + \mathrm{d}t)\Psi(\mathbf{x}, t_0)\end{aligned} \tag{2.4}$$

where only the first-order terms in $\mathrm{d}t$ have been retained and

$$\hat{U}(t_0, t_0 + \mathrm{d}t) = 1 - \frac{\mathrm{i}\mathrm{d}t}{\hbar}\hat{H}(t_0) \tag{2.5}$$

is the infinitesimal time evolution operator from time t_0 to $t_0 + \mathrm{d}t$. The above expression for $\hat{U}(t_0, t_0 + \mathrm{d}t)$ is generally valid, even for a time-dependent Hamiltonian. Note that the wavefunction $\Psi(\mathbf{x}, t)$ is inherently a complex-valued quantity: In fact, as $\hat{U}(t_0, t_0 + \mathrm{d}t)$ contains the imaginary unit, even if we start with a real Ψ at t_0, it will become complex at later (or previous) times.

2.1.1 Observables

Let $\hat{X}$ be a linear operator. Its adjoint $\hat{X}^\dagger$ is defined by requiring that the equality

$$\int_{all\ space} \psi^* \hat{X}^\dagger \phi \mathrm{d}\mathbf{x} = \int_{all\ space} \phi^* \hat{X} \psi \mathrm{d}\mathbf{x} \tag{2.6}$$

is valid for any pair of wavefunctions ϕ and ψ. In Dirac notation:

$$\left\langle \psi \left| \hat{X}^\dagger \right| \phi \right\rangle = \left\langle \phi \left| \hat{X} \right| \psi \right\rangle \qquad \forall\ \phi, \psi\ . \tag{2.7}$$

An operator $\hat{X}$ is said to be Hermitian if $\hat{X} = \hat{X}^\dagger$, or equivalently

$$\left\langle \psi \left| \hat{X} \right| \phi \right\rangle = \left\langle \phi \left| \hat{X} \right| \psi \right\rangle^* \qquad \forall\ \phi, \psi\ . \tag{2.8}$$

The complex number λ is an eigenvalue of $\hat{X}$ if $\hat{X}\phi = \lambda\phi$, and ϕ is the corresponding eigenfunction. The spectrum of an operator is the full set of its eigenvalues. For a Hermitian operator we have that the eigenvalues are real numbers and the eigenvectors are mutually orthogonal (or at least they can be chosen so as to be orthogonal) and represent a basis for the vector space on which the operator is defined.

In quantum mechanics a physical observable is associated with a Hermitian operator. For example, for position $\hat{x}$, linear momentum $\hat{p}_x$ and kinetic energy $\hat{T}$ we have:

$$\hat{x} = x \qquad \hat{p} = -\mathrm{i}\hbar \frac{\partial}{\partial x} \qquad \hat{T} = -\frac{\hbar^2}{2m}\nabla^2\ . \tag{2.9}$$

The spectrum of a Hermitian operator $\hat{X}$ can be discrete, Eq. (2.10), or continuous, Eq. (2.11):

$$\hat{X}\phi_i = \lambda_i \phi_i \quad i = 1, 2, \ldots \tag{2.10}$$

$$\hat{X}\phi_\lambda = \lambda \phi_\lambda \quad \lambda \in \mathbb{R}\ . \tag{2.11}$$

The eigenfunctions of an observable $\hat{O}$ with a discrete spectrum are normalizable in the sense of Eq. (2.3), while those of an observable with a continuous spectrum require a different normalization because the integral (2.2) does not exist (see Appendix C). In fact, a wavefunction is normalizable only if it tends to zero when any space coordinate takes values far from a limited interval ("bound state"): but this requirement is satisfied only by some "special" eigenfunctions (those satisfying the boundary conditions), making the spectrum discrete.

We now consider a system in a physical state described by the normalized wavefunction $\Psi(t)$, and an observable $\hat{O}$ with a discrete spectrum: $\hat{O}\phi_i = \lambda_i \phi_i$. We assume that $\hat{O}$ is not explicitly dependent on time. We choose the eigenfunctions ϕ_i to be orthonormal, i.e.,

$$\langle \phi_i \, | \phi_j \rangle = \delta_{ij} \ . \tag{2.12}$$

The wavefunction $\Psi(t)$ can be expanded on the basis of the eigenfunctions of $\hat{O}$:

$$\Psi(t) = \sum_i c_i(t)\phi_i \tag{2.13}$$

and exploiting Eq. (2.12) we have $c_i(t) = \langle \phi_i \, | \Psi \rangle$. Assuming that $\Psi(t)$ is normalized we have $\sum_i |c_i(t)|^2 = 1$. The averaged measured value of the observable is the expectation value:

$$\begin{aligned} \left\langle \Psi \left| \hat{O} \right| \Psi \right\rangle &= \sum_{i,j} c_i(t)^* c_j(t) \left\langle \phi_i \left| \hat{O} \right| \phi_j \right\rangle \\ &= \sum_i |c_i(t)|^2 \lambda_i \ . \end{aligned} \tag{2.14}$$

Note that $\left\langle \Psi \left| \hat{O} \right| \Psi \right\rangle$ is a real quantity. According to the quantum theory of measurement, a single determination of the observable $\hat{O}$ can only give one of its eigenvalues λ_i and $|c_i(t)|^2$ is the probability of finding the system in the eigenstate ϕ_i.

If the observable $\hat{O}$ has a continuous spectrum, $\hat{O}\phi_\lambda = \lambda\phi_\lambda$, its eigenvectors cannot be normalized as the integral $\langle \phi_\lambda \, | \phi_\lambda \rangle$ diverges. However, a different normalization condition may be imposed:

$$\langle \phi_\lambda \, | \phi_{\lambda'} \rangle = \delta(\lambda - \lambda') \tag{2.15}$$

where $\delta(x)$ is the Dirac delta function; see Appendix C. In this way we have, for a normalized wavefunction $\Psi(t)$

$$\begin{aligned} \Psi(t) &= \int c(\lambda, t)\phi_\lambda \mathrm{d}\lambda \\ c(\lambda, t) &= \langle \phi_\lambda \, | \Psi \rangle \\ \langle \Psi \, | \Psi \rangle &= 1 = \int |c(\lambda, t)|^2 \, \mathrm{d}\lambda \end{aligned} \tag{2.16}$$

and the expectation value is

$$\begin{aligned} \left\langle \Psi \left| \hat{O} \right| \Psi \right\rangle &= \iint c(\lambda, t)^* c(\lambda', t) \left\langle \phi_\lambda \left| \hat{O} \right| \phi_{\lambda'} \right\rangle \mathrm{d}\lambda \mathrm{d}\lambda' \\ &= \int |c(\lambda, t)|^2 \, \lambda \mathrm{d}\lambda \ . \end{aligned} \tag{2.17}$$

Similar to the discrete case, $|c(\lambda, t)|^2$ is the probability density of finding the system in the eigenstate ψ_λ.

An important example is offered by linear momentum. The eigenvalue equation for $\hat{p}_x$ is

$$-\mathrm{i}\hbar\frac{\partial\phi_p(x)}{\partial x} = p\phi_p(x) \tag{2.18}$$

which is solved by the plane waves $\phi_p = A\mathrm{e}^{\mathrm{i}px/\hbar}$, with $p \in (-\infty, +\infty)$. Note that a complex value of p would give divergent eigenvectors, physically inacceptable. The constant A is determined requiring

$$\int_{-\infty}^{+\infty} \phi_p^*(x)\phi_{p'}(x)\mathrm{d}x = \delta(p - p') \ . \tag{2.19}$$

Remembering that, from Fourier analysis

$$\delta(x) = \frac{1}{2\pi}\int_{-\infty}^{+\infty} \mathrm{e}^{\mathrm{i}kx}\mathrm{d}k \tag{2.20}$$

we get $A = 1/\sqrt{2\pi\hbar}$. Therefore

$$\phi_p(x) = \frac{\mathrm{e}^{\mathrm{i}px/\hbar}}{\sqrt{2\pi\hbar}} \ . \tag{2.21}$$

According to (2.16), a normalized wavefunction $\Psi(x, t)$ can be written as

$$\Psi(x, t) = \int_{-\infty}^{+\infty} \tilde{\Psi}(p, t)\frac{\mathrm{e}^{\mathrm{i}px/\hbar}}{\sqrt{2\pi\hbar}}\mathrm{d}p \tag{2.22}$$

and $\left|\tilde{\Psi}(p, t)\right|^2 \mathrm{d}p$ is the probability of finding the momentum in the interval $[p,\ p+\mathrm{d}p]$ at time t. So, $\tilde{\Psi}(p, t)$ corresponds to the wavefunction in the momentum representation. Note that we have as well

$$\tilde{\Psi}(p, t) = \int_{-\infty}^{+\infty} \Psi(q, t)\frac{\mathrm{e}^{-\mathrm{i}px/\hbar}}{\sqrt{2\pi\hbar}}\mathrm{d}x \ . \tag{2.23}$$

Moreover from Eq. (2.16):

$$\int_{-\infty}^{+\infty} |\Psi(x, t)|^2\,\mathrm{d}x = \int_{-\infty}^{+\infty} \left|\tilde{\Psi}(p, t)\right|^2 \mathrm{d}p \tag{2.24}$$

which is consistent with the fact the norm is conserved by a Fourier transform.

2.1.2 Stationary States

The eigenvalue equation for the Hamiltonian operator:

$$\hat{H}\psi_k = E_k\psi_k \tag{2.25}$$

is called time-independent Schrödinger equation, and the corresponding eigenvectors are the stationary states. We assume here that $\hat{H}$ is not directly dependent on time (otherwise, the concept of stationary state would be meaningless). In that case the TDSE is formally solved by $\Psi(t) = \hat{U}(t_0, t)\Psi(t_0)$, where

$$\hat{U}(t_0, t) = \mathrm{e}^{-\mathrm{i}(t-t_0)\hat{H}/\hbar} \tag{2.26}$$

is the time evolution operator for the finite time interval $t - t_0$. We stress here that the above equation is only valid if $\hat{H}$ is time independent. It is clear from Eq. (2.1) that the stationary states play a very important role. If the system considered, at a given time t_0, is found on ψ_k, so that $\Psi(t_0) = \psi_k$, we have

$$\Psi(t) = \mathrm{e}^{-\mathrm{i}E_k(t-t_0)/\hbar}\psi_k \tag{2.27}$$

as it may be readily verified by using the time evolution operator or by direct substitution in the TDSE. Therefore, the time evolution of ψ_k is just a time-dependent phase factor: when the system is in a stationary state, the probability density $|\Psi|^2$ and the other measurable quantities are constant in time. Moreover, the TDSE with the initial condition $\Psi(t = 0) \equiv \Psi(0)$ is solved by

$$\Psi(t) = \sum_k \langle\psi_k\,|\Psi(0)\rangle\,\mathrm{e}^{-\mathrm{i}E_k t/\hbar}\psi_k \tag{2.28}$$

so that the knowledge of the stationary states allows to easily obtain the time evolution of the system.

Using Eq. (2.28) we see that the mean value of energy is conserved, i.e., constant in time:

$$\begin{aligned}\left\langle\Psi\left|\hat{H}\right|\Psi\right\rangle &= \sum_{k,l}\langle\psi_k\,|\Psi(0)\rangle^*\,\langle\psi_l\,|\Psi(0)\rangle\,\mathrm{e}^{-\mathrm{i}(E_l-E_k)t/\hbar}\left\langle\psi_k\left|\hat{H}\right|\psi_l\right\rangle \\ &= \sum_k |\langle\psi_k\,|\Psi(0)\rangle|^2\,E_k\end{aligned} \tag{2.29}$$

where we have exploited Eq. (2.25) and the orthonormality of the stationary states. Moreover, the probability of measuring energy E_k, which is $|\langle\psi_k\,|\Psi(0)\rangle|^2$, is also invariant in time. This means the distribution of energy values obtained by a large number of measurements on a system always prepared in the same state at time $t = 0$ is independent on the elapsed time.

By the same argument, a physical observable is conserved if its associated operator $\hat{O}$ is not directly dependent on time and has a common set of eigenvectors with $\hat{H}$, which corresponds to say that $[\hat{H}, \hat{O}] = 0$. Therefore, an observable which commutes with the Hamiltonian is a constant of motion, otherwise its mean value evolves as

$$\left\langle \Psi \left| \hat{O} \right| \Psi \right\rangle = \sum_{k,l} \langle \psi_k \, | \Psi(0) \rangle^* \, \langle \psi_l \, | \Psi(0) \rangle \, \mathrm{e}^{-\mathrm{i}(E_l - E_k)t/\hbar} \left\langle \psi_k \left| \hat{O} \right| \psi_l \right\rangle . \tag{2.30}$$

In the general case in which the Hamiltonian has both a discrete and a continuous spectra, Eq. (2.28) generalizes to

$$\Psi(t) = \sum_k \langle \psi_k \, | \Psi(0) \rangle \, \mathrm{e}^{-\mathrm{i}E_k t/\hbar} \psi_k + \int \langle \psi_E \, | \Psi(0) \rangle \, \mathrm{e}^{-\mathrm{i}Et/\hbar} \psi_E \, \mathrm{d}E \tag{2.31}$$

where we have assumed the normalization condition $\langle \psi_E \, | \psi_{E'} \rangle = \delta(E - E')$ (see Appendix C).

2.2 Molecular Dynamics and the Separation of Variables

In the previous section we have seen that the TDSE is easily solved if the eigenstates of the Hamiltonian are known. In this sense, the complete solution of the eigenvalue Eq. (2.25) allows to determine in full the dynamic behavior of a molecular system. Let us consider a molecule with N_n nuclei and N_e electrons. The molecular Hamiltonian is

$$\hat{H}_{mol} = \hat{T}_n + \hat{T}_e + V_{el} + \hat{V}_s \tag{2.32}$$

$$\hat{T}_n = -\sum_{\alpha}^{N_n} \frac{\hbar^2}{2M_\alpha} \nabla_\alpha^2 \qquad \hat{T}_e = -\frac{\hbar^2}{2m_e} \sum_{i}^{N_e} \nabla_i^2 \tag{2.33}$$

where index α runs on nuclei and i on electrons, and M_α and m_e are nuclear and electronic masses, respectively. $\hat{T}_n$ and $\hat{T}_e$ constitute the nuclear and electronic kinetic energy, while $V_{el} + \hat{V}_s$ represents the electromagnetic interaction among the particles. In particular, the multiplicative operator V_{el} is the electrostatic interaction

$$V_{el} = \frac{e^2}{4\pi\varepsilon_0} \left[\sum_{i<j}^{N_e} \frac{1}{|\mathbf{r}_i - \mathbf{r}_j|} - \sum_{i}^{N_e} \sum_{\alpha}^{N_n} \frac{Z_\alpha}{|\mathbf{r}_i - \mathbf{R}_\alpha|} + \sum_{\alpha<\beta}^{N_n} \frac{Z_\alpha Z_\beta}{|\mathbf{R}_\alpha - \mathbf{R}_\beta|} \right] \tag{2.34}$$

where Z_α are the atomic numbers and $-e$ is the electronic charge. The operator $\hat{V}_s$ represents smaller interaction terms, depending on the spins of electrons and nuclei, some of which are important in photochemistry, as it will be discussed in Sect. 2.4.

However, neglecting $\hat{V}_s$ one is left with the electrostatic Hamiltonian

$$\hat{H}_{mol,SF} = \hat{T}_n + \hat{T}_e + V_{el} \tag{2.35}$$

where the subscript SF stands for "spin free." Even with this simplification, to solve the eigenvalue equation for the molecular Hamiltonian represents a formidable task, which may be undertaken as such only for a very small number of particles. It is therefore necessary to introduce some simplifications, which are based on the concept of separation of variables. As we shall see in this chapter, this concept is particularly important because of the physical representation of a molecular system and of its dynamics that it provides.

2.2.1 Independent Variables

We consider a Hamiltonian operator which is dependent on two groups of variables $\hat{H}(\mathbf{x}, \mathbf{y})$. If we have $\hat{H}(\mathbf{x}, \mathbf{y}) = \hat{H}_A(\mathbf{x}) + \hat{H}_B(\mathbf{y})$, the variables $\mathbf{x}$ and $\mathbf{y}$ are separable: the probability density to find the system in $\mathbf{x}$ is independent on $\mathbf{y}$ and vice versa. In fact, if $\psi_{A,i}$ are the eigenstates of $\hat{H}_A$, so that $\hat{H}_A(\mathbf{x})\psi_{A,i}(\mathbf{x}) = E_{A,i}\psi_{A,i}(\mathbf{x})$, and similarly for $\hat{H}_B(\mathbf{y})$, the stationary states ψ_{ij} are given by the products $\psi_{A,i}\psi_{B,j}$

$$\begin{aligned} \hat{H}(\mathbf{x}, \mathbf{y})\psi_{ij}(\mathbf{x}, \mathbf{y}) &= (\hat{H}_A(\mathbf{x}) + \hat{H}_B(\mathbf{y}))\psi_{A,i}(\mathbf{x})\psi_{B,j}(\mathbf{y}) \\ &= (E_{A,i} + E_{B,j})\psi_{ij}(\mathbf{x}, \mathbf{y}) \ . \end{aligned} \tag{2.36}$$

In this way, in the stationary state ψ_{ij} the probability density for finding the system in $\mathbf{x}$, $\mathbf{y}$ is the product of the probabilities for $\mathbf{x}$ and $\mathbf{y}$

$$\left|\psi_{ij}(\mathbf{x}, \mathbf{y})\right|^2 = \left|\psi_{A,i}(\mathbf{x})\right|^2 \left|\psi_{B,j}(\mathbf{y})\right|^2 \tag{2.37}$$

which confirms that the two events are mutually independent.

The same is true for a time-dependent state, if the wavefunction at a given time $t = 0$ is the product of two factors, one dependent on $\mathbf{x}$ and the other on $\mathbf{y}$:

$$\begin{aligned} \Psi(\mathbf{x}, \mathbf{y}, 0) &= \Psi_A(\mathbf{x})\Psi_B(\mathbf{y}) \\ &= \left[\sum_i A_i \psi_{A,i}(\mathbf{x})\right]\left[\sum_j B_j \psi_{B,j}(\mathbf{y})\right] \end{aligned} \tag{2.38}$$

where $X_i = \langle \psi_{X,i} | \Psi_X \rangle$, with $X = A, \ B$. By applying the time evolution operator (2.26) we see that the separation of the variables is preserved in time

$$\Psi(\mathbf{x},\mathbf{y},t)=\left[\sum_i A_i\psi_{A,i}(\mathbf{x})\mathrm{e}^{-\mathrm{i}E_{A,i}t/\hbar}\right]\left[\sum_j B_j\psi_{B,j}(\mathbf{y})\mathrm{e}^{-\mathrm{i}E_{B,j}t/\hbar}\right]. \tag{2.39}$$

Note that, if $\mathbf{x}$ and $\mathbf{y}$ are not separable, it is always possible to write $\hat{H}(\mathbf{x},\mathbf{y}) = \hat{H}_A(\mathbf{x})+\hat{H}_B(\mathbf{y})+\hat{H}_{AB}(\mathbf{x},\mathbf{y})$, and since the eigenvectors of $\hat{H}_A$ and $\hat{H}_B$ have anyway to represent complete sets we may write

$$\Psi(\mathbf{x},\mathbf{y},0)=\sum_{ij} C_{ij}\psi_{A,i}(\mathbf{x})\psi_{B,j}(\mathbf{y}) \tag{2.40}$$

where $C_{ij} = \langle\psi_{A,i}\psi_{B,j}|\Psi\rangle$. To put the above equation in the form of (2.38) one would have to evaluate the coefficients A_i and B_j in such a way that $A_iB_j = C_{ij}$. But that system has, in general, no solution (more equations than unknowns).

As a simple example of separation of variables we may consider two molecules, A and B, very far from each other so that they do not interact. Then, the total Hamiltonian is just the sum of the molecular Hamiltonians of A and B. The wavefunctions are products as in Eq. (2.36) or (2.39): molecule A behaves in a way that is completely independent to what happens to B and vice versa. Moreover, their energies are separately conserved. However, if A and B get closer, their mutual interaction is no longer negligible, so the time-dependent wavefunction is not in the form of Eq. (2.39). Nevertheless, if the coupling between A and B is small, it may be treated as a perturbation, taking the products $\psi_{A,i}(\mathbf{x})\psi_{B,j}(\mathbf{y})$ as zero-order stationary states. If the system, at time $t = 0$, is found in one of these zero-order states, it will evolve in time, populating the other states. This means that energy can be exchanged between A and B: an energy transfer between systems that are approximately independent, but coupled by a small perturbation, is typically governed by the Fermi golden rule (see Sect. 3.11 and Chap. 6).

2.2.2 Separation of Translation and Rotation

The state of an isolated molecule does not change if the system as a whole (or, equivalently, the fixed reference frame) is translated or rotated. In other words, the molecular Hamiltonian is invariant with respect to rotations and translations so that it commutes with the respective operators, which are represented by the total linear and angular momentum $\hat{\mathbf{P}}$ and $\hat{\mathbf{J}}$ (generators of infinitesimal translations and rotations, respectively). As a consequence, $\mathbf{P}$ and $\mathbf{J}$ are conserved quantities, as much as in classical mechanics (for the relationship between infinitesimal transformations and constants of motion, see for instance, Merzbacher [1]).

The translational invariance, which implies the conservation of the total momentum, leads to the separation of the center of mass coordinates. To this aim, a transformation of the Cartesian coordinates of electrons and nuclei has to be done. As such

a transformation does not mix the different Cartesian components x, y, and z among them, we will show it for x only. In particular, we consider a generic system of N particles with coordinates x_a and masses m_a. We define, in matrix notation

$$\begin{bmatrix} X_{CM} \\ x'_2 \\ \vdots \\ x'_N \end{bmatrix} = \mathbf{A} \begin{bmatrix} x_1 \\ x_2 \\ \vdots \\ x_N \end{bmatrix} \tag{2.41}$$

with

$$\mathbf{A} = \left[\begin{array}{ccc} \frac{m_1}{M} & \frac{m_2}{M} \cdots & \frac{m_N}{M} \\ \hline & \mathbf{B} & \end{array}\right] . \tag{2.42}$$

Here X_{CM} is the center of mass coordinate, $M = \sum_a m_a$ is the total mass, and $\mathbf{B}$ is a $(N-1) \times N$ matrix of constant coefficients. We want $x'_2, \ldots, x'_N$ to represent internal coordinates: they must be invariant in a translation. Imposing that the x'_a are unaltered when the x_a are changed to $x_a + \Delta_x$ we obtain the following relations for the rows of $\mathbf{B}$

$$\sum_{a=1}^{N} B_{ba} = 0 \quad \forall b = 1, \ldots, N-1 \tag{2.43}$$

The interaction terms V_{el} and $\hat{V}_s$ in the molecular Hamiltonian are functions of the relative positions of the particles. Hence, they do not depend on the center of mass coordinates. For the kinetic energy $\hat{T}$ we first observe that, using the chain rule for differentiation

$$\nabla_x = \mathbf{A}^t \nabla_{x'} \tag{2.44}$$

where ∇_x is a column vector collecting the terms $\partial/\partial x_a$ and

$$\nabla^t_{x'} = \left(\frac{\partial}{\partial X'_{CM}}, \frac{\partial}{\partial x'_2}, \ldots, \frac{\partial}{\partial x'_N} \right) . \tag{2.45}$$

The superscript t indicates transposition of vectors and matrices. Then

$$\hat{T} = -\frac{\hbar^2}{2} \nabla^t_x \mathbf{M}^{-1} \nabla_x = -\frac{\hbar^2}{2} \nabla^t_{x'} \mathbf{A} \mathbf{M}^{-1} \mathbf{A}^t \nabla_{x'} \tag{2.46}$$

where $\mathbf{M}$ is a diagonal matrix with $M_{aa} = m_a$. We note at this point that $(\mathbf{A}\mathbf{M}^{-1})_{1a} = 1/M$. Using this relation and Eq. (2.43) we obtain

$$(\mathbf{A}\mathbf{M}^{-1}\mathbf{A}^t)_{1b} = 0 \quad \forall b = 2, \ldots, N \tag{2.47}$$

so that the kinetic energy does not contain terms coupling X_{CM} with the other coordinates x'_b. In particular we have

$$\hat{T} = -\frac{\hbar^2}{2M}\frac{\partial^2}{\partial X_{CM}^2} - \frac{\hbar^2}{2}\sum_{b=2}^{N}\sum_{a=1}^{N}\frac{B_{b'a}^2}{m_a}\frac{\partial^2}{\partial x_b'^2} - \hbar^2\sum_{c=2}^{N-1}\sum_{b>c}^{N}\sum_{a=1}^{N}\frac{B_{b'a}B_{c'a}}{m_a}\frac{\partial}{\partial x'_b}\frac{\partial}{\partial x'_c} \tag{2.48}$$

where for the indices of the matrix $\mathbf{B}$ we used the shorthand $b' = b-1$ and $c' = c-1$. The matrix $\mathbf{B}$ may be determined (not univocally) requiring that

$$\sum_{a=1}^{N}\frac{B_{ba}B_{ca}}{m_a} = 0 \qquad \text{for} \quad b \neq c \tag{2.49}$$

so as to avoid cross terms in the kinetic energy (last term of Eq. (2.48)). The main problem in this way to proceed for a molecule is that such kind of transformation would mix the electronic and the nuclear coordinates, which is definitely not desirable, because it would complicate the expression of the potential energy. What is usually done instead is to mix only the nuclear coordinates among them in such a way that Eq. (2.49) is satisfied. The new electronic coordinates are then defined with respect to the center of mass of the nuclei alone. In this way the distinction between nuclei and electrons is preserved. Moreover, the kinetic energy does not contain nuclear/nuclear and nuclear/electronic cross terms, but just a small electronic/electronic cross term, usually neglected.

In any case, whatever the choice of $\mathbf{B}$ (giving for granted that condition (2.43) is fulfilled), the above procedure allows to separate the center of mass coordinates $\mathbf{R}_{CM}$ from the other (internal) ones. We have then

$$\hat{H}_{mol}(\mathbf{R}_{CM}, \mathbf{q}_{int}) = -\frac{\hbar^2}{2M}\left(\frac{\partial^2}{\partial X_{CM}^2} + \frac{\partial^2}{\partial Y_{CM}^2} + \frac{\partial^2}{\partial Z_{CM}^2}\right) + \hat{H}_{mol,int}(\mathbf{q}_{int}) \tag{2.50}$$

where $\mathbf{q}_{int}$ collectively labels the $3(N_n + N_e - 1)$ internal coordinates. A stationary state ψ may therefore be written as a product

$$\psi = \frac{e^{i\mathbf{P}\cdot\mathbf{R}_{CM}/\hbar}}{(2\pi\hbar)^{3/2}}\,\psi_{int}(\mathbf{q}_{int}) \tag{2.51}$$

where $\hat{H}_{mol,int}\psi_{int} = E_{int}\psi_{int}$, and the corresponding energy is given by the sum

$$E = \frac{P^2}{2M} + E_{int}\ . \tag{2.52}$$

The rotational invariance of the molecular Hamiltonian entails the conservation of total angular momentum. However, it is not possible to separate exactly the rotational motion. Let us consider a Cartesian reference system centered in the center of mass

of the molecule. To separate the rotational motion one has first to define a vector $\boldsymbol{\omega}$ representing the angular velocity of rotation of the whole molecule, which plays the same role as $\dot{\mathbf{R}}_{CM}$ for translations, and then to set up a reference frame rotating at angular velocity $\boldsymbol{\omega}$. If the system is formed by only two particles, the vector $\boldsymbol{\omega}$ is easily defined, because in the reference frame centered in the center of mass, the two particles necessarily rotate at the same angular velocity $\boldsymbol{\omega} = \mathbf{J}/\mu r^2$, where μ is the reduced mass and r is the interparticle distance. Of course, in general we may always define $\boldsymbol{\omega}$ in such a way that $\mathbf{J} = \mathbf{I}\boldsymbol{\omega}$, where $\mathbf{I}$ is the inertia tensor. However, $\mathbf{I}$ is not known *a priori*: its form depends on the positions of all the particles constituting the molecular system. Therefore, apart from the simple case of a two-particle system, the rotational motion cannot be separated exactly. An approximate separation is however possible: we shall come back on this point in Sect. 2.5.

2.3 The Born–Oppenheimer Approximation and Its Breakdown: The Nonadiabatic Couplings

In a molecule, the interaction between electrons and nuclei is never negligible. In fact, at least in bound states it is the Hamiltonian term with the largest mean value in module. As a consequence, the complete separation of nuclear and electronic variables is not possible, not even approximately. However, the electron mass is at least three orders of magnitude smaller than the nuclear masses, so that the timescales for the respective motions are different (femtoseconds for nuclei and attoseconds for electrons). This entails a different kind of separation of variables. We start observing that a given eigenfunction $\psi(\mathbf{r}, \mathbf{R})$ of the molecular Hamiltonian can always be written in this way

$$\psi(\mathbf{r}, \mathbf{R}) = \varphi(\mathbf{r}; \mathbf{R})\chi(\mathbf{R}) \tag{2.53}$$

where $\mathbf{r}$ and $\mathbf{R}$ collect the electronic and nuclear Cartesian coordinates, respectively. For the sake of simplicity the dependence on spin, which does not play a relevant role in this context, is omitted. We also assume that ψ is normalized. In the above equation φ and χ are, respectively, electronic and nuclear wavefunctions. In fact, we want $|\chi(\mathbf{R})|^2$ to be the probability density to find the nuclei in $\mathbf{R}$, which can be obtained by integrating $|\psi(\mathbf{r}, \mathbf{R})|^2$ with respect to the electronic coordinates:

$$|\chi(\mathbf{R})|^2 = \int_{-\infty}^{+\infty} |\varphi(\mathbf{r}; \mathbf{R})\chi(\mathbf{R})|^2 \, \mathrm{d}r_1^3 \ldots \mathrm{d}r_{N_e}^3 \, . \tag{2.54}$$

This identity requires $\varphi(\mathbf{r}; \mathbf{R})$ to be normalized for any fixed set of nuclear coordinates:

$$\langle \varphi \, | \varphi \, \rangle_{\mathbf{r}} = 1 \qquad \forall \, \mathbf{R} \, . \tag{2.55}$$

Here and in the following, a subscript added to a bracket expression indicates the integration variables, when needed for clarity. Moreover, $|\varphi(\mathbf{r};\mathbf{R})|^2$ (which is given by the ratio $|\psi|^2 / |\chi|^2$) represents the probability density to find the electrons in $\mathbf{r}$, once the nuclei have been fixed in the positions $\mathbf{R}$: it is then a conditional probability. Note that $\varphi(\mathbf{r};\mathbf{R})$ is by no means a nuclear wavefunction, but of course it depends parametrically on the nuclear coordinates $\mathbf{R}$.

The Born–Oppenheimer (BO) approximation consists in assuming specific forms of the electronic and the nuclear wavefunctions, consistent with the above requirements (2.54) and (2.55). In particular, the electronic wavefunctions are defined as the eigenfunctions of the electronic Hamiltonian $\hat{H}_{el}$:

$$\hat{H}_{el} = \hat{H}_{mol} - \hat{T}_n = \hat{T}_e + V_{el} + \hat{V}_s \tag{2.56}$$

$$\hat{H}_{el}(\mathbf{r},\mathbf{R})\varphi_k(\mathbf{r};\mathbf{R}) = U_k(\mathbf{R})\varphi_k(\mathbf{r};\mathbf{R}) \tag{2.57}$$

where $U_k(\mathbf{R})$ is the electronic energy and k is the index enumerating the eigenstates. The energies and wavefunctions so defined are called "adiabatic." Since $\hat{H}_{el}$ is Hermitian, we can require $\langle \varphi_k | \varphi_l \rangle_{\mathbf{r}} = \delta_{kl}$. Given that the electronic motion is much faster than the nuclear one, it is assumed that the electronic energy U_k plays the role of potential energy surface for the nuclear motion. In particular, the nuclear wavefunctions belonging to the electronic potential energy surface (PES) $U_k(\mathbf{R})$ are determined as eigenfunctions of the nuclear Hamiltonian $\hat{H}_n^{(k)}$

$$\hat{H}_n^{(k)} = \hat{T}_n + U_k \tag{2.58}$$

$$\hat{H}_n^{(k)}(\mathbf{R})\chi_{kv}(\mathbf{R}) = E_{kv}\chi_{kv}(\mathbf{R}) \tag{2.59}$$

where v is the index enumerating the nuclear (vibrational) states and E_{kv} is the total energy. In the above, $\mathbf{R}$ represents the $3N_n$ Cartesian coordinates of the nuclei, or the $3N_n - 6$ internal coordinates, after separation of translations and rotations. In the latter case M_α have to be replaced by the relevant reduced masses in $\hat{T}_n$, and we assume anyway that the internal coordinates are fixed and orthogonal (i.e., they verify Eqs. (2.41) and (2.49)), so that $\hat{T}_n$ keeps the diagonal form of Eq. (2.33).

Within the BO approximation, a given eigenstate of the molecular Hamiltonian is equal to the "vibronic" product $\varphi_k(\mathbf{r};\mathbf{R})\chi_{kv}(\mathbf{R})$, and the corresponding energy is E_{kv} (see Eqs. (2.57) and (2.59)). To judge about the quality of the BO approximation, let us evaluate the matrix elements of $\hat{H}_{mol}$ between BO functions. We have

$$\begin{aligned}
\left\langle \varphi_l \chi_{lu} \left| \hat{H}_{mol} \right| \varphi_k \chi_{kv} \right\rangle &= \left\langle \chi_{lu} \left| \left\langle \varphi_l \left| \hat{T}_n + \hat{H}_{el} \right| \varphi_k \right\rangle_{\mathbf{r}} \right| \chi_{kv} \right\rangle_{\mathbf{R}} \\
&= \left\langle \chi_{lu} \left| \left\langle \varphi_l \left| \hat{T}_n \right| \varphi_k \right\rangle_{\mathbf{r}} + U_k \delta_{kl} \right| \chi_{kv} \right\rangle_{\mathbf{R}} \\
&= \left\langle \chi_{lu} \left| \hat{V}_{kl}^{BO} + (\hat{T}_n + U_k)\delta_{kl} \right| \chi_{kv} \right\rangle_{\mathbf{R}} \\
&= \left\langle \chi_{lu} \left| \hat{V}_{kl}^{BO} \right| \chi_{kv} \right\rangle_{\mathbf{R}} + E_{kv}\delta_{lk}\delta_{uv}
\end{aligned} \tag{2.60}$$

where we have exploited Eqs. (2.57) and (2.59). The form of the operators $\hat{V}_{kl}^{BO}$ can be obtained observing that, if both φ and χ depend on x:

$$\frac{\partial^2 \varphi\chi}{\partial x^2} = \frac{\partial^2 \varphi}{\partial x^2}\chi + 2\frac{\partial \varphi}{\partial x}\frac{\partial \chi}{\partial x} + \varphi\frac{\partial^2 \chi}{\partial x^2} \ . \tag{2.61}$$

We have therefore

$$\hat{V}_{kl}^{BO} = -\sum_{\alpha} \frac{\hbar^2}{2M_\alpha}\left[t_{kl}^{(\alpha)} + 2g_{kl}^{(\alpha)}\frac{\partial}{\partial R_\alpha}\right] \tag{2.62}$$

where

$$g_{kl}^{(\alpha)}(\mathbf{R}) = \left\langle \varphi_k \left| \frac{\partial}{\partial R_\alpha} \right| \varphi_l \right\rangle \qquad t_{kl}^{(\alpha)}(\mathbf{R}) = \left\langle \varphi_k \left| \frac{\partial^2}{\partial R_\alpha^2} \right| \varphi_l \right\rangle \tag{2.63}$$

are the α components of the nonadiabatic coupling vectors $\mathbf{g}_{kl}$ and $\mathbf{t}_{kl}$. If the nonadiabatic couplings are small, the off-diagonal terms of $\hat{H}_{mol}$ in the basis represented by the BO functions $\varphi_k\chi_{kv}$ will also be small (see Eq. (2.60)), and the products $\varphi_k\chi_{kv}$ will be good approximations of stationary states. In that case, from the point of view of the time evolution, if the molecular system is found at a given time on the electronic state φ_k, it will stay on φ_k, and the time evolution of the nuclei will be ruled by the potential energy surface $U_k(\mathbf{R})$.

2.3.1 Properties of Nonadiabatic Couplings

We start noting that the matrix of nonadiabatic couplings $\mathbf{g}^{(\alpha)}$ is anti-Hermitian. We have in fact:

$$\mathbf{g}_{kl} + \mathbf{g}_{lk}^{*} = \langle \varphi_k | \nabla_{\mathbf{R}} \varphi_l \rangle + \langle \nabla_{\mathbf{R}} \varphi_k | \varphi_l \rangle = \nabla_{\mathbf{R}} \langle \varphi_k | \varphi_l \rangle = 0. \tag{2.64}$$

If spin terms are neglected, the electronic Hamiltonian is real and its wavefunctions can always be chosen as real. Then, $\mathbf{g}_{kl}$ is antisymmetric and $\mathbf{g}_{kk} = 0$.

The term $\mathbf{t}_{kl}$ containing the second derivatives is, in general, neither symmetric nor antisymmetric; its diagonal elements $\mathbf{t}_{kk}$ merely represent a modification of the adiabatic energies U_k. In particular, by replacing U_k with

$$U_k' = U_k - \sum_{\alpha} \frac{\hbar^2}{2M_\alpha} t_{kk}^{(\alpha)} \tag{2.65}$$

in the nuclear Hamiltonian $\hat{H}_n^{(k)}$, one has $\hat{V}_{kk}^{BO} = 0$, at least for real electronic functions. Therefore, the BO interaction only couples vibronic wavefunctions $\varphi_k\chi_{kv}$ and $\varphi_l\chi_{lu}$ belonging to different electronic states ($k \neq l$). By deriving $g_{kl}^{(\alpha)}$ with

respect to R_α we get a relation involving the second derivative coupling

$$t_{kl}^{(\alpha)} = \frac{\partial g_{kl}^{(\alpha)}}{\partial R_\alpha} - \left\langle \frac{\partial \varphi_k}{\partial R_\alpha} \middle| \frac{\partial \varphi_l}{\partial R_\alpha} \right\rangle \tag{2.66}$$

which can be recast in the following form

$$t_{kl}^{(\alpha)} = \frac{\partial g_{kl}^{(\alpha)}}{\partial R_\alpha} + \sum_m g_{km}^{(\alpha)} g_{ml}^{(\alpha)} \tag{2.67}$$

where the index m runs over a complete set of adiabatic states. In a region where the adiabatic states φ_k depend smoothly on $\mathbf{R}$, both $\mathbf{g}_{kl}$ and a fortiori $\mathbf{t}_{kl}$ are expected to be small.

By deriving both members of Eq. (2.57) with respect to the nuclear coordinates one has

$$\nabla_{\mathbf{R}}(\hat{H}_{el}) \, |\varphi_l\rangle + \hat{H}_{el} \nabla_{\mathbf{R}} \, |\varphi_l\rangle = |\varphi_l\rangle \, \nabla_{\mathbf{R}} U_l + U_l \nabla_{\mathbf{R}} \, |\varphi_l\rangle \tag{2.68}$$

By premultiplying by $\langle \varphi_l |$ we get Hellmann–Feynman's theorem for the energy gradient:

$$\nabla_{\mathbf{R}} U_l = \left\langle \varphi_l \middle| \nabla_{\mathbf{R}} \hat{H}_{el} \middle| \varphi_l \right\rangle \tag{2.69}$$

By premultiplying by $\langle \varphi_k |$ (with $k \neq l$) we get a useful Hellmann–Feynman like expression for the nonadiabatic couplings

$$\mathbf{g}_{kl} = \frac{\left\langle \varphi_k \middle| \nabla_{\mathbf{R}} \hat{H}_{el} \middle| \varphi_l \right\rangle}{U_l - U_k} \qquad (k \neq l) \; . \tag{2.70}$$

According to the above expression, for nuclear geometries where the energy difference $U_l - U_k$ is large, $\mathbf{g}_{kl}$ is expected to be small. Conversely, in regions where $U_l - U_k \to 0$ the coupling $\mathbf{g}_{kl}$ diverges and the BO approximation is not reliable.

2.3.2 *Validity of the BO Approximation*

According to Eqs. (2.60) and (2.65), we can rewrite the molecular Hamiltonian in this form

$$\hat{H}_{mol} = \sum_k |\varphi_k\rangle \, (\hat{T}_n + U'_k) \, \langle \varphi_k | + \sum_k \sum_{l \neq k} |\varphi_k\rangle \, \hat{V}_{kl}^{BO} \, \langle \varphi_l | \tag{2.71}$$

$$= \hat{H}^{BO} + \hat{V}^{BO} \tag{2.72}$$

which is appropriate for real φ_k (otherwise one has to take into account that $\mathbf{g}_{kk} \neq 0$). The above partition is suited for a perturbative development (see for instance, Merzbacher [1] or Atkins and Friedman [3]): $\hat{H}_{BO}$ is the zero-order Hamiltonian, and its eigenvectors and eigenvalues are the BO vibronic states $\varphi_k \chi_{kv}$ and energies E_{kv}. The first-order correction to the energies is zero, as $\hat{V}_{kk}^{BO} = 0$. If the potential energy U_k has not been corrected according to Eq. (2.65), the first-order correction is just

$$E_{kv}^{(1)} = -\sum_{\alpha} \frac{\hbar^2}{2M_\alpha} \left\langle \chi_{kv} \left| t_{kk}^{(\alpha)} \right| \chi_{kv} \right\rangle . \tag{2.73}$$

The second-order correction to E_{kv} and the first-order correction to $\psi_{kv}^{(0)} = \varphi_k \chi_{kv}$ are given by

$$E_{kv}^{(2)} = -\sum_{l \neq k} \sum_{u} \frac{\left| V_{kv,lu}^{BO} \right|^2}{E_{lu} - E_{kv}} \tag{2.74}$$

$$\psi_{kv}^{(1)} = -\sum_{l \neq k} \sum_{u} \frac{V_{lu,kv}^{BO}}{E_{lu} - E_{kv}} \varphi_l \chi_{lu} . \tag{2.75}$$

Therefore, the BO approximation is valid for a given vibronic state $\varphi_k \chi_{kv}$ if the condition

$$\left| V_{kv,lu}^{BO} \right| \ll |E_{kv} - E_{lu}| \tag{2.76}$$

is verified for all l, u (with $l \neq k$).

The vibronic states $\varphi_0 \chi_{0v}$, where φ_0 is the ground electronic state, are coupled through the matrix elements $V_{0v,lu}^{BO}$ only with excited electronic states $l \geq 1$. Now, in most closed shell molecules, at geometries close to the ground state minimum, the energy difference $U_l - U_0$ is quite large (usually of the order of 0.1 a.u.). Large energy differences, as suggested by Eq. (2.70), correspond to small nonadiabatic couplings, so the BO approximation is well justified for the ground state. More in detail, we start by noting that the order of magnitude of the electronic energy differences is determined by the strong Coulomb potentials that bind the electrons to the nuclei. On the contrary, the PESs that bind the atoms together in the molecule have relatively shallow minima, so the much larger nuclear masses give place to vibrational levels with energy separations $\hbar\omega$ one or two orders of magnitude smaller than the electronic ones (remember that a vibrational frequency is $\omega = (k/\mu)^{1/2}$, where k is the force constant and μ the reduced mass). As we have seen, the nonadiabatic couplings derive from the action of the nuclear kinetic energy operator on the electronic wavefunctions. In comparison with the kinetic energy of a vibration (at most ≈ 0.01 a.u. for the lowest vibrational states) the nonadiabatic coupling matrix elements are much smaller. This is because the derivatives with respect to nuclear coordinates of the electronic wavefunctions are much smaller than those of the vibrational ones. In fact, the former do not change drastically for the displacement of, say, 1 bohr, while

the latter may have several nodes, maxima and minima within the same interval (even the $v = 0$ wavefunction normally goes from almost zero to the maximum value and back to zero in a fraction of bohr). Then, the denominators of Eqs. (2.74) and (2.75) are much larger than the nonadiabatic couplings, if we consider low-lying vibrational levels. For larger values of the vibrational quantum number v, the energy difference $E_{lu} - E_{0v}$ decreases and χ_{0v} explores a larger portion of the nuclear configurational space, making more likely to reach regions where $U_l - U_0$ is small. In these conditions, it may be important to take into account the nonadiabatic couplings. This amounts to say that for highly distorted molecular geometries (e.g., at a transition state) the BO approximation is less valid than at the equilibrium geometry.

The excited electronic states behave in a very different way. In fact, for any vibronic state $\varphi_k \chi_{kv}$ belonging to an electronically excited state φ_k ($k \geq 1$) we may find some state $\varphi_l \chi_{lu}$ with $U_l < U_k$, such that $E_{lu} - E_{kv} \simeq 0$. Normally, χ_{lu} will be a highly excited vibrational state showing many oscillations (see Fig. 2.1), so that the matrix element $V^{BO}_{kv,lu}$ will be very small, because positive and negative contributions to the integral cancel out. Nevertheless, the two vibronic states are almost degenerate, giving rise to a potentially large perturbative correction, i.e., a non-negligible mixing of $\varphi_k \chi_{kv}$ with $\varphi_l \chi_{lu}$. Therefore, if the molecular system is prepared in the state $\varphi_k \chi_{kv}$, it will evolve in time, populating nonradiatively the vibronic states close in energy, which amounts to convert electronic energy into vibrational energy (see also Fig. 1.1). Note that when the energy difference $U_k - U_l$ increases the nonadiabatic coupling $V^{BO}_{kv,lu}$ becomes smaller so that the larger is the amount of electronic energy which has to be transformed in nuclear kinetic energy, the less likely is the process. If the χ_{lv} belong to the continuous spectrum of dissociative states of U_l, the radiationless transition from $\varphi_k \chi_{kv}$ to these states can lead to the dissociation of the molecule (a process called electronic predissociation, see Sect. 3.10).

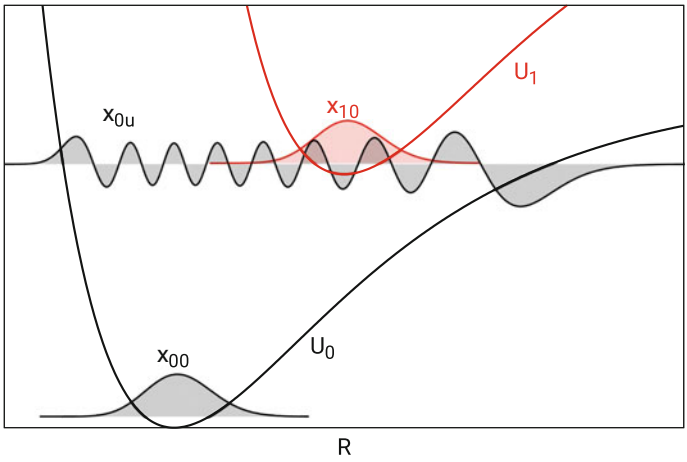

Fig. 2.1 Interaction of vibronic states in a diatomic molecule

2.3.3 Time Evolution in the BO Framework

A time-dependent molecular wavefunction can be expressed using the Born–Huang expansion

$$\Psi(\mathbf{R}, \mathbf{r}, t) = \sum_k \Theta_k(\mathbf{R}, t)\varphi_k(\mathbf{r}; \mathbf{R}) \tag{2.77}$$

where the sum is extended to all the electronic states, and $\Theta_k(\mathbf{R}, t)$ is a *nuclear wavepacket* belonging to the electronic state φ_k. The total wavefunction Ψ and the φ_k are normalized, so that $P_k(t) = \int |\Theta_k(\mathbf{R}, t)|^2 \, \mathrm{d}\mathbf{R}$ represents the probability (or population) of the electronic state φ_k at time t. Note that $\sum_k P_k(t) = 1$, irrespective of time. The equation of motion for the nuclear wavepackets is found by inserting the Born–Huang expansion (2.77) in the TDSE. Considering real functions φ_k we get

$$\mathrm{i}\hbar \frac{\mathrm{d}\Theta_k}{\mathrm{d}t} = \left(\hat{T}_n + U'_k\right)\Theta_k + \sum_{l \neq k} \hat{V}_{kl}^{BO}\Theta_l \ . \tag{2.78}$$

The first term of the RHS of the above equation leads to the concept of nuclear wavefunctions $\Theta_k(\mathbf{R}, t)$ evolving on potential energy surfaces $U'_k(\mathbf{R})$. The second term describes population transfer to nuclear wavepackets belonging to different electronic states, i.e., nonradiative transitions. This is the physical representation of the dynamics of a molecular system to which we make reference throughout this book.

The quantum wavepacket view of the molecular dynamics has a classical counterpart in which the nuclear positions and momenta are well defined and change in time according to Newton's equations. The potential energy surfaces of the electronic states determine the forces to which the nuclei are subjected. We shall see in Chap. 4 how this classical view of the nuclear motion is justified, but we anticipate it here because chemistry and photochemistry are most frequently discussed in a language that refers to classical physics. It is worth here to anticipate the Franck–Condon principle (see Chap. 3), asserting that the electronic excitation does not affect instantaneously the nuclear dynamics, which changes only afterward under the influence of a different potential energy surface. In the quantum language, this means that, under certain conditions, the wavepacket is promoted from the initial electronic state to the final one without change. In the classical language, the nuclear positions and momenta remain the same upon excitation and, if we take as starting geometry the equilibrium geometry of the ground electronic state, the molecules end up in a corresponding point of the excited PES called the Franck–Condon point. In both cases, *after* excitation the nuclear dynamics runs on the new PES and therefore can differ radically from what it was in the initial state.

2.4 The Electrostatic Approximation: Spin and Magnetic Couplings

In the electrostatic approximation we neglect the spin terms in the electronic Hamiltonian, which is written as (see Eq. (2.35))

$$\hat{H}_{el,SF} = \hat{T}_e + V_{el} \ . \tag{2.79}$$

The total electronic spin $\hat{\mathbf{S}} = \sum_i^{N_e} \hat{\mathbf{s}}_i$ commutes with $\hat{H}_{el,SF}$ so that, in the electrostatic approximation, the electronic wavefunctions $\varphi_k(\mathbf{x}; \mathbf{R})$ can be chosen as eigenstates of $\hat{S}^2$ and $\hat{S}_z$

$$\hat{S}^2 \varphi_k(\mathbf{x}; \mathbf{R}) = \hbar^2 S_k(S_k + 1)\varphi_k(\mathbf{x}; \mathbf{R}) \tag{2.80}$$

$$\hat{S}_z \varphi_k(\mathbf{x}; \mathbf{R}) = \hbar M_{S_k} \varphi_k(\mathbf{x}; \mathbf{R}) \tag{2.81}$$

where $\mathbf{x}$ collects the spin and space electronic degrees of freedom. For a given value of S_k, the projection M_{S_k} of the spin on a quantization axis has $2S_k + 1$ different values, which correspond to the same energy.

To be more specific, the electronic wavefunctions φ_k are usually built from one-electron states, called *spin-orbitals*, written as the product of a space part (the *orbital*) times a spin part

$$\theta(\mathbf{r}, s) = \phi(\mathbf{r})\sigma(s) \ . \tag{2.82}$$

The one-electron spin function σ can be chosen to be α or β, with

$$\hat{s}_z \alpha = \frac{\hbar}{2}\alpha \tag{2.83}$$

$$\hat{s}_z \beta = -\frac{\hbar}{2}\beta \ . \tag{2.84}$$

We assume here that the orbitals are orthonormalized: $\langle \phi_i \, | \phi_j \rangle = \delta_{ij}$. In obeyance with the antisymmetry of the electronic wavefunction with respect to the exchange of two electrons, we expand φ_k as a combination of antisymmetrized products of spin-orbitals, in which each spin-orbital can accommodate only one electron (the Pauli exclusion principle). A single antisymmetrized product of n spin-orbitals, including the normalization factor, can be written as

$$\theta_{i_1} \wedge \theta_{i_2} \wedge \cdots \wedge \theta_{i_n} = \frac{1}{\sqrt{n!}} \begin{vmatrix} \theta_{i_1}(\mathbf{x}_1) & \theta_{i_1}(\mathbf{x}_2) & \cdots & \theta_{i_1}(\mathbf{x}_n) \\ \theta_{i_2}(\mathbf{x}_1) & \theta_{i_2}(\mathbf{x}_2) & \cdots & \theta_{i_2}(\mathbf{x}_n) \\ \vdots & \vdots & & \vdots \\ \theta_{i_n}(\mathbf{x}_1) & \theta_{i_n}(\mathbf{x}_2) & \cdots & \theta_{i_n}(\mathbf{x}_n) \end{vmatrix} \tag{2.85}$$

and it is called a *Slater determinant*. The spin-orbitals must be different, otherwise the Slater determinant vanishes (see Levine [4] or McWeeny [7] for a deeper discussion of the representation of electronic wavefunctions).

2.4.1 Singlet and Triplet Wavefunctions

A couple of *paired* electrons in the same orbital ϕ_a is necessarily described by a wavefunction of this kind

$$\phi_a(\mathbf{r}_1)\phi_a(\mathbf{r}_2)\left[\frac{\alpha(s_1)\beta(s_2)-\beta(s_1)\alpha(s_2)}{\sqrt{2}}\right] \tag{2.86}$$

where the spin factor corresponds to a singlet state (i.e., $S = 0$ and, necessarily, $M_s = 0$). This can be shown making use of the fundamental commutation relations, valid for angular momentum operators

$$\left[\hat{S}_x, \hat{S}_y\right] = \mathrm{i}\hbar\hat{S}_z \ , \quad \left[\hat{S}_y, \hat{S}_z\right] = \mathrm{i}\hbar\hat{S}_x \ , \quad \left[\hat{S}_z, \hat{S}_x\right] = \mathrm{i}\hbar\hat{S}_y \ , \tag{2.87}$$

from which, defining

$$\hat{S}_\pm = \hat{S}_x \pm \mathrm{i}\hat{S}_y \tag{2.88}$$

one gets

$$\hat{S}^2 = \hat{S}_+\hat{S}_- + \hat{S}_z^2 - \hbar\hat{S}_z \ . \tag{2.89}$$

Here we use capital letters for the components of the n-particle spin operator: $\hat{S}_\lambda = \sum_{i=1}^{n}\hat{s}_{i,\lambda}$, with $\lambda = x, y, z, +$ or $-$. Each $\hat{s}_{i,\lambda}$ operates only on spin functions of the ith electron. $\hat{s}_+$ and $\hat{s}_-$ are the raising and lowering operators for spin, such that $\hat{s}_-\alpha = \beta$, $\hat{s}_+\alpha = 0$, $\hat{s}_-\beta = 0$ and $\hat{s}_+\beta = \alpha$ (this implies a consistent choice of phase factors between the α and β functions). We have then

$$\begin{aligned}\hat{S}^2\left[\alpha(s_1)\beta(s_2)-\beta(s_1)\alpha(s_2)\right] = \\ \hat{S}_+\hat{S}_-\left[\alpha(s_1)\beta(s_2)-\beta(s_1)\alpha(s_2)\right] = \\ \hat{S}_+\left[\beta(s_1)\beta(s_2)-\beta(s_1)\beta(s_2)\right] = 0 \ .\end{aligned} \tag{2.90}$$

From the point of view of the total spin, it does not matter how many paired couples one has, so that we can focus on the unpaired electrons only. Of course, with one unpaired electron we have a doublet: $S = 1/2$ and two choices for M_S, $\pm 1/2$. With two unpaired electrons we get a triplet and a singlet. The three components of the triplet are

$$\frac{\phi_a\phi_b - \phi_b\phi_a}{\sqrt{2}} \cdot \begin{cases} \alpha\alpha & S = 1,\ M_S = 1 \\ \dfrac{\alpha\beta + \beta\alpha}{\sqrt{2}} & S = 1,\ M_S = 0 \\ \beta\beta & S = 1,\ M_S = -1 \end{cases} \tag{2.91}$$

where we have used the convention that in a product of monoelectronic functions, the ordering of the terms corresponds with that of the particles (i.e., $\phi_a\phi_b \equiv \phi_a(\mathbf{r}_1)\phi_b(\mathbf{r}_2)$). The $M_S = 0$ component can be obtained by applying $\hat{S}_-$ to $\alpha\alpha$. Note that the triplet has a symmetric spin part and an antisymmetric space part. At variance, for the singlet we have an antisymmetric spin part (see (2.86)) and a symmetric space part

$$\frac{\phi_a\phi_b + \phi_b\phi_a}{\sqrt{2}} \frac{\alpha\beta - \beta\alpha}{\sqrt{2}} \qquad (S = 0) \tag{2.92}$$

This has important consequences on the energetics: the triplet wavefunction (2.91) goes to zero when $\mathbf{r}_1 \to \mathbf{r}_2$, while the singlet one, Eq. (2.92), does not. So, in a singlet state the electrons can get closer and the electron–electron repulsion is larger. Therefore, a singlet state is higher in energy than the corresponding triplet where the electrons occupy the same spin-orbitals. From the quantitative point of view, the energy difference between the two wavefunctions (2.92) and (2.91) is given by $2K_{\phi_a,\phi_b}$, where K_{ϕ_a,ϕ_b} is the exchange integral of the two singly occupied orbitals

$$K_{\phi_a,\phi_b} = \int \frac{\phi_a^*(\mathbf{r}_1)\phi_b^*(\mathbf{r}_2)\phi_b(\mathbf{r}_1)\phi_a(\mathbf{r}_2)}{|\mathbf{r}_1 - \mathbf{r}_2|} \mathrm{d}\mathbf{r}_1 \mathrm{d}\mathbf{r}_2 \tag{2.93}$$

in atomic units (see Appendix A).

If the ground-state wavefunction φ_{S_0} is approximated as in Eq. (2.86) and that of an excited singlet φ_{S_n} as in Eq. (2.92), the transition matrix elements of one-electron operators between the two states are very simple. For a general spinless one-electron operator $\hat{D} = \sum_i^{N_e} \hat{d}(\mathbf{r}_i)$ we have

$$\left\langle \varphi_{S_0} \middle| \hat{D} \middle| \varphi_{S_n} \right\rangle = \sqrt{2} \left\langle \phi_a \middle| \hat{d} \middle| \phi_b \right\rangle \tag{2.94}$$

independently of the presence of other doubly occupied orbitals in S_0 and S_n. Therefore, to evaluate the radiative transition probability between S_0 and S_1 (see Sect. 3.5) one just needs $\boldsymbol{\mu}_{\phi_a\phi_b}$. Because of the orthogonality of the spin factors between singlets and triplets, $\left\langle \varphi_{S_0} \middle| \hat{D} \middle| \varphi_{T_n} \right\rangle = 0$, no matter what level of approximation is used for the wavefunctions of the two states.

We could proceed considering more unpaired electrons (for a more systematic approach, see, e.g., de Graaf and Broer [8]). However, in most organic molecules the ground electronic state is well represented by a wavefunction in which each occupied orbital has two electrons (often called a closed shell) and the lowest lying excited states are singlets or triplets with no more than two unpaired electrons (see also Sect. 1.4). Therefore, the above discussion is sufficient to approach spin problems in many molecular systems.

2.4.2 Spin–Orbit Coupling

As we have seen, in the electrostatic approximation the molecular Hamiltonian does not depend on spin. Therefore, the components of an electronic spin multiplet, which share the same space parts (see e.g., (2.91)), are degenerate. More importantly, two electronic states φ_k and φ_l having different spin part do not interact (i.e., $\hat{V}_{kl}^{BO} = 0$) so that the time evolution of the corresponding nuclear wavepackets does not lead to any population transfer between Θ_k and Θ_l. It is therefore mandatory to include the small interaction terms dependent on electronic spin in the electronic Hamiltonian to account for radiative and nonradiative "spin-forbidden" processes (i.e., ISC and phosphorescence, see Fig. 1.1). The most important interaction in this respect is the spin–orbit (SO) coupling, which is considered in the present section.

An appraisal of the SO interaction can be obtained by the following argument of classical electromagnetism. With the spin of the electron comes a magnetic moment

$$\boldsymbol{\mu}_s = -g_e \frac{e}{2m_e} \mathbf{s} \tag{2.95}$$

where $g_e = 2.002319\ldots$ is a dimensionless factor (the g-factor) characteristic of the electron spin. Note that for the orbital angular momentum the g-factor is 1. The magnetic moment $\boldsymbol{\mu}_s$ interacts with the magnetic field experienced by the electron as it moves through the electric field $\mathbf{E}$ produced by a charged particle. Let us consider a nucleus with charge Ze at rest in the origin. In a reference frame centered on the electron, the nucleus moves with velocity $\mathbf{v}$ and gives rise to a magnetic field $\mathbf{B} = \mathbf{v} \times \mathbf{E}/c^2$, which interacts with the magnetic moment of the electron through the energy term $-\boldsymbol{\mu}_s \cdot \mathbf{B}$. The classical evaluation of the magnetic field $\mathbf{B}$ is, however, grossly inaccurate, the correct relativistic expression being one half of the classical value, as first pointed out by Thomas in 1926. Reverting to the inertial reference frame centered on the nucleus, $\mathbf{v}$ changes its sign so that

$$\hat{h}_{SO} = -\boldsymbol{\mu}_s \cdot \mathbf{B} = -\boldsymbol{\mu}_s \cdot \frac{\mathbf{E} \times \mathbf{p}}{2m_e c^2} \tag{2.96}$$

$$= \frac{g_e Z e^2}{16\pi \varepsilon_0 m_e^2 c^2} \frac{\mathbf{s} \cdot \mathbf{l}}{r^3} \tag{2.97}$$

is the one-electron spin–orbit Hamiltonian ($\mathbf{l} = \mathbf{r} \times \mathbf{p}$). However, it is clear from the above that a correct account of the spin–orbit interaction would imply a full relativistic approach, which is far beyond the aim of this book (see, e.g., Greiner's textbooks [9, 10]). In the following, we will limit ourselves to show some of the most used spin–orbit Hamiltonians, giving just a brief comment about their derivation.

The relativistic quantum mechanical equation of motion for the free electron is the Dirac equation, where the wavefunction has four components, as it can describe an electron or a positron with spin $\pm 1/2$. In particular, positive energy solutions of the Dirac equation represent electrons, while negative energy solutions represent positrons. The four components of the wavefunction are coupled, nevertheless a simplification of the Dirac equation can be obtained by applying a transformation which reduces the coupling between electronic and positronic solutions, yielding a two-component one-electron Hamiltonian, from which the spin–orbit interaction can be extracted. However, such a transformation may be performed in many different ways, and correspondingly different forms of the SO interaction are obtained. In particular, three among the most well-known SO Hamiltonian are, for one electron in an external potential $V = -Z/r$ (using atomic units) [11]

$$\hat{h}_{SO}^{Pauli} = \frac{\alpha^2 Z}{2} \frac{\mathbf{s} \cdot \mathbf{l}}{r^3} \tag{2.98}$$

$$\hat{h}_{SO}^{DKH} = \alpha^2 Z Q \frac{\mathbf{s} \cdot \mathbf{l}}{r^3} Q \quad \text{where} \quad Q = \left(\frac{c^2}{c^2 + p^2 + c\sqrt{c^2 + p^2}} \right)^{1/2} \tag{2.99}$$

$$\hat{h}_{SO}^{ZORA} = 2\alpha^2 W (\nabla \mathrm{V} \times \mathbf{p}) \cdot \mathbf{s} = 2\alpha^2 Z W \frac{\mathbf{s} \cdot \mathbf{l}}{r^3} \quad \text{where} \quad W = \frac{c^4}{(2c^2 - V)^2} \tag{2.100}$$

Here α is the dimensionless *fine structure constant*, $\alpha = e/4\pi\varepsilon_0 \hbar c \simeq 1/137$. In the above equations one has $g_e = 2$. In fact, the departure of the electron g-factor from 2 is not accounted for by the Dirac equation. Note that the Pauli SO Hamiltonian of Eq. (2.98) corresponds to the one obtained in Eq. (2.97) by classical ad hoc arguments (apart from the different units). The Douglas–Kroll–Hess (DKH) and zero-order regular approximation (ZORA) Hamiltonians of Eqs. (2.99) and (2.100) are more involved with respect to the Pauli one, but present the advantage of being variationally stable (i.e., they are bounded from below).

The ZORA Hamiltonian [12] is mostly used in the framework of density functional theory (DFT). In its expression, the SO coupling is accounted by the one-electron Hamiltonian shown above (middle part of Eq. (2.100)), where V contains the nuclear attraction and the electron Coulomb and correlation-exchange potentials.

When the interaction among the particles in a molecular system is taken into account (which is not an easy task in relativistic quantum mechanics and therefore involves several approximations) one obtains for the Pauli and the DKH spin–orbit Hamiltonians [7, 13, 14], using again atomic units

$$\hat{H}_{SO}^{BP} = \frac{\alpha^2}{2}\left[\sum_{i,v} Z_v \frac{\mathbf{l}_{iv}}{r_{iv}^3}\cdot\mathbf{s}_i - \sum_{i\neq j}\frac{\mathbf{l}_{ij}}{r_{ij}^3}\cdot(\mathbf{s}_i + 2\mathbf{s}_j)\right] \tag{2.101}$$

$$\hat{H}_{SO}^{DKH} = 2\alpha^2\left[\sum_{i,v} A_i K_i Z_v \frac{\mathbf{l}_{iv}}{r_{iv}^3}\cdot\mathbf{s}_i K_i A_i - \sum_{i\neq j} A_i K_i A_j \frac{\mathbf{l}_{ij}}{r_{ij}^3}\cdot(\mathbf{s}_i + 2\mathbf{s}_j) A_j K_i A_i\right] \tag{2.102}$$

with

$$A_i = \left(\frac{E_i + c^2}{2E_i}\right)^{1/2} \qquad K_i = \frac{c^2}{E_i + c^2} \qquad E_i = \sqrt{p_i^2 c^2 + c^4} \tag{2.103}$$

where BP stands for Breit–Pauli. Here $\mathbf{r}_{iv} = \mathbf{r}_i - \mathbf{R}_v$, and $\mathbf{l}_{iv} = \mathbf{r}_{iv} \times \mathbf{p}_i$ represents the orbital angular moment of electron i around nucleus v. Similarly $\mathbf{r}_{ij} = \mathbf{r}_i - \mathbf{r}_j$, and $\mathbf{l}_{ij} = \mathbf{r}_{ij} \times \mathbf{p}_i$ is the angular moment of electron i around electron j. Therefore, in the above SO Hamiltonians, the first part of the second sum is the "spin–same orbit" interaction, and the second part "spin–other orbit."

Due to the presence of the $1/r^3$ term, the largest contribution in the SO interaction comes from the electrons that are close to the nuclei. For this reason, and also because of the dependence on the nuclear charge, the SO interaction increases with the atomic numbers of the nuclei: this is the so-called heavy atom effect. As a rough rule of thumb, with second-row atoms one may expect an order of magnitude of 10 cm^{-1} for the SO coupling, which increases by a factor of 10 if third-row atoms are present.

From the computational point of view, the BP and DKH Hamiltonians are quite expensive, in particular because of the presence of two-electron terms (second sum in Eqs. (2.101) and (2.102)). Therefore, they are often approximated with one-electron SO Hamiltonians in which the two-electron terms are neglected and the nuclear charges Z_v are replaced by empirically determined effective charges Z_v^{eff}. A more refined approach would consist in incorporating the effect of the two-electron terms with a mean-field approach. An effective one-electron SO Hamiltonian can be formally written in this way

$$\hat{H}_{SO}^{eff} = \mathbf{D}\cdot\mathbf{S} = \sum_i \mathbf{d}_i \cdot \mathbf{s}_i \tag{2.104}$$

where $\mathbf{D}$ is a spin-free one-electron operator. In the simple effective charge approximation $\mathbf{d}_i = \frac{1}{2}\alpha^2 \sum_v Z_v^{eff} r_{iv}^{-3}\mathbf{l}_i$, but more elaborated formulations have been proposed [14]. Note that $\mathbf{D}$ and $\mathbf{d}_i$ are imaginary and Hermitian (like the angular momentum operators $\mathbf{l}_i$), so their diagonal matrix elements with real wavefunctions are zero. Let us now evaluate the SO coupling between the triplet and the singlet states defined in Eqs. (2.91) and (2.92). Using the effective one-electron SO Hamiltonian $\hat{H}_{SO}^{eff}$ defined above we get

$$\left\langle S \left| \hat{H}_{SO}^{eff} \right| T^{(1)} \right\rangle = \frac{1}{2\sqrt{2}} \sum_{i=1}^{2} \langle \phi_a\phi_b + \phi_b\phi_a \left| \mathbf{d}_i \right| \phi_a\phi_b - \phi_b\phi_a \rangle \cdot \langle \alpha\beta - \beta\alpha \left| \mathbf{s}_i \right| \alpha\alpha \rangle$$
$$= \frac{1}{\sqrt{2}} \left(\langle \phi_b \left| \mathbf{d} \right| \phi_b \rangle - \langle \phi_a \left| \mathbf{d} \right| \phi_a \rangle \right) \cdot \langle \beta \left| \mathbf{s} \right| \alpha \rangle = 0 \tag{2.105}$$

$$\left\langle S \left| \hat{H}_{SO}^{eff} \right| T^{(-1)} \right\rangle = \frac{1}{2\sqrt{2}} \sum_{i=1}^{2} \langle \phi_a\phi_b + \phi_b\phi_a \left| \mathbf{d}_i \right| \phi_a\phi_b - \phi_b\phi_a \rangle \cdot \langle \alpha\beta - \beta\alpha \left| \mathbf{s}_i \right| \beta\beta \rangle$$
$$= \frac{1}{\sqrt{2}} \left(\langle \phi_a \left| \mathbf{d} \right| \phi_a \rangle - \langle \phi_b \left| \mathbf{d} \right| \phi_b \rangle \right) \cdot \langle \alpha \left| \mathbf{s} \right| \beta \rangle = 0 \tag{2.106}$$

$$\left\langle S \left| \hat{H}_{SO}^{eff} \right| T^{(0)} \right\rangle = \frac{1}{4} \sum_{i=1}^{2} \langle \phi_a\phi_b + \phi_b\phi_a \left| \mathbf{d}_i \right| \phi_a\phi_b - \phi_b\phi_a \rangle \cdot \langle \alpha\beta - \beta\alpha \left| \mathbf{s}_i \right| \alpha\beta + \beta\alpha \rangle$$
$$= \frac{\hbar}{2} \left(\left\langle \phi_a \left| \hat{d}_z \right| \phi_a \right\rangle - \left\langle \phi_b \left| \hat{d}_z \right| \phi_b \right\rangle \right) = 0 \tag{2.107}$$

where S labels the singlet state, and $T^{(m)}$ represents the component of the triplet state with $M_s = m$, and we exploited the fact that $\langle \phi \left| \mathbf{d} \right| \phi \rangle = \mathbf{0}$ for any real orbital ϕ. Therefore, very low SO coupling is expected between a singlet state and a triplet state sharing the same spatial configuration. This is a manifestation of the *El-Sayed rules*, of which we shall see examples in the next sections.

2.5 Vibrational and Rotational States

In the framework of the BO approximation, the nuclear Hamiltonian $\hat{H}_n^{(k)}$ for a molecular system in the electronic state φ_k is given by Eq. (2.58). We assume that $\hat{H}_n^{(k)}$ is written in terms of the Cartesian coordinates of the nuclei, in an inertial reference frame centered in the nuclear center of mass, so as to separate the translational motion. The eigenfunctions of $\hat{H}_n^{(k)}$ describe the nuclear internal (i.e., vibrational) motion as well as the rotation of the molecule as a whole. Of course in this way we are completely neglecting the contribution of the electronic angular momentum (including spin) to the total angular momentum of the molecule. However, the interaction between the electronic rotation and the nuclear motion is normally of little interest in photochemistry: for example, the roto-electronic coupling may lead to transitions between different electronic states but it is usually negligible with respect to nonadiabatic couplings. In fact, the latter take larger values especially in regions of degeneracy or near degeneracy between potential energy surfaces.

The potential energy surface U_k may have several minima, which correspond to different isomers or conformers. Let $\mathbf{R}_{eq}^{(k)}$ be the nuclear Cartesian coordinates defining one of these minima. Assuming that the nuclear motion is confined in the vicinity of $\mathbf{R}_{eq}^{(k)}$, the rotation of the molecule can be approximately separated from the internal motions as follows

$$\hat{H}_n^{(k)} \simeq \hat{H}_{rot}^{(k)} + \hat{H}_{vib}^{(k)} \tag{2.108}$$

$$\hat{H}_{rot}^{(k)} = \frac{1}{2}\mathbf{J}_n(\mathbf{I}^{(k)})^{-1}\mathbf{J}_n \tag{2.109}$$

where $\mathbf{J}_n$ is the nuclear angular momentum and $\mathbf{I}^{(k)}$ is the inertia tensor for the nuclear configuration corresponding to $\mathbf{R}_{eq}^{(k)}$. The vibrational Hamiltonian $\hat{H}_{vib}^{(k)}$ has the same functional form as $\hat{H}_n^{(k)}$ of Eq. (2.58), but is written in terms of the Cartesian coordinates in the rotating reference frame where $\mathbf{I}^{(k)}$ is diagonal (i.e., in the principal axis system of the molecule). In this way any roto-vibrational coupling between nuclear internal and rotational motions is neglected. Note however that these couplings are not connecting different electronic states, so that they are not able to promote electronic transitions. For simplicity, in the following sections we will drop the superscript $^{(k)}$ indicating the electronic state to which the vibrational and rotational Hamiltonians are referred.

2.5.1 Rotational States

In the rotating reference frame referred above the Hamiltonian $\hat{H}_{rot}$ simplifies to

$$\hat{H}_{rot} = \frac{\hat{J}_{n\xi}^2}{2I_{\xi\xi}} + \frac{\hat{J}_{n\eta}^2}{2I_{\eta\eta}} + \frac{\hat{J}_{n\zeta}^2}{2I_{\zeta\zeta}} \tag{2.110}$$

where ξ, η, ζ label the three components of the rotating frame. The eigenfunctions of $\hat{H}_{rot}$ are the rotational functions, which depend on the Euler angles α, β, and γ relating the fixed reference frame (x, y, z) to the rotating one (ξ, η, ζ). As a consequence of the isotropy of space the angular momentum (in the present case the nuclear angular momentum) is a conserved quantity. Then, the rotational Hamiltonian $\hat{H}_{rot}$ commutes with $\hat{J}_n^2$ and $\hat{J}_{nz}$; its eigenstates ψ_{rot}^{JM} can be written as linear combinations of the rigid spherical rotor wavefunctions, which represent a complete basis and correspond to the Wigner functions $D_{KM}^{(J)}$

$$\psi_{rot}^{JM} = \sum_{K=-J}^{J} C_K^{(J)} D_{KM}^{(J)}(\alpha, \beta, \gamma) \; . \tag{2.111}$$

The Wigner functions are common eigenfunctions of the set of commuting operators $\hat{J}_n^2$, $\hat{J}_{nz}$ and $\hat{J}_{n\zeta}$, so that

$$\begin{aligned} \hat{J}_n^2 D_{KM}^{(J)} &= \hbar^2 J(J+1) D_{KM}^{(J)} \\ \hat{J}_{nz} D_{KM}^{(J)} &= \hbar M D_{KM}^{(J)} \\ \hat{J}_{n\zeta} D_{KM}^{(J)} &= \hbar K D_{KM}^{(J)} \; . \end{aligned} \tag{2.112}$$

$\mathbf{J}_n$ being an orbital angular momentum, the quantum number J takes only integer values, and so do M and K, which go from $-J$ to J. Contrary to $\hat{J}_{nz}$, in general $\hat{J}_{n\zeta}$ does not commute with $\hat{H}_{rot}$, so that $D^{(J)}_{KM}$ are not, in general, eigenfunctions of the rotational Hamiltonian: to find the ψ^{JM}_{rot} and the corresponding rotational energies one has to evaluate the matrix element of $\hat{H}_{rot}$ on the basis of the Wigner functions and diagonalize.

If two of the three principal moments of inertia are equal, the molecule is called a *symmetric top*. In that case we can define $I_{\xi\xi} = I_{\eta\eta} = I_a$ and $I_{\zeta\zeta} = I_b$ so that $\hat{H}_{rot}$ simplifies to

$$\hat{H}_{rot} = \frac{1}{2I_a}(\hat{J}_n^2 - \hat{J}_{n\zeta}^2) + \frac{1}{2I_b}\hat{J}_{n\zeta}^2 \tag{2.113}$$

which shows that $\hat{J}_{n\zeta}$ commutes with $\hat{H}_{rot}$. Therefore the eigenstates ψ^{JM}_{rot} of the rotational Hamiltonian are also eigenfunctions of $\hat{J}_{n\zeta}$ and directly correspond (apart from a normalization factor) to the Wigner functions $D^{(J)}_{KM}$, with eigenvalues E^{rot}_{JK} given by

$$E^{rot}_{JK} = \frac{\hbar^2}{2I_a}J(J+1) + \frac{\hbar^2}{2}\left(\frac{1}{I_b} - \frac{1}{I_a}\right)K^2 \,. \tag{2.114}$$

For a *spherical top* all the three principal moments of inertia are equal: $I_{\xi\xi} = I_{\eta\eta} = I_{\zeta\zeta} = I$. Hence, $\hat{H}_{rot}$ and the rotational energy further simplify

$$\begin{aligned} \hat{H}_{rot} &= \frac{\hat{J}_n^2}{2I} \\ E^{rot}_J &= \frac{\hbar^2}{2I}J(J+1) \,. \end{aligned} \tag{2.115}$$

In general, the rotational energy of a molecular system cannot depend on the orientation of the molecule with respect to the fixed reference frame; i.e., it cannot depend on the quantum number M (again, this is due to the isotropy of space). Therefore, the rotational levels are $2J+1$ times degenerate. The degeneracy increases to $2(2J+1)$ for symmetric tops (note in fact that $E^{rot}_{JK} = E^{rot}_{J,-K}$ in that case) and to $(2J+1)^2$ for spherical tops, where E^{rot}_J is independent on K. We note that the rotational energies increase quadratically with J, so the spacing between the levels J and $J+1$ increases linearly. Since the number of states (degenerate or not) with a given J also increases quadratically, the density of states $\rho(E^{rot})$ is roughly proportional to J, i.e., to $\sqrt{E^{rot}}$. By density of states we mean the ratio $N_{st}/\Delta E$, where N_{st} is the number of states in the (small) interval of energies ΔE. Of course we can consider ρ as an almost continuous function of E^{rot} only if N_{st} is very large. ρ can be seen as the product of degeneracy times the average reciprocal spacing between rotational levels. For low J, the spacings are of the order of $\hbar^2/I_\lambda$, where I_λ is a component of the inertia tensor. We get the largest spacings, up to tens of cm^{-1}, for small molecules made of light atoms. Going to larger molecules, the moments of inertia increase rapidly, because the contributions of more atoms sum

up and their distances from the center of mass increase. As a result, for medium to large molecules and/or large J it is often reasonable to neglect the quantization of levels and to consider the overall rotation of the molecule as a classical motion. We also note that, when talking about the molecular ground state, one usually refers to the electronic and vibrational degrees of freedom, while rotations (and a fortiori translations) are not considered, because a number of rotational states are always populated, except at extremely low temperatures.

2.5.2 Vibrational States

The nuclear internal (or vibrational) motion is described by the vibrational Hamiltonian $\hat{H}_{vib}$. The eigenvalue equation for $\hat{H}_{vib}$ is greatly simplified if the nuclear motion is confined in a neighborhood of the minimum point $\mathbf{R}_{eq}$. In fact, in that case the potential energy function U can be expanded in a Taylor series centered in $\mathbf{R}_{eq}$ and truncated at the second order

$$U(\mathbf{X}) = U_0 + \frac{1}{2}\sum_{\alpha,\beta} K_{\alpha\beta} X_\alpha X_\beta + \dots \tag{2.116}$$

where $U_0 = U(\mathbf{R}_{eq})$, $\mathbf{X} = \mathbf{R} - \mathbf{R}_{eq}$ is the vector collecting the Cartesian displacements from the minimum point and

$$K_{\alpha\beta} = \left.\frac{\partial^2 U}{\partial X_\alpha \partial X_\beta}\right|_{\mathbf{X}=\mathbf{0}} . \tag{2.117}$$

We define the symmetric matrix $\mathbf{K}'$ of the mass weighted Cartesian force constants

$$K'_{\alpha\beta} = (M_\alpha M_\beta)^{-1/2} K_{\alpha\beta} . \tag{2.118}$$

Let $\mathbf{L}$ be the orthogonal matrix which diagonalizes $\mathbf{K}'$, in such a way that $\mathbf{L}^t\mathbf{K}'\mathbf{L}$ is the diagonal matrix collecting the eigenvalues ω_r^2 of $\mathbf{K}'$. We have then, up to the second order

$$U = U_0 + \frac{1}{2}\sum_r \omega_r^2 Q_r^2 \tag{2.119}$$

where

$$Q_r = \sum_\alpha L_{\alpha r} X_\alpha \sqrt{M_\alpha} \tag{2.120}$$

are the normal coordinates. Note that, as $\mathbf{Q} = \mathbf{0}$ is a minimum of U, $\omega_r^2 \geq 0$ for all coordinates; i.e., the ω_r are all real. The potential U cannot depend on the 6 coordinates describing translations and rotations of the system as a whole; therefore, 6 of the ω_r will be equal to 0 (5 in the case $\mathbf{R}_{eq}$ corresponds to a linear arrangement of nuclei). In terms of the normal coordinates $\hat{H}_{vib}$ is given by a sum of equivalent terms, each one depending on a single Q_r

$$\begin{aligned} \hat{H}_{vib} &= U_0 + \sum_r \hat{h}_{harm}(Q_r) \\ \hat{h}_{harm}(Q_r) &= -\frac{\hbar^2}{2}\frac{\partial^2}{\partial Q_r^2} + \frac{1}{2}\omega_r^2 Q_r^2 \end{aligned} \tag{2.121}$$

where $\hat{h}_{harm}(Q_r)$ is the Hamiltonian of a harmonic oscillator with unit mass and frequency ω_r (see Appendix F). In this way, the eigenvalue equation $\hat{H}_{vib}\chi_v = E_v^{vib}\chi_v$ can be solved exactly. We have

$$\begin{aligned} \chi_v(Q_1, \ldots, Q_s) &= \prod_{r=1}^{s} \chi_{v_r}(Q_r) \\ E_v^{vib} &= U_0 + \sum_{r=1}^{s} \hbar\omega_r \left(v_r + \frac{1}{2}\right) \end{aligned} \tag{2.122}$$

where $s = 3N_n - 6$ (or $s = 3N_n - 5$) is the number of internal coordinates, the integer v_r gives the degree of excitation of the normal mode r, v is formally a compound index collecting all the v_r, and $\chi_{v_r}(Q_r)$ is a harmonic oscillator eigenfunction. In the ground vibrational state all the v_r are equal to zero and the corresponding vibrational energy is $E_0^{vib} = \sum_r \hbar\omega_r/2$, which is called the zero-point energy (ZPE). In a polyatomic molecule the vibrational frequencies $\omega_r/2\pi$ (or better the wavenumbers $\omega_r/2\pi c$) take values in the range 10–4000 cm^{-1}.

The harmonic approximation referred above describes correctly the nuclear motion only for small oscillations of the nuclei around $\mathbf{R}_{eq}$, i.e., for the lowest vibrational states. For larger v_r, the portion of potential energy surface U explored by the nuclei increases (more rapidly for the normal modes with smaller frequencies) and the anharmonic terms neglected in Eq. (2.121) become important. Usually, the harmonic approximation overestimates the potential energy U in certain regions of the PES, for instance, for large bond distances. As a consequence, taking into account the anharmonicity, the energy levels of a given normal mode are not anymore evenly spaced, but rather the energy difference between two successive levels v and $v + 1$ decreases with v.

A more important consequence of anharmonicity is that an exact eigenfunction of $\hat{H}_{vib}$ cannot be written as the product of harmonic oscillator eigenstates of Eq. (2.122). In other words, the normal modes are coupled: the vibrational excitation can be transferred from a normal mode to another. In particular, if the system is prepared with some degree of vibrational excitation concentrated in a single normal mode,

it will evolve transferring the excitation to the other modes. This phenomenon is called intramolecular vibrational energy redistribution (IVR) and is usually quite fast in polyatomic molecules (see Sect. 4.3). IVR depends on the density of vibrational states and on their coupling. Clearly, it has a strong influence on the kinetics of thermal unimolecular reactions, which depend on the ability to concentrate the available vibrational energy along the reaction coordinate. For example, in the Rice, Ramsperger, Kassel, and Marcus (RRKM) theory of unimolecular reactions it is assumed that the vibrational energy is statistically distributed among the oscillators: the microcanonical rate constant, which depends on the probability of gathering enough energy in the reaction coordinate, is then related to the density of vibrational states of the reactant [15].

By applying the harmonic approximation, the density of vibrational states is easily obtained if we make the simplifying assumption that all the vibrational frequencies are equal, so that $\omega_r = \omega_0$ for all $r = 1, \ldots, s$. In this way, the vibrational levels are evenly spaced by the same amount $\hbar\omega_0$, and their energy only depends on ω_0 and on the total number of vibrational quanta $q = \sum_r v_r$. The degeneracy of a level corresponds to the number of ways q objects (the vibrational quanta) can be distributed among s boxes (the oscillators), and the density of vibrational states (number of states per unit energy) is obtained dividing the degeneracy by $\hbar\omega_0$

$$\rho_{vib} = \frac{1}{\hbar\omega_0} \frac{(q+s-1)!}{q!(s-1)!} \,. \tag{2.123}$$

Clearly ρ_{vib} is a rapidly increasing function of q. In particular, when q is large (i.e., for $q \gg s$), using the Stirling approximation $q! \simeq \sqrt{2\pi q}(q/\mathrm{e})^q$ and $(1+s/q)^q \simeq \mathrm{e}^s$ we obtain

$$\rho_{vib} \simeq \frac{q^{s-1}}{\hbar\omega_0(s-1)!} = \frac{E^{s-1}}{(\hbar\omega_0)^s(s-1)!} \tag{2.124}$$

where $E = q\hbar\omega_0$ is the excess vibrational energy above the ZPE. A large value for q corresponds to the classical limit for the oscillators (large energy with respect to $\hbar\omega_r$). Actually, the classical expression for the density of states of a system of s oscillators can be easily worked out [16] without assuming that all the ω_r are equal. In fact, from the classical point of view, $\mathrm{d}\varepsilon/\hbar\omega_r$ is the number of states in the energy interval from ε to $\varepsilon + \mathrm{d}\varepsilon$ (for any $\varepsilon > 0$) for a harmonic oscillator with frequency ω_r. Then, the total number of states of a system of s harmonic oscillators having energies less than a given value E is

$$N^{cl}(E) = \left(\prod_{r=1}^{s} \hbar\omega_r\right)^{-1} \int\limits_{\varepsilon_1+\ldots+\varepsilon_s \le E} \cdots \int \mathrm{d}\varepsilon_1 \ldots \mathrm{d}\varepsilon_s \tag{2.125}$$

where $\varepsilon_r \ge 0$ for all $r = 1, \ldots, s$. The integral in the above expression is the volume of the *simplex* $T_s(E)$, defined as the region of $\mathbb{R}^s$ such that $\sum_r x_r \le E$ and $x_r \ge 0$ for all r (a triangle for $s = 2$ and a tetrahedron for $s = 3$). It can be shown that

Table 2.1 Density of vibrational states in the harmonic approximation. The vibrational energy E above the ZPE is given in cm^{-1} and ρ_{vib} in states/cm^{-1}. The density of states was obtained evaluating first $N(E)$ by the Beyer–Swinehart [17] exact counting algorithm and then performing numerical differentiation. We used experimental vibrational frequencies, from NIST (https://cccbdb.nist.gov)

Molecule	N_n	s	E	ρ_{vib}
NH_3	4	6	5000	$6 \cdot 10^{-3}$
NH_3	4	6	10000	$8 \cdot 10^{-2}$
NH_3	4	6	30000	5
CH_4	5	9	5000	0.01
CH_4	5	9	10000	0.6
CH_4	5	9	30000	300
Acetone	10	24	5000	10^3
Acetone	10	24	10000	$7 \cdot 10^5$
Acetone	10	24	30000	10^{12}
Benzene	12	30	5000	$3 \cdot 10^2$
Benzene	12	30	10000	$3 \cdot 10^5$
Benzene	12	30	30000	$5 \cdot 10^{12}$

the volume of $T_s(E)$ is given by $E^s/s!$, so that the classical expression for the total number of states is

$$N^{cl}(E) = \left(\prod_{r=1}^{s} \hbar\omega_r\right)^{-1} \frac{E^s}{s!} \tag{2.126}$$

which, derived with respect to E, gives the density of states

$$\rho_{vib}^{cl} = \left(\prod_{r=1}^{s} \hbar\omega_r\right)^{-1} \frac{E^{s-1}}{(s-1)!} \,. \tag{2.127}$$

As expected, ρ_{vib} coincides with ρ_{vib}^{cl} in the limit of large E (see Eq. (2.124)). In any case, taking the anharmonicity into account, ρ_{vib} is expected to grow with the vibrational energy even faster than the harmonic expressions reported above.

In Table 2.1 we show a few values of ρ_{vib} for some selected molecules, obtained by exact count of the number of states, in the harmonic approximation. Even with a very modest number of atoms (say, larger than 4) the density of states rapidly becomes so high to challenge the resolution of any experimental apparatus.

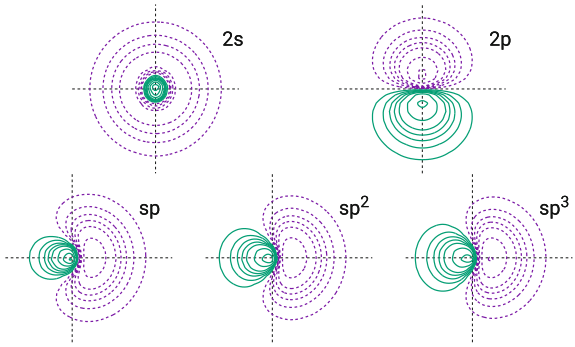

Fig. 2.2 Atomic orbitals and hybridization. Isodensity contour lines, unevenly spaced. Solid and dashed lines are used to represent positive and negative values of the functions

2.6 Electronic States of Polyatomics and Photoreactivity

2.6.1 Molecular Orbitals

As already discussed in Sect. 2.4, the electronic wavefunctions are often written in the form of antisymmetrized products of one-electron functions: the molecular (spin)orbitals. In fact, the approximation of considering the motions of the electrons as independent from each other works surprisingly well, provided the mandatory requirement of antisymmetry is taken into account. The shape of a molecular orbital is then determined by the electrostatic interaction with the nuclei and with the mean-field generated by the motion of the other electrons.

In the following we will rely on the simplest description of the molecular orbitals, which consists in approximating them as linear combinations of atomic orbitals. It is often convenient to consider "hybrid" atomic orbitals, which present the advantage of being oriented in space more conveniently for the formation of chemical bonds. For example, with atomic orbitals s and p, three main types of hybrids can be built (sp, sp^2, and sp^3) as shown in Fig. 2.2, although one may have any intermediate shape between pure s and pure p.

From the combinations of two atomic orbitals of two adjacent atoms we get a molecular orbital which describes the chemical bond in a schematic way. The mixing is influenced by the relative energy of the two atomic orbitals and by their interaction which, in turn, may be taken as proportional to their overlap. Four typical cases in this respect are shown in Fig. 2.3. The shape of a molecular orbital depends on the kind of atomic orbitals which are mixed: in the simplest case (H_2), combining the two $1s$ orbitals we get a bonding (σ) and an antibonding (σ^*) orbital with axial symmetry, as shown in Fig. 2.4. The other orbitals shown in Fig. 2.4 are suited, for example, to the description of the C-H bond in an alkane, where the σ orbital is obtained by mixing one of the four sp^3 hybrids of the carbon atom with the $1s$ of H. In double and triple bonds, the molecular orbitals are formed combining two parallel p orbitals orthogonal to the bond axis. We have in this case π and π^* orbitals, characterized by a nodal plane containing the bond axis (see Fig. 2.5). In this case, the interaction between

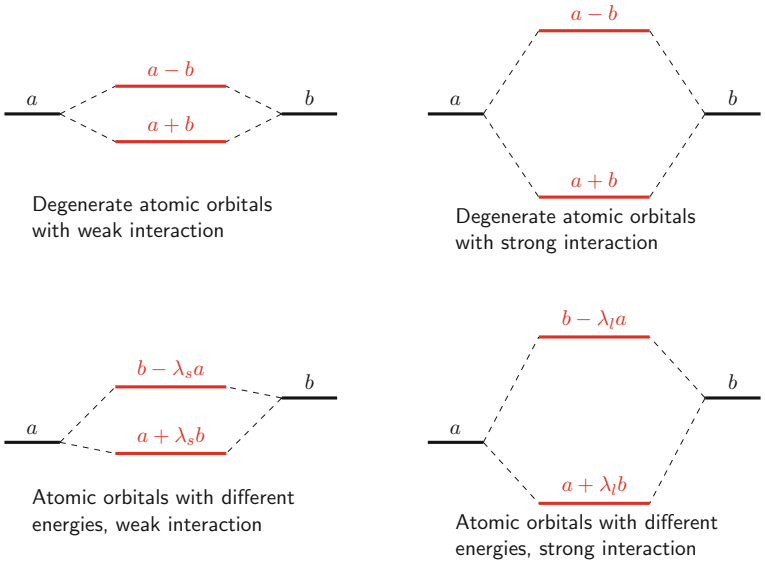

Fig. 2.3 Four typical cases of interaction between two atomic orbitals a and b. The energy levels of atomic and molecular orbitals are shown as black and red thick lines, respectively. λ_s is a small mixing coefficient, while λ_l is a larger one

Fig. 2.4 Molecular orbitals, type σ

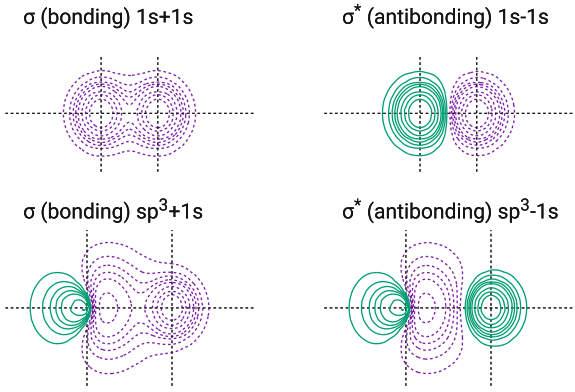

atomic orbitals is normally weaker with respect to the σ bonds. *Nonbonding* orbitals, indicated as n, are atomic orbitals or hybrids that already contain two electrons ("lone pairs") before the bonds are formed and therefore do not mix with other orbitals as in Fig. 2.3. This happens when the s and p orbitals and their hybrids contain more than four valence electrons, as in N, O, P, S and the halogens. As a rule of thumb the energetic ordering of the molecular orbitals is then $\sigma < \pi < n < \pi^* < \sigma^*$.

The electronic ground state S_0 of an organic molecule, at least in the vicinity of its equilibrium geometry, is well described by a configuration in which the first

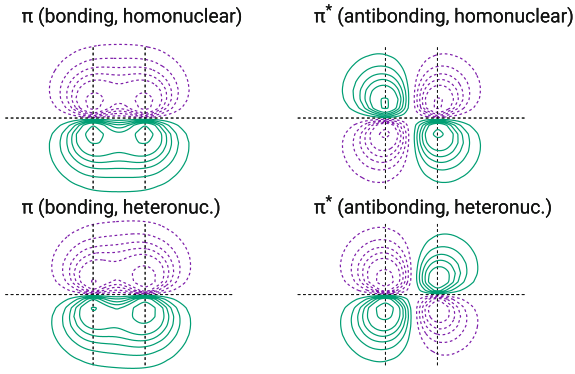

Fig. 2.5 Molecular orbitals, type π

$N_e/2$ molecular orbitals are occupied (stable organic species have usually an even number of electrons). Therefore, the lowest lying excited electronic states (S_1 and T_1) have a couple of unpaired electrons and are obtained by promoting an electron from the highest occupied molecular orbital (HOMO) to the lowest unoccupied molecular orbital (LUMO). Once that the double occupation characteristic of the ground state is abandoned, the number of ways the electrons can be placed in the molecular orbitals increases: therefore, the energetic separation between excited states is usually much smaller than the energy difference between S_1 and S_0. Things may be much more complicated for molecules containing transition metal complexes, with partly filled d or f shells (not covered here).

In the following the features of the lowest lying excited electronic states in organic molecules are analyzed on the basis of the frontier orbitals (HOMO and LUMO) involved in the excitation.

2.6.2 *Excited States $\sigma \rightarrow \sigma^*$*

A molecule only containing single bonds and no lone pairs, as an alkane, only has valence orbitals of σ and σ^* types. In this case the frontier orbitals HOMO and LUMO are a σ and a σ^*, respectively, so that S_1 and T_1 are approximately described by singly excited configurations $\sigma \rightarrow \sigma^*$. We will only consider the frontier orbitals, which are occupied in a different way in the ground and in the excited states. Assuming that the two frontier orbitals σ and σ^* describe the bond between two atoms A and B in the molecular system considered, they can be represented in terms of two atomic orbitals a and b (centered respectively on A and B), as in Fig. 2.3

$$\sigma(\mathbf{r}) = \frac{a(\mathbf{r}) + \lambda b(\mathbf{r})}{\sqrt{1+\lambda^2}} \tag{2.128}$$

$$\sigma^*(\mathbf{r}) = \frac{b(\mathbf{r}) - \lambda a(\mathbf{r})}{\sqrt{1+\lambda^2}} \,. \tag{2.129}$$

For the sake of simplicity, here we have assumed that a and b are orthogonal: $s = \langle a\,|b\,\rangle = 0$. Of course this is in general not the case for two atomic orbitals belonging to different atoms, especially if they have to form a bonding MO. However, one can orthogonalize two atomic orbitals, generating orbitals as similar as possible to the original ones (see Appendix E). The mixing coefficient $\lambda > 0$ depends on the internuclear distance R_{AB} and on the chemical environment. In particular, if we assume A more electronegative than B, then $\lambda \leq 1$. Note that $\lambda = 1$ when A and B are identical (symmetric case, see Fig. 2.3). Moreover, increasing R_{AB} the interaction becomes smaller, so that λ tends to zero, and the two molecular orbitals σ and σ^* boil down to a and b (except in the symmetric case where $\lambda = 1$ independently of R_{AB}).

According to Sect. 2.4, the electronic wavefunctions for S_0, S_1, and T_1, omitting the spin factors, can be approximated as

$$\varphi_{S_0} = \sigma^2 = \frac{a^2 + \lambda^2 b^2 + \lambda(ab + ba)}{1 + \lambda^2} \tag{2.130}$$

$$\varphi_{S_1} = \frac{\sigma\sigma^* + \sigma^*\sigma}{\sqrt{2}} = \frac{(1 - \lambda^2)(ab + ba) + 2\lambda(b^2 - a^2)}{(1 + \lambda^2)\sqrt{2}} \tag{2.131}$$

$$\varphi_{T_1} = \frac{\sigma\sigma^* - \sigma^*\sigma}{\sqrt{2}} = \frac{ab - ba}{\sqrt{2}}\,. \tag{2.132}$$

Here, as in Sect. 2.4, $a^2 \equiv a(\mathbf{r}_1)a(\mathbf{r}_2)$, $ab \equiv a(\mathbf{r}_1)b(\mathbf{r}_2)$, etc. In valence bond (VB) theory, the functions a^2 and b^2 are called ionic structures, while $ab \pm ba$ is a neutral, or covalent, structure. The triplet wavefunction contains no ionic structures: this is a general result, due to the fact that two electrons in the same orbital make a symmetric space factor that necessarily goes with an antisymmetric (singlet) spin factor.

The ground-state function of Eq. (2.130) has a qualitatively wrong behavior at large R_{AB} (see Fig. 2.6). In fact, the ionization potentials of atoms or groups are normally much larger than their electronic affinities, so that the ground-state dissociation of an isolated molecule is homolytic (ionic dissociation normally occurs in polar solvents). Therefore, the ionic configurations should disappear from φ_{S_0} for large R_{AB}, and this is evidently not the case in Eq. (2.130), neither in the symmetric ($\lambda = 1$) nor in the nonsymmetric ($\lambda \to 0$) case: the wavefunction (2.130) overestimates the importance of the ionic configurations. A better representation for S_0 could be obtained by writing φ_{S_0} as a linear combination of the three singlet configurations which can be built with two electrons in two molecular orbitals

$$\varphi_{S_0} = C_0\sigma^2 + C_1\frac{\sigma\sigma^* + \sigma^*\sigma}{\sqrt{2}} + C_2\sigma^{*2} \tag{2.133}$$

where the coefficients C_0, C_1, and C_2 are determined by minimizing the energy $E_{S_0} = \left\langle \varphi_{S_0} \middle| \hat{H}_{el} \middle| \varphi_{S_0} \right\rangle$, i.e., by diagonalizing $\hat{H}_{el}$ on the basis of the three configurations. This is an example of application of the "configurations interaction" (CI) method.

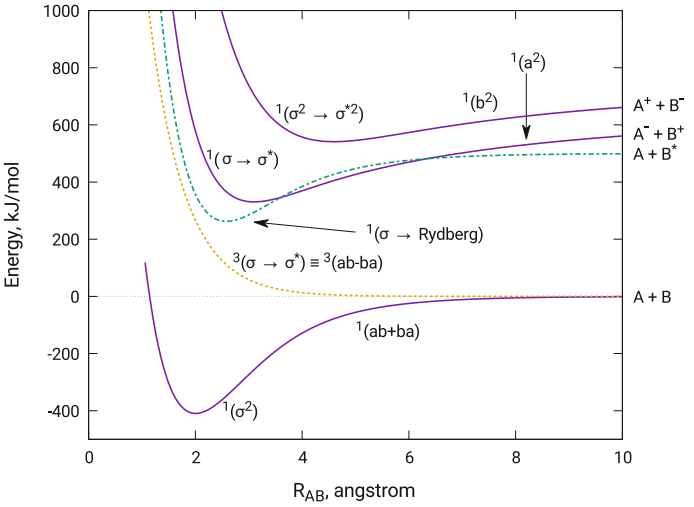

Fig. 2.6 Potential energy curves for $\sigma \rightarrow \sigma^*$ states. R_{AB} is the distance between the two atoms giving rise to the σ bond

The same procedure could be applied to S_1: note in fact that the asymptotic behavior of φ_{S_1} of Eq. (2.131) is also incorrect, as the S_1 wavefunction should correlate with the ionic configuration a^2 (corresponding to A^-B^+) for large R_{AB} (see Fig. 2.6). Due to the attractive long-range electrostatic interaction between the two ions A^- and B^+, the S_1 potential energy curve along R_{AB} normally has a minimum, but shallower and with a larger equilibrium distance with respect to the ground state, because of the antibonding effect of the σ^* orbital, which is occupied by one electron. In the symmetric case S_1 is given by a combination of the two ionic structures, with the same weight (a "zwitterionic" state). Conversely, if the difference in electronegativity between A and B is large, at short distances S_0 and S_1 will mainly have ionic and neutral character, respectively. At large R_{AB} the situation is reversed: therefore, in that case, the potential energy curve of the ionic VB structure must cross that of the covalent structure for some value of the distance. At that point, the potential energy curves of S_0 and S_1 may get close, too. This subject will be developed in greater detail in Sect. 5.1.

The potential energy curve of T_1, which has a neutral wavefunction, is usually repulsive and correlates with the same asymptote as the ground state (see Fig. 2.6).

Besides valence excited states, for small molecules one has also to consider "Rydberg" states, which can be described as excitations from an occupied orbital (σ in the present case) to a Rydberg orbital. The latter is a very diffuse hydrogen-like orbital, because an electron in a Rydberg orbital sees the rest of the molecule approximately as a point charge. A Rydberg orbital is indicated by the generic symbol Ry, or by the symbol of the hydrogenoid orbital it resembles: $3s$, $3p$, $3d$, $4s$ ... The energies of

Rydberg states form series converging to the energy of the cation and can be fitted by the following formula

$$E_n \simeq IP - \frac{\mathrm{Ry}}{(n-\delta)^2} \tag{2.134}$$

where IP is the ionization potential, $\mathrm{Ry} = m_e\alpha^2c^2/2$ is the Rydberg energy, n is the principal quantum number of the singly occupied hydrogen-like orbital, and δ is the so-called quantum defect, which takes into account the deviation from the point charge model. Often the first $\sigma \rightarrow Ry$ Rydberg states are found at lower energies with respect to $\sigma \rightarrow \sigma^*$, but they usually show quite low radiative transition probabilities, rapidly decreasing with n, because of the small overlap of the Rydberg orbitals with the MO occupied in the ground state. For the same reason, the exchange integral $K_{\sigma,Ry}$ is expected to be small, and therefore the energetic splitting between the singlet and triplet states sharing the same $\sigma \rightarrow Ry$ configuration is normally small (see Eq. (2.93)). Usually the potential energy surface of a Rydberg state looks like that of the corresponding cation, as the electron in the Rydberg orbital is weekly affected by changes in the molecular geometry. Large molecules, which cannot be approximated as point charges, do not show well-characterized Rydberg states.

2.6.3 Excited States $n \rightarrow \sigma^*$

According to the energetic ordering of molecular orbitals referred above, in molecules containing σ bonds and lone pairs, such as water, ammonia, alcohols, ethers, the frontier orbitals are n and σ^*. Then, the first excited states are normally of $n \rightarrow \sigma^*$ character (or $n \rightarrow Ry$ in small molecules). At variance with $\sigma \rightarrow \sigma^*$, the excited singlet $n \rightarrow \sigma^*$ has a homolytic dissociation, giving rise to two neutral fragments, like S_0. In fact, if A is the atom containing the lone pair n, when the A-B bond is broken, A will have two nonbonding orbitals (n_1 and n_2, probably very close in energy). It will be therefore possible to place the unpaired electron in n_1 or n_2, producing two degenerate or quasi-degenerate singlets.

As a simple example we consider the water photolysis [18, 19]. The first excited singlet state of water has a mixed valence/Rydberg character (i.e., it can be represented as a combination of the $n \rightarrow \sigma^*$ and $n \rightarrow 3s$ configurations). The corresponding absorption band, with a maximum at 166 nm, has a weak intensity and is a continuum, which is the signature of a dissociative potential energy surface. In fact, the $n \rightarrow \sigma^*$ configuration has a repulsive potential energy surface and the S_1 state, which has a substantial Rydberg character at the S_0 equilibrium geometry, evolves to become a valence $n \rightarrow \sigma^*$ state when the O-H bond is stretched. The orbital correlation diagram of Fig. 2.7 shows that the ground state and the $n \rightarrow \sigma^*$ singlet are degenerate at dissociation, where two equivalent configurations may be produced placing the unpaired electron on the OH moiety in one of the two degenerate p orbitals of the oxygen atom. This simple description is also suited to the dissociation of O-H and O-C bonds in alcohols and ethers.

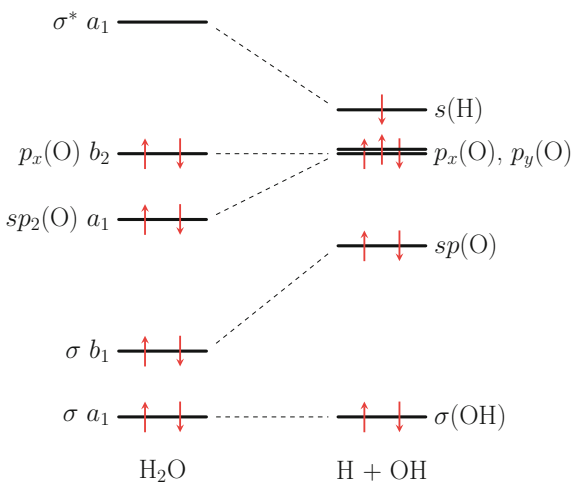

Fig. 2.7 Schematic orbital correlation diagram for the OH bond dissociation in a water molecule. The occupation of the orbitals is referred to the ground state. For the orbitals of the water molecule (which is assumed to lie in the yz plane) the C_{2v} symmetry labels are shown. The OH fragment lies on the z-axis

2.6.4 Excited States $\pi \rightarrow \pi^*$

In monoalkenes the frontier orbitals are π and π^*, so the first excited states have $\pi \rightarrow \pi^*$ character (in small molecules, low-lying Rydberg states may be present as well). The same mixing scheme as in Eqs. (2.128) and (2.129) can be applied to π orbitals. In particular, in this case the two mixing atomic orbitals a and b (two p orbitals of two C atoms) are likely to have very similar energies, so that the mixing coefficient λ will be close to 1. Then, at the equilibrium geometry of S_0, both ionic and covalent structures are expected to contribute to the ground-state wavefunction, while the $\pi \rightarrow \pi^*$ S_1 state is mainly described by the zwitterionic configuration $a^2 - b^2$. The π bond can be broken without dissociating the molecule, with a torsion around the bond axis. Such a torsion represents the reaction coordinate for the *cis–trans* isomerization; see Fig. 2.8. Along this coordinate, the energy of the ground state increases, until the torsion angle is about 90°, and at the same time the energy of S_1 decreases.

At 90° degree of rotation, which corresponds to a geometry close to the transition state for the thermal *cis–trans* isomerization, the two p orbitals are perpendicular to each other and their interaction is close to zero. Therefore, their combinations π and π^* are degenerate, or nearly degenerate. The S_0 state is well described by a diradical configuration $ab + ba$, while S_1 and S_2 are ionic. In particular, if the two fragments are perfectly equivalent (symmetric case), S_1 and S_2 are well described by the two zwitterionic combinations $a^2 - b^2$ and $a^2 + b^2$, respectively. Conversely, in an asymmetric case where, say, a^2 is lower in energy than b^2, given the negligible interaction between a and b, S_1 and S_2 will be well described by pure a^2 and b^2 ionic states, respectively. In other words, at geometries close to the transition state for the isomerization, the zwitterionic states are very polarizable. Note that an asymmetry between the two centers can always be produced by a geometrical deformation:

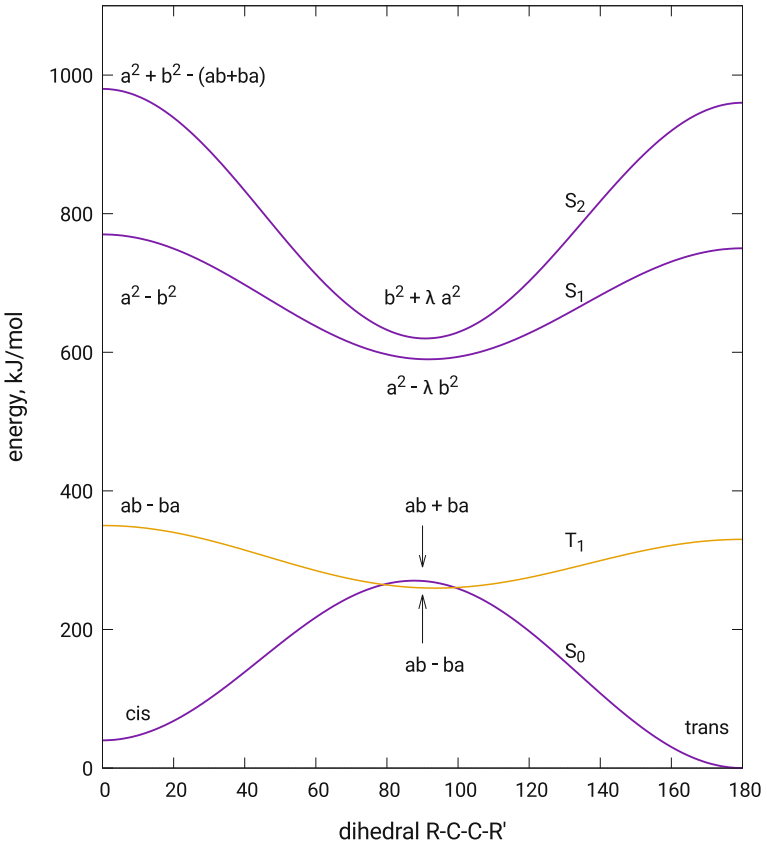

Fig. 2.8 Energies of the electronic states of a monoalkene CHR=CHR′, as a function of the torsion angle R-C-C-R′. The leading configurations for the different states are also shown, in terms of atomic orbitals, at the ground-state equilibrium geometry and at 90° of torsion. In a symmetric case (i.e., with R = R′) the parameter λ is equal to 1, while it tends to zero when an asymmetry is introduced (see text)

for example, the pyramidalization of the carbon atom A, with hybridization going from sp^2 to sp^3, slightly lowers the energy of the a^2 ionic configuration. Therefore along that coordinate the energy of S_1 slightly decreases, while the energy of S_0 increases: eventually, the two states may cross. In any case, with that deformation the energy difference between S_1 and S_0 is further reduced with respect to the value at the transition state for *cis–trans* isomerization. Hence in that region, which can be accessed very easily on the S_1 surface from the Franck–Condon point, nonadiabatic transitions between the two electronic states are very likely to happen. For that reason, alkene molecules which are free to rotate around the C-C double bond and to pyramidalize one of the two carbon atoms, after electronic excitation show a very fast decay to S_0, and are therefore not fluorescent.

It is evident from Fig. 2.8 that electronic excitation of a monoalkene may easily lead to isomerization: in fact, when the molecule goes back to the ground state from a geometry close to the transition state, it follows the S_0 potential energy surface ending with either a *trans* or *cis* final geometry, independently of the starting isomer on S_0.

The first band in the absorption spectrum of monoalkenes has mixed character $\pi \rightarrow \pi^*$ and Rydberg and peaks around 180–200 nm. It is very broad, given the different shapes of the S_0 and S_1 potential energy surfaces, as shown in Fig. 2.8.

The energetic separation between two $\pi \rightarrow \pi^*$ T_1 and S_1 states is large: in fact, given the substantial overlap between $|\pi|$ and $|\pi^*|$, the exchange integral $K_{\pi\pi^*}$ is not small, except when the double bond is twisted. The T_1 potential energy surface has a behavior similar to S_1 with respect to the torsion around the double bond axis and is closer to S_0: population of the T_1 state, when feasible, may lead to *cis–trans* isomerization as well.

2.6.5 Excited States $n \rightarrow \pi^*$

In nonconjugated molecules like imines, carbonyl compounds, azocompounds, where the double bond involves an atom with a lone pair, the frontier orbitals are n and π^*, so the first excited states have $n \rightarrow \pi^*$ character. There are significant differences between $n \rightarrow \pi^*$ and $\pi \rightarrow \pi^*$ states. In particular, the singlet–triplet energetic separation is smaller for $n \rightarrow \pi^*$ states than for $\pi \rightarrow \pi^*$ states. In fact, n and π^* orbitals occupy quite different space regions, so that concerning the exchange integrals we have $K_{n\pi^*} \ll K_{\pi\pi^*}$. This has an important consequence on the photophysics, since with a smaller energy difference, the ISC $S_1 \rightarrow T_1$ is easier. Therefore, systems with $n \rightarrow \pi^*$ transitions have larger triplet quantum yield with respect to molecules with $\pi \rightarrow \pi^*$ states only. For example, in acetone the $n \rightarrow \pi^*$ states S_1 and T_1 have minima at about 3.8 and 3.5 eV above the ground state, respectively. Now, the spin–orbit coupling between S_1 and T_1 is very small because of the El-Sayed rules (about 1 cm^{-1}), see Sect. 2.4. However, the $\pi \rightarrow \pi^*$ state T_2, with minimum at about 4.5 eV above S_0, is not far from S_1 and the SO coupling S_1/T_2 is not negligible (about 60 cm^{-1}). As a result, the triplet quantum yield of acetone is close to 1 (at least at excitation energies below the threshold for C-C bond dissociation, which is a process in competition with ISC).

Another remarkable difference is due to the fact that, for symmetry reasons, the $\boldsymbol{\mu}_{n\pi^*}$ is zero or close to zero. Hence the radiative transition from S_0 is (almost) dipole forbidden for $n \rightarrow \pi^*$ states (see Eq. (2.94)), at variance with the $\pi \rightarrow \pi^*$ states. Let us consider, for example, a carbonyl compound: the C=O group has a local C_{2v} symmetry, with n and π^* belonging to b_1 and b_2 irreducible representations, so $\boldsymbol{\mu}_{n\pi^*} = 0$ (see also Sect. 3.7). The C_{2v} symmetry may be disrupted by the groups linked to the carbonyl; however, $\boldsymbol{\mu}_{n\pi^*}$ will be small, as n and π^* are localized on the C=O, for a nonconjugated carbonyl compound. In the absorption spectrum the

$n \rightarrow \pi^*$ transitions have molar extinction coefficients roughly in the range $\varepsilon_{max} \approx$ 10–100 mol^{-1} L cm^{-1}, while for $\pi \rightarrow \pi^*$ states one may easily have $\varepsilon_{max} \approx 10^4$.

In the absorption spectrum of nonconjugated carbonyl compounds the $n \rightarrow \pi^*$ band is found at about 300 nm and usually has an extended vibrational structure. In fact, at variance with S_0 which has a planar structure, in the $n \rightarrow \pi^*$ state the carbon atom tends to pyramidalize, with an ibridation going from sp^2 to sp^3, due to the antibonding interaction of the π^* electron. The $\pi \rightarrow \pi^*$ band is usually found around 190 nm.

In compounds with a C=N or a N=N double bond (imines or azocompounds, respectively) the ground and the first excited states S_1 and T_1 show a behavior similar to that of Fig. 2.8 with respect to the torsion about the double bond. However, the energy gap between S_1 and T_1, which have $n \rightarrow \pi^*$ character, is smaller, while S_1 is normally lower in energy than in alkenes. For example, in azomethane the first absorption band has maximum at about 360 nm. In general, imines and azocompounds are not fluorescent and photoisomerize with a mechanism similar to that of alkenes.

2.6.6 *Excited States of Conjugated Systems*

The distinctive feature of a conjugated π system with $2n_c$ centers is that, being the π orbitals delocalized, the energy gap between two consecutive π orbitals (hence the HOMO-LUMO gap) decreases with n_c, in analogy with the levels of a particle in a box. The $\pi \rightarrow \pi^*$ transitions are therefore displaced at lower energies, as shown in Fig. 2.9. If present, $n \rightarrow \pi^*$ transitions show a similar behavior, but to a lesser extent (the energy of the n orbital being not affected by the extension of the π system). Therefore, increasing n_c, $n \rightarrow \pi^*$ and $\pi \rightarrow \pi^*$ bands tend to approach, with the $n \rightarrow \pi^*$ absorption disappearing below the more intense $\pi \rightarrow \pi^*$ one for n_c large enough. For that reason in Fig. 2.9 the plot is interrupted at $n_c = 3$ for $n \rightarrow \pi^*$ bands.

In aromatic compounds the first absorption band is again displaced to shorter wavelengths, because aromaticity stabilizes the ground state: for instance, the S_1 absorption band in hexatriene peaks at 270 nm, while in benzene it is found at about 250 nm. Moreover, the easy torsion of the double bonds in linear polyenes completely obscures the vibrational structure, which is instead quite apparent in the first absorption band of aromatic compounds. A quite analogous effect is instead the shift to longer wavelengths which is observed by extending the conjugated systems: from 250 nm in benzene we go to 270 nm in naphthalene, 345 nm in anthracene, and 470 nm in tetracene. Polycyclic aromatic hydrocarbons (PAH) are quite rigid, so the S_1 PES cannot get close to the S_0 one, as it does by double-bond torsion in linear polyenes. As a result, the S_1 lifetime is long and PAH compounds are often fluorescent, see Table 2.2.

In general $n \rightarrow \pi^*$ triplets have larger radiative transition rates with respect to $\pi \rightarrow \pi^*$ triplets. In fact, due to the El-Sayed rules, $n \rightarrow \pi^*$ triplet states are

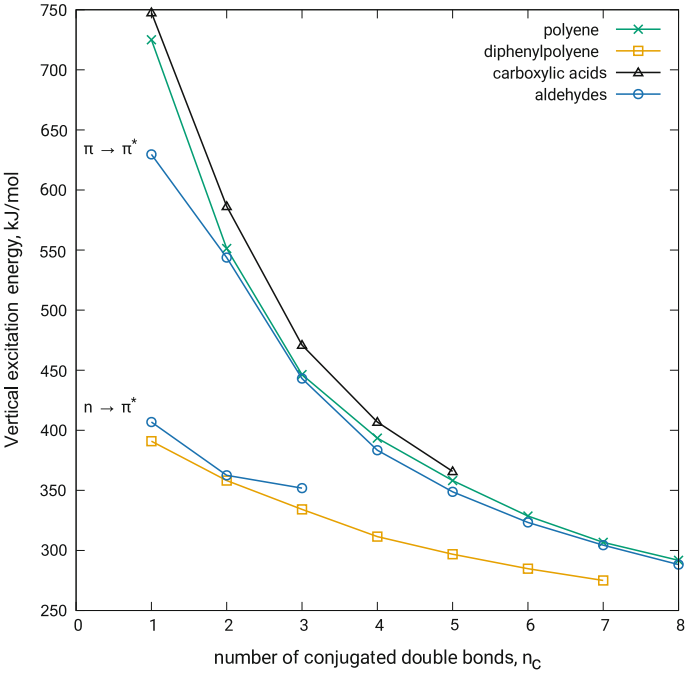

Fig. 2.9 Vertical transition energies $\pi \rightarrow \pi^*$ in conjugated systems, from absorption maxima. Simple polyenes, H(CH=CH)$_{n_c}$H; diphenylpolyenes, Ph-(CH=CH)$_{n_c}$-Ph; aldehydes, CH$_3$-(CH=CH)$_{n_c-1}$-CHO; carboxylic acids, CH$_3$-(CH=CH)$_{n_c-1}$-COOH. For aldehydes with n_c = 1-3, the $n \rightarrow \pi^*$ transition is shown as well. Data from [20]

Table 2.2 Photophysical properties of selected aromatic compounds in solution. τ_S is the singlet lifetime. Φ_F and Φ_T are the fluorescence and triplet quantum yields, respectively. Data from [21, 22]

Molecule	τ_S (ns)	Φ_F	Φ_T
Benzene	34	0.06	0.25
Naphthalene	96	0.19	0.75
Anthracene	6	0.27	0.71
Phenanthrene	57	0.14	0.73
Pyrene	650	0.65	0.37
Chrysene	45	0.12	0.85
Tetracene	6	0.17	0.62

more strongly coupled and therefore mixed with $\pi \rightarrow \pi^*$ singlets, which in turn have large transition dipoles with S_0. Therefore, molecules where S_1 and T_1 have $n \rightarrow \pi^*$ character usually have $\Phi_P \gg \Phi_F$ (where Φ_F and Φ_P are the fluorescence and phosphorescence quantum yields, respectively). This happens in many carbonyl compounds, especially the aromatic ones. For example, benzophenone has $\Phi_F \approx 10^{-5}$ and $\Phi_P \simeq 0.9$ (in rigid glasses at 77 K).

2.6.7 Charge Transfer States

Molecules containing electron-rich (donor, D) and electron-poor (acceptor, A) moieties are called push–pull systems. Considering A and D as separate entities, one expects for A a large electron affinity and for D a small ionization potential. In other words, the LUMO of A is particularly low in energy, while HOMO of D is particularly high. In these systems the first excited state usually corresponds to the transition HOMO(D) $\rightarrow$ LUMO(A): a charge transfer (CT) state. An organic chemistry example is represented by the so-called Reichardt's dye of Fig. 2.10, but this kind of excited states is very common in transition metal complexes, because different oxidation states of the metal center are accessible at relatively low energies.

If A and D belong to different molecules we may have intermolecular charge transfer states. An example is the A/D complex tetracyanoethylene/1,2,4,5-tetramethylbenzene. In this case the dipole moment, which is 1.3 D in the ground state, increases in the charge transfer state up to 11.6 D. The presence of the charge transfer state can be detected from the absorption spectrum, where a low energy band, not corresponding to localized excitations in A or D (or combinations of these) appears. The charge transfer band is usually broad and featureless, as the interaction between A and D is clearly quite different in the ground and in the CT state.

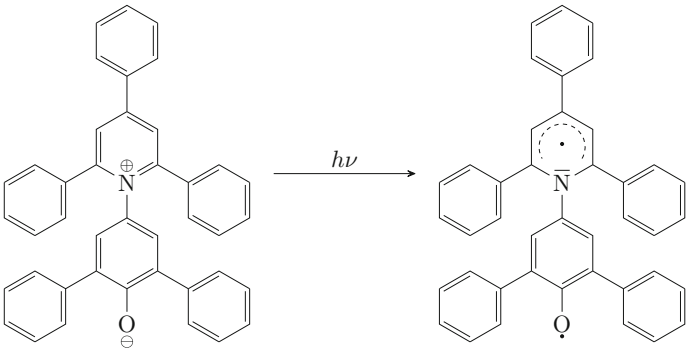

Fig. 2.10 Charge transfer in the Reichardt's dye (pyridynium N-phenolate betaine, PNPB). The ground-state dipole moment of PNPB is 15 D. Upon excitation it decreases in modulus to 6 D, reversing its direction

2.7 Unimolecular Photochemical Reactions in Organic Molecules

We give here a short account of the photochemical reactivity of organic molecules, considering only some of the main photochemical processes. More information on organic photochemistry can be found in Klán and Wirz [23] or Turro et al. [24].

2.7.1 Photoisomerization of Alkenes

In the ground state, the *cis–trans* isomerization in alkenes has a high activation energy (around 250 kJ/mol in monoalkenes, see Fig. 2.8) and requires therefore high temperatures, or the use of a catalyzer. In any case, in the end the (thermodynamic) equilibrium mixture of the two isomers is obtained. At variance, the photoisomerization is usually easy and fast, and both *cis* → *trans* and *trans* → *cis* photoisomerizations can be obtained. In particular, at the photostationary state, the ratio between the two isomers is given by (see Eq. (1.79))

$$\frac{[cis]}{[trans]} = \frac{\varepsilon_{trans}\Phi_{trans\to cis}}{\varepsilon_{cis}\Phi_{cis\to trans}} \tag{2.135}$$

and, as already observed in Sect. 1.6.4, may in principle be modified by tuning the excitation wavelength.

The quantum yields $\Phi_{trans\to cis}$ and $\Phi_{cis\to trans}$ depend mainly on the potential energy surfaces of S_0 and S_1. Typically one has $\Phi_{trans\to cis}$ and $\Phi_{cis\to trans}$ close to 0.5, with a slightly larger value for the reaction leading to the more stable isomer.

2.7.2 Electrocyclic Reactions

Alkenes with a conjugated π system may give rise to ring-closure and/or ring-opening "electrocyclic" reactions. In an electrocyclic ring-closure, n_c conjugated double bonds are reduced to $n_c - 1$, and a new σ bond is formed between the two terminal carbon atoms of the π system. These reactions may happen either thermally or photochemically. Clearly, in the latter case it is easy to obtain a photostationary state which is far from the thermodynamic equilibrium: in fact, the ring-opened compound, with an additional double bond, absorbs at longer wavelengths and can be selectively excited. To form the σ bond between the two terminal carbon atoms, the groups bonded to them have to move out of the plane of the conjugated π system. As shown in Fig. 2.11, that motion can be *conrotatory* or *disrotatory*, ending in two stereochemically distinct products.

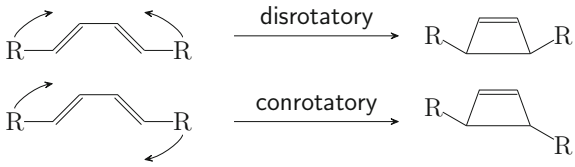

Fig. 2.11 Conrotatory and disrotatory ring-closure in an electrocyclic reaction

Table 2.3 Stereochemistry of an electrocyclic reaction

Electrons involved ($2n_c$)	Thermal reaction	Photochemical reaction
$4n$	Conrotatory	Disrotatory
$4n+2$	Disrotatory	Conrotatory

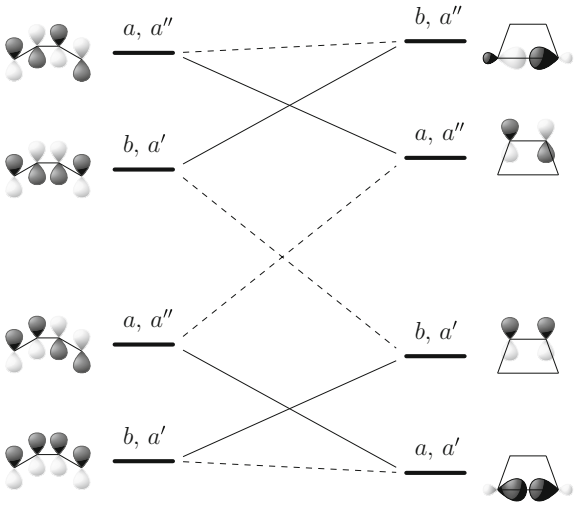

Fig. 2.12 Orbital correlation scheme for the electrocyclic ring-closure of a diene. The molecular orbitals involved are labeled according to the irreps of the C_2 and the C_s symmetry groups, which are relevant for conrotatory or disrotatory mechanism, respectively. The full lines connecting the orbitals of the reactant and the product refer to the conrotatory pathway, the dashed lines to the disrotatory one

Electrocyclic reactions are concerted processes. In fact, as shown in Table 2.3, there is a sharp correlation between the number of π electrons in the ring-opened system ($2n_c$) and the stereochemistry of the product. This correlation is different for photochemical and thermal reactions and can be explained by the Woodward–Hoffmann principle of conservation of orbital symmetry [25], as schematically shown in Fig. 2.12 for the butadiene/cyclobutene system. Note in fact that along a conrotatory (respectively, disrotatory) pathway a C_2 (respectively, C_s) symmetry is kept, and the orbital symmetry is conserved during the reaction. In particular, focussing on the photochemical process, the HOMO and LUMO (the second and third orbital in Fig. 2.12) are both occupied with one electron. Then an activation barrier is expected following the conrotatory path, where orbitals are labeled according to the irreps a and b of the C_s symmetry group, as the LUMO of the reactant correlates with LUMO+1 of the product. Conversely, the disrotatory mechanism appears to be favorable, as HOMO and LUMO of the reactant correlate with LUMO and HOMO of the product.

Quite the opposite is true for the thermal reaction, which prefers the conrotatory pathway. Note that symmetry conservation is just a way to identify which orbitals of the reactant can be gradually transformed into which orbitals of the reaction product. In fact, the orbital correlations can also be established without reference to symmetry, on the basis of continuous transformations along a reaction pathway.

2.7.3 Sigmatropic Reactions

In sigmatropic rearrangements one has a conjugated π system formed by carbon atoms C_2–C_{n_s} plus an aliphatic (sp^3) carbon atom C_1 connected to C_2: a hydrogen atom migrates from C_1 to C_{n_s} and the double bonds are displaced accordingly. Similar to the electrocyclic processes, sigmatropic rearrangements are concerted reactions, and one may have stereospecific thermal or photochemical sigmatropic rearrangements, with a stereochemical course depending on the number of electrons involved in the reaction, $n_s + 1$. For example, for a diene we have a thermal shift "[1, 5] supra"

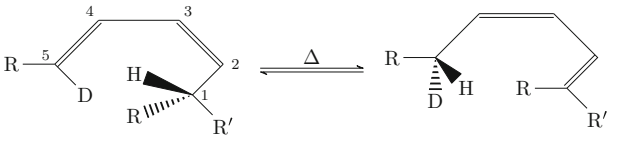

(2.136)

where, thanks to the deuteration, we can see that the hydrogen atom has migrated from C_1 to C_5 remaining on the same side of the molecular plane (*suprafacial* shift). A sigmatropic rearrangement where the hydrogen atom crosses the plane of the π system is called *antarafacial*.

The correlation between the number of electrons involved in the rearrangement (the $n_s - 1$ π and the two σ electrons of the C-H bond) and the stereochemistry is shown in Table 2.4. Being a concerted process, a sigmatropic rearrangement involves a cyclic intermediate with partly broken C_1-H and partly formed C_{n_s}-H bonds. Therefore an antarafacial shift is only possible if the molecule has an helicoidal twist such that C_1 and C_{n_s} can be found on top of each other. As a consequence, monoolefins are stable

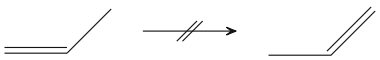

(2.137)

Table 2.4 Stereochemistry of a sigmatropic rearrangement

Electrons involved ($n_s + 1$)	Shift	Thermal reaction	Photochemical reaction
$4n$	[1, 3], [1, 7] ...	antara	supra
$4n + 2$	[1, 5], [1, 9] ...	supra	antara

as the shift [1, 3] cannot be antarafacial, and the photochemical shift [1, 3] supra would require UV light with $\lambda < 200$ nm.

The stereochemical behavior shown in Table 2.4 can be explained considering the cyclic intermediate referred above. In that system, HOMO and LUMO orbitals are obtained from the linear combination of the $1s$ orbital of the H atom which is transferred and the SOMO (singly occupied molecular orbital) of the remaining molecular fragment. In turn, the SOMO is a π orbital of a conjugated system with n_s centers and n_s electrons (note that in the intermediate C_1 and C_{n_s} belong to the π system, both contributing with one electron and a partly hybridated p orbital). In a suprafacial mechanism, a SOMO with an even number of nodes has a bonding interaction with the $1s$ orbital: in fact, in that case the linear combination of p orbitals which represents the SOMO is such that the p orbitals on C_1 and C_{n_s} are in phase. Noting that n_s is odd and the number of nodes in the SOMO is $(n_s - 1)/2$, we obtain the correlation Table 2.4 for thermal reactions. Concerning the photochemical process, one has to consider the interaction of the $1s$ orbital with SOMO+1, which of course has $(n_s + 1)/2$ nodes, yielding an inverted stereospecificity with respect to the thermal reaction.

The stereochemistry of a sigmatropic rearrangement in which atoms or groups different from hydrogen are transferred, can be analyzed in a similar way. However, if the unpaired electron of the migrating group is in a p orbital, as in the methyl radical, it can establish bonding interactions with p or hybrid orbitals of opposite signs on C_1 and C_{n_s}, so inverting the rules of Table 2.4.

2.7.4 Photodissociation of Carbonyl Compounds

The carbonyl compounds have a rich photochemistry. Here we focus on the "Norrish type I" reaction, which is the photodissociation of the C-C bond in α position with respect to C=O. In aliphatic aldehydes and ketones S_1 and T_1 have $n \rightarrow \pi^*$ character and are close in energy, with similar potential energy surfaces and efficient ISC. Therefore, the α-cleavage (as well as other photochemical processes) may take place either in S_1 or in T_1.

The Norrish type I reaction involves quite a complex rearrangement of molecular orbitals (see Fig. 2.13). In particular, considering the following α-cleavage

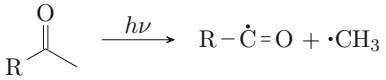

(2.138)

we have in short a mixing between the nonbonding p orbital of the oxygen atom ($p(O)$), singly occupied after the $n \rightarrow \pi^*$ transition, and the doubly occupied σ C-CH_3 bond ($\sigma(CC)$). At dissociation $p(O)$ is practically unaltered, but its occupation increases from 1 to 2 electrons. In other words, the singly occupied $p(O)$ behaves as an electrophilic center with respect to the $\sigma(CC)$ orbital, leading to the

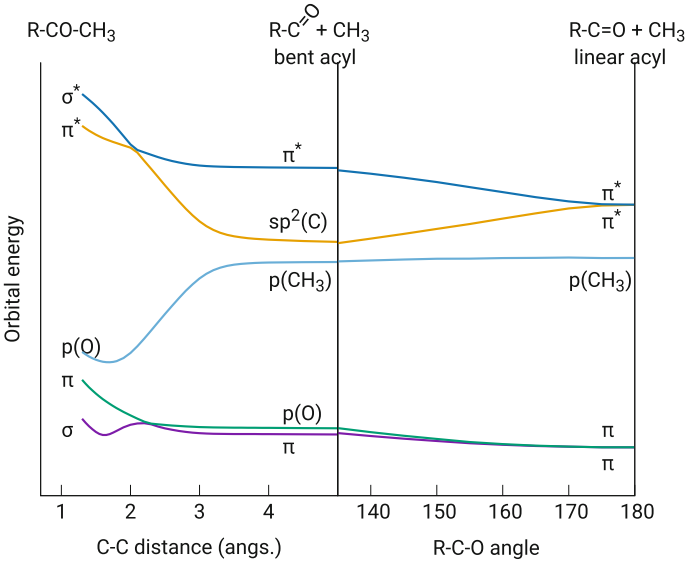

Fig. 2.13 Orbital correlation scheme for the Norrish type I reaction (2.138). The left panel describes the α-cleavage, ending with a bent R-C=O acyl group, which progressively becomes linear in the right panel

breaking of the C-C bond. The acyl radical R-C=O is bent in the ground state, with the unpaired electron in the sp^2 hybrid of the carbonylic C atom. It has a low-lying excited state where the unpaired electron occupies the π^* orbital. That excited state has a linear equilibrium geometry, where sp^2 becomes $p(C)$ which in turn mixes with $p(O)$ to give a pair of π, π^* orbitals. Hence, at the linear geometry the two states of the acyl radical are degenerate as the unpaired electron can choose between two equivalent π^* orbitals. This is a manifestation of the Renner–Teller effect, see Sect. 5.4.4.

The S_0 and T_1 states of the reactant correlate with the bent ground state of the acyl radical, while S_1 correlates with the linear excited state. Therefore, the potential energy surface of T_1 is normally more favorable to the photodissociation than that of S_1. Usually the primary process of Eq. (2.138) is followed by the second α-cleavage, which may lead to decarbonylation if the two radicals recombine.

The energy needed for the α-cleavage is close to the $S_0 \rightarrow S_1$ excitation energy of the carbonyl compound. Then, photodissociation is easily inhibited. In condensed phase, the small amount of excess vibrational energy in the excited state can be rapidly transferred to the environment (see Sect. 4.5), leading to the recombination of the radical pair: this is an example of solvent cage effect. As a rule, in small saturated ketones like acetone the photodissociation occurs in the gas phase but is inhibited in solution. Moreover, the α-cleavage does not occur in aromatic ketones, like benzophenone, where the C-C bond is stabilized by conjugation. Conversely, the photodissociation is easy in strained cyclic ketones (cyclobutanone, cyclopentanone) or if the radicals produced are particularly stable. For example

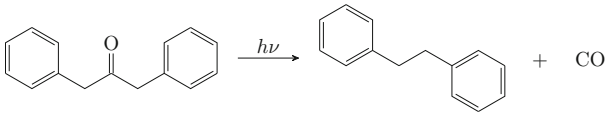

(2.139)

2.8 Solvent Effects on Absorption and Emission Spectra

The interaction with a solvent has an influence on the shape and the position of bands of a chromophore in electronic spectroscopy. As to the shape, the spectral bands of a molecule in solution are broader than in gas phase because of fluctuations in the solute-solvent interactions. In fact, such interactions change slightly among solute molecules and in time, and so do the energy differences between their electronic and vibrational levels. This is an important source of *inhomogeneous broadening*, meaning the broadening due to the inhomogeneous conditions experienced by the absorbing or emitting molecules (see Sect. 3.5). In this section, we will make some qualitative considerations about the shift in the absorption and emission bands of a solute in different solvents, a phenomenon called *solvatochromism*. For deeper and more extended discussions the interested reader is referred to references [26–28].

As discussed in Sect. 2.6, in organic molecules the electronic excited states involve electronic promotions to virtual orbitals (LUMO, LUMO+1, etc.) which are more diffuse with respect to the occupied orbitals. As a result, excited states have usually larger polarizabilities with respect to the ground state, thus stronger stabilization by van der Waals interaction with a solvent. This effect, always present, causes a red shift in the absorption and emission spectra. Dispersion interactions may be important, for instance, in the case of "stacked" aromatic molecules, where two polarizable π systems are close to each other. For polar molecules, electrostatic interactions are usually stronger and may override the red shift due to dispersion.

For a polar molecule, it is important to consider that the ground-state dipole moment $\boldsymbol{\mu}_0$ may differ from that of the excited state responsible of the absorption or the emission, $\boldsymbol{\mu}_e$. When the solute is in the ground state, the solvent molecules close to it are oriented in agreement to $\boldsymbol{\mu}_0$. In particular, $\boldsymbol{\mu}_0$ gives rise to a field which determines the induced dipole moments of the surrounding solvent molecules (and possibly orients the permanent dipoles, if the solvent is polar) in such a way to minimize the interaction energy. In turn, the solvent molecules give rise to a "reaction field" that polarizes the solute itself. Upon absorption the solute dipole moment suddenly changes to $\boldsymbol{\mu}_e$ and, in agreement with the Franck–Condon principle, the permanent dipole moments of the solvent are not able to quickly reorient. Instead, the induced dipoles of the solvent readjust almost instantaneously to the new dipole $\boldsymbol{\mu}_e$. The absorption spectrum is a snapshot of this nonequilibrium state. What happens in emission depend on the time required for the reorganization of solvent molecules around the solute: if this is short compared to the fluorescence lifetime, the solvent shell is in equilibrium with the emitter, stabilizing it and causing a red shift of the fluorescence, the entity of which depends on the solvent polarity (note that the

Table 2.5 Solvatochromic shifts of absorption bands. The maximum absorption wavelength (λ_{max}, nm) for the given band ($n \rightarrow \pi^*$, $\pi \rightarrow \pi^*$ or CT) is reported. PNPB is the molecule shown in Fig. 2.10, for which the color of the solution is indicated in parenthesis. ε_r is the dielectric constant of the solvent. Data from [26, 29]

Solvent		Pyrimidine	Benzophenone	Benzophenone	PNPB
Molecule	ε_r	$n \rightarrow \pi^*$	$n \rightarrow \pi^*$	$\pi \rightarrow \pi^*$	CT
n-hexane	1.89	–	347	248	–
Anisole	4.33	–	–	–	771 (yellow)
Ether	4.34	290	344	249	–
Acetone	20.7	–	–	–	667 (green)
Isopentanol	14.7	–	–	–	583 (blue)
Acetonitrile	37.5	287	339	251	–
Ethanol	25.1	–	332	252	550 (violet)
Methanol	32.6	280	331	253	516 (red)
Water	78.5	271	322	258	453

ground state will also be out of equilibrium after photon emission, so contributing to the red shift). This is what happens in many cases for fluorescent molecules in low viscosity solvents. Conversely, if the solvent relaxation is slow and/or the lifetime of the excited state is too short, the fluorescence is emitted from the nonequilibrium Franck–Condon state, with no shift due to reorganization.

In general, $n \rightarrow \pi^*$ transitions entail a sizeable decrease in polarity. In fact, in a $n \rightarrow \pi^*$ state an electron is displaced from a nonbonding orbital, usually localized in an outlying region, to a more central and delocalized orbital. Therefore, the interaction with the solvent stabilizes more the ground than the excited $n \rightarrow \pi^*$ state, and the resulting blue shift of the absorption band increases with the solvent polarity (see Table 2.5). Especially large blue shift are expected in protic solvents, where the n lone pair is involved in a hydrogen bond. This may lead to the inversion of $n \rightarrow \pi^*$ and $\pi \rightarrow \pi^*$ bands in solution. In particular, the S_1 state may change its nature from $n \rightarrow \pi^*$ in the gas phase to $\pi \rightarrow \pi^*$ in solution, with important consequences on the molecular photochemistry and photophysics. In fact, as we shall see in Sect. 3.11, fluorescence and other slow processes normally take place in the S_1 state (Kasha's rule). As an example, 1-pyrenecarboxaldehyde shows an increase of the fluorescence quantum yield by three orders of magnitude when changing the solvent from cyclohexane to methanol, because the emission rate of the $\pi \rightarrow \pi^*$ state is much higher than that of the $n \rightarrow \pi^*$ state [30].

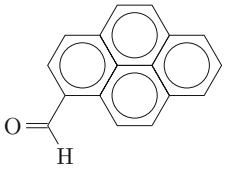

1-pyrenecarboxaldehyde

In acidic media the heteroatom that provides the n orbital may be protonated: in that limiting case the lone pair is not anymore available and the $n \rightarrow \pi^*$ band disappears. Of course, charge transfer transitions are strongly affected by the interaction with a polar solvent, due to the large difference between the ground and the excited state polarity, see Table 2.5. The Reichardt's dye of Fig. 2.10, thanks to its impressive solvatochromism, can be used as a polarity probe.

2.9 Computational Note: The Determination of Electronic Excited States

This short section is devoted to readers that are at least minimally acquainted with quantum chemistry methods. Excellent textbooks, both at introductory level [4, 31] and more advanced [7, 32], can be consulted for a deeper understanding of theory and techniques. Here we shall be concerned with the application of quantum chemistry to the determination of the properties of excited states and in particular of their PESs and spectra.

The simplest approximate method to solve the time-independent Schrödinger equation $\hat{H}_{el}\varphi = U\varphi$ for the electronic ground state of a molecular system is represented by the Hartree–Fock self consistent field (SCF) theory, where φ is written in the form of a single Slater determinant. Usually, the SCF method provides a good qualitative description of the ground state of organic molecules near to their equilibrium geometry. One could extend the SCF theory to excited states, however we know from Sect. 2.6 that in most cases an excited state cannot be represented by just one Slater determinant, so the Hartree–Fock approximation is normally qualitatively wrong for excited states. For the same reason, the SCF method cannot be used to obtain a potential energy surface: in fact, it behaves incorrectly at dissociation (see Sect. 2.6.2), close to a transition state, and in general in degeneracy situations, where it is mandatory to consider more than one Slater determinant.

The methods which build on the SCF determinant Φ_0 to obtain a more refined (ground state) wavefunction are called *single-reference*. Examples are single-reference configurations interaction (CI) and coupled cluster (CC). In most cases it is possible to obtain from these methods excited state wavefunctions and/or energies. However, the description is clearly biased in favor of the ground state (e.g., the molecular orbitals are optimized for it). Moreover, problems are expected in regions where the single determinant approximation is not valid.

To have a balanced treatment of ground and excited states one has to rely on *multireference* methods, which also allow for full PES exploration. In particular, the most used version of multiconfigurational SCF (MCSCF) is complete active space SCF (CASSCF), in which a set of active electrons and orbitals is defined, and a full CI within that set is performed. This is effective from the computational point of view and simplifies the choice of the configurations to include in the wavefunction. However, in many cases a valence CASSCF calculation gives too high $S_0 \rightarrow S_n$

Franck–Condon transition energies. Loosely speaking, this is due to the fact that normally, at the ground-state geometry, the ionic configurations are more important in the description of singlet excited states than for S_0. Now, in CASSCF the orbitals are optimized in an averaged field corresponding to a neutral charge distribution, and therefore are more suited to covalent than to ionic configurations [33, 34], thus introducing a bias in favor of S_0. This phenomenon may be especially important for $\pi \rightarrow \pi^*$ states (see Sect. 2.6.4), less for $n \rightarrow \pi^*$ states. To obtain quantitative agreement with experimental spectroscopic data, the CASSCF results can be refined either variationally, by multireference CI (MRCI) or, more commonly, perturbatively (using CASPT2 [35] or NEVPT2 [36]). However, due to the high computational cost of these multireference methods, their applicability is limited to small molecules (say, ∼20 second row atoms).

An alternative to ab initio methods is provided by density functional theory (DFT), a single-reference scheme for which excited state properties are available from the "time-dependent" approach (TD-DFT). Due to its low computational cost, TD-DFT is usually the method of choice for large systems, and in many cases, at geometries close to the ground-state minimum, gives results in good agreement with the best ab initio methods. At distorted geometries it suffers from the problems of single-reference methods mentioned above.

Problems

2.1 Consider a one dimensional system described by the following Hamiltonian

$$\hat{H}(x) = -\frac{\hbar^2}{2m}\frac{\mathrm{d}^2}{\mathrm{d}x^2} - Fx \qquad (F > 0)$$

appropriate, for example, for a particle of mass m and charge q in the presence of a constant electric field E_0 (in that case $F = qE_0$). Working in the momentum representation (use $x = \mathrm{i}\hbar\mathrm{d}/\mathrm{d}p$), evaluate the time evolution of a Gaussian wavepacket, i.e., find $\Psi(p,t)$ given $\Psi(p,0) = (2\alpha/\pi)^{-1/4}\exp(-\alpha p^2)$, with $\alpha > 0$.

2.2 The potential energy of a Morse oscillator is $V(x) = D(1 - \mathrm{e}^{-a(x-x_0)})^2$, where D is the well depth. The corresponding energy eigenvalues are

$$E_v = \hbar\omega(v + 1/2) + \frac{\hbar^2\omega^2}{4D}(v + 1/2)^2 \qquad \omega = a\sqrt{2D/m}$$

where $v = 0, 1, \ldots$ and m is the mass of the oscillator. Evaluate the density of states for a single Morse oscillator and use it to obtain a classical expression (i.e., without taking into account the quantization of energy) for the density of states of two noninteracting identical Morse oscillators.

2.3 In molecules where S_1 and T_1 are close in energy, the "inverse" ISC from T_1 to S_1 may be characterized by a non-negligible rate constant K_{invISC}. Compute K_{invISC} for acetone, according to the following data/assumptions: (i) the molecule is isolated, so that its energy is constant, and in particular $E = 1$ eV above the ZPE of T_1; (ii) the lifetimes of S_1 and T_1 are long enough to reach microcanonical equilibrium before decaying to S_0; (iii) the adiabatic (i.e., minimum-minimum) energy difference between S_1 and T_1 is $\Delta E = 0.25$ eV; (iv) S_1 and T_1 have the same vibrational frequencies; (v) the rate constant for the ISC $S_1 \rightarrow T_1$ is $K_{ISC} = 3.5\ \text{ns}^{-1}$.

2.4 Four different Slater determinants can be written with two electrons in two orbitals. The related matrix elements of H_{el} are

$$\left\langle \phi_i \wedge \overline{\phi}_i \left| \hat{H}_{el} \right| \phi_i \wedge \overline{\phi}_i \right\rangle = 2\varepsilon_i + J_{ii}$$
$$\left\langle \phi_i \wedge \overline{\phi}_j \left| \hat{H}_{el} \right| \phi_i \wedge \overline{\phi}_j \right\rangle = \varepsilon_i + \varepsilon_j + J_{ij}$$
$$\left\langle \overline{\phi_i} \wedge \phi_j \left| \hat{H}_{el} \right| \phi_i \wedge \overline{\phi}_j \right\rangle = -K_{ij}$$

with $i, j = 1, 2$ and where ϕ_i (respectively, $\overline{\phi}_i$) label a spin-orbital with spin part α (respectively, β). ε_i are the orbital energies ($\varepsilon_1 \leq \varepsilon_2$). J_{ij} are the Coulomb integrals, representing the electrostatic repulsion between the two charge clouds $|\phi_i|^2$ and $|\phi_j|^2$. K_{12} is the exchange integral, see Eq. (2.93). Both the Coulomb and the exchange integrals are positive quantities and we assume $J_{ii} > J_{ij}$. Write φ_{S_0}, φ_{S_1} and φ_{T_1} in terms of the three Slater determinants $\phi_1 \wedge \overline{\phi}_1$, $\phi_1 \wedge \overline{\phi}_2$, and $\overline{\phi}_1 \wedge \phi_2$. Evaluate the corresponding energies. Which one is the ground state when the two orbitals are degenerate (i.e., $\varepsilon_1 = \varepsilon_2$)?

References

1. Merzbacher, E.: Quantum Mechanics. Wiley, New York (1998)
2. Sakurai, J., Napolitano, J.: Modern Quantum Mechanics. Cambridge University Press, Cambridge (2017)
3. Atkins, P.W., Friedman, R.S.: Molecular Quantum Mechanics. Oxford University Press, Oxford (2010)
4. Levine, I.N.: Quantum Chemistry. Pearson, Cambridge (2014)
5. Michl, J., Bonačić-Koutecký, V.: Electronic Aspects of Organic Photochemistry. Wiley, New York (1990)
6. Klessinger, M., Michl, J.: Excited States and Photochemistry of Organic Molecules. VCH, New York (1995)
7. McWeeny, R.: Methods of Molecular Quantum Mechanics. Academic Press, London (1992)
8. de Graaf, C., Broer, R.: Magnetic Interactions in Molecules and Solids. Springer, Cham (2016)
9. Greiner, W.: Quantum Mechanics. An Introduction. Springer, Heidelberg (2000)
10. Greiner, W.: Relativistic Quantum Mechanics. Wave Equations. Springer, Heidelberg (2000)
11. Li, Z., Xiao, Y., Liu, W.: On the spin separation of algebraic two-component relativistic Hamiltonians. J. Chem. Phys. **137**, 154114 (2012)

12. van Lenthe, E., Snijders, J.G., Baerends, E.J.: The zero-order regular approximation for relativistic effects: the effect of spin-orbit coupling in closed shell molecules. J. Chem. Phys. **105**, 6505–6516 (1996)
13. Nakajima, T., Hirao, W.: The Douglas-Kroll-Hess approach. Chem. Rev. **112**, 385–402 (2012)
14. Marian, C.M.: Spin-orbit coupling and intersystem crossing in molecules. WIREs Comput. Mol. Sci. **2**, 187–203 (2012)
15. Holbrook, K.A., Pilling, M.J., Robertson, S.H.: Unimolecular Reactions. Wiley, Chichester (1996)
16. Tolman, R.C.: The Principles of Statistical Mechanics. Dover, Mineola (1979)
17. Beyer, T., Swinehart, D.F.: Algorithm 448. Number of multiply-restricted partitions. Comm. ACM **16**, 379 (1973)
18. Mota, R., Parafita, R., Giuliani, A., Hubin-Franskin, M.-J., Lourenço, J.M.C., Garcia, G., Hoffmann, S.V., Mason, N.J., Ribeiro, P.A., Raposo, M., Limão-Vieira, P.: Water VUV electronic state spectroscopy by synchrotron radiation. Chem. Phys. Lett. **416**, 152–159 (2005)
19. Rubio, M., Serrano-Andrés, L., Merchán, M.: Excited states of the water molecule: analysis of the valence and Rydberg character. J. Chem. Phys. **128**, 104305 (2008)
20. Jaffé, H.H., Orchin, M.: Theory and Applications of Ultraviolet Spectroscopy. Wiley, New York (1962)
21. Montalti, M., Credi, A., Prodi, L., Gandolfi, M.T.: Handbook of Photochemistry. CRC Press, Boca Raton (2006)
22. Dabestani, R., Ivanov, I.N.: A compilation of physical, spectroscopic and photophysical properties of polycyclic aromatic hydrocarbons. Photochem. Photobiol. **70**, 10–34 (1999)
23. Klán, P., Wirz, J.: Photochemistry Of Organic Compounds: From Concepts to Practice. Wiley, Chichester (2009)
24. Turro, N.J., Ramamurthy, V., Scaiano, J.C.: Modern Molecular Photochemistry of Organic Molecules. University Science Books, Sausalito (2010)
25. Hoffmann, R., Woodward, R.B.: Conservation of orbital symmetry. Acc. Chem. Res. **1**, 17–22 (1968)
26. Reichardt, C., Welton, T.: Solvents and Solvent Effects in Organic Chemistry. Wiley-VCH, Weinheim (2011)
27. Lakowicz, J.R.: Principles of Fluorescence Spectroscopy. Springer, New York (2006)
28. Mennucci, B., Cammi, R. (eds.): Continuum Solvation Models in Chemical Physics. Wiley, Chichester (2007)
29. Baba, H., Goodman, L., Valenti, P.C.: Solvent effects on the fluorescence spectra of diazines. Dipole moments in the (n,π^*) excited states. J. Am. Chem. Soc. **88**, 5410–5415 (1966)
30. Kumar, ChV, Chattopadhyay, S.K., Das, P.K.: A laser flash photolysis study of pyrene-1-aldehyde. Intersystem crossing efficiency, photoreactivity and triplet state properties in various solvents. Photochem. Photobiol. **38**, 141–152 (1983)
31. Szabo, A., Ostlund, N.S.: Modern Quantum Chemistry. Introduction to Advanced Electronic Structure Theory. Dover, Mineola (1996)
32. Helgaker, T., Jørgensen, P., Olsen, J.: Molecular Electronic-Structure Theory. Wiley, Chichester (2000)
33. Hiberty, P.C., Humbel, S., Byrman, C.P., van Lenthe, J.H.: Compact valence bond functions with breathing orbitals: application to the bond dissociation energies of F_2 and FH. J. Chem. Phys. **101**, 5969–5976 (1994)
34. Schmidt, M.W., Gordon, M.S.: The construction and interpretation of MCSCF wavefunctions. Annu. Rev. Phys. Chem. **49**, 233–266 (1998)
35. Andersson, K., Malmqvist, P., Roos, B.O.: Second-order perturbation theory with a complete active space self-consistent field reference function. J. Chem. Phys. **96**, 1218–1226 (1992)
36. Angeli, C., Pastore, M., Cimiraglia, R.: New perspectives in multireference perturbation theory: the n-electron valence state approach. Theor. Chem. Acc. **117**, 743–754 (2007)

Chapter 3
Electronic Excitation and Decay

Abstract This chapter deals with the optical excitation processes that bring about transitions between electronic states and with some of the dynamical processes that may follow. The excited states created by photon absorption can be nonstationary under two basic aspects: first, they can undergo radiationless electronic transitions (nonadiabatic dynamics), and second, internal motions can occur in the new potential energy surface as the nuclear wavefunction or "wavepacket" evolves in time (adiabatic dynamics). After presenting the basic aspects of optical excitation, in this chapter we shall consider the slow radiationless transitions between electronic states caused by nonadiabatic or spin–orbit couplings. The adiabatic dynamics, i.e., the nuclear motion in a single potential energy surface, will be dealt with in the next chapter. Finally, in Chap. 5 we shall tackle the ultrafast nonadiabatic transitions that occur when two or more PESs are close in energy. In such events, the nonadiabatic dynamics and the nuclear motion are inextricably coupled. To begin with, we shall introduce and make use of some important formalisms, such as the time-dependent perturbation theory or the relationship between autocorrelation functions and spectra. In presenting such concepts and tools, we shall focus rather on their physical meaning and their applicability to real phenomena, than on the mathematical formalism.

Keywords Rabi oscillations · Time dependent perturbation theory
Autocorrelation function · Franck-Condon factors · Fermi golden rule
Quasi-continuum

3.1 Constant and Time-Dependent Perturbations

Several common phenomena in molecular physics can be described as a system, initially in a stationary state, being perturbed by an external force that drives a dynamical response. For instance, the source of perturbation can be a static electric or magnetic field, a light pulse, or the interaction with an approaching molecule. If we call $\hat{H}^{(0)}$ the Hamiltonian of the unperturbed system, and $\hat{V}$ the perturbation, then the complete Hamiltonian is

$$\hat{H} = \hat{H}^{(0)} + \hat{V} \tag{3.1}$$

M. Persico and G. Granucci, *Photochemistry*, Theoretical Chemistry
and Computational Modelling, https://doi.org/10.1007/978-3-319-89972-5_3

A formally similar situation can also be found in the absence of external perturbations, when the full molecular Hamiltonian is split in two terms, $\hat{H}^{(0)}$ and $\hat{V}$, and one can assume the initial state to be an eigenstate $\left|\psi_i^{(0)}\right\rangle$ of $\hat{H}^{(0)}$:

$$\hat{H}^{(0)} \left|\psi_i^{(0)}\right\rangle = \varepsilon_i \left|\psi_i^{(0)}\right\rangle . \tag{3.2}$$

Let us write the time-dependent wavefunction as a linear combination of the $\psi_j^{(0)}$ eigenstates:

$$|\psi(t)\rangle = \sum_j c_j(t)\, \mathrm{e}^{-\mathrm{i}\varepsilon_j t/\hbar} \left|\psi_j^{(0)}\right\rangle . \tag{3.3}$$

As we know from Sect. 2.1.2, without the perturbation $\hat{V}$ this expression would represent the time evolution of the system with constant coefficients: $c_j(t) = c_j(0)$. By using this expansion, the time-dependent Schrödinger equation

$$\mathrm{i}\hbar \frac{\mathrm{d}}{\mathrm{d}t} |\psi(t)\rangle = \hat{H} \ |\psi(t)\rangle \tag{3.4}$$

becomes

$$\sum_j \left[\dot{c}_j - \frac{\mathrm{i}\varepsilon_j}{\hbar} c_j\right] \mathrm{e}^{-\mathrm{i}\varepsilon_j t/\hbar} \left|\psi_j^{(0)}\right\rangle = -\frac{\mathrm{i}}{\hbar} \sum_j c_j \ \mathrm{e}^{-\mathrm{i}\varepsilon_j t/\hbar} \left[\varepsilon_j + \hat{V}\right] \left|\psi_j^{(0)}\right\rangle . \tag{3.5}$$

Thanks to the introduction of the exponential factors $\exp(-\mathrm{i}\varepsilon_j t/\hbar)$ in Eq. (3.3) the terms $-\mathrm{i}\varepsilon_j c_j/\hbar$ cancel out. We can single out the time derivative of coefficient c_i by multiplying on the left both members of this equation by $\left\langle\psi_i^{(0)}\right|$:

$$\dot{c}_i = -\frac{\mathrm{i}}{\hbar} \sum_j c_j \ \mathrm{e}^{\mathrm{i}\omega_{ij} t} \ V_{ij} \qquad \forall\, i \tag{3.6}$$

where

$$V_{ij} = \left\langle\psi_i^{(0)}\right| \hat{V} \left|\psi_j^{(0)}\right\rangle \tag{3.7}$$

and

$$\omega_{ij} = \frac{\varepsilon_i - \varepsilon_j}{\hbar} . \tag{3.8}$$

The (3.6) are a set of coupled equations, one for each c_i coefficient, the solution of which yields the full information about the time evolution of the system. The squared module of each coefficient in the development (3.3), $P_i = |c_i(t)|^2$, is the probability of finding the system in state $\psi_i^{(0)}$ at time t, also called the state population. When the probability P_i increases in time, we say that transitions occur from other states $\psi_j^{(0)}$ to state $\psi_i^{(0)}$. According to Eq. (3.6) this is possible only when at least one other

$\psi_j^{(0)}$ state is populated (i.e., $c_j \neq 0$) and $V_{ij} \neq 0$. This is the basis of all "selection rules," in spectroscopy as in other aspects of molecular dynamics. When $V_{ij} \neq 0$ we say that the perturbation $\hat{V}$ "couples" states $\psi_i^{(0)}$ and $\psi_j^{(0)}$. The V_{ij} matrix element is called the "coupling" or "interaction" between the two states.

Notice that, as far as $\hat{H}^{(0)} \neq \hat{H}$, the quantity $\sum_j \left|c_j\right|^2 \varepsilon_j$ is not the total energy of the system; at best, it is an approximation of it, valid for small couplings V_{ij}. However, if $\hat{V}$ depends on time, there may be times at which $\hat{H}^{(0)}$ coincides with the total Hamiltonian. For instance, if the system is perturbed by a light pulse, before the pulse is switched on and after it dies off we have $\hat{V} = 0$: so, the $\left|c_j\right|^2$ probabilities correctly describe the molecular energy distributions before and after the interaction with the light pulse.

3.2 Light–Molecule Interaction

Since we are particularly interested in the light absorption process, we shall consider the case where $\hat{V}$ is the radiation–molecule interaction. Molecules interact with light mainly through the electric field. Consider, for instance, electric and magnetic dipoles with the usual orders of magnitude of 1 a.u., i.e., respectively, two proton/electron charges separated by 1 bohr, and the orbital or spin angular momentum of an electron. Since the field magnitudes in Eqs. (1.1) and (1.2) are related by $E_0 = cB_0$, the field-dipole interaction is about 100 times larger for the electric field than for the magnetic one. As we shall see, the effect of such perturbations in many circumstances is proportional to the square of the interaction, so the electric field of light affects a molecule about 10^4 times more than the magnetic field.

The interaction energy of a molecule with a time- and space-dependent electric field is, in atomic units

$$\hat{V} = -\sum_\alpha Z_\alpha \mathbf{r}_\alpha \cdot \mathbf{E}(\mathbf{r}_\alpha, t) + \sum_i \mathbf{r}_i \cdot \mathbf{E}(\mathbf{r}_i, t) \tag{3.9}$$

where α numbers the nuclei and i the electrons. For UV, visible or NIR light of interest in photochemistry, the wavelengths we consider are larger than 100 nm, i.e., much larger than many molecules or at least of the part of a molecule where the excitation is localized. As a consequence, in Eq. (3.9) we can replace $\mathbf{E}(\mathbf{r}_i, t)$ with its value at an arbitrary location $\mathbf{r}_0$ within the molecule, for instance, its center of mass. Then, we shall drop the dependence on position and write

$$\hat{V} = -\boldsymbol{\mu} \cdot \mathbf{E}(t) \tag{3.10}$$

where

$$\boldsymbol{\mu} = \sum_\alpha Z_\alpha \mathbf{r}_\alpha - \sum_i \mathbf{r}_i \tag{3.11}$$

is the molecular dipole. For obvious reasons, this is called the dipolar approximation. The matrix elements V_{ij} are then related to the dipole matrix elements $\boldsymbol{\mu}_{ij} = \left\langle \psi_i^{(0)} \left| \boldsymbol{\mu} \right| \psi_j^{(0)} \right\rangle$:

$$V_{ij} = -\boldsymbol{\mu}_{ij} \cdot \mathbf{E}(t) \ . \tag{3.12}$$

For simplicity, we shall consider a linearly polarized wave, Eq. (1.1), dropping the constant term $-\mathbf{k} \cdot \mathbf{r}_0$ that can be incorporated in the phase φ:

$$\mathbf{E}(t) = \mathbf{E}_0 \ \cos(\omega t - \varphi) \ . \tag{3.13}$$

The phase may be important in particular conditions (light pulses with a duration of few optical cycles or, more generally, radiation very suddenly switched on or off). In such cases, one must remember that molecules in different positions will experience different electric fields because of the term $-\mathbf{k} \cdot \mathbf{r}_0$ included in φ. More general formulations can be envisaged, e.g., the elliptic or circular polarization as in Eq. (1.3).

In some of the following sections we shall focus on radiation pulses, described by a vector $\mathbf{E}_0(t)$ (the "pulse envelope") that depends on time, usually with a much slower variation with respect to $\cos(\omega t)$. If $E_0(t)$ tends to zero for $t \to \pm\infty$ fast enough, its Fourier transform

$$\tilde{\mathbf{E}}_0(\Delta\omega) = (2\pi)^{-1/2} \int_{-\infty}^{+\infty} \mathbf{E}_0(t) \ \mathrm{e}^{-\mathrm{i}\Delta\omega t} \ \mathrm{d}t \tag{3.14}$$

together with the carrier frequency ω, defines the spectrum of the radiation pulse:

$$\tilde{\mathbf{E}}(\omega') = \frac{1}{2} \left[\mathrm{e}^{\mathrm{i}\varphi} \tilde{\mathbf{E}}_0(\omega' + \omega) + \mathrm{e}^{-\mathrm{i}\varphi} \tilde{\mathbf{E}}_0(\omega' - \omega) \right] \tag{3.15}$$

(each component of a time-dependent vector is independently Fourier transformed). Notice that, if $E_0(t)$ is a smoothly varying function, $\tilde{\mathbf{E}}_0(\Delta\omega)$ will peak around $\Delta\omega = 0$. Then, the frequency distribution expressed by Eq. (3.15) will have two peaks, one due to the term $\tilde{\mathbf{E}}_0(\omega' + \omega)$ at $\omega' \simeq -\omega$ and the other due to the term $\tilde{\mathbf{E}}_0(\omega' - \omega)$ at $\omega' \simeq \omega$. We can define the duration of the pulse in various ways, for instance, as the full width at half maximum (FWHM_t) of the function $E_0^2(t)$. Similarly, we have a width FWHM_ω in the frequency domain, by considering the FWHM of the function $\left| \tilde{\mathbf{E}}_0(\Delta\omega) \right|^2$. If the pulse envelope is modified by a scaling factor α to $E_0(\alpha t)$, the pulse duration changes to FWHM_t/α and the frequency width to $\alpha \ \mathrm{FWHM}_\omega$. So, for a given pulse shape, longer pulses correspond to narrower frequency distributions and the product $\mathrm{FWHM}_t \ \mathrm{FWHM}_\omega$ is not altered by scaling.

3.3 The Two-State Model: Rabi Oscillations

We shall first tackle an exactly solvable model, involving two states $\psi_1^{(0)}$ and $\psi_2^{(0)}$ with a constant interaction. For simplicity, we assume the diagonal elements of the perturbation $\hat{V}$ to vanish: $\left\langle \psi_i^{(0)} \middle| \hat{V} \middle| \psi_i^{(0)} \right\rangle = 0$ (this requirement could be relaxed without spoiling the exact solvability of the model). The off-diagonal matrix elements of $\hat{V}$ will be called $V_{12} = V$ and $V_{21} = V^*$. The coupled equations (3.6) reduce to

$$\begin{cases} \dot{c}_1 = -\mathrm{i}\hbar^{-1}\, c_2\, V\, \mathrm{e}^{-\mathrm{i}\omega_{21}t} \\ \dot{c}_2 = -\mathrm{i}\hbar^{-1}\, c_1\, V^*\, \mathrm{e}^{\mathrm{i}\omega_{21}t} \end{cases} \tag{3.16}$$

By differentiating both equations we get

$$\begin{cases} \ddot{c}_1 = -\hbar^{-1}\, [\mathrm{i}\dot{c}_2 + c_2\omega_{21}]\, V\, \mathrm{e}^{-\mathrm{i}\omega_{21}t} \\ \ddot{c}_2 = -\hbar^{-1}\, [\mathrm{i}\dot{c}_1 - c_1\omega_{21}]\, V^*\, \mathrm{e}^{\mathrm{i}\omega_{21}t} \end{cases} \tag{3.17}$$

In the right hand sides c_1, c_2, $\dot{c}_1$ and $\dot{c}_2$ can be replaced by expressions obtained from Eq. (3.16), in order to decouple the differential equations for the two coefficients:

$$\begin{cases} \ddot{c}_1 = -\dfrac{|V|^2}{\hbar^2}\, c_1 - \mathrm{i}\omega_{21}\dot{c}_1 \\ \ddot{c}_2 = -\dfrac{|V|^2}{\hbar^2}\, c_2 + \mathrm{i}\omega_{21}\dot{c}_2 \end{cases} \tag{3.18}$$

Notice that such a decoupling operation is not warranted for more than two states. A solution of each of these equations can be sought in the form of an exponential function. For instance, by trying $c_1 = \exp(\mathrm{i}\Omega t)$ in the first equation, one obtains the condition

$$\Omega^2 + \omega_{21}\Omega - \frac{|V|^2}{\hbar^2} = 0\,. \tag{3.19}$$

This condition is satisfied for two values of Ω:

$$\Omega_\pm = \frac{1}{2}\left[-\omega_{21} \pm (\omega_{21}^2 + 4\,|V|^2/\hbar^2)^{1/2}\right]\,. \tag{3.20}$$

The same is obtained for the second equation, except that the sign of $\Omega\pm$ is reversed. Since there are two solutions, with $\pm\Omega_+$ and $\pm\Omega_-$, for each equation, the general solutions are

$$\begin{cases} c_1 = A_+\mathrm{e}^{\mathrm{i}\Omega_+ t} + A_-\mathrm{e}^{\mathrm{i}\Omega_- t} \\ c_2 = B_+\mathrm{e}^{-\mathrm{i}\Omega_+ t} + B_-\mathrm{e}^{-\mathrm{i}\Omega_- t} \end{cases} \tag{3.21}$$

However, the c_1 and c_2 coefficients are related through Eq. (3.16) and the normalization of the wavefunction. Suppose the system at $t = 0$ is in state $\psi_1^{(0)}$, i.e., $c_1 = 1$ and $c_2 = 0$. Then $A_+ + A_- = 1$ and $B_+ = -B_-$. By substitution either in the first or in the second of Eq. (3.16) one finds:

$$A_+ = -\frac{\Omega_-}{\Omega_+ - \Omega_-}, \quad A_- = \frac{\Omega_+}{\Omega_+ - \Omega_-}, \quad B_- = -B_+ = \frac{\hbar}{V}\frac{\Omega_+\Omega_-}{\Omega_+ - \Omega_-} \ . \tag{3.22}$$

Then, the population of the "final" state $\psi_2^{(0)}$ turns out to be

$$P_2(t) = |c_2(t)|^2 = \frac{4\,|V|^2}{\Delta\varepsilon^2 + 4\,|V|^2} \ \sin^2\left(\frac{\Omega_R\, t}{2}\right) \ . \tag{3.23}$$

Here $\Delta\varepsilon = \hbar\omega_{21} = \varepsilon_2 - \varepsilon_1$ and

$$\Omega_R = \hbar^{-1}\sqrt{\Delta\varepsilon^2 + 4\,|V|^2} \tag{3.24}$$

is called the Rabi frequency. Of course $|c_1(t)|^2 = 1 - |c_2(t)|^2$. We see that the final state populations oscillate in time with a period $2\pi/\Omega_R$. After half a period P_2 reaches for the first time its maximum

$$P_{max} = P_2(\pi/\Omega_R) = \frac{4\,|V|^2}{\Delta\varepsilon^2 + 4\,|V|^2} = \frac{1}{\alpha^2 + 1} \tag{3.25}$$

which is a Lorentzian function of the parameter $\alpha = \Delta\varepsilon/|2V|$. For $|V| \gg |\Delta\varepsilon|$ the population approaches 1, but only with $\Delta\varepsilon = 0$ (degenerate states) can we obtain a complete switch to the final state ("population inversion"). Note that the long-time average (or the average over a period $2\pi/\Omega_R$) of P_2 is just half of P_{max}, so it depends on α in the same way.

$\hbar\Omega_R$ is simply the energy difference between the eigenvalues of the two-state Hamiltonian (see Appendix A). In fact, the oscillatory behavior of the state populations in the two-state model is the simplest example of a general rule: if the eigenenergies E_J of the populated eigenstates $|\Psi_J\rangle$ are equispaced, i.e., $E_{J+1} = E_J + \Delta E$, then all the properties of the system oscillate in time with a frequency that depends on the energy spacing ΔE. In fact, the time-dependent wavefunction is

$$|\Psi(t)\rangle = \sum_J |\Psi_J\rangle\,\langle\Psi_J\,|\Psi(0)\rangle\ \mathrm{e}^{-\mathrm{i}E_J t/\hbar} \tag{3.26}$$

and the expectation value of an observable $\hat{A}$ is

$$\left\langle\Psi(t)\left|\hat{A}\right|\Psi(t)\right\rangle = \sum_{J,J'} \langle\Psi(0)\,|\Psi_J\rangle\left\langle\Psi_J\left|\hat{A}\right|\Psi_{J'}\right\rangle\langle\Psi_{J'}\,|\Psi(0)\rangle\,\mathrm{e}^{-\mathrm{i}\Delta E(J'-J)t/\hbar} \ . \tag{3.27}$$

All the time-dependent factors $\exp[-\mathrm{i}\Delta E(J'-J)t/\hbar]$ share the common period $T = 2\pi\hbar/\Delta E$, corresponding to the frequency $\Omega = \Delta E/\hbar$, so the same value of any given property recurs after a time interval T.

It is easy to extend the above results (3.23) and (3.24) to the case of a periodic perturbation, but then an approximation is needed to get a closed-form solution. If

$$V_{12}(t) = W\ \cos(\omega t - \varphi) = \frac{W}{2}\ \left(\mathrm{e}^{\mathrm{i}(\omega t-\varphi)} + \mathrm{e}^{-\mathrm{i}(\omega t-\varphi)}\right) \tag{3.28}$$

Eq. (3.16) are replaced by

$$\begin{cases} \dot{c}_1 = -\mathrm{i}\hbar^{-1}\ c_2\ \dfrac{W}{2}\ \left[\mathrm{e}^{-\mathrm{i}(\omega_{21}-\omega)t}\mathrm{e}^{-\mathrm{i}\varphi} + \mathrm{e}^{-\mathrm{i}(\omega_{21}+\omega)t}\mathrm{e}^{\mathrm{i}\varphi}\right] \\ \dot{c}_2 = -\mathrm{i}\hbar^{-1}\ c_1\ \dfrac{W}{2}\ \left[\mathrm{e}^{\mathrm{i}(\omega_{21}-\omega)t}\mathrm{e}^{\mathrm{i}\varphi} + \mathrm{e}^{\mathrm{i}(\omega_{21}+\omega)t}\mathrm{e}^{-\mathrm{i}\varphi}\right] \end{cases} \tag{3.29}$$

If $\omega \simeq \omega_{21} > 0$, the exponentials $\mathrm{e}^{\pm\mathrm{i}(\omega_{21}+\omega)t}$ oscillate at a much larger frequency than $\mathrm{e}^{\pm\mathrm{i}(\omega_{21}-\omega)t}$. The high-frequency terms integrate to almost zero, so their contributions to $c_i(t)$ after several optical cycles can be neglected: this is called the "rotating wave approximation" (RWA). Vice versa, with $\omega_{21} < 0$ the RWA consists in neglecting the high-frequency terms $\mathrm{e}^{\pm i(\omega_{21}-\omega)t}$. With only one exponential term left, Eq. (3.29) shows the same structure as (3.16):

$$\begin{cases} \dot{c}_1 = -\mathrm{i}\hbar^{-1}\ c_2\ \dfrac{W}{2}\ \mathrm{e}^{\pm\mathrm{i}\varphi}\ \mathrm{e}^{-\mathrm{i}(\omega_{21}\pm\omega)t} \\ \dot{c}_2 = -\mathrm{i}\hbar^{-1}\ c_1\ \dfrac{W}{2}\ \mathrm{e}^{\mp\mathrm{i}\varphi}\ \mathrm{e}^{\mathrm{i}(\omega_{21}\pm\omega)t} \end{cases} \tag{3.30}$$

These equations would be identical to the (3.16) by replacing V with $W\mathrm{e}^{\pm\mathrm{i}\varphi}/2$ and ω_{21} with $\omega_{21} \pm \omega$ (here the $\pm$ sign is opposite to the sign of ω_{21}). Then, the final state population is

$$P_2(t) = \frac{W^2}{\hbar^2\Delta\omega^2 + W^2}\ \ \sin^2\left(\frac{\Omega_R\ t}{2}\right)\ . \tag{3.31}$$

Here, the Rabi frequency is

$$\Omega_R = \sqrt{\Delta\omega^2 + W^2/\hbar^2} \tag{3.32}$$

and $\Delta\omega = \omega - |\omega_{21}|$ will be called the detuning of the radiation frequency with respect to the transition frequency. The maximum population P_{max} of the final state is still given by the Lorentzian function of Eq. (3.25), but here $\alpha = \hbar\Delta\omega/W$. The population inversion is obtained only when the resonance condition $\Delta\omega = 0$ is met: this means that the absorbed photon energy $\hbar\omega$ equals the energy gap $|\Delta\varepsilon|$. However, the final state can be populated at nonresonant frequencies, and the tolerance on the detuning can be measured as the half-width at half maximum (HWHM) of the Lorentzian (3.25), which is $\mathrm{HWHM}_\omega = |W|/\hbar$. So, a stronger molecule-radiation coupling corresponds to a broader lineshape in the frequency domain. The time needed to reach the maximum P_2 population at resonance is $\Delta t = \pi/\Omega_R = \pi\hbar/|W|$. In other words, we need a "rectangular pulse" of this duration, called a "π pulse," to

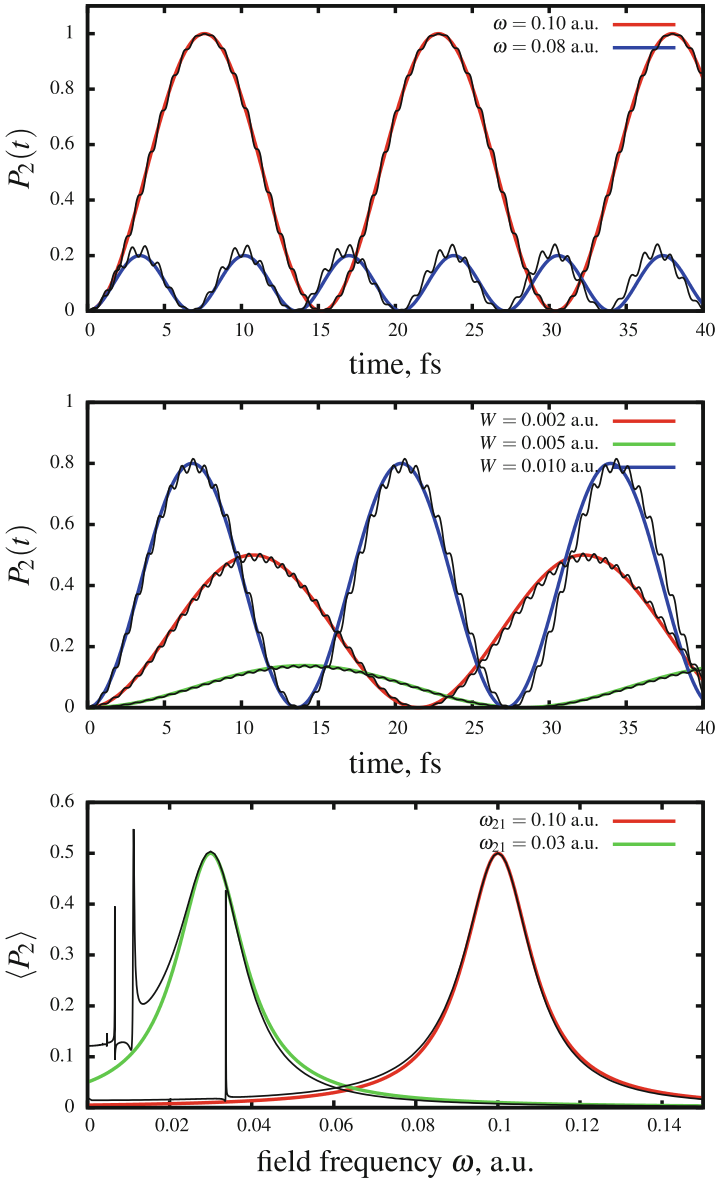

Fig. 3.1 Dynamics of a two-level system with radiation. Colored curves, RWA results; black curves, numerically exact calculations. Upper panel: state 2 population $P_2(t)$ with $\omega_{21} = 0.10$ a.u., $W = 0.01$ a.u. and two different radiation frequencies. Middle panel: $P_2(t)$ with $\omega_{21} = 0.10$ a.u., $\omega = 0.105$ a.u. and different radiation–molecule couplings. Lower panel: long-time average of P_2 as a function of the field frequency, with $W = 0.01$ and two different transition frequencies

produce a full population inversion. The product Δt HWHM$_\omega$ is π, in agreement with what we found in Sect. 3.2 concerning the properties of a finite radiation pulse.

The RWA is a poor approximation when the detuning $\Delta\omega$ is of the same order of magnitude as $|\omega_{21}|$, because then one cannot assume $||\omega_{21}| - \omega| \ll ||\omega_{21}| + \omega|$. However, even in this case Eq. (3.31) yields $P_{max} \ll 1$ when $\Delta\omega \gg$ HWHM$_\omega$. So, the RWA absorption profile as a function of $\Delta\omega$ is close to the exact one, as far as HWHM$_\omega \ll |\omega_{21}|$, i.e., $|W| \ll |\Delta\varepsilon|$. Figure 3.1 illustrates the accuracy of the RWA in various cases, by comparison with virtually exact numerical calculations. The narrow peaks that appear at approximately $\omega_{21}/3$ and $\omega_{21}/5$ are due to multiphoton resonances that cannot be accounted for by the RWA in the form we have applied it (see Ref. [1] for this topic that exceeds the scope of this book).

3.4 Time-Dependent Perturbation Theory

Let us recall here the set of coupled equations (3.6) that were derived without approximations:

$$\frac{\mathrm{d}c_i}{\mathrm{d}t} = -\frac{\mathrm{i}}{\hbar}\sum_j c_j(t)\ \mathrm{e}^{\mathrm{i}(\varepsilon_i-\varepsilon_j)t/\hbar}\left\langle \psi_i^{(0)}\left|\hat{V}\right|\psi_j^{(0)}\right\rangle \qquad \forall\ i\ .$$

In order to find a general solution for an arbitrary number of states, we now introduce the first-order perturbative approximation that consists in evaluating the RHS of these equations by replacing the $c_j(t)$ coefficients with their initial values. This approximation is only valid if the perturbation is applied for a short time. As we shall see, how short this time interval must be depends on the strength of the perturbation, i.e., on the magnitude of the relevant V_{ij} matrix elements. The main advantage of first-order time-dependent perturbation theory (TDPT) is to decouple Eq. (3.6), i.e., to enable us to evaluate each time- dependent coefficient independently of the others. In fact, time integration yields

$$c_i(t) = c_i(t_0) - \frac{\mathrm{i}}{\hbar}\sum_j c_j(t_0)\ \int_{t_0}^{t} \mathrm{e}^{\mathrm{i}\omega_{ij}t'}\,V_{ij}(t')\ \mathrm{d}t' \tag{3.33}$$

where $\hbar\omega_{ij} \equiv hv_{ij} = \varepsilon_i - \varepsilon_j$. The initial time t_0 can be any time at which the coefficients $c_j(t_0)$ are known.

Let's assume for simplicity that one state, $\psi_0^{(0)}$, is initially populated, i.e.,

$$\begin{aligned} c_0 &= 1 \\ c_i &= 0 \quad \forall\ i \neq 0\ . \end{aligned} \tag{3.34}$$

Then, from Eq. (3.33) we get

$$c_i(t) = -\frac{\mathrm{i}}{\hbar}\int_{t_0}^{t} \mathrm{e}^{\mathrm{i}\omega_{i0}t'} V_{i0}(t')\,\mathrm{d}t' \quad \forall\ i \neq 0\ . \tag{3.35}$$

In many cases, only off-diagonal couplings exist, i.e., $V_{ii} = 0$, so at $t = 0$: $\mathrm{d}c_0/\mathrm{d}t = 0$. This shows that the approximations $c_0 \simeq 1$ in such cases is valid to second order in t. If $V_{i0}(t)$ vanishes sufficiently fast for large $|t|$ and we take as the starting time $t_0 = -\infty$, the total effect of the perturbation over its whole duration is related to the Fourier transform of the $V_{i0}(t)$ function:

$$c_i(\infty) = -\frac{\mathrm{i}}{\hbar}\int_{-\infty}^{\infty} \mathrm{e}^{\mathrm{i}\omega_{i0}t'} V_{i0}(t')\,\mathrm{d}t' = -\frac{\mathrm{i}}{\hbar}\,(2\pi)^{1/2}\,\tilde{V}_{i0}(-\omega_{i0})\ . \tag{3.36}$$

The population of state i is then

$$|c_i(\infty)|^2 = \frac{2\pi}{\hbar^2}\,\left|\tilde{V}_{i0}(-\omega_{i0})\right|^2\ . \tag{3.37}$$

If a different time interval is considered, say $[t_0, t]$, formally we can write a relationship similar to (3.36) by zeroing the interaction matrix element outside the chosen interval:

$$c_i(t) = -\mathrm{i}\frac{(2\pi)^{1/2}}{\hbar}\,\tilde{V}'_{i0}(-\omega_{i0}) \tag{3.38}$$

with

$$\begin{aligned} V'_{i0}(t') &= V_{i0}(t') \quad \text{for } t' \in [t_0, t] \\ V'_{i0}(t') &= 0 \qquad\quad \text{for } t' \notin [t_0, t]\ . \end{aligned} \tag{3.39}$$

Note that the first-order TDPT approximation does not preserve the normalization of the wavefunction, because $|c_0|^2$ remains 1 at all times, while the other probabilities are in general nonvanishing for $t > t_0$. Of course, according to the exact solution of Eq. (3.6), $|c_0|^2$ decreases in time at least shortly after the perturbation begins to take effect, since

$$|c_0|^2 = 1 - \sum_{i(\neq 0)} |c_i(t)|^2\ . \tag{3.40}$$

It follows that the first-order TDPT approximation, i.e., using the initial values of the coefficients in evaluating the RHS of Eq. (3.6), is only valid when

$$\sum_{i(\neq 0)} |c_i(t)|^2 \ll 1\ . \tag{3.41}$$

In fact this requirement ensures at once that c_0 is close to 1 and all the other c_i coefficients are small enough as to be neglected ("perturbative limit"). To fulfill this condition for an infinite time interval the Fourier transform of the perturbation must be negligibly small:

$$\sum_{i(\neq 0)} \left| \tilde{V}_{i0}(-\omega_{i0}) \right|^2 \ll \frac{\hbar^2}{2\pi} \,. \tag{3.42}$$

For a finite time interval, the same must hold for V'_{i0}, which is always true if $t - t_0$ is small enough.

3.5 Excitation by a Continuous Wave

As a first example of application of TDPT we shall consider the perturbation caused by a continuous electromagnetic wave:

$$\mathbf{E}(t) = \mathbf{E}_{00} \, \cos(\omega t - \varphi) \tag{3.43}$$

where $\mathbf{E}_{00}$ is constant in time. If the light is switched on at $t = 0$ and we examine the molecular wavefunction at a later time t, we get the same result as with a radiation pulse of duration t. From Eq. (3.35) we get the coefficient of state ψ_i (from now on we drop the superscript $^{(0)}$ to indicate the exact eigenstates in the absence of radiation and we shall indicate their energies with E instead of ε):

$$\begin{aligned} c_i(t) &= \frac{\mathrm{i}}{\hbar} \, \boldsymbol{\mu}_{i0} \cdot \mathbf{E}_{00} \int_0^t \cos(\omega t' - \varphi) \, \mathrm{e}^{\mathrm{i}\omega_{i0} t'} \, \mathrm{d}t' = \\ &= \frac{\mathrm{i}}{2\hbar} \, \boldsymbol{\mu}_{i0} \cdot \mathbf{E}_{00} \int_0^t \left[\mathrm{e}^{-\mathrm{i}\varphi} \, \mathrm{e}^{\mathrm{i}(\omega_{i0}+\omega)t'} + \mathrm{e}^{\mathrm{i}\varphi} \, \mathrm{e}^{\mathrm{i}(\omega_{i0}-\omega)t'} \right] \mathrm{d}t' = \\ &= \frac{1}{2\hbar} \, \boldsymbol{\mu}_{i0} \cdot \mathbf{E}_{00} \left[\mathrm{e}^{-\mathrm{i}\varphi} \, \frac{\mathrm{e}^{\mathrm{i}(\omega_{i0}+\omega)t} - 1}{\omega_{i0} + \omega} + \mathrm{e}^{\mathrm{i}\varphi} \, \frac{\mathrm{e}^{\mathrm{i}(\omega_{i0}-\omega)t} - 1}{\omega_{i0} - \omega} \right] . \end{aligned} \tag{3.44}$$

Here too we can apply the RWA, neglecting the term with $\omega_{i0} + \omega$ if $\omega_{i0} > 0$ and the one with $\omega_{i0} - \omega$ if $\omega_{i0} < 0$. When the transition goes from a lower to an upper level ($\omega_{i0} > 0$), a photon of frequency approximately equal to ω_{i0} is absorbed. On the contrary, when the initial level is higher than the final one ($\omega_{i0} < 0$), a photon of frequency $\sim |\omega_{i0}|$ is emitted. In the RWA, the final coefficient of state i is then

$$c_i(t) = \pm \frac{1}{2\hbar} \, \boldsymbol{\mu}_{i0} \cdot \mathbf{E}_{00} \, \mathrm{e}^{\pm \mathrm{i}\varphi} \, \frac{1 - \mathrm{e}^{\mp \mathrm{i} \Delta\omega_{i0} t}}{\Delta\omega_{i0}} \,. \tag{3.45}$$

Here the $\pm$ sign is plus for photon absorption and minus for stimulated emission, while $\Delta\omega_{i0} = \omega - |\omega_{i0}|$ is the detuning for the $0 \to i$ transition. The corresponding population is

$$P_i(t) = |c_i(t)|^2 = \frac{\left| \boldsymbol{\mu}_{i0} \cdot \mathbf{E}_{00} \right|^2}{\hbar^2} \left[\frac{\sin(\Delta\omega_{i0} \, t/2)}{\Delta\omega_{i0}} \right]^2 . \tag{3.46}$$

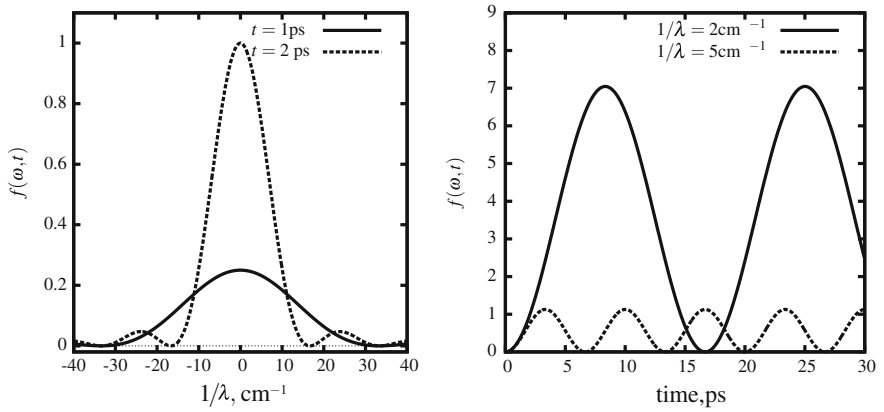

Fig. 3.2 Plot of $f(\omega, t) = \dfrac{\sin^2(\omega t/2)}{\omega^2}$ as a function of $\omega = 2\pi c/\lambda$ (left panel) and as a function of t (right panel)

With $\Delta\omega \neq 0$, the function $f(\Delta\omega, t) = \sin^2(\Delta\omega t/2)/\Delta\omega^2$ oscillates in time from 0 to $\Delta\omega^{-2}$, with a period $2\pi/\Delta\omega$ (see Fig. 3.2). For $\Delta\omega = 0$, $f(\Delta\omega, t)$ increases quadratically in time:

$$\lim_{\Delta\omega\to 0}\left[\frac{\sin(\Delta\omega t/2)}{\Delta\omega}\right]^2 = \frac{t^2}{4}\,. \tag{3.47}$$

Considering $f(\Delta\omega, t)$ as a function of $\Delta\omega$, we see a main peak centered at $\Delta\omega = 0$ that gets taller and narrower as the time interval t increases (see again Fig. 3.2 and animation 3.1). In fact, the two zeroes that bracket the peak occur at $\Delta\omega = \pm 2\pi/t$, while all other maxima decrease approximately as $\Delta\omega^2$. This means that a relatively weak periodic field acting for a time interval t long enough can hardly induce transitions if the detuning exceeds h/t. For instance, with $t = 1$ ps the resonance condition $\omega \simeq |\omega_{12}|$ is obeyed with an error bar $\text{HWHM}_\omega \approx 10\ \text{cm}^{-1}$, while with $t = 1$ ns, $\text{HWHM}_\omega \approx 10^{-2}\ \text{cm}^{-1}$.

In many real situations, the values of ω_{12} and ω are not precisely defined and their uncertainties largely exceed HWHM_ω. For instance, different molecules in a sample can experience slightly different environments which modify the transition energy $E_i - E_0$. Moreover, as we shall see in Sect. 3.10, instead of a single-state ψ_i (or ψ_0) we may deal with many or infinite states with (slightly) different energy levels and transition dipoles. These two sources of "broadening" of the spectral lines are called "inhomogeneous broadening" and "homogeneous broadening," respectively, because the first originates from the inhomogeneity of the sample, while the second is inherent to the single molecule spectral properties.

The field frequency ω can also cover a rather wide interval, in which case the light is not monochromatic, as that of normal lamps: even when the emitters are gas phase atoms, inhomogeneous broadening works in the same way as in the irradiated sample, affecting the emission frequency. In this case E_{00} becomes a function of

ω and the electric field is given as an integral over a range of frequencies as in Eq. (1.9). We shall therefore compute the transition probability by integrating the expression (3.46) as a function of the detuning $\Delta\omega_{i0}$, with approximations based on the assumption that HWHM_ω is much smaller than the variation of ω and/or ω_{i0}. We assume $\boldsymbol{\mu}_{i0} \cdot \mathbf{E}_{00}$ to be constant within a small interval of a few HWHM_ω units around $\Delta\omega_{i0} = 0$. Outside this interval the integrand is negligibly small, so we can set the integration limits to $\pm\infty$:

$$P_i(t) = \frac{\left|\boldsymbol{\mu}_{i0} \cdot \mathbf{E}_{00}\right|^2}{\hbar^2} \int_{-\infty}^{+\infty} \frac{\sin^2(\Delta\omega_{i0}\, t/2)}{\Delta\omega_{i0}^2} \mathrm{d}\Delta\omega_{i0} = \frac{\pi \left|\boldsymbol{\mu}_{i0} \cdot \mathbf{E}_{00}\right|^2}{2\hbar^2}\, t \,. \tag{3.48}$$

Since the probability of being in state ψ_i increases linearly with time, we can define a constant transition rate

$$\frac{\mathrm{d}P_i}{\mathrm{d}t} = \frac{\pi \left|\boldsymbol{\mu}_{i0} \cdot \mathbf{E}_{00}\right|^2}{2\hbar^2} \,. \tag{3.49}$$

We remind that this expression holds in the TDPT approximation; i.e., when the population of state ψ_0 is very close to 1. Therefore $\frac{\mathrm{d}P_i}{\mathrm{d}t}$ is actually the transition rate constant, which multiplies the number of molecules in state ψ_0 in kinetic treatments.

In isotropic samples, typically gases or liquids, we find molecules with random orientations. If we consider a Cartesian frame with the z axis in the $\mathbf{E}_{00}$ direction and the $\boldsymbol{\mu}_{i0}$ orientation given by the polar angles θ and ϕ, the average value of $\left|\boldsymbol{\mu}_{i0} \cdot \mathbf{E}_{00}\right|^2$ is obtained by integrating over both angles:

$$\overline{\left|\boldsymbol{\mu}_{i0} \cdot \mathbf{E}_{00}\right|^2} = \frac{\mu_{i0}^2 E_{00}^2}{4\pi} \int_0^{2\pi} \mathrm{d}\phi \int_0^{\pi} \cos^2\theta \, \sin\theta \, \mathrm{d}\theta = \frac{1}{3}\mu_{i0}^2 E_{00}^2 \,. \tag{3.50}$$

So, in isotropic samples the average transition rate constant is

$$\overline{\frac{\mathrm{d}P_i}{\mathrm{d}t}} = \frac{\pi \mu_{i0}^2 E_{00}^2}{6\hbar^2} \,. \tag{3.51}$$

Considering the relationship between E_{00}^2 and the energy density or the spectral irradiance (see Sect. 1.2.2), we get

$$\overline{\frac{\mathrm{d}P_i}{\mathrm{d}t}} = \frac{\pi \mu_{i0}^2 U_\omega}{3\hbar^2 \varepsilon_0} = \frac{\mu_{i0}^2 U_\nu}{6\hbar^2 \varepsilon_0} = \frac{\mu_{i0}^2 I_\nu}{6\hbar^2 \varepsilon_0 c} \,. \tag{3.52}$$

The proportionality coefficient between the $0 \to i$ transition rate and the energy density U_ν is called the Einstein's $B_{0,i}$ coefficient and within the approximations made here, it is proportional to the square of the transition dipole moment. For the $i \to 0$ transition with stimulated emission the theory developed in this section predicts the same rate constant as for photon absorption, so $B_{i,0} = B_{0,i}$ or, more generally

$$B_{i,j} = B_{j,i} = \frac{\mu_{ij}^2}{6\hbar^2\varepsilon_0} \,. \tag{3.53}$$

In atomic units:

$$B_{i,j} = B_{j,i} = \frac{2\pi\,\mu_{ij}^2}{3} \,. \tag{3.54}$$

To relate the Einstein coefficients with the experimental spectra, let us consider an absorption band in the interval $[\nu_a, \nu_b]$, made of one or more $0 \to i$ transitions. From Sect. 1.6.1 we know that the excitation rate per unit volume (1 m^3) is

$$R_{exc}^{(\nu_a,\nu_b)} = N \int_{\nu_a}^{\nu_b} \sigma(\nu)\; I_{ph,\nu}(\nu)\; \mathrm{d}\nu = \frac{\ln(10)\; N}{10\; N_A} \int_{\nu_a}^{\nu_b} \varepsilon(\nu)\; I_{ph,\nu}(\nu)\; \mathrm{d}\nu \tag{3.55}$$

where N is the number density (m^{-3}), σ is the absorption cross section and ε the molar extinction coefficient in mol^{-1} L cm^{-1}. On the other hand, from Eqs. (3.52) and (3.53) we have

$$R_{exc}^{(\nu_a,\nu_b)} = N \sum_i \frac{B_{0,i}\; I_\nu(\nu_{i0})}{c} = N \sum_i \frac{B_{0,i}\; I_{ph,\nu}(\nu_{i0})\; h\nu_{i0}}{c} \tag{3.56}$$

where the index i runs over the transitions with frequencies falling in the interval $[\nu_a, \nu_b]$. If we consider $I_{ph,\nu}(\nu)$ as constant, equating the RHS of Eqs. (3.55) and (3.56) yields

$$\sum_i \nu_{i0}\; B_{0,i} = \frac{c}{h} \int_{\nu_a}^{\nu_b} \sigma(\nu)\; \mathrm{d}\nu = \frac{\ln(10)\; c}{10\; N_A h} \int_{\nu_a}^{\nu_b} \varepsilon(\nu)\; \mathrm{d}\nu \tag{3.57}$$

i.e.,

$$\sum_i \nu_{i0}\; \mu_{i0}^2 = \frac{3\hbar\varepsilon_0 c}{\pi} \int_{\nu_a}^{\nu_b} \sigma(\nu)\; \mathrm{d}\nu = \frac{3\ln(10)\;\hbar\varepsilon_0 c}{10\;\pi N_A} \int_{\nu_a}^{\nu_b} \varepsilon(\nu)\; \mathrm{d}\nu \,. \tag{3.58}$$

We now define the dimensionless quantity called "oscillator strength," either for a single spectral line:

$$f_{ij} = \frac{4\pi m_e}{3\hbar e^2}\; \nu_{ij}\; \mu_{ij}^2 \tag{3.59}$$

or for the whole band:

$$f(\nu_a, \nu_b) = \frac{4\pi m_e}{3\hbar e^2} \sum_i \nu_{i0}\; \mu_{i0}^2 = \frac{4\ln(10)\;\varepsilon_0 m_e c}{10\; N_A e^2} \int_{\nu_a}^{\nu_b} \varepsilon(\nu)\; \mathrm{d}\nu \,. \tag{3.60}$$

The conventional factor that makes the oscillator strength dimensionless is $4\pi m_e/(3\hbar e^2) = 1.40955 \cdot 10^{42}$ s·m^{-2}C^{-2}. Equation (3.60) can be rewritten as

$$f(\nu_a, \nu_b) = 1.4407 \cdot 10^{-19} \int_{\nu_a}^{\nu_b} \varepsilon(\nu)\, \mathrm{d}\nu = 4.3190 \cdot 10^{-9} \int_{\overline{\nu}_a}^{\overline{\nu}_b} \varepsilon(\overline{\nu})\, \mathrm{d}\overline{\nu} \quad (3.61)$$

where, in the second integral, the frequency unit is cm^{-1} instead of Hz.

Equations (3.57–3.60) show that the quantities $\nu_{i0}\ B_{0,i}$, $\nu_{i0}\ \mu_{i0}^2$, and f_{i0}, all proportional to each other, are additive contributions to the absorption spectrum, while $B_{0,i}$ or μ_{i0}^2 are not. So, when spectral lines that are broadened coalesce to a single band, with or without a structure (i.e., distinguishable peaks), their f_{i0} add up to make the total $f(\nu_a, \nu_b)$ of the band. Of course, any interaction that causes a broadening can also alter the oscillator strengths, but the comparison between two different situations (say, for instance, gas phase and solution) should be based on (a sum of) the oscillator strengths. The same holds for the comparisons between theory, which very often only determines transition frequencies and dipole moments, and experiment, which offers spectral bands with variable heights and widths depending on the environment and other conditions, but fairly invariant oscillator strengths.

3.6 Spontaneous Emission

In 1916 Einstein showed that photon absorption and stimulated emission would never lead to a state of equilibrium between matter and radiation and concluded that a different emission mechanism must exist [2]. Equilibrium between molecules and photons is not the common situation in photochemical experiments and in natural (planetary or cosmic) conditions. Most frequently, hot objects emit light that is absorbed by the colder ones or escapes in regions where matter is rarefied. However, we can imagine a system where photons are confined (by mirror walls) and a gas of atoms or molecules absorbs and emits light. The interactions among molecules and between molecules and photons allow the exchange of energy among all components (note that photons do not interact among themselves). So, if the system is thermostated, in the long term the population N_i of any molecular state $|i\rangle$ will be proportional to $\exp(-E_i/K_B T)$. The equilibrium distribution of photons in the frequency spectrum gives place to the spectral energy density

$$U_\nu(\nu) = \frac{8\pi\ h\nu^3}{c^3} \left[\mathrm{e}^{h\nu/K_B T} - 1\right]^{-1} \quad (3.62)$$

which is the famous "black body" formula proposed by Max Planck in 1900.

If we consider any two molecular states i and j, with $E_i < E_j$, there will be $i \to j$ transitions with photon absorption and $j \to i$ transitions with stimulated emission. Both transition rates will be proportional to $B_{i,j}\ U_\nu(\nu_{ij})$ and to the respective populations of the initial states. Since $N_i > N_j$, more photons will be absorbed than emitted, which is the normal situation when a sample at room temperature is irradiated with

UV or visible light. However, this condition is incompatible with thermodynamical equilibrium, so we need another kind of $j \rightarrow i$ transitions to balance absorption and emission. In the equation

$$N_j \; A_{ji} + N_j \; B_{ij} U_\nu(\nu_{ij}) = N_i \; B_{ij} U_\nu(\nu_{ij}) \tag{3.63}$$

the LHS is the emission rate and the RHS is the absorption rate. The new term $N_j \; A_{ji}$ contains the unknown quantity A_{ji} which can be determined using Eqs. (3.62) and (3.63):

$$A_{ji} = \frac{N_i - N_j}{N_j} \; B_{ij} U_\nu(\nu_{ij}) = \left[\mathrm{e}^{(E_j - E_i)/K_B T} - 1 \right] \; B_{ij} U_\nu(\nu_{ij}) = \frac{8\pi \; h\nu_{ij}^3}{c^3} \; B_{ij} \; . \tag{3.64}$$

We see that the Einstein coefficient A_{ji} does not depend on the energy density of radiation nor on temperature. Since the emission associated with such transitions occurs even in the absence of radiation, it is called "spontaneous emission." The relationship between A_{ji} and $B_{ij} = B_{ji}$ is valid for any pair of states, whether they are coupled (mainly) through the electric or magnetic dipole. In the dipolar approximation, Eq. (3.53) allows to write explicitly

$$A_{ji} = \frac{8\pi^2 \; \nu_{ij}^3 \; \mu_{ij}^2}{3\hbar\varepsilon_0 c^3} \tag{3.65}$$

or, in atomic units,

$$A_{ji} = \frac{4\omega_{ij}^3 \; \mu_{ij}^2}{3c^3} \; . \tag{3.66}$$

While the stimulated emission adds to the impinging radiation with the same frequency, direction of propagation and polarization, the spontaneous emission only depends on the molecular properties. In particular, for dipole allowed transitions the direction of propagation and the polarization depend on the orientation of the transition dipole moment (see, for instance, Lakowicz [3]). For isotropic samples, the spontaneous emission is isotropic as well. Spontaneous emission prevails in hot light sources: stars, hot lamps, or flames. Lasers are instead based on stimulated emission: "laser" is an acronym for "Light Amplification by Stimulated Emission of Radiation." For stimulated emission to prevail on absorption, one needs an inversion of population, i.e., the upper level must be more populated than the lower one. For the various ways to achieve such condition and the uses of lasers in chemistry see, for instance, Andrews [4].

3.7 Vibrational Structure of Electronic Spectra

The absorption or emission of UV, visible, or NIR light implies a transition between electronic states, which is often complemented by a certain degree of vibrational excitation. We shall assume that the exciting light is sufficiently monochromatic as to promote transitions between vibronic eigenstates. In the Born–Oppenheimer approximation, the initial and final wavefunctions are the products $\varphi_l \chi_{lu}$ e $\varphi_k \chi_{kv}$, respectively. If the molecule is initially in the electronic ground state, i.e., usually the S_0 singlet state, then $l = 0$. At room temperature, the vibrational state too is normally the lowest in energy ($u = 0$). Exceptions are due to low-frequency vibrations, when present, having $h\nu$ of the order of $K_B T$ or lower, in which case some of the first vibrational states can have non-negligible populations. This means that normally the initial molecular geometry is close to the equilibrium one in S_0.

From Sect. 3.5 we know that the intensity of an absorption band, i.e., the integrated area under the corresponding peak of the extinction coefficient $\varepsilon(\nu)$, is proportional to $\nu_{00,kv}\ \mu^2_{00,kv}$. For emission bands, the relevant factor is $\nu^3_{0u,10}\ \mu^2_{0u,10}$, where the electronic index 1 refers to the S_1 state. In fact, as we shall see in Sect. 3.11, the higher excited states usually decay in a very short time to S_1, and fluorescence emission then follows. If the triplet states are populated by ISC, then T_1 is normally the emitting state (phosphorescence). Moreover, if the excited state lifetime is long enough and the transfer of vibrational energy to the environment is efficient, as normal in condensed phase, by far the most populated vibrational state is the lowest one, just as in S_0 (see Sect. 4.5). Figures 3.3, 3.4, and 3.5 illustrate these concepts: they show schematically the potential energy curves U_0 and U_1, belonging to S_0 and S_1, the relevant vibrational levels and the transitions giving place to absorption and fluorescence bands.

The transition dipole for the $l, u \rightarrow k, v$ transition is the result of two integrations, one over the electronic coordinates and one over the nuclear ones. The electronic transition dipole, computed for a given set of nuclear coordinates $\mathbf{R}$, is

$$\boldsymbol{\mu}_{lk}(\mathbf{R}) = \langle \varphi_l(\mathbf{R}) \, |\boldsymbol{\mu}| \, \varphi_k(\mathbf{R}) \rangle_{\mathbf{r}} \ . \tag{3.67}$$

If the φ_l and φ_k have different spin multiplicities, the matrix element vanishes and the transition is "spin-forbidden." Such transition occur because of the existence of magnetic couplings, both between radiation and molecules and, more important, between molecular states of different spin (see Sect. 2.4). $\boldsymbol{\mu}_{lk}$ can also be zero by symmetry, when the product $\varphi_l \varphi_k$ belongs to an irreducible representation of the point group that none of the components of the $\boldsymbol{\mu}$ vector does match. For instance, in the C_{2v} group, x, y, and z belong to the B_2, B_1, and A_1 representations, so the transitions between A_1 and A_2 states are "symmetry-forbidden," and those between B_1 and B_2 states as well. Note that the symmetry considerations concern the equilibrium geometry $\mathbf{R}_{eq}$ of the starting state, but in polyatomics a symmetric geometry can always be modified by molecular vibrations, in such a way that $\boldsymbol{\mu}_{lk}(\mathbf{R}) \neq 0$. The matrix element of the dipole between vibronic states is

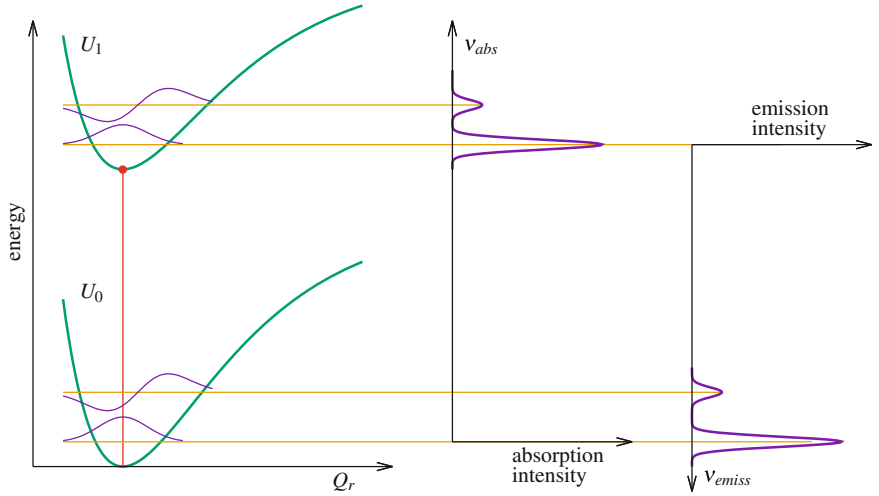

Fig. 3.3 Potential energy curves and electronic spectra. The ground and excited PES and their equilibrium geometries are similar. The red dot indicates the Franck–Condon point

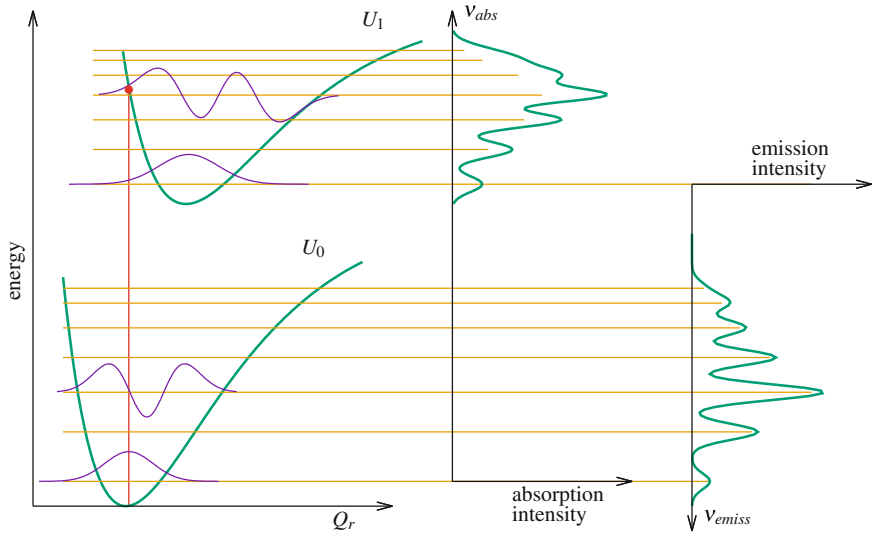

Fig. 3.4 Potential energy curves and electronic spectra. The ground and excited PES are similar but the respective minima are displaced along the coordinate Q_r. The red dot indicates the Franck–Condon point

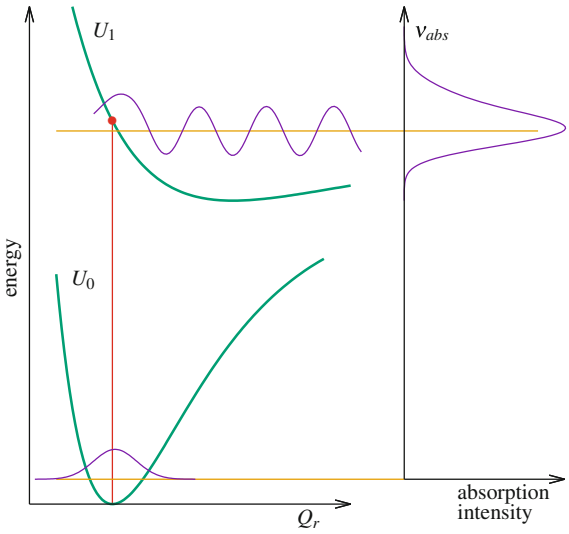

Fig. 3.5 Potential energy curves and electronic spectra. The Franck–Condon point in the excited PES is above the dissociation limit along the coordinate Q_r. The red dot indicates the Franck–Condon point

$$\boldsymbol{\mu}_{lu,kv} = \left\langle \chi_{lu} \left| \boldsymbol{\mu}_{lk}(\mathbf{R}) \right| \chi_{kv} \right\rangle_{\mathbf{R}} \ . \tag{3.68}$$

The completeness of the basis of vibrational states χ_{kv} leads to the sum rule:

$$\sum_v \mu^2_{lu,kv} = \left\langle \chi_{lu} \left| \mu^2_{lk} \right| \chi_{lu} \right\rangle \ . \tag{3.69}$$

If the transition is symmetry-allowed, i.e., $\boldsymbol{\mu}_{lk}(\mathbf{R}_{eq}) \neq 0$, one can apply the Franck–Condon approximation, i.e., consider $\boldsymbol{\mu}_{lk}(\mathbf{R})$ as constant and replace it by its value at the equilibrium geometry. Then

$$\boldsymbol{\mu}_{lu,kv} \simeq \boldsymbol{\mu}_{lk}(\mathbf{R}_{eq}) \ \langle \chi_{lu} \, | \chi_{kv} \rangle \tag{3.70}$$

and

$$\sum_v \mu^2_{lu,kv} \simeq \mu^2_{lk}(\mathbf{R}_{eq}) \ . \tag{3.71}$$

If the relative intensities of the vibrational sub-bands are approximately proportional to the squared overlap integrals $\langle \chi_{lu} \, | \chi_{kv} \rangle^2$, the strongest band in the absorption spectrum is due to the χ_{kv} state that best overlaps with χ_{00}.

In Fig. 3.3 we show the potential energy curves of S_0 and S_1 and the related absorption and emission spectra. We represent the case where the U_0 and U_1 are similar and their minima approximately coincide. Then, the largest overlap is obtained for $v = 0$ (0-0 band), while all the upper states, with one or more nodes, give place to much weaker sub-bands at higher frequencies. Overall, the whole electronic band

is narrow and shows one or very few peaks. The same occurs in emission, with the difference that the weaker sub-bands are at lower frequencies than the 0-0 one.

Consider now the case of two quite different potential energy surfaces, with minima at substantially different geometries. In Fig. 3.4, U_0 and U_1 are displaced along a coordinate Q_r, with the equilibrium value of Q_r larger in S_1 than in S_0. In such a case, the most intense sub-band in the absorption spectrum is due to a transition to a vibrational level that puts the inner turning point close to the Franck–Condon point (it would be the outer turning point for a displacement of the minima in the opposite direction).[1] In fact, the first maximum in the χ_{1v} wavefunction is close to that of χ_{00} and its first node is sufficiently far on the right (see Fig. 3.4). The overlaps with other χ_{1v} wavefunctions, both higher and lower in energy, decrease gradually, so that overall the electronic band is quite broad. Similarly, in the emission band the strongest peak corresponds to a χ_{0u} state with the outer turning point close to the minimum geometry in the excited state.

In the last example (Fig. 3.5), Q_r is a bond stretching coordinate and presents a very shallow minimum in the excited state. The Franck–Condon point is well above dissociation, so the states that best overlap χ_{00} belong to the dissociative continuum and will be indicated by $\chi_{0\varepsilon}$, where ε is the asymptotic kinetic energy (see Appendix C). Then, the Franck–Condon factor $\langle \chi_{00} \,|\chi_{0\varepsilon}\rangle^2$ is a function of ε and the absorption band profile is smooth, without peaks corresponding to the quantized vibrational levels. The maximum of the band occurs again in correspondence to a vibrational level such that the turning point approximately coincides with the Franck–Condon point (note that here only the inner turning point exists). After excitation above the dissociation threshold, the molecule promptly dissociates and no fluorescence can be observed. This kind of photodissociation is called "direct," meaning it takes place in the same electronic state where the molecule was initially excited. Predissociation, on the contrary, requires a nonadiabatic transition to occur (see Sect. 3.10). In conclusion, we see that the maximum intensity of a band coincides approximately with the vertical excitation energy, i.e., the energy difference between the two PESs at the equilibrium geometry in the initial state. Remember, however, that this statement relies on the hypothesis that only the $v = 0$ state is populated in the initial electronic state, plus at most some of the closest lying vibrational states. For fluorescence (or phosphorescence to which the same considerations apply), this assumption is only true when the vibrational energy loss of the chromophore occurs in a time much shorter than the excited state lifetime (see Sects. 4.3 and 4.5). The electronic bands can be structured, i.e., show one or more "progressions" belonging to discrete vibrational levels, or featureless, because the final states belong to a dissociative continuum (this can also occur in emission bands of exciplexes, see Sect. 6.3). However, vibrational progressions can be blurred and give place to essentially continuous bands because of line broadening and the closeness of vibrational levels: this frequently

[1] In classical mechanics, the motion of a particle in one dimension has a turning point when the potential and the total energies are equal, i.e., the kinetic energy vanishes. For a bound state in quantum mechanics, the potential energy coincides with the eigenenergy in at least two points: the inner turning point, Q_i, and the outer one, Q_o, with $Q_i < Q_o$. The Franck–Condon point is the point in the excited PES corresponding to the equilibrium geometry of the ground state.

occurs for large molecules and in condensed phase. In all cases, the broadness of the electronic band is an indication of how much the PESs differ. The only sub-band the absorption and fluorescence spectra have in common normally corresponds to the 0-0 transition between S_0 and S_1, which can be easily identified if both spectra have been recorded. The frequency of this transition corresponds to the energy difference between the minima of S_0 and S_1 (the "adiabatic" energy difference), in the approximation of neglecting the change in the zero point energies between the two PESs. As a last remark, we remind the basic asymmetry between absorption and spontaneous emission: when using monochromatic light, the former occurs at a well-defined frequency with little uncertainty, while the latter unavoidably produces the whole spectrum.

3.8 Excitation by Radiation Pulses

We now consider the excited state created by a radiation pulse of the form

$$\mathbf{E}(t) = \mathbf{E}_0(t)\ \cos(\omega t - \varphi) \tag{3.72}$$

already discussed at the end of Sect. 3.2. By combining Eqs. (3.15) and (3.36) we find

$$\begin{aligned} c_i(\infty) &= \frac{(2\pi)^{1/2}\mathrm{i}}{\hbar}\ \boldsymbol{\mu}_{i0}\cdot\tilde{\mathbf{E}}(-\omega_{i0}) = \\ &= \frac{\pi^{1/2}\mathrm{i}}{2^{1/2}\hbar}\ \boldsymbol{\mu}_{i0}\cdot\left[\mathrm{e}^{\mathrm{i}\varphi}\ \tilde{\mathbf{E}}_0(\omega-\omega_{i0}) + \mathrm{e}^{-\mathrm{i}\varphi}\ \tilde{\mathbf{E}}_0(-\omega-\omega_{i0})\right]. \end{aligned} \tag{3.73}$$

Once again we apply the RWA, keeping only the term $\tilde{\mathbf{E}}_0(\omega-\omega_{i0})$ if $\omega_{i0} > 0$ (photon absorption) and the term $\tilde{\mathbf{E}}_0(-\omega-\omega_{i0})$ if $\omega_{i0} < 0$ (photon emission). Then, the final coefficient of state i is

$$c_i(\infty) = \frac{\pi^{1/2}\mathrm{i}}{2^{1/2}\hbar}\ \mathrm{e}^{\pm\mathrm{i}\varphi}\ \boldsymbol{\mu}_{i0}\cdot\tilde{\mathbf{E}}_0(\pm\Delta\omega_{i0})\ . \tag{3.74}$$

Here the detuning $\Delta\omega_{i0} = \omega - |\omega_{i0}|$ gets the plus sign for photon absorption and the minus sign for stimulated emission. The final-state probability is

$$P_i(\infty) = |c_i(\infty)|^2 = \frac{\pi}{2\hbar^2}\ \left|\boldsymbol{\mu}_{i0}\cdot\tilde{\mathbf{E}}_0(\pm\Delta\omega_{i0})\right|^2\ . \tag{3.75}$$

So, according to the conclusions of Sect. 3.2, we see that the range of final energy levels with non-negligible populations is within a few units of FWHM_ω from the carrier frequency ω. To obtain a better resolution, i.e., a smaller bandwidth FWHM_ω, the pulse duration must be proportionally increased.

Consider, for instance, the commonly assumed Gaussian pulse

$$\mathbf{E}_0(t) = \mathbf{E}_{max}\ \mathrm{e}^{-t^2/4\tau^2} \tag{3.76}$$

and its Fourier transform

$$\tilde{\mathbf{E}}_0(\Delta\omega) = \sqrt{2}\,\mathbf{E}_{max}\ \tau\ \mathrm{e}^{-\tau^2\Delta\omega^2}\ . \tag{3.77}$$

The final coefficient of state i is then

$$c_i(\infty) = \mathrm{i}\frac{\pi^{1/2}\tau}{\hbar}\ \ \boldsymbol{\mu}_{i0}\cdot\mathbf{E}_{max}\ \mathrm{e}^{\pm\mathrm{i}\varphi}\ \mathrm{e}^{-\tau^2\Delta\omega_{i0}^2} \tag{3.78}$$

and its population is

$$|c_i(\infty)|^2 = \frac{\pi\tau^2\left|\boldsymbol{\mu}_{i0}\cdot\mathbf{E}_{max}\right|^2}{\hbar^2}\ \mathrm{e}^{-2\tau^2\Delta\omega_{i0}^2}\ . \tag{3.79}$$

The pulse duration is $\mathrm{FWHM}_t = 2\sqrt{2\ln 2}\ \tau$ and the bandwidth is $\mathrm{FWHM}_\omega = \sqrt{2\ln 2}/\tau$. In terms of standard deviations, the (half) length of the pulse is τ and the frequency resolution is $1/2\tau$. So, for a Gaussian pulse the (energy) x (time) uncertainty product is $\hbar/2$. This relationship is mathematically analogous to Heisenberg's uncertainty principle (see, for instance, Merzbacher [5] or Sakurai [6]): in both cases the Gaussian shape corresponds to the smallest possible uncertainty product.

3.9 Spectrum and Autocorrelation Function

We define the "autocorrelation function" of a time-dependent wavefunction as the superposition of two wavefunctions taken at different times. If we consider the times 0 and t, the autocorrelation function is

$$A(t) = \langle\Psi(t)\,|\Psi(0)\rangle\ . \tag{3.80}$$

Assuming the Hamiltonian is not time-dependent, as $\hat{H}^{(0)}$ in the previous sections, we develop $|\Psi\rangle$ in the basis of its eigenstates:

$$|\Psi(0)\rangle = \sum_i c_i\,|\psi_i\rangle \tag{3.81}$$

and

$$|\Psi(t)\rangle = \sum_i c_i\ \mathrm{e}^{-\mathrm{i}E_i t/\hbar}\,|\psi_i\rangle\ . \tag{3.82}$$

The autocorrelation function is then

$$A(t) = \sum_i |c_i|^2 \ \mathrm{e}^{\mathrm{i}E_i t/\hbar} \ . \tag{3.83}$$

The energy spectrum of Ψ is given by the eigenenergies E_i and by the associated probabilities $|c_i|^2$. If we want to express it as a frequency distribution, we make use of δ functions:

$$S(\omega) = \sum_i |c_i|^2 \, \delta(\omega - E_i/\hbar) \ . \tag{3.84}$$

It is interesting to realize that the spectrum is connected with the autocorrelation function by a Fourier transform:

$$\begin{aligned} \tilde{A}(\omega) &= (2\pi)^{-1/2} \sum_i |c_i|^2 \int_{-\infty}^{+\infty} \mathrm{e}^{\mathrm{i}(E_i/\hbar - \omega)t} \, \mathrm{d}t = \\ &= (2\pi)^{1/2} \sum_i |c_i|^2 \ \delta(E_i/\hbar - \omega) = (2\pi)^{1/2} \ S(\omega) \ . \end{aligned} \tag{3.85}$$

The vice versa is of course true:

$$\begin{aligned} \tilde{S}(t) &= (2\pi)^{-1/2} \sum_i |c_i|^2 \int_{-\infty}^{+\infty} \delta(\omega - E_i/\hbar) \mathrm{e}^{-\mathrm{i}\omega t} \, \mathrm{d}\omega = \\ &= (2\pi)^{-1/2} \sum_i |c_i|^2 \ \mathrm{e}^{-\mathrm{i}E_i t/\hbar} = (2\pi)^{-1/2} \ A(-t) \ . \end{aligned} \tag{3.86}$$

So, the energy spectrum and the autocorrelation function in principle contain the same information.

The eigenstates may belong to a continuum spectrum, in which case the expansion (3.81) is replaced by

$$|\Psi(0)\rangle = \int_{E_{min}}^{\infty} c(E) \, |\psi_E\rangle \ \mathrm{d}E \tag{3.87}$$

where $|\psi_E\rangle$ denotes the state of energy E. The spectrum is then simply

$$S(\omega) = \hbar \ |c(\hbar\omega)|^2 \ . \tag{3.88}$$

Notice that $|c(E)|^2$ is a probability density in the energy domain, so its dimensions are (energy)$^{-1}$. The autocorrelation function in this case is

$$A(t) = \int_{E_{min}}^{\infty} |c(E)|^2 \ \mathrm{e}^{\mathrm{i}Et/\hbar} \, \mathrm{d}E \ . \tag{3.89}$$

It is easy to see that the relationships (3.85) and (3.86) also hold for a continuum spectrum.

The nonstationary state $|\Psi(0)\rangle$ can be generated by a light pulse. Suppose an atom or molecule is initially in state $|G\rangle$ (the ground state or another low-lying state). After a radiation pulse, according to TDPT the state of the system is $|G\rangle + |\Psi_{exc}\rangle$, where

$$|\Psi_{exc}(0)\rangle = \frac{\pi^{1/2}\mathrm{i}}{2^{1/2}\hbar}\ \mathrm{e}^{\mathrm{i}\varphi}\ \sum_i \boldsymbol{\mu}_{i,G}\cdot\tilde{\mathbf{E}}_0(\Delta\omega_{i,G})\,|\psi_i\rangle\ . \tag{3.90}$$

Here we have reset the zero of the time scale just after the end of the almost instantaneous pulse. This amounts to ignore the phase factors $\exp(-\mathrm{i}E_i t/\hbar)$ associated with each state $|\psi_i\rangle$, which is a good approximation in the conditions discussed below. The same approximation will be applied again in other contexts, namely in Eqs. (3.114) and (4.1). The ψ_i states can be, for instance, the vibrational states of the excited PES involved in an electronic absorption band. If the states $|\psi_i\rangle$ that compose $|\Psi_{exc}\rangle$ are well separated in energy from $|G\rangle$, we can forget about the latter because the interesting dynamics will occur in the excited state. In fact, only the state $|\Psi_{exc}\rangle$, which is not stationary, will evolve in time even after the light pulse has died off.

We shall assume the light pulse to be very short, so that (1) we can neglect the internal dynamics of the system during the pulse itself and (2) we can take $\tilde{\mathbf{E}}_0(\Delta\omega_{i,G})$ as independent on $\Delta\omega_{i,G}$ for all the states involved in the transition: $\tilde{\mathbf{E}}_0(\Delta\omega_{i,G}) \simeq \tilde{\mathbf{E}}_0(0)$. These two requirements are indeed equivalent. As we know from Sect. 2.1.2, the properties of the system evolve in time as a combination of complex exponentials of the kind $\mathrm{e}^{-\mathrm{i}(E_i-E_j)t/\hbar}$. Now, the fastest oscillating terms contain the highest and the lowest energies, E_{max} and E_{min}, and have a period $2\pi\hbar/(E_{max}-E_{min})$. So, the first condition requires that $\mathrm{FWHM}_t \ll \hbar/(E_{max}-E_{min})$. The second condition means that the pulse bandwidth is much larger than the whole absorption band: $\mathrm{FWHM}_\omega \gg (E_{max}-E_{min})/\hbar$. Since the dimensionless product $\mathrm{FWHM}_t\mathrm{FWHM}_\omega$ has a value of a few units ($4\ln 2$ for a Gaussian pulse), the two conditions are simultaneously either satisfied or not satisfied. Then

$$|\Psi_{exc}(0)\rangle = \frac{\pi^{1/2}\mathrm{i}}{2^{1/2}\hbar}\ \mathrm{e}^{\mathrm{i}\varphi}\ \tilde{\mathbf{E}}_0(0)\ \cdot\ \sum_i \boldsymbol{\mu}_{i,G}\,|\psi_i\rangle\ . \tag{3.91}$$

The energy spectrum is

$$S(\omega) = \frac{\pi}{2\hbar^2}\ \sum_i \left|\tilde{\mathbf{E}}_0(0)\ \cdot\ \boldsymbol{\mu}_{i,G}\right|^2 \delta(\omega - E_i/\hbar)\ . \tag{3.92}$$

We see that the strength of each spectral line is proportional to its squared transition dipole, just as in the standard steady-state absorption spectrum obtained by scanning the same frequency range with (almost) monochromatic light.[2] If the approximation

[2] Actually there is a difference between $S(\omega)$ and a standard spectrum: in Eq. (3.92) only the component of $\boldsymbol{\mu}_{i,G}$ along the light polarization matters, so in principle the $S(\omega)$ function depends on the orientation of each molecule, while normally the spectra of isotropic samples are averaged over all orientations. This is not important if all the spectral lines involved have the same polar-

of constant $\tilde{\mathbf{E}}_0(\Delta\omega_{i,G})$ is not quite valid, at the end of the pulse the $S(\omega)$ function will be similar to the standard spectrum, but somewhat altered. Equations (3.85) and (3.86) are then relationships between the absorption spectrum of state $|G\rangle$ and the autocorrelation function of the excited state created by a light pulse. This result is in principle more accurate, the shorter is the pulse.

To illustrate how the autocorrelation function can be connected with measurable dynamic properties of the system, we discuss a very simple model. Suppose that only two states close in energy, $|B\rangle$ and $|D\rangle$, are within the frequency range covered by the radiation pulse. $|B\rangle$ and $|D\rangle$ are not eigenstates of the Hamiltonian: they are coupled by a small interaction $V = |V|e^{i\gamma}$ and their energy expectation values are ε_B and ε_D. $|B\rangle$ is a "bright state," i.e., it is coupled to the ground state by a nonvanishing transition dipole $\boldsymbol{\mu}_{B,G}$. $|D\rangle$ is instead a "dark state," i.e., $\boldsymbol{\mu}_{D,G} = 0$. The exact eigenstates (see Appendix D) are

$$\begin{aligned} |\psi_1\rangle &= \cos\theta\ |B\rangle + \sin\theta e^{-i\gamma}\ |D\rangle \\ |\psi_2\rangle &= -\sin\theta\ |B\rangle + \cos\theta e^{-i\gamma}\ |D\rangle \end{aligned} \tag{3.93}$$

where

$$\operatorname{tg}\theta = \frac{(\varepsilon_D - \varepsilon_B) - \sqrt{(\varepsilon_D - \varepsilon_B)^2 + 4|V|^2}}{2|V|} . \tag{3.94}$$

The corresponding eigenenergies are

$$E_\pm = \frac{1}{2}\left[\varepsilon_D + \varepsilon_B \pm \sqrt{(\varepsilon_D - \varepsilon_B)^2 + 4|V|^2}\right] . \tag{3.95}$$

where the $-$ for ψ_1 and the $+$ sign for ψ_2. The relevant transition dipoles are then

$$\begin{aligned} \mu_{1,G} &= \langle\psi_1 |\boldsymbol{\mu}| G\rangle = \cos\theta\ \boldsymbol{\mu}_{B,G} \\ \mu_{2,G} &= \langle\psi_2 |\boldsymbol{\mu}| G\rangle = -\sin\theta\ \boldsymbol{\mu}_{B,G} \end{aligned} \tag{3.96}$$

and the excited wavefunction is

$$|\Psi_{exc}(0)\rangle = \cos\theta\ |\psi_1\rangle - \sin\theta\ |\psi_2\rangle = |B\rangle\ . \tag{3.97}$$

Here we have dropped the inessential constant factors of Eq. (3.91), so that $|\Psi_{exc}(0)\rangle$ is normalized. The excitation by a very short pulse only populates the bright state and not the dark one. We see that we are just in the conditions of the two-state Rabi problem. The population of state $|B\rangle$, which is the squared module of the autocorrelation function, will oscillate as

---

ization, i.e. all the $\boldsymbol{\mu}_{i,G}$ vectors are parallel, because then we can replace $\left|\tilde{\mathbf{E}}_0(0)\cdot\boldsymbol{\mu}_{i,G}\right|^2$ with $\left|\tilde{\mathbf{E}}_0(0)\right|^2 |\boldsymbol{\mu}_{i,G}|^2 \cos^2\alpha$, where α is the angle between the light polarization and the $\boldsymbol{\mu}_{i,G}$ vectors. In this case, the molecular orientation only affects the common factor $\cos^2\alpha$ and not the relative weights of the spectral lines.

$$|\langle \Psi_{exc}(t)\,|\Psi_{exc}(0)\rangle|^2 = 1 - \frac{4\,|V|^2}{(\varepsilon_D - \varepsilon_B)^2 + 4\,|V|^2}\ \sin^2\left(\frac{\Omega_R\ t}{2}\right) \tag{3.98}$$

where

$$\Omega_R = \hbar^{-1}\sqrt{(\varepsilon_D - \varepsilon_B)^2 + 4\,|V|^2}\ . \tag{3.99}$$

The population of the bright state may be monitored by time-resolved fluorescence or stimulated emission, while the dark state is neutral with respect to these detection techniques. So, one can experimentally measure the autocorrelation function. The normalized spectrum, which is measured by steady-state absorption spectroscopy, is

$$S(\omega) = \cos^2\theta\ \delta(\omega - E_-/\hbar) + \sin^2\theta\ \delta(\omega - E_+/\hbar)\ . \tag{3.100}$$

We leave to the reader as an exercise to verify that the spectrum and the autocorrelation function are connected by Fourier transforms as shown in the general case.

3.10 Predissociation and Fermi's Golden Rule

Many atomic and molecular processes can be modeled as a small set of bound states interacting with one or more continuum sets of dissociative states. The bound levels can be "embedded" in the continuum; i.e., their energies fall above the lowest continuum limit. As a result, the system can be "prepared" in a bound state which is "metastable," i.e., may decay irreversibly into the dissociative states. Typical cases are:

- The Auger electron emission [7]. After core electron ionization of an atom, a valence electron can fill the core hole and the energy so released can be disposed of by emitting another electron (or an X-ray photon). We can identify a state with a core hole where all electrons are bound, and several continuum sets with holes in different valence shells and a free electron. The interaction of the bound state with the continuum states determines the Auger electron emission rate.
- The electronic predissociation. One or more bound vibrational states belonging to a molecular electronically excited state are populated by photon absorption. If their energies are higher than the dissociation limit of other electronic states (for instance, the ground state), a radiationless transition (internal conversion or intersystem crossing) can lead to molecular dissociation.
- The vibrational predissociation. A bound state where high frequency vibrational modes are excited can be populated either through a mere vibrational transition caused by IR light, or through an electronic transition caused by UV-visible light leading to some degree of vibrational excitation. If the dissociation limit for the elongation of a weak bond is lower than the available vibrational energy, the bound state is embedded in a dissociative continuum made of states with less energy in high-frequency modes and more energy in the low-frequency dissociative mode.

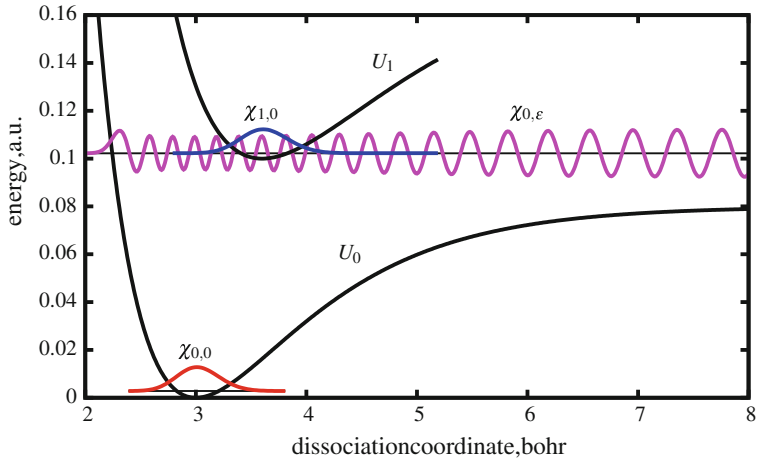

Fig. 3.6 Predissociation

This is a common situation in weakly bound molecular complexes. The anharmonic terms in the PES can transfer energy from the high to the low-frequency modes, so causing dissociation.

Electronic predissociation is an important dissociation mechanism for diatomic and polyatomic molecules. The relationship between the electronic PESs and the vibrational states involved is illustrated in Fig. 3.6. We shall consider Born–Oppenheimer states, expressed as products of electronic and nuclear factors $\varphi_k(\mathbf{r};\mathbf{R})\chi_{k,v}(\mathbf{R})$, where $\mathbf{r}$ and $\mathbf{R}$ are the electronic and the nuclear coordinates, respectively. We shall here tackle the excitation and decay processes for the simple case of one bound state $|B\rangle \equiv |\varphi_k \chi_{k,v}\rangle$, embedded in a continuum of dissociative states $|D_\varepsilon\rangle \equiv |\varphi_l \chi_{l,\varepsilon}\rangle$. Here each dissociative state is identified by its energy ε, while the bound state has got the integer index v and energy $\varepsilon_{k,v}$. In Fig. 3.6, $k = 1, l = 0$ and $v = 0$. The dissociative wavefunction $\chi_{0,\varepsilon}$ plotted in the figure is degenerate with the bound state $\chi_{1,0}$: $\varepsilon = \varepsilon_{1,0}$.

The generic symbols $|B\rangle$ and $|D_\varepsilon\rangle$ are here used because the model we are going to discuss can be used for other processes, besides electronic predissociation due to internal conversion or intersystem crossing. In the partition of the total Hamiltonian used throughout this section, $\hat{H}^{(0)}$ is the Born–Oppenheimer electrostatic Hamiltonian and $\hat{V}$ is either the nonadiabatic coupling if the states k and l belong to the same spin multiplicity or the spin–orbit coupling if k and l have different spins. To model the vibrational predissociation process, $\hat{H}^{(0)}$ would be the harmonic approximation Hamiltonian and $\hat{V}$ the coupling due to anharmonic terms.

The states $|B\rangle$ and $|D_\varepsilon\rangle$ are eigenstates of $\hat{H}^{(0)}$:

$$\hat{H}^{(0)} \ |B\rangle = \varepsilon_B \ |B\rangle \tag{3.101}$$

and

$$\hat{H}^{(0)} \ |D_\varepsilon\rangle = \varepsilon \ |D_\varepsilon\rangle \ . \tag{3.102}$$

The continuum states are normalized to the δ of energy, i.e.,

$$\left\langle D_\varepsilon \left| D'_\varepsilon \right.\right\rangle = \delta(\varepsilon - \varepsilon') \tag{3.103}$$

(see Appendix C). The perturbation only couples the bound and the continuum states:

$$\begin{aligned} \left\langle B \left| \hat{V} \right| B \right\rangle &= 0 \ , & \left\langle D_\varepsilon \left| \hat{V} \right| D_\varepsilon \right\rangle &= 0 \ , \\ \left\langle B \left| \hat{V} \right| D_\varepsilon \right\rangle &= V_B(\varepsilon) \ , & \left\langle D_\varepsilon \left| \hat{V} \right| B \right\rangle &= V_B^*(\varepsilon) \ . \end{aligned} \tag{3.104}$$

In the energy region close to ε_B and far from other bound states, the exact eigenstates are essentially linear combinations of $|B\rangle$ and of the continuum states:

$$|E\rangle = |B\rangle \langle B|E\rangle + \int_{\varepsilon_{diss}}^{\infty} |D_\varepsilon\rangle \langle D_\varepsilon|E\rangle \ \mathrm{d}\varepsilon \tag{3.105}$$

where ε_{diss} is the lower limit for the continuum energies (in the electronic predissociation process, this is the dissociation limit for state φ_l). The $|E\rangle$ states are normalized just as the $|D_\varepsilon\rangle$ ones: $\left\langle E \left| E' \right.\right\rangle = \delta(E - E')$. Using the development (3.105), the eigenvalue equation

$$\hat{H} \ |E\rangle = E \ |E\rangle \tag{3.106}$$

becomes

$$(\varepsilon_B - E + \hat{V}) \, |B\rangle \langle B|E\rangle + \int_{\varepsilon_{diss}}^{\infty} (\varepsilon - E + \hat{V}) \ |D_\varepsilon\rangle \langle D_\varepsilon|E\rangle \ \mathrm{d}\varepsilon = 0 \ . \tag{3.107}$$

Premultiplying either by $\langle B|$ or by $\langle D_\varepsilon|$ one gets, respectively

$$(E - \varepsilon_B) \langle B|E\rangle = \int_{\varepsilon_{diss}}^{\infty} V_B(\varepsilon) \langle D_\varepsilon|E\rangle \ \mathrm{d}\varepsilon = \left\langle B \left| \hat{V} \right| E \right\rangle \tag{3.108}$$

and

$$(E - \varepsilon) \ \langle D_\varepsilon|E\rangle = V_B^*(\varepsilon) \langle B|E\rangle \ . \tag{3.109}$$

From Eq. (3.108) we see that the coefficient $\langle B|E\rangle$ is proportional to the coupling strength $\left\langle B \left| \hat{V} \right| E \right\rangle$ and inversely proportional to $E - \varepsilon_B$. So, for weak couplings and E far from ε_B, $\langle B|E\rangle$ becomes negligible. When the potential energy surfaces U_k and U_l are well separated, the couplings $V_B(\varepsilon)$ tend to be small. The reason is that the $\chi_{l,\varepsilon}$ wavefunction has many nodes in the coordinate region where $\chi_{k,v}$ has none or few (see Fig. 3.6). In fact, the "wavelength" of a vibrational wavefunction is a

decreasing function of its kinetic energy, so for two (almost) degenerate vibrational states belonging to electronic terms with a large potential energy gap the wavelengths must be very different. As a consequence, integrals containing the product of two such wavefunctions are small and tend to decrease with the energy gap between the two PESs. In typical electronic predissociation conditions, the range of $E - \varepsilon_B$ values where the coefficient $\langle B\,|E\,\rangle$ is not negligible can vary from $\ll 1\ \ \mathrm{cm}^{-1}$ to several cm^{-1} (as we shall see, these ranges correspond to the experimentally known line widths). Outside that range, $|E\rangle$ can be essentially identified with the dissociative state $|D_\varepsilon\rangle$ of the same energy.

Suppose now the molecule is initially in an eigenstate $|G\rangle$, for which the adiabatic and the electrostatic approximations are quite accurate (this is usually the case for the ground state), so that we can assume $|G\rangle = \left|\varphi_0 \chi_{0,v'}\right\rangle$. We then excite the molecule with a radiation pulse of carrier frequency $\omega \simeq \varepsilon_B - E_G$, where E_G is the eigenenergy of state $|G\rangle$. Perturbation theory, Eq. (3.74), tells us that the final coefficient of state $|E\rangle$ is

$$c(E) = \frac{\pi^{1/2}\mathrm{i}}{2^{1/2}\hbar}\ \mathrm{e}^{\mathrm{i}\varphi}\ \ \langle E\,|\boldsymbol{\mu}|\,G\rangle \cdot \tilde{\mathbf{E}}_0(\omega - \omega_{E,G})\ . \tag{3.110}$$

Here $\omega_{E,G} = (E - E_G)/\hbar$. In this expression, the transition dipole moment can be decomposed using Eq. (3.105):

$$\langle E\,|\boldsymbol{\mu}|\,G\rangle = \langle E\,|B\,\rangle\,\langle B\,|\boldsymbol{\mu}|\,G\rangle + \int_{\varepsilon_{diss}}^{\infty} \langle E\,|D_\varepsilon\,\rangle\,\langle D_\varepsilon\,|\boldsymbol{\mu}|\,G\rangle\,\mathrm{d}\varepsilon \simeq \langle E\,|B\,\rangle\,\langle B\,|\boldsymbol{\mu}|\,G\rangle\ . \tag{3.111}$$

The approximation of neglecting the $\langle D_\varepsilon\,|\boldsymbol{\mu}|\,G\rangle$ integrals is normally a very good one, again because of the fast oscillations of the $\chi_{k,\varepsilon}$ wavefunction. This is the reason why high overtones, i.e., transitions to high lying vibrational states, cannot be observed spectroscopically without resorting to multiphoton absorption. Notice that the argument we use here is the same we applied to the coupling matrix elements $V_B(\varepsilon)$, but the conclusion is somewhat different, because the contribution to $\langle D_\varepsilon\,|\boldsymbol{\mu}|\,G\rangle$ we have neglected adds to the much larger $\langle B\,|\boldsymbol{\mu}|\,G\rangle$ transition dipole, while the effect of the coupling $V_B(\varepsilon)$, however small, is just what we want to study. The transition dipole (3.111) is therefore proportional to $\langle E\,|B\,\rangle$, so it also vanishes for large $|E - \varepsilon_B|$. The coefficient of state $|E\rangle$ is then

$$c(E) = \frac{\pi^{1/2}\mathrm{i}}{2^{1/2}\hbar}\ \mathrm{e}^{\mathrm{i}\varphi}\ \ \langle E\,|B\,\rangle\,\langle B\,|\boldsymbol{\mu}|\,G\rangle \cdot \tilde{\mathbf{E}}_0(\omega - \omega_{E,G})\ . \tag{3.112}$$

If the pulse is short enough, such that FWHM_ω largely exceeds the width of the absorption line, we can introduce the approximation $\tilde{\mathbf{E}}_0(\omega - \omega_{E,G}) \simeq \tilde{\mathbf{E}}_0(0)$, thus

$$c(E) = \frac{\pi^{1/2}\mathrm{i}}{2^{1/2}\hbar}\ \mathrm{e}^{\mathrm{i}\varphi}\,\langle B\,|\boldsymbol{\mu}|\,G\rangle \cdot \tilde{\mathbf{E}}_0(0)\ \ \langle E\,|B\,\rangle\ . \tag{3.113}$$

The excited state is then

$$|\Psi_{exc}(0)\rangle \simeq \frac{\pi^{1/2}\mathrm{i}}{2^{1/2}\hbar}\ \mathrm{e}^{\mathrm{i}\varphi}\ \langle B\,|\boldsymbol{\mu}|\,G\rangle \cdot \tilde{\mathbf{E}}_0(0)\ \int_{E_{min}}^{\infty} |E\rangle\ \langle E\,|B\rangle\ \mathrm{d}E = \\ = \frac{\pi^{1/2}\mathrm{i}}{2^{1/2}\hbar}\ \mathrm{e}^{\mathrm{i}\varphi}\ \langle B\,|\boldsymbol{\mu}|\,G\rangle \cdot \tilde{\mathbf{E}}_0(0)\ |B\rangle\ . \tag{3.114}$$

Apart from the constant coefficient, the square module of which is the excitation probability, this is just the $|B\rangle$ state. The heuristic interpretation is that one cannot directly populate the "dark" states $|D_\varepsilon\rangle$, but only the "bright" state $|B\rangle$. However, remember that this is only true for a short pulse with a poor frequency resolution that does not enable to distinguish among eigenstates with slightly different energies.

Let us turn to the field-free time evolution of the initial state $|B\rangle$. We shall write the time-dependent wavefunction as

$$|\Psi(t)\rangle = b(t)\mathrm{e}^{-\mathrm{i}\varepsilon_B t/\hbar}\ |B\rangle + \int_{\varepsilon_{min}}^{\infty} d_\varepsilon(t)\ \mathrm{e}^{-\mathrm{i}\varepsilon t/\hbar}\ |D_\varepsilon\rangle\ \mathrm{d}\varepsilon \tag{3.115}$$

with $b(0) = 1$ and $d_\varepsilon(0) = 0$. For this wavefunction the TDSE yields, in analogy with Eq. (3.6):

$$\dot{b}(t) = -\frac{\mathrm{i}}{\hbar}\int_{\varepsilon_{min}}^{\infty} d_\varepsilon(t)\ \mathrm{e}^{-\mathrm{i}(\varepsilon-\varepsilon_B)t/\hbar}\ V_B(\varepsilon)\ \mathrm{d}\varepsilon \tag{3.116}$$

and

$$\dot{d}_\varepsilon(t) = -\frac{\mathrm{i}}{\hbar}\ b(t)\ \mathrm{e}^{\mathrm{i}(\varepsilon-\varepsilon_B)t/\hbar}\ V_B^*(\varepsilon)\ . \tag{3.117}$$

We note that the integrand in Eq. (3.116) is negligible if $|\varepsilon - \varepsilon_B|$ largely exceeds the linewidth, because then the $|E\rangle$ eigenstates practically coincide with the $|D_\varepsilon\rangle$ states and their population tends to vanish. From Eq. (3.117) we get

$$d_\varepsilon(t) = -\frac{\mathrm{i}}{\hbar}\ V_B^*(\varepsilon)\ \int_0^t b(t')\ \mathrm{e}^{\mathrm{i}(\varepsilon-\varepsilon_B)t'/\hbar}\ \mathrm{d}t' \tag{3.118}$$

and substituting this result into Eq. (3.116):

$$\dot{b}(t) = -\frac{1}{\hbar^2}\int_{\varepsilon_{min}}^{\infty}\left[\int_0^t b(t')\ \mathrm{e}^{-\mathrm{i}(\varepsilon-\varepsilon_B)(t-t')/\hbar}\ \mathrm{d}t'\right]\ |V_B(\varepsilon)|^2\ \mathrm{d}\varepsilon\ . \tag{3.119}$$

This equation must be solved to get $b(t)$, which is directly connected with the autocorrelation function: $A(t) = b^*(t)\ \exp(\mathrm{i}\varepsilon_B t/\hbar)$. The solution can be easily found by introducing two approximations: to replace the integration limit ε_{min} with $-\infty$ and to consider $V_B(\varepsilon)$ as constant. Both approximations are based on the fact that the integrand vanishes when $|\varepsilon - \varepsilon_B|$ is much larger than the linewidth, so they are quite appropriate for very small linewidths. By putting $V_B(\varepsilon) \simeq V_B(\varepsilon_B)$ we get

$$\dot{b}(t) \simeq -\frac{1}{\hbar^2}\,|V_B(\varepsilon_B)|^2 \int_0^t b(t') \left[\int_{-\infty}^{\infty} \mathrm{e}^{-\mathrm{i}(\varepsilon-\varepsilon_B)(t-t')/\hbar}\,\mathrm{d}\varepsilon\right] \mathrm{d}t' = \\ = \frac{|2\pi\, V_B(\varepsilon_B)|^2}{\hbar} \int_0^t b(t')\,\delta(t-t')\,\mathrm{d}t' = \frac{\pi\,|V_B(\varepsilon_B)|^2}{\hbar}\,b(t) \tag{3.120}$$

(see Appendix C for the properties of the δ function). The solution of this differential equation is any combination of the two exponentials $\exp(\pm t/2\tau)$. Actually, we must choose $\exp(-t/2\tau)$ for $t > 0$ and $\exp(t/2\tau)$ for $t < 0$ to avoid a divergence (we shall see later why we are also interested in negative times). So, we can write

$$b(t) = \mathrm{e}^{-|t|/2\tau} \tag{3.121}$$

and

$$|b(t)|^2 = \mathrm{e}^{-|t|/\tau} \tag{3.122}$$

where

$$\tau = \frac{\hbar}{2\pi\,|V_B(\varepsilon_B)|^2}\,. \tag{3.123}$$

We see that the population of the bound state decays exponentially, with a rate constant τ^{-1} that is proportional to $|V_B(\varepsilon_B)|^2$, i.e., the squared module of the interaction between $|B\rangle$ and the dissociative state degenerate with it. This result is the celebrated Fermi Golden Rule.

The autocorrelation function of $|\Psi(t)\rangle$ is

$$A(t) = \mathrm{e}^{-|t|/2\tau + \mathrm{i}\varepsilon_B t/\hbar} \tag{3.124}$$

and its Fourier transform yields the spectrum

$$S(\omega) = \hbar\,|\langle B\,|E\,\rangle|^2 = (2\pi)^{-1} \int_{-\infty}^{+\infty} \mathrm{e}^{-|t|/2\tau}\,\mathrm{e}^{-\mathrm{i}(\omega-\varepsilon_B/\hbar)t}\,\mathrm{d}t = \\ = \frac{(2\pi\tau)^{-1}}{(\omega-\varepsilon_B/\hbar)^2 + (2\tau)^{-2}} = \frac{\hbar\,|V_B(\varepsilon_B)|^2}{(E-\varepsilon_B)^2 + \pi^2|V_B(\varepsilon_B)|^4}\,. \tag{3.125}$$

This is a Lorentzian function, centered at $E = \hbar\omega = \varepsilon_B$, with the linewidth $\mathrm{FWHM}_\omega = \tau^{-1} = 2\pi\,|V_B(\varepsilon_B)|^2/\hbar$. We see that the linewidth is inversely proportional to the lifetime and both are determined by $|V_B(\varepsilon_B)|^2$. For instance, a linewidth of 1 cm^{-1} corresponds to $\tau = 5.3$ ps. A light pulse much shorter than τ produces an excited state without appreciable interference with the decay process. On the other hand, its frequency width is large enough as to guarantee the approximation of constant $\tilde{\mathbf{E}}_0$ within a range of several linewidths.

In Fig. 3.7 we see the results of two simulations for a system with $V_B(\varepsilon)^2 = 0.5$ cm^{-1}, which corresponds to a linewidth $\mathrm{FWHM}_\omega = 3.14$ cm^{-1}. According to Fermi's rule the lifetime is $\tau = 1890$ fs. The excitation from the ground state is done with a constant amplitude pulse as in the Rabi model, tuned to the $G \to B$

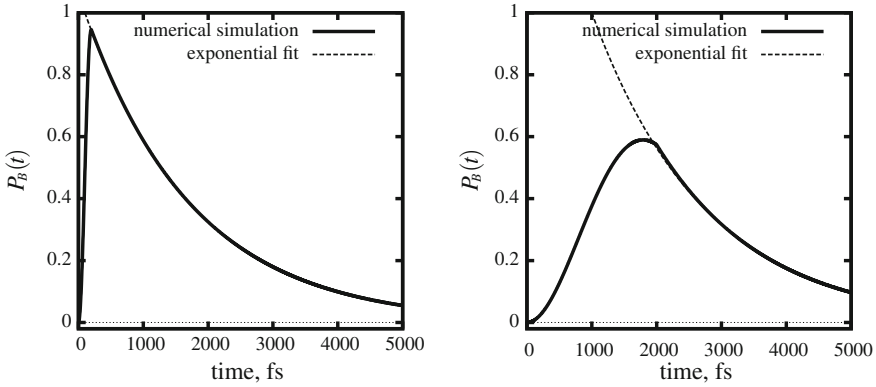

Fig. 3.7 Plot of the probability of the bright state $|\langle \Psi(t) \,|B\rangle|^2$ as a function of time. The excitation is made with a pulse of constant amplitude. In the left panel the duration of the pulse is $\Delta t = 200$ fs and in the right one is 2000 fs

transition. Two different pulse lengths Δt are used and the amplitude is adjusted in order to obtain a π pulse: $E_0 \langle G \,|\mu|\, B\rangle \, \Delta t = \pi$ (see end of Sect. 3.3). In the left panel $\Delta t = 200$ fs $\ll \tau$, so the interference between the excitation and decay processes is minimal: at the end of the pulse the population of the bound state, P_B, is almost 1. The bandwidth FWHM_ω of the light pulse (see Fig. 3.2) is of the order of 200 cm^{-1}, much larger than the absorption linewidth. These are the ideal conditions described above. On the contrary, when $\Delta t = 2000$ fs the FWHM_ω of the light pulse reduces to about six times the linewidth. Moreover, a considerable loss of population by decay to the continuum states takes place during the excitation. However, in both cases the computed $P_B(t)$ function is perfectly fitted by the exponential $\exp[-(t - \Delta t/2)/\tau]$ for $t > \Delta t$.

Without the approximation of constant $V_B(\varepsilon)$, the decay of the $|B\rangle$ population and the line shape would not be simple exponential and Lorentzian functions, respectively. The exact line shape $S(\omega)$ can be found by solving the coupled equations (3.108) and (3.109) for the $\langle B \,|E\rangle$ coefficient, while the decay law $A(t)$ is determined by the integro-differential equation (3.119). A famous paper by U. Fano [8] shows how to go beyond the constant V_B approximation. Of course $A(t)$ can be used to determine $S(\omega)$, as we have done in this section, or vice versa. The same is true if either quantity is determined experimentally: in principle, high-resolution spectroscopy or time-resolved techniques yield the same information.

3.11 Excited State Decay to a Quasi-continuum

The results of the previous section are valid beyond the case of weak coupling between one bright bound state $|B\rangle$ and a continuum of dark dissociative states $|D_\varepsilon\rangle$. First of all, the same treatment can be applied to several bound states, when their spectral lines are too wide to be treated separately (see again Ref. [8]).

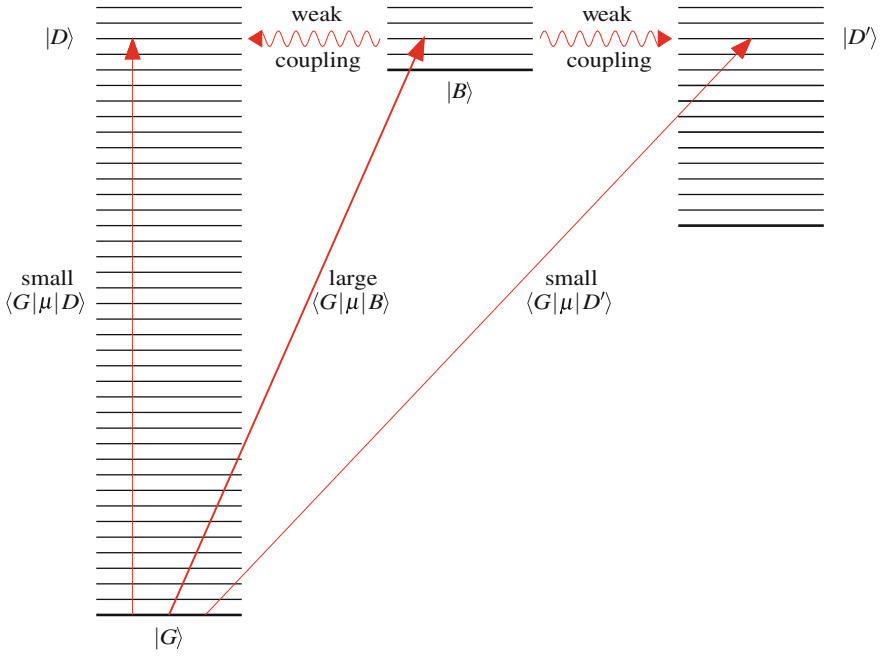

Fig. 3.8 Diagram for the excitation and decay of a bright state interacting with a quasi-continuum of dark states. No attempt is made to represent the different level densities, which increase sharply as functions of the vibrational energy

More important, the dark states to which the bright one decays are not necessarily dissociative. In fact, the essential feature is that there is a high density ρ of dark states around the energy of the bright state $|B\rangle$ (see Fig. 3.8). This is the case in polyatomics when the two PESs to which the vibrational states belong are well separated in energy and therefore the vibrational energy in the lower PES must be large. In fact, the density of states increases with energy and with the number of atoms or vibrational modes (see Sect. 2.5.2). A state with several vibrational quanta is "dark," i.e., its transition dipole to the ground state is practically zero even if each mode is not excited by more than one or two quanta. This is normally true whether the initial and final state belong to the same electronic term, as $|G\rangle$ and $|D\rangle$ in Fig. 3.8, or not, as $|G\rangle$ and $\left|D'\right\rangle$ in the same figure. The reason is that, contrary to state $|G\rangle$, the wavefunctions of $|D\rangle$ or $\left|D'\right\rangle$ contain many nodes that may concern several normal coordinates but have basically the same effect as those of the dissociative wavefunction of Fig. 3.6. Also the nonadiabatic or spin–orbit couplings between the bright state $|B\rangle$ and the almost degenerate vibrational states of the lower electronic terms $|D\rangle$ and $\left|D'\right\rangle$ are weak, for the same reason.

The treatment of this problem is quite analogous to that of a true continuum, except that instead of integrals for the continuum states $|D_\varepsilon\rangle$ we have here summations for the discrete states $|D_K\rangle$. In particular, Eq. (3.119) is replaced by

$$\dot{b}(t) = -\frac{1}{\hbar^2} \sum_K \left[\int_0^t b(t') \, \mathrm{e}^{-\mathrm{i}(\varepsilon_K - \varepsilon_B)(t-t')/\hbar} \, \mathrm{d}t' \right] \left| V_{B,K} \right|^2 \tag{3.126}$$

where $V_{B,K} = \left\langle B \left| \hat{V} \right| D_K \right\rangle$. If the density of states is very high, one can define an average $\left| V_{B,K} \right|^2$ for the $|D_K\rangle$ states having $\varepsilon_K \in [\varepsilon, \varepsilon + \delta\varepsilon]$. The (large) number of states in this (small) interval is $\rho(\varepsilon)\delta\varepsilon$. We shall indicate the average as $\overline{|V_B(\varepsilon)|^2}$ and we can go back to the integral formulation (3.119) by replacing $|V_B(\varepsilon)|^2$ with $\overline{|V_B(\varepsilon)|^2}\rho(\varepsilon)$:

$$\dot{b}(t) = -\frac{1}{\hbar^2} \int_{\varepsilon_{min}}^{\infty} \left[\int_0^t b(t') \, \mathrm{e}^{-\mathrm{i}(\varepsilon - \varepsilon_B)(t-t')/\hbar} \, \mathrm{d}t' \right] \overline{|V_B(\varepsilon)|^2} \, \rho(\varepsilon) \, \mathrm{d}\varepsilon \, . \tag{3.127}$$

We now apply the same approximations as in the previous section and in particular we assume the product of squared coupling times state density to be constant. In this way we get Fermi's Golden Rule for a quasi-continuum of states, where the exponential lifetime is

$$\tau = \frac{\hbar}{2\pi \overline{|V_B(\varepsilon_B)|^2} \rho(\varepsilon_B)} \tag{3.128}$$

and the lineshape is

$$S(\omega) = \frac{(2\pi\tau)^{-1}}{(\omega - \varepsilon_B/\hbar)^2 + (2\tau)^{-2}} = \frac{\hbar \, \overline{|V_B(\varepsilon_B)|^2} \, \rho(\varepsilon_B)}{(E - \varepsilon_B)^2 + \pi^2 \left[\overline{|V_B(\varepsilon_B)|^2} \rho(\varepsilon_B) \right]^2} \, . \tag{3.129}$$

In one of the simplest models to which these equations can be applied, proposed by Bixon and Jortner [9], the dark levels are equispaced ($\varepsilon_{K+1} = \varepsilon_K + \Delta\varepsilon$) and $V_{B,K} = V$ is independent on K. Actually the numerical simulations of Fig. 3.7 were performed by using this model, with a sufficiently high density of states $\rho = 1/\Delta\varepsilon$. It is interesting to see what happens when the density ρ is lower, i.e., the separation between consecutive levels is comparable with the linewidth $\hbar \, \mathrm{FWHM}_\omega = 2\pi \overline{|V_B(\varepsilon_B)|^2} \rho(\varepsilon_B)$. Within the Bixon-Jortner model this means $\Delta\varepsilon \approx V$. Figure 3.9 shows the results obtained with $\Delta\varepsilon = 2 \ \mathrm{cm}^{-1}$ and $V = 1 \ \mathrm{cm}^{-1}$. With such a low density of states, another parameter of the Bixon-Jortner model becomes important, namely the difference $\varepsilon_C - \varepsilon_B$, where ε_C is the dark level closest to ε_B. In our example, the two closest levels differ from ε_B by $\pm\Delta\varepsilon$.

The upper panel of Fig. 3.9 shows the time dependence of the bright-state probability with such parameters. After an exponential decay in agreement with Fermi's rule down to very low values of $P_B(t)$, we see a sudden revival of the population.

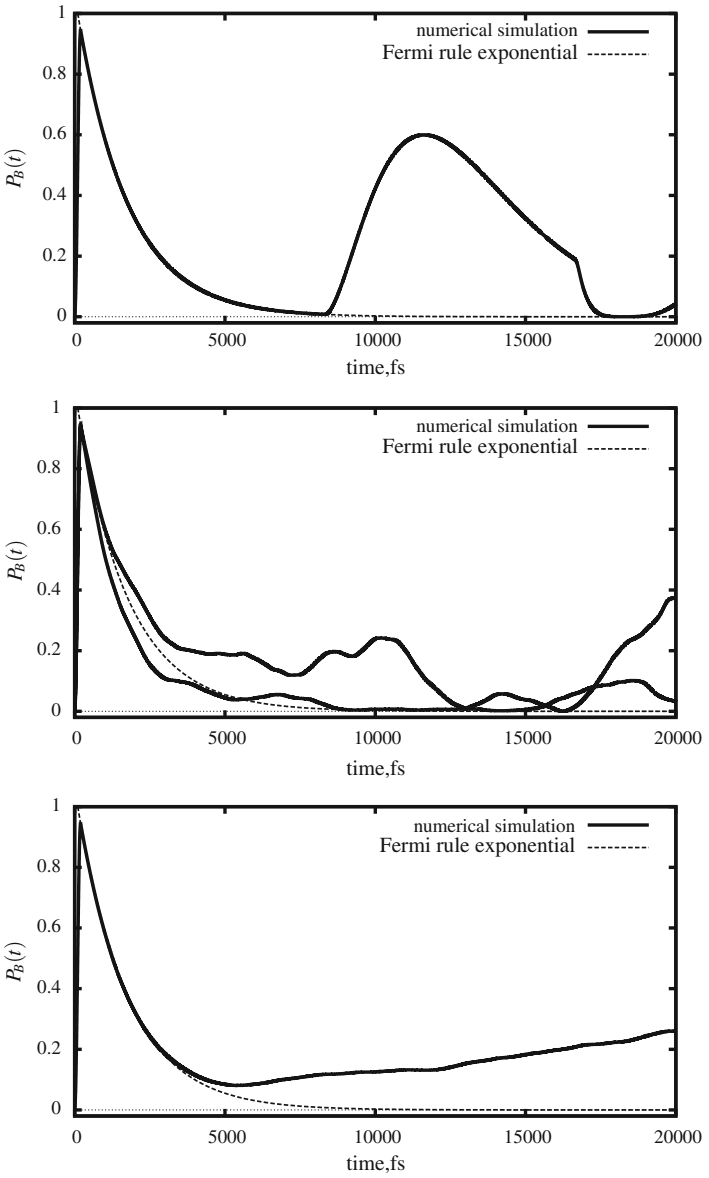

Fig. 3.9 Plot of the probability of the bright state $P_B(t) = |\langle \Psi(t) | B \rangle|^2$ as a function of time. The excitation is made with a pulse of constant amplitude and duration of 200 fs. Upper panel: Bixon-Jortner model with $\Delta\varepsilon = 2$ cm^{-1} and $V = 0.5$ cm^{-1}. Middle panel: the same with two random sequences of ε_K levels and $V_{B,K}$ couplings. Lower panel: average probability obtained from 50 random choices of the ε_K and $V_{B,K}$

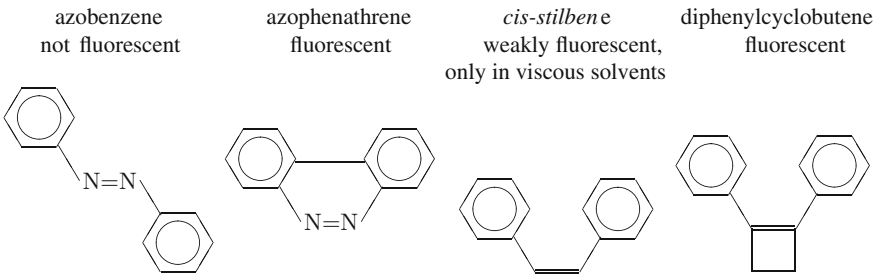

Fig. 3.10 Fluorescence and structure

This is due to the fact that the three eigenstates with the largest populations, i.e., those closest in energy to the bright state are approximately equispaced. Because of the symmetric distribution of ε_K levels around ε_B, one of the eigenvalues is just ε_B and the nearest ones are $\varepsilon_B \pm 2.68$ cm^{-1}. So, as discussed in Sect. 3.3, we expect recurrencies at times multiple of about 12.5 ps. Although instructive, this example is not realistic, because in the radiationless transitions between electronic states we can hardly find equispaced levels. As a variant of the Bixon-Jortner model, we show in the middle panel of Fig. 3.9 the results obtained with two different random sequences of ε_K levels and $V_{B,K}$ couplings, still keeping the same average density of states ρ and coupling $\overline{|V_B|^2}$. In this case the initial exponential decay is followed by irregular oscillations. In a molecular sample, with molecules in slightly different situations, for instance, because of the interactions with the environment, one would observe an averaged situation. The lower panel in Fig. 3.9 shows the averaged result of 50 simulations with different random sequences of levels and couplings. The random oscillations are averaged out, but after about 5 ps the exponential decay is replaced by a slow increase. Overall, these results illustrate the fact that the decay of the initial (bright) state of an isolated molecule is truly irreversible only with a very high density of final (dark) states.

The irreversible decay of electronically excited states can be observed even with a relatively low density of states if the final state populations are depleted by further processes. For instance, collisions in gas phase or interactions with the neighboring molecules in condensed phase lead to vibrational energy transfer. The time scale of such a process in solution is normally of the order of 10 ps. The population of the vibrationally excited states $|D_K\rangle$ is then transferred to lower levels and cannot replete the initial state $|B\rangle$. In practice, a slow decay characterized by a lifetime in the ns range or longer is very often perfectly exponential: in fact, the almost ubiquitous final state depleting processes override any long-time revival of the initial state population.

As already discussed, the coupling matrix elements between vibronic states are small when the numbers of nodes of the two vibrational wavefunctions are very different. As the number of nodes of the vibrational wavefunction in the lower electronic state increases with the energy gap between the two PESs, so decrease the coupling and the transition rate. Typically, the internal conversion from S_1 to S_0 is slow in fairly

rigid molecules, as for instance naphthalene (see Sect. 1.6.2). For such molecules, S_1 lifetimes are at least 1 ns or much longer. However, when the molecular geometry can undergo large rearrangements, as for instance by twisting a double bond, the S_1 and S_0 PESs can get much closer and the S_1 lifetime decreases dramatically. A clue about different lifetimes in analogous compounds is the fluorescence quantum yield, which is inversely proportional to the S_1 lifetime. Figure 3.10 shows two examples of the effect of structural rigidity imposed to otherwise flexible molecules. In Chap. 5 we shall analyze the fast decay of excited states and we shall see that it is often related to the intersection of potential energy surfaces.

The energy gaps between excited singlet states are usually much smaller than the gap between S_1 and S_0, and similarly for triplets. As already discussed in Chap. 2, the "crowding" of states beyond S_1 is due to the many ways one can promote an electron from bonding or nonbonding orbitals to the virtual ones, for approximately the same energetic cost, especially in large molecules. It follows that the internal conversion between excited electronic states of the same spin is usually very fast, with typical times of 1 ps or less. No matter which state the molecule was initially excited to, in a very short time it will be found in S_1 or, if ISC is very efficient, in T_1. Kasha's rule states that fluorescence is related to $S_1 \rightarrow S_0$ transitions, irrespective of the exciting wavelength. In a similar way, phosphorescence normally starts from T_1. Other slow processes, such as bimolecular reactions between partners that need to collide in gas phase or meet by diffusion in liquid phase, also occur only after the excited molecule has decayed to S_1 or T_1. Moreover, as already anticipated, in condensed phase the vibrational energy loss to the environment is also fast, so in a short time only the lowest vibrational level(s) of S_1 or T_1 are populated. In this way, the exciting photon wavelength does not affect the fluorescence and phosphorescence spectra, nor their quantum yields and those of slow photoreactions. Exceptions to Kasha's rule are very fast processes, such as direct photodissociations or the twisting of double bonds, that may outcompete the decay of higher excited states. Other interesting exceptions are molecules such as azulene, where the $S_2 - S_1$ and $S_1 - S_1$ energy gaps are both large and almost equal: as a result, fluorescence from S_2 can be observed.

3.12 Computational Note: Franck–Condon Factors and Coupling Matrix Elements

The calculation of absorption and emission spectra is a common task, which aims at assigning the experimental bands and at predicting optical properties of new molecules and materials. We have reviewed in the previous chapter how the electronic problem is tackled by deploying several quantum chemistry methods. The comparison with recorded electronic spectra or their prediction is often done by resorting to simplifying assumptions. For instance, vertical energy differences are put in relation with the intensity maxima of absorption and emission bands. More accurately, adi-

abatic energy differences are computed to approximate the 0-0 vibronic transition frequencies.

The oscillator strength of absorption or emission bands is often predicted by rewriting the sum rules (3.69) and (3.71) as

$$f(\nu_a, \nu_b) \simeq \frac{2m_e}{3\hbar^2 e^2}\, \Delta E_{vert} \sum_v \mu^2_{l0,kv} = \frac{2m_e}{3\hbar^2 e^2}\, \Delta E_{vert} \left\langle \chi_{l0} \left| \mu^2_{lk} \right| \chi_{l0} \right\rangle \tag{3.130}$$

and

$$f(\nu_a, \nu_b) \simeq \frac{2m_e}{3\hbar^2 e^2}\, \Delta E_{vert}\, \mu^2_{lk}(\mathbf{R}_{eq}) \,. \tag{3.131}$$

Here ν_a and ν_b are the boundaries of the spectral band, l is the starting electronic state where only the $v = 0$ is assumed to be populated, and ΔE_{vert} is the vertical excitation energy which replaces as an average the individual $h\nu_{l0,kv}$ transition energies. The second formula, Eq. (3.131) only applies to symmetry-allowed transitions and for the symmetry-forbidden ones just predicts vanishing oscillator strengths. The first one, Eq. (3.130), is more accurate and allows to evaluate the strength of symmetry-forbidden transitions. The χ_{l0} wavefunction can be approximated by a normal mode treatment and, in the same spirit, $\boldsymbol{\mu}_{lk}(\mathbf{R})$ can be expanded in the normal coordinates system as

$$\boldsymbol{\mu}_{lk}(\mathbf{Q}) \simeq \boldsymbol{\mu}_{lk}(0) + \sum_r \left(\frac{\partial \boldsymbol{\mu}_{lk}}{\partial Q_r} \right)_{\mathbf{Q}=0} Q_r \,. \tag{3.132}$$

Of course, for symmetry-forbidden transitions the first term vanishes, as well as all the terms concerning total-symmetric coordinates. With these approximations, the $\left\langle \chi_{l0} \left| \mu^2_{lk} \right| \chi_{l0} \right\rangle$ integral is easily computed. Anharmonic potentials and more general $\boldsymbol{\mu}_{lk}(\mathbf{Q})$ functions can be dealt with by numerical integration, for few coordinates (see, for instance, the treatment of the $n \rightarrow \pi^*$ transition in *trans*-azobenzene [10]). Anharmonicity can be particularly important for large amplitude motions with low vibrational frequencies, in which case not only the lowest vibrational state is populated at room temperature. For such modes it is reasonable to approximate the nuclear motion by classical mechanics and sample many points along nuclear trajectories to compute averaged spectra. In this way one can treat very large systems and simulate the effect of solvents or other environments as well (see Refs. [11–13] for examples and details on the techniques).

The prediction of the structure of an $l \rightarrow k$ electronic band requires the determination of the vibrational states χ_{kv}. This can be done again within the harmonic approximation, although anharmonicity is here more important because of the higher vibrational levels which are involved. Moreover, one is here confronted with the more difficult task of computing Franck–Condon factors in many coordinates, taking into account that two different normal mode systems are associated with the two PESs (Duschinsky effect) [14].

To evaluate the internal conversion rates one needs the matrix elements

$$V_{lu,kv} = \left\langle \chi_{lu} \left| -\sum_{\alpha} \frac{\hbar^2}{M_\alpha} \left[\frac{1}{2} t_{kl}^{(\alpha)} + g_{kl}^{(\alpha)} \frac{\partial}{\partial R_\alpha} \right] \right| \chi_{kv} \right\rangle . \tag{3.133}$$

If the vibrational wavefunctions are once again obtained within the normal modes approximation, it is convenient to rewrite the nonadiabatic coupling operator using the normal coordinates $\mathbf{Q}$ pertaining to state k:

$$V_{lu,kv} = \left\langle \chi_{lu} \left| -\hbar^2 \sum_{r} \left[\frac{1}{2} t_{kl}^{(r)}(\mathbf{Q}) + 2 g_{kl}^{(r)}(\mathbf{Q}) \frac{\partial}{\partial Q_r} \right] \right| \chi_{kv} \right\rangle . \tag{3.134}$$

The differential operator $\frac{\partial}{\partial Q_r}$ applies to the factorized wavefunction $\chi_{kv} = \prod_s \chi_{v_s}(Q_s)$ (see Sect. 2.5.2), namely to the factor $\chi_{v_r}(Q_r)$:

$$\frac{\partial}{\partial Q_r} \chi_{v_r}(Q_r) = \left(\frac{\omega_r}{2\hbar} \right)^{1/2} \left[v_r^{1/2} \chi_{v_r - 1}(Q_r) - (v_r + 1)^{1/2} \chi_{v_r + 1}(Q_r) \right] . \tag{3.135}$$

Then, the coupling matrix elements (3.134) reduce to matrix elements of the functions $t_{kl}^{(r)}(\mathbf{Q})$ and $g_{kl}^{(r)}(\mathbf{Q})$, which can be expanded in the same way as $\boldsymbol{\mu}_{kl}$, Eq. (3.132). The same can be done with the spin–orbit coupling, which does not imply a differentiation of the vibrational wavefunctions. Once the electronic matrix elements have been replaced by linear functions of the Q_rs, closed formulas are available for the relevant integrals. However, the number of integrals to be computed can be huge, as the density of the states χ_{kv} increases combinatorially with the size of the molecule and the energy difference between states k and l (see Sect. 2.5.2). Some of the different strategies devised to tackle this computational problem are presented in Refs. [14–17], with examples of applications. In simpler cases, anharmonic coordinates such as single bond torsions can also be taken into account [16, 17].

Problems

3.1 A system irradiated with a continuous wave as in Eq. (3.43), tuned to the transition between states 1 and 2, can be considered a two-state system, as far as its interaction with light is concerned, provided other states cannot be populated. Let us consider a molecule initially in its ground state (state 1). We want to transfer the whole population of state 1 to a vibronic level (state 2) that lies 20000 cm^{-1} higher up. There are other vibronic levels at 19900 and 20100 cm^{-1}. Apply Rabi theory to estimate the minimum duration of a rectangular pulse that can achieve this task still keeping the population of the nearby levels lower than 10^{-4}. Assume all the transition dipole moments between the ground and the excited states to be about equal.

3.2 Solve the two-state problem with constant V coupling by time-dependent perturbation theory. Compare the TDPT solution with the exact Rabi formula and show that the approximate solution is accurate for short times, in two cases: (A) $|V| \ll \Delta\varepsilon$ and (B) $\Delta\varepsilon = 0$.

3.3 Verify that the spectrum/autocorrelation relationships (3.85) and (3.86) also hold for a continuum spectrum, i.e., that they are consistent with Eqs. (3.88) and (3.89).

3.4 Derive the Rabi expression (3.98) from the spectrum of two states, one bright and one dark, given in Eq. (3.100). Make use of the connection between spectrum and autocorrelation function.

3.5 Derive the expression of the oscillator strength of an absorption or emission electronic band by applying approximations (3.131) and (3.132) and the normal coordinate treatment. Use the atomic units system and the formulas of Appendix F.

References

1. Shirley, J.H.: Solution of the Schrödinger equation with a Hamiltonian periodic in time. Phys. Rev. **138**, B979–987 (1965)
2. Einstein, A.: Strahlungs-Emission und -Absorption nach der Quantentheorie. Verhandlungen der Deutschen Physikalischen Gesellschaft **18**, 318–323 (1916)
3. Lakowicz, J.R.: Principles of Fluorescence Spectroscopy. Springer, New York (2006)
4. Andrews, D.L.: Lasers in Chemistry. Springer, Berlin (1997)
5. Merzbacher, E.: Quantum Mechanics. Wiley, New York (1998)
6. Sakurai, J., Napolitano, J.: Modern Quantum Mechanics. Cambridge University Press, Cambridge (2017)
7. Chattarji, D.: The Theory of Auger Transitions. Academic Press, London (1976)
8. Fano, U.: Effects of configuration interaction on intensities and phase shifts. Phys. Rev. **124**, 1866–1878 (1961)
9. Bixon, M., Jortner, J.: Intramolecular radiationless transitions. J. Chem. Phys. **48**, 715–726 (1968)
10. Cusati, T., Granucci, G., Persico, M., Spighi, G.: Oscillator strength and polarization of the forbidden $n \rightarrow \pi^*$ band of *trans*-azobenzene. A computational study. J. Chem. Phys. **128**, 194312/1–9 (2008)
11. Cascella, M., Cuendet, M.L., Tavernelli, I., Rothlisberger, U.: Optical spectra of Cu(II)-azurin by hybrid TDDFT-molecular dynamics simulations. J. Phys. Chem. B **111**, 10248–10252 (2007)
12. Gebauer, R., De Angelis, F.: A combined molecular dynamics and computational spectroscopy study of a dye-sensitized solar cell. New J. Phys. **13**, 085013/1–10 (2011)
13. Srebro-Hooper, M., Autschbach, J.: Calculating natural optical activity of molecules from first principles. Ann. Rev. Phys. Chem. **68**, 399–420 (2017)
14. Kupka, H.: Transitions in Molecular Systems. Wiley-VCH, Weinheim (2010)
15. Peluso, A., Santoro, F., Del Re, G.: Vibronic coupling in electronic transitions with significant Duschinsky effect. Int. J. Quantum Chem. **63**, 233–244 (1997)
16. Toniolo, A., Persico, M.: Efficient calculation of Franck-Condon factors and vibronic couplings in polyatomics. J. Comput. Chem. **22**, 968–975 (2001)
17. Toniolo, A., Persico, M.: A theoretical study of spectroscopy and predissociation dynamics in nitrosoalkanes. J. Chem. Phys. **115**, 1817–1827 (2001)

Chapter 4
Wavepacket Dynamics and Geometrical Relaxation

Abstract In this chapter we shall present the dynamics that takes place after electronic excitation, under the influence of the new potential energy surface (PES). Nonadiabatic transitions to other electronic states will be assumed to be slow enough as to be neglected, so we shall qualify this topic as "adiabatic dynamics." We shall examine the basic features of quantum wavepacket dynamics, and we shall find that some details of the excitation process affect the nature and the time evolution of the excited state even after the end of the radiation pulse. We shall see how, in certain conditions, quantum dynamics can be described with classical concepts, that are easier to grasp and provide the common language of qualitative arguments about reaction dynamics. The effects of the chemical environment on the dynamics of excited molecules will also be considered, trying to distinguish between interactions that change the PES and energy flow processes, i.e., the "static" and the "dynamic" effects, respectively.

Keywords Franck-Condon excitation · Adiabatic dynamics · Ehrenfest theorem Intramolecular vibrational energy redistribution · Thermalization · Environmental effects

4.1 Franck–Condon Excitation

We now explore the excitation by light pulses even shorter than in the previous chapter, down to few fs, i.e., the realm of "femtochemistry" that was opened in the 1980s by pioneers such as Ahmed Zewail [1]. A 10 fs pulse has a bandwidth FWHM_ω larger than 1500 cm^{-1}, so it can excite simultaneously several vibrational states, depending on the spacing of the vibrational levels. The "interesting" vibrational modes in photochemistry often have low frequencies, because they are associated with shallower minima than in the ground state: along such coordinates large amplitude motions occur, leading to conformational changes, isomerizations or other reactions.

We consider therefore the excitation from the vibronic state $\varphi_0 \chi_{0,u}$, belonging to the ground electronic term, to a set of states $\varphi_k \chi_{k,v}$ with different vibrational quantum numbers v. According to Eq. (3.74) the excited wavefunction will be

M. Persico and G. Granucci, *Photochemistry*, Theoretical Chemistry and Computational Modelling, https://doi.org/10.1007/978-3-319-89972-5_4

$$|\Psi_{exc}\rangle = \frac{\pi^{1/2}\mathrm{i}}{2^{1/2}\hbar}\ \mathrm{e}^{\mathrm{i}\phi}\ \sum_v \left|\varphi_k \chi_{k,v}\right\rangle \boldsymbol{\mu}_{kv,0u} \cdot \tilde{\mathbf{E}}_0(\Delta\omega_{kv,0u}) \tag{4.1}$$

where $\boldsymbol{\mu}_{kv,0u} = \langle \varphi_k \chi_{k,v} |\boldsymbol{\mu}| \varphi_0 \chi_{0,u} \rangle$ is the transition dipole moment and $\Delta\omega_{kv,0u} = \omega - (E_{kv} - E_{0u})/\hbar$ is the detuning. Here we adopt the Born–Oppenheimer electrostatic approximation because we have seen in Sects. 3.10 and 3.11 that the coupling with vibrationally excited dark states can be neglected as far as the excitation with short light pulses is concerned. As before, we shall also replace $\tilde{\mathbf{E}}_0(\Delta\omega_{kv,0u})$ with its value at zero detuning, although the wider range of the final energies E_{kv} makes this approximation less accurate. So, leaving aside the inessential factors, we get

$$|\Psi_{exc}\rangle = \sum_v \left|\varphi_k \chi_{k,v}\right\rangle \boldsymbol{\mu}_{kv,0u} \cdot \hat{e}_p \tag{4.2}$$

where $\hat{e}_p$ is the polarization versor of the exciting light. This expression describes a nuclear "wavepacket" in the electronic state φ_k with a shape that depends on the vibrational eigenstates $\chi_{k,v}$ and their transition dipoles $\boldsymbol{\mu}_{kv,0u}$, but not on the features of the radiation pulse, provided it is short enough. By wavepacket we mean a nonstationary normalizable wavefunction and this term is most often used for well-localized distributions in the coordinate space. A generalization of Eq. 4.2 to more electronic states can be envisaged if their PESs are close enough. A further simplification is possible when the Franck–Condon approximation is valid, i.e., in the case of dipole allowed electronic transitions. We assume $\boldsymbol{\mu}_{kv,0u} \simeq \boldsymbol{\mu}_{k,0}(\mathbf{R}_0^{(eq)})\langle \chi_{k,v} \left| \chi_{0,u} \right\rangle$ where $\mathbf{R}_0^{(eq)}$ are the equilibrium coordinates in the ground state. Then

$$|\Psi_{exc}\rangle = \boldsymbol{\mu}_{k,0}(\mathbf{R}_0^{(eq)}) \cdot \hat{e}_p \sum_v \left|\varphi_k \chi_{k,v}\right\rangle \langle \chi_{k,v} \left| \chi_{0,u} \right\rangle = \boldsymbol{\mu}_{k,0}(\mathbf{R}_0^{(eq)}) \cdot \hat{e}_p \ \left|\varphi_k \chi_{0,u}\right\rangle \ . \tag{4.3}$$

The last equality stems from the completeness of the $\left|\chi_{k,v}\right\rangle$ set of vibrational states as a basis for wavefunctions of the nuclear coordinates (actually it is sufficient to assume that the $\chi_{0,u}$ function can be expanded on a subset of the $\chi_{k,v}$ with energies well within the bandwidth of the light pulse). The excitation then generates a wavepacket with the same shape as the initial vibrational wavefunction $\chi_{0,u}$, translated into the excited PES of state φ_k. This is called a "Franck–Condon" excitation, and the region of the excited PES occupied by the wavepacket is called the Franck–Condon region. Of course in the new PES the $\chi_{0,u}$ wavepacket is not anymore a vibrational eigenstate, so it will evolve in time as shown in the next section. On the contrary a long pulse with a good frequency resolution (small FWHM_ω) allows to select a single vibrational eigenstate in the upper potential, thus creating a stationary state (apart from the almost ubiquitous decay to lower states, with or without photon emission).

In classical terms, it is often stated that the excitation process is so fast that the positions and momenta of the nuclei cannot change. What happens is then a "vertical excitation" whereby the point representing the molecule in the nuclear phase space (coordinates and momenta) is translated from the ground-state PES to the excited

one. From the above considerations about the relationship between ultrashort pulses and the generation of well-localized excited wavepackets, we see that the shorter the pulse, the closer to the real process is the vertical excitation assumption.

4.2 Vibrational Wavepacket Dynamics

When a wavepacket representing the nuclear motion is sufficiently well localized in the nuclear phase space, it moves in a way that can be approximately described by Newton-like equations. For objects with a large mass and momentum the indetermination on both position and momentum is physically irrelevant and Newton's laws of dynamics apply. Nuclei, especially lower down in the periodic table, are heavy enough as to be treated by classical mechanics as a first approximation, although important details, such as the quantization of vibrational levels and tunneling, are lost. Ehrenfest's theorem shows that there is a relationship between quantum wavepacket dynamics and Newton's laws even for light particles.

Consider the time dependence of the expectation value of an observable $\hat{A}$, for a wavepacket $\psi(\mathbf{x}, t)$. Here $\mathbf{x}$ is the collection of the particles coordinates x_i. From the TDSE, Eq. (2.1), we have:

$$\frac{\mathrm{d}}{\mathrm{d}t}\left\langle \psi \left| \hat{A} \right| \psi \right\rangle = \left\langle \frac{\mathrm{d}\psi}{\mathrm{d}t} \left| \hat{A} \right| \psi \right\rangle + \left\langle \psi \left| \hat{A} \right| \frac{\mathrm{d}\psi}{\mathrm{d}t} \right\rangle = \frac{\mathrm{i}}{\hbar}\left\langle \psi \left| \left[\hat{H}, \hat{A}\right] \right| \psi \right\rangle . \tag{4.4}$$

In the Hamiltonian $\hat{H}$, we must distinguish the potential energy term $V(\mathbf{x})$ and the kinetic energy

$$\hat{T} = -\sum_j \frac{\hbar^2}{2m_j}\frac{\partial^2}{\partial x_j^2} . \tag{4.5}$$

Here m_j is the mass of the particle associated with the x_j coordinate. If $\hat{A}$ is one of the coordinates, say x_i, it commutes with $V(\mathbf{x})$ but not with $\hat{T}$. By indicating with the shorthand $\langle x_i \rangle$ its expectation value, we can write

$$\frac{\mathrm{d}\langle x_i \rangle}{\mathrm{d}t} = \frac{\mathrm{i}}{\hbar}\left\langle \psi \left| \left[\hat{T}, x_i\right] \right| \psi \right\rangle = \frac{\langle \hat{p}_i \rangle}{m_i} \tag{4.6}$$

where $\hat{p}_i$ is the linear momentum operator associated with the coordinate x_i. Note that only the derivative with respect to x_i contributes to the commutator. Consider now the time derivative of the expectation value of $\hat{p}_i$. Here the only contribution to the commutator is due to $V(\mathbf{x})$:

$$\frac{\mathrm{d}\langle \hat{p}_i \rangle}{\mathrm{d}t} = \frac{\mathrm{i}}{\hbar}\left\langle \psi \left| -\mathrm{i}\hbar\left[V(\mathbf{x}), \frac{\partial}{\partial x_i}\right] \right| \psi \right\rangle = -\left\langle \frac{\partial V}{\partial x_i} \right\rangle . \tag{4.7}$$

Ehrenfest's equations (4.6) and (4.7) are the quantum equivalent of Newton's equations, i.e.,

$$\dot{x_i} = \frac{p_i}{m_i} \quad \text{and} \quad \dot{p_i} = -\frac{\partial V}{\partial x_i} \,. \tag{4.8}$$

The difference is that Ehrenfest's equations of course apply to the expectation values of x_i, $\hat{p}_i$ and $\partial V/\partial x_i$, i.e., to averages taken over all coordinates, while Newton's equations concern a single point in the phase space. Knowing $\langle x_i \rangle$ and $\langle \hat{p}_i \rangle$ is a very valuable information if the coordinate and momentum distributions are sharply peaked around the average values, but of course the indetermination principle limits the localization of a wavepacket in both variables.

The shape of the potential energy function is also important. Let's expand $V(\mathbf{x})$ as a Taylor series of $\Delta\mathbf{x} = \mathbf{x} - \langle \mathbf{x} \rangle$:

$$V(\mathbf{x}) = V(\langle \mathbf{x} \rangle) + \Delta\mathbf{x}^t \mathbf{G}(\langle \mathbf{x} \rangle) + \frac{1}{2} \Delta\mathbf{x}^t \mathbf{H}(\langle \mathbf{x} \rangle) \Delta\mathbf{x} + O\left(|\Delta\mathbf{x}|^3\right) \tag{4.9}$$

where $\mathbf{G}$ is the gradient of $V(\mathbf{x})$ and $\mathbf{H}$ its Hessian matrix. Then

$$\frac{\partial V}{\partial x_i} = G_i(\langle \mathbf{x} \rangle) + \sum_j H_{ij}(\langle \mathbf{x} \rangle) \Delta x_j + O\left(|\Delta\mathbf{x}|^2\right) \tag{4.10}$$

When we take the average of this distribution the linear term containing the Hessian does not contribute, so by neglecting the terms of the order of $|\Delta\mathbf{x}|^3$ in the potential we get

$$\left\langle \frac{\partial V}{\partial x_i} \right\rangle \simeq \left(\frac{\partial V}{\partial x_i} \right)_{\langle x \rangle} \,. \tag{4.11}$$

Then, the time evolution of $\langle \mathbf{x} \rangle$ and $\langle \mathbf{p} \rangle$ does not depend on the average of $\mathbf{G}$, but just on its value in $\langle \mathbf{x} \rangle$. This result is even closer to classical mechanics than Eq. (4.7) and is valid as far as the wavepacket is sufficiently localized in space; otherwise one cannot neglect the higher powers of $|\Delta\mathbf{x}|$.

For harmonic potentials Eq. (4.11) is exact, so the evolution of $\langle \mathbf{x} \rangle$ and $\langle \mathbf{p} \rangle$ is perfectly classical. By converting to the normal coordinates system (see Sect. 2.5), the motion is periodic along each coordinate Q_α. The periodicity of quantum dynamics is a more general property of the harmonic oscillator and is due to the equal spacing of the energy levels $E_v = (v + 1/2)\hbar\omega$. The time-dependent wavefunction for a given mode Q can be expressed as

$$\chi(Q,t) = \sum_{v=0}^{\infty} c_v \, \mathrm{e}^{-\mathrm{i}(v+1/2)\omega t} \, \chi_v(Q) = \mathrm{e}^{-\mathrm{i}\omega t/2} \sum_{v=0}^{\infty} c_v \, \mathrm{e}^{-\mathrm{i}v\omega t} \, \chi_v(Q) \tag{4.12}$$

where the χ_v are the vibrational eigenfunctions. All the $\exp(-\mathrm{i}v\omega t)$ factors are periodic functions of time, with a common period $T = 2\pi/\omega$. So, apart from the irrelevant

factor $\exp(-i\omega t/2)$, the system is back to the initial wavefunction at times that are integer multiples of T: $\chi(Q, nT) = \chi(Q, 0)$. Moreover, at half-integer multiples of T all coefficients with even v take their initial values, while those with odd v change in sign, so the wavefunction converts to the specular image of the initial one with respect to the equilibrium point $Q = 0$, i.e., $\chi(Q, T/2 + nT) = \chi(-Q, 0)$.

Putting together the concepts of Franck–Condon excitation, Ehrenfest's theorem and the harmonic approximation, we can sketch the short-time dynamics as follows:

1. Excitation by an ultrashort pulse creates a localized nuclear wavepacket in an excited state PES. The wavepacket resembles the starting vibrational state in the ground-state PES.
2. Radiationless transitions to other states can be neglected, unless they are very fast, as in the presence of conical intersections (see next chapter). The dynamics is therefore "adiabatic."
3. The center of the wavepacket moves in the excited PES according to classical mechanics, as far as the wavepacket is sufficiently well localized in the coordinate space.
4. If the excited PES is approximately harmonic and the wavepacket can be decomposed as a product of factors, each depending on one normal coordinate, it will oscillate along each coordinate according to the relative frequency.

Note that the harmonic approximation is usually a good one for the lowest vibrational levels in the ground-state PES and yields wavefunctions that are factorized in the normal coordinates $\mathbf{Q}^{(gs)}$: $\chi_{\mathbf{v}}(\mathbf{Q}^{(gs)}) = \prod_r \chi_{v_r}^{(r)}(Q_r^{(gs)})$. In the Franck–Condon approximation, this wavepacket is translated into the excited state PES without modification. However, independent oscillations along each normal coordinate, as referred to in the last point of the above list, only occur if the wavepacket is factorized as a function of the excited state normal coordinates $\mathbf{Q}^{(ex)}$. Unfortunately the $\mathbf{Q}^{(ex)}$ are linear combinations of the Cartesian coordinates of the nuclei just as the $\mathbf{Q}^{(gs)}$, but with different coefficients. The factorization of $\chi_{\mathbf{v}}$ in the $\mathbf{Q}^{(ex)}$ coordinates is therefore approximately true only if one can neglect the difference between the two normal coordinates systems, i.e., the so-called Duschinsky effect.

Figures 4.1, 4.2, and 4.3 illustrate the relationship between the excitation process and the adiabatic dynamics for one-dimensional potentials, i.e., for a model diatomic molecule in which we consider two electronic states. The transition dipole moment is assumed to be independent on the internuclear distance and the radiation pulse has a Gaussian shape as in Eq. (3.76). Its amplitude has been kept sufficiently low as to be in the first-order TDPT regime, the excitation probability being less than 1% in all cases: however, the results illustrated in this section are based on numerically exact calculations. The carrier frequency ω is tuned to the vibronic transition with the largest Franck–Condon factor, i.e., to $\chi_{e,24}$ for the harmonic potentials and to $\chi_{e,40}$ for the Morse ones (see Fig. 4.1). Figures 4.2 and 4.3 show the average internuclear distance $\langle R \rangle$ in the excited state as a function of time.

In the harmonic model $\langle R \rangle$ undergoes perfectly periodic oscillations between two turning points. With an ultrashort pulse ($\tau = 10$ fs) the requirements for a Franck–Condon excitation are fulfilled; thus the inner turning point is close to the equilibrium

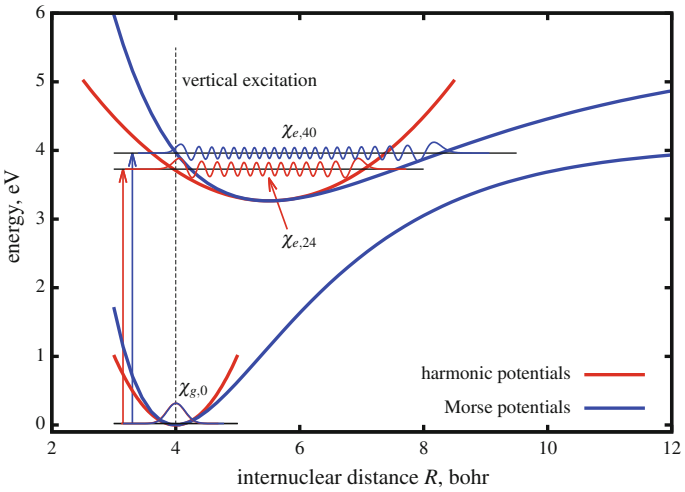

Fig. 4.1 Harmonic and Morse potentials for the diatomic molecule model with two electronic states.The vibrational levels and wavefunctions shown are $\chi_{g,0}$ (electronic ground state, $v = 0$), which is practically the same for either the harmonic and the Morse potential; $\chi_{e,24}$ and $\chi_{e,40}$, which are the wavefunctions with the largest overlap with $\chi_{g,0}$, respectively for the harmonic and the Morse excited potentials

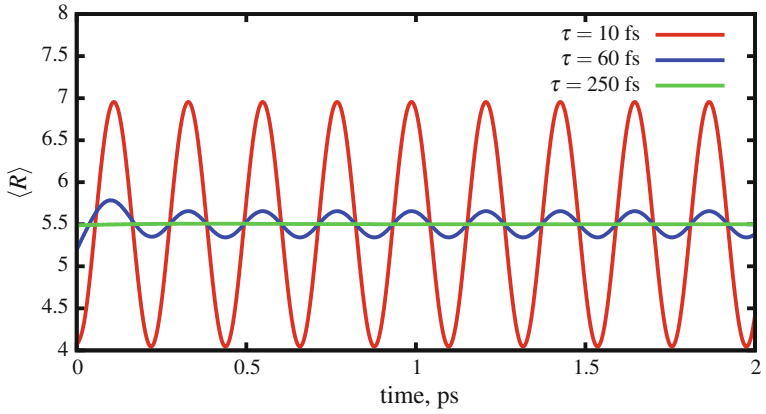

Fig. 4.2 Plot of the average internuclear distance $\langle R \rangle$ of a diatomic molecule as a function of time, for a wavepacket created in the excited electronic state by an ultrashort radiation pulse. The radiation pulse is Gaussian as in Eq. (3.76), centered at $t = 0$, and three different pulse lengths τ have been simulated. The ground and excited potentials are assumed to be the harmonic functions of Fig. 4.1

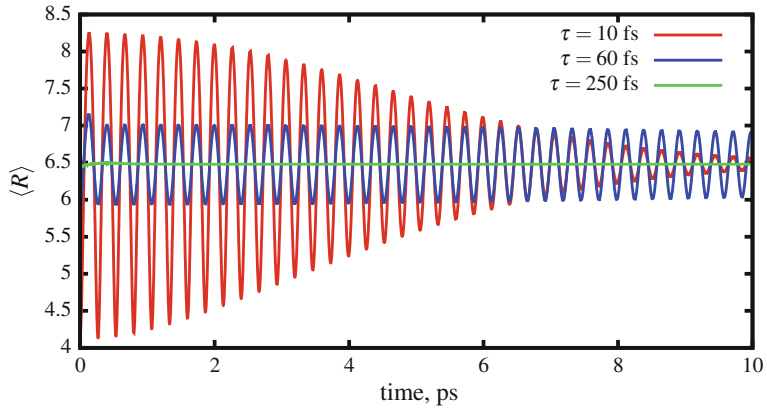

Fig. 4.3 Plot of the average internuclear distance $\langle R \rangle$ as in Fig. 4.2, but with the Morse potentials depicted in Fig. 4.1

distance in the ground state (4 bohr). With a longer pulse (60 fs) the oscillation amplitude is much reduced, because few vibrational states in the upper potential are populated and the initial wavepacket is not a faithful image of the ground-state vibrational wavefunction translated in the excited PES. With $\tau = 250$ fs only the $\chi_{e,24}$ state is populated, so the excited wavefunction is practically stationary and $\langle R \rangle$ is constant in time. Animations 4.1–4.3 show the time dependence of the excited wavepacket, plotted as $|\chi(R)|^2$ in arbitrary units. One can appreciate that the Franck–Condon excitation with $\tau = 10$ fs creates a well-localized wavepacket that maintains this character indefinitely although its width in the R coordinate undergoes periodic changes. The 60 fs pulse creates a much broader wavepacket, with the two most pronounced maxima at the turning points and a periodic alternation among which of the two is prevalent. The animation for the 250 fs pulse confirms that the wavepacket is almost perfectly stationary. We also note that, with the shortest pulse, the growth of the wavepacket due to optical excitation is much faster than, and almost decoupled from, the motion in the excited state potential. On the contrary, with the intermediate pulse (60 fs), the excitation process and the vibrational dynamics occur in the same timescale.

Switching from the harmonic to the Morse potentials (see Fig. 4.3 and Animations 4.4–4.6), the most important features remain similar, but not quite. The main difference occurs in a relatively long timescale (few ps), after excitation with the ultrashort pulse of 10 fs. We observe a steady decrease in the amplitude of the $\langle R \rangle$ oscillations, and the animation shows that the initially well-localized wavepacket spreads out, occupying the whole classically allowed region. One can detect oscillations from left to right and back (similarly to the harmonic case with the 60 ps pulse), but the shape of the wavepacket is less regular. The lack of periodicity of the dynamics in anharmonic potentials is a manifestation of a frequently met feature of quantum dynamics, called "decoherence." Decoherence occurs when different

components of a wavefunction (here, the vibrational eigenstates) do not keep the same relationships among them while evolving in time. In the case of anharmonic potentials the reason is dephasing (i.e., change of the relative phases) of the coefficients of the eigenstates: in fact, the coefficients do not change with a common time period as those of Eq. (4.12), because the vibrational levels in the Morse potential are not equispaced. This is confirmed by comparing the dynamics triggered by the $\tau = 10$ and $\tau = 60$ fs pulses: with the latter, as already seen in the harmonic case, very few vibrational eigenstates are significantly populated (those with $v = 39, 40$ and 41), so the wavepacket is delocalized and the amplitude of the $\langle R \rangle$ oscillations is initially smaller than with the 10 fs pulse. However, the amplitude decreases much more slowly than with the 10 fs pulse and the animation shows almost no decoherence effects. The reason is that dephasing is minimal, because the $E_{40} - E_{39}$ and $E_{41} - E_{40}$ energy differences are almost equal. Decoherence is much faster when the wavepacket is expanded on a dozen of states, as with the shorter pulse, because then the spread in the energy differences is larger.

The above results highlight the importance of considering the uncertainties of x_i and $\hat{p}_i$, in addition to their averages. The squared uncertainties (second moments or variances) are

$$\Delta x_i^2 = \left\langle \psi \left| (x_i - \langle x_i \rangle)^2 \right| \psi \right\rangle = \left\langle \psi \left| x_i^2 \right| \psi \right\rangle - \langle x_i \rangle^2 \tag{4.13}$$

and

$$\Delta p_i^2 = \left\langle \psi \left| (\hat{p}_i - \langle \hat{p}_i \rangle)^2 \right| \psi \right\rangle = \left\langle \psi \left| \hat{p}_i^2 \right| \psi \right\rangle - \left\langle \hat{p}_i \right\rangle^2 \ . \tag{4.14}$$

The equations of motion for these two quantities can be deduced as follows:

$$\frac{\mathrm{d}}{\mathrm{d}t} \left\langle \psi \left| (x_i - \langle x_i \rangle)^2 \right| \psi \right\rangle = \frac{i}{\hbar} \left\langle \psi \left| [\hat{H}, x_i^2] \right| \psi \right\rangle - 2 \langle x_i \rangle \frac{\mathrm{d} \langle x_i \rangle}{\mathrm{d}t} \ . \tag{4.15}$$

Using the rule $[\hat{A}, \hat{B}\hat{C}] = \hat{B}[\hat{A}, \hat{C}] + [\hat{A}, \hat{B}]\hat{C}$ for the first term and Ehrenfest's theorem for the second one, we get:

$$\begin{aligned} &\frac{\mathrm{d}}{\mathrm{d}t} \left\langle \psi \left| (x_i - \langle x_i \rangle)^2 \right| \psi \right\rangle = \frac{\mathrm{i}}{\hbar} \left\langle \psi \left| x_i [\hat{H}, x_i] + [\hat{H}, x_i] x_i \right| \psi \right\rangle - 2 \langle x_i \rangle \frac{\left\langle \hat{p}_i \right\rangle}{m_i} = \\ &= m_i^{-1} \left[\left\langle \psi \left| x_i \hat{p}_i + \hat{p}_i x_i \right| \psi \right\rangle - 2 \langle x_i \rangle \left\langle \hat{p}_i \right\rangle \right] = \\ &= m_i^{-1} \left\langle \psi \left| (x_i - \langle x_i \rangle)(\hat{p}_i - \left\langle \hat{p}_i \right\rangle) + (\hat{p}_i - \left\langle \hat{p}_i \right\rangle)(x_i - \langle x_i \rangle) \right| \psi \right\rangle \ . \end{aligned} \tag{4.16}$$

We similarly find:

$$\begin{aligned} &\frac{\mathrm{d}}{\mathrm{d}t} \left\langle \psi \left| (\hat{p}_i - \left\langle \hat{p}_i \right\rangle)^2 \right| \psi \right\rangle = \\ &= -\left\langle \psi \left| (\hat{p}_i - \left\langle \hat{p}_i \right\rangle) \left(\frac{\partial V}{\partial x_i} - \left\langle \frac{\partial V}{\partial x_i} \right\rangle \right) + \left(\frac{\partial V}{\partial x_i} - \left\langle \frac{\partial V}{\partial x_i} \right\rangle \right) (\hat{p}_i - \left\langle \hat{p}_i \right\rangle) \right| \psi \right\rangle \ . \end{aligned} \tag{4.17}$$

These equations too have classical analogues. Consider a set of classical trajectories with different initial conditions for a system of particles, that give place to a distribution of values for the variables x_i and p_i. We define averages over all trajectories for these variables and their second moments, and we indicate them as $\overline{x_i}$, $\overline{p_i}$, and so on, to distinguish them from the quantum expectation values. Equation (4.8) trivially yield the time dependence of $\overline{x}$ and $\overline{p_i}$:

$$\frac{d}{dt}\,\overline{x_i} = \frac{\overline{p_i}}{m_i} \qquad \text{and} \qquad \frac{d}{dt}\,\overline{p_i} = -\overline{\left(\frac{\partial V}{\partial x_i}\right)}\,. \tag{4.18}$$

For the second moments we get

$$\frac{d}{dt}\,\overline{(x_i - \overline{x_i})^2} = 2\overline{(x_i - \overline{x_i})\left(\dot{x}_i - \overline{\dot{x}_i}\right)} = 2m_i^{-1}\,\overline{(x_i - \overline{x_i})\,(p_i - \overline{p_i})} \tag{4.19}$$

$$\frac{d}{dt}\,\overline{(p_i - \overline{p_i})^2} = -2\overline{(p_i - \overline{p_i})\left(\frac{\partial V}{\partial x_i} - \overline{\frac{\partial V}{\partial x_i}}\right)}\,. \tag{4.20}$$

We see that Eqs. (4.19) and (4.20) are perfectly analogue to Eqs. (4.16) and (4.17), except that in the quantum case $\hat{p}_i$ does not commute with x_i and $V(\mathbf{x})$, so we have the sum of two distinct quantities such as $x_i\hat{p}_i$ and $\hat{p}_i x_i$ instead of the classical expression $2x_i p_i$. The physical meaning of both pairs of equations concerns the correlation between positions, momenta, and forces, which is more easily understood in classical terms. According to Eq. (4.19) the x_i distribution broadens in time if $x_i - \overline{x_i}$ and $p_i - \overline{p_i}$ are mostly of the same sign, whereas it narrows if x_i and p_i tend to deviate from their averages in opposite directions. Equation (4.20) similarly means that the p_i distribution spreads out when the momentum p_i and the force $-\partial V/\partial x_i$ deviate from their averages in a concordant way, while it narrows when the deviations are discordant.

The consequences of such correlations for quantum dynamics are most clearly illustrated by the Animations 4.1 and 4.4, which show the motion of well-localized wavepackets created by Franck–Condon excitation. While the wavepacket oscillates back and forth, its width in the R coordinate also changes. The width variation of course is perfectly periodic in the harmonic potential and only approximately so in the Morse one. The ground-state $v = 0$ eigenfunction that is translated into the excited PES by an ultrashort pulse is a minimum uncertainty Gaussian wavepacket with vanishing average momentum. Its R and $\hat{P}$ (the associate momentum) distributions are independent, so the expression Eq. 4.16 vanishes. However, if put in a constant potential, the wavepacket would spread out indefinitely in the R coordinate, while its momentum distribution would remain unchanged. Also in a linear potential, with constant $\partial V/\partial R$, the wavepacket would spread, but in this case $\left\langle \hat{P} \right\rangle$ would change in time according to (4.7), still keeping the same distribution of $\hat{P} - \left\langle \hat{P} \right\rangle$. We easily see why a swarm of trajectories with the same distributions of coordinates and momenta

as the Gaussian wavepacket mimics well the wavepacket behavior, at least for short times: trajectories with $P > \overline{P}$ soon or later will be at the forefront of the swarm, while those with $P < \overline{P}$ will lag behind, which produces a broadening of the swarm corresponding to a positive result for the average (4.19). To counteract this broadening effect, one needs a potential with positive curvature, such as to decrease the momentum in regions where $(R - \langle R \rangle)(P - \langle P \rangle) > 0$ and to increase it when the two factors are opposite in sign. The curvature that exactly annihilates the broadening effect is by definition that of the harmonic oscillator of which the wavepacket is an eigenfunction. Larger curvatures have a narrowing effect and smaller curvatures, as in our model, permit a temporary broadening (see the animations referred to above).

Negative curvatures occur at saddle points, such as one finds in $n \rightarrow \pi^*$ or $\pi \rightarrow \pi^*$ excited states along the double-bond torsional coordinate of imines or azo-compounds. In that case, the wavepacket initially broadens and then splits in two components, one on each side of the saddle point. The two components will correspond to distinct photoisomerization pathways. The pathways may be equivalent, if the PES is symmetric, as is the case when starting from planar structures. A good example is the $trans \rightarrow cis$ photoisomerization of azobenzene [2, 3], as illustrated in Fig. 4.4. In other cases, the PES is not symmetric with respect to the torsional coordinate and the two pathways are not equivalent, one of them leading more easily to the reaction product. This is the case for the $cis \rightarrow trans$ photoisomerization of azobenzene, also shown in Fig. 4.4. In fact, the cis isomer exists in two enantiomeric conformers and, starting from each of them, the torsion of the double bond can increase the distance of the two phenyl rings or push them closer. In the former case

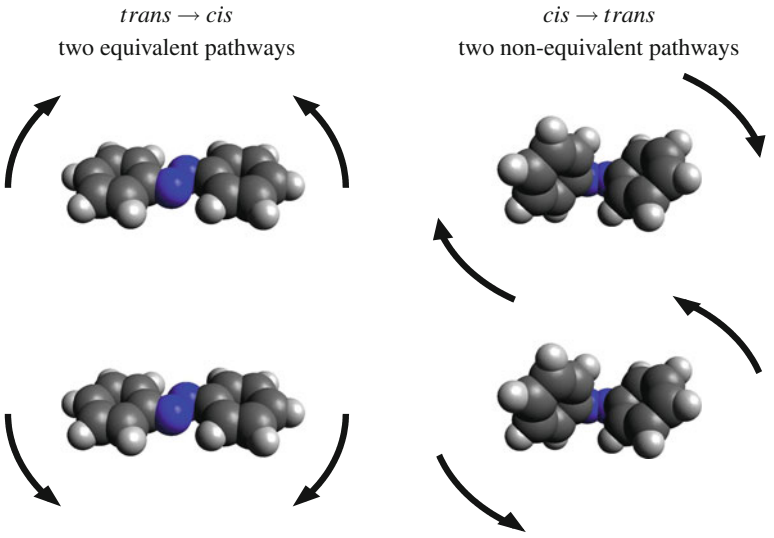

Fig. 4.4 Photoisomerization of azobenzene. Two equivalent pathways exist for the $trans \rightarrow cis$ conversion and two nonequivalent ones for the $cis \rightarrow trans$ conversion

the chirality is conserved till the achiral product is formed, while in the latter case a chirality inversion occurs. Simulations show that the chirality conserving pathway is preferred when exciting in the $n \rightarrow \pi^*$ band, while the more energetic $\pi \rightarrow \pi^*$ excitation overrides this bias [2, 3].

4.3 Intramolecular Vibrational Energy Redistribution

As we have seen, the electronic excitation is normally associated with a certain degree of vibrational excitation. Depending on the light wavelength, bandwidth, and polarization, a single vibrational eigenstate or a time-dependent wavepacket may be produced. In both cases, the vibrational energy in the excited state is $h\nu - (E_{k,0} - E_{0,u})$. Here $E_{0,u}$ is the energy of the starting state and $E_{k,0}$ is the energy of the lowest vibrational state in the excited PES k. This relationship is exact in the case of monochromatic light and is usually a good approximation of the mean value of the wavepacket energy when using broadband light pulses. In polyatomics, if the vibrational energy excess is a few thousands cm^{-1} or more, it is hard to populate a chosen eigenstate, because the huge density of states (see Table 2.1) prevents to resolve single levels. However, even when the outcome is a nonstationary wavepacket, i.e., a superposition of eigenstates, the initial distribution of the vibrational excitation is not statistical but can privilege one or a few vibrational modes. This bias depends on the characteristics of the exciting light and on the transition dipoles between the initial vibronic state $\varphi_0 \chi_{0,u}$ and the possible final states $\varphi_k \chi_{k,v}$. The transition dipoles in turn depend very much on the shapes of the initial and final PESs through the Franck–Condon factors $\langle \chi_{0,u} \,|\, \chi_{k,v} \rangle$; see Eq. 3.70. As a consequence, excitation will mostly concern vibrational coordinates along which the two PESs are sharply different, as we have seen in Sect. 3.7.

Franck–Condon excitation and its classical analogue, vertical excitation, provide the simplest illustration of the above considerations. The center of the excited wavepacket approximately lies, in the normal coordinate system $\mathbf{Q}^{(ex)}$ of the excited PES, in the position $\Delta\mathbf{Q}$, which is determined by the difference between the equilibrium geometries of ground and excited state. Classically, for each normal mode, ΔQ_α is the maximum elongation of the oscillatory motion that follows the excitation. $E_\alpha = \omega_\alpha^2 \Delta Q_\alpha^2/2$ is the classical normal mode vibrational energy and is a good approximation for the quantum mechanical expectation value too. The short-time dynamics is determined by the ΔQ_α elongations and E_α energies, so for instance if E_α for a bond stretching coordinate exceeds the dissociation energy, bond breaking is likely to occur promptly. However, the E_α distribution of energies in the vibrational modes does not remain unaltered for many oscillations, mainly because of anharmonicity. This phenomenon is called "internal" or 'intramolecular vibrational energy redistribution" (IVR). The IVR is important in photochemistry, because several elementary processes can happen only when enough energy is concentrated in one or few vibrational modes. IVR can provide or subtract energy to a particular vibrational mode, so triggering or inhibiting such "activated" processes. Examples

are bond breakings (when the corresponding potential energy curve is bound), all reactions that require to overcome potential energy barriers, and radiationless decay processes that only occur when high energy surface crossings are reached (see next chapter).

As already observed in Sect. 3.10, the harmonic vibrational Hamiltonian (2.121) can be taken as a zero-order approximation, while the anharmonic terms provide a perturbation that promotes transitions between the zero-order eigenstates. Transitions will be fast between almost degenerate states strongly coupled by the anharmonic terms. The coupling matrix elements depend on the shape of the potential and on the vibrational quantum numbers of the states involved: in general, the magnitude of the anharmonic terms in the potential increases with the amplitude of the vibrational motions. For instance, if we add a cubic potential term of the form $k_{rst}\,Q_r\,Q_s\,Q_t$ to the zero-order Hamiltonian (2.121), we couple vibrational states differing by one quantum in each of the three modes. Suppose a state with quantum numbers v_r, v_s, v_t for the Q_r, Q_s, Q_t modes is initially populated. This state is coupled to eight states with $v'_r = v_r \pm 1$, $v'_s = v_s \pm 1$, $v'_t = v_t \pm 1$ by the cubic potential. Their energies differ from the initial one by $\pm\,\omega_r \pm \omega_s \pm \omega_t$, which may be accidentally a small energy if the sum of two frequencies approximately coincides with the third one. In a large molecule, with a rich choice of frequencies, it is very probable to find almost degenerate states that are coupled by cubic or higher order terms. In our example, the coupling matrix element is

$$\left\langle v_r, v_s, v_t \,|k_{rst}\,Q_r\,Q_s\,Q_t|\, v'_r, v'_s, v'_t \right\rangle = k_{rst} \left[\frac{\max(v_r, v'_r)\,\max(v_s, v'_s)\,\max(v_t, v'_t)\;\hbar^3}{8\omega_r\;\omega_s\;\omega_t} \right]^{1/2} \tag{4.21}$$

where $\max(n, n')$ is the larger of the two numbers. Considering that the classical amplitude of the oscillation along the Q_r coordinate is $[(2v_r + 1)\hbar/\omega_r]^{1/2}$, we see that the coupling increases roughly proportionally to the amplitudes of the three modes. In fact the IVR is faster for high vibrational levels and low frequencies, because both the couplings and the number of almost degenerate states are larger. Typical times for the transfer of energy among different modes can be of the order of 1 ps. The IVR can be much slower if the initial state has one quantum in a high-frequency mode, and all other modes are of much lower frequency: this is the case in the phenomenon of vibrational predissociation (see Sect. 3.10).

For an isolated molecule with constant energy E_{vib}, at sufficiently long times the microcanonical equilibrium distribution will be established. In quantum mechanics, this means every state with energy close to E_{vib} has the same probability to be populated. In classical mechanics, the probability density, as a function of the coordinates $\mathbf{Q}$ and momenta $\mathbf{P}$, is the same for all points in the phase space with total energy E_{vib}. These two statements are not equivalent, namely they imply different energy distributions in the vibrational modes. Note that the lowest possible energy in classical mechanics coincides with the potential energy at the equilibrium geometry, while in quantum mechanics it is the zero-point energy $\sum_{r=1}^{N_{modes}} \hbar\omega_r/2$. Therefore in this context we shall take as zero of the energy scale these two different references when discussing classical and quantum mechanical energies, respectively (this holds both for E_{tot} and for the single-mode energies). The microcanonical classical energy

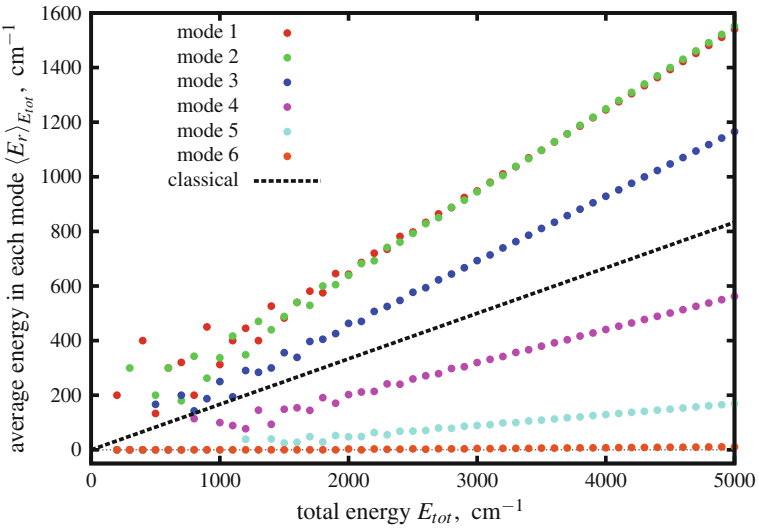

Fig. 4.5 Average energy stored in each vibrational mode as a function of the total energy, according to the microcanonical distribution for a tetratomic molecule with harmonic frequencies of 200, 300, 500, 800, 1200, and 2000 cm^{-1}. The plotted energies, both E_{tot} and the single-mode ones, take as reference the ZPE for the quantum distribution and the minimum of the PES for the classical one

distribution is very simple: all modes share the same fraction of the total energy, so the energy per mode is E_{tot}/N_{modes} ("equipartition"). The quantization of vibrational levels implies a basic change in the statistics, which reduces the energy share of the high-frequency modes with respect to the low-frequency ones. To understand this, consider the limiting case of $\hbar\omega_r > E_{tot}$: only the $v_r = 0$ state can be populated for the mode Q_r, so its energy excess is zero. The opposite limit is reached when the average available energy per mode, E_{tot}/N_{modes}, is much larger than all frequencies: then the quantization of the levels becomes irrelevant and the equipartition principle is verified. Figure 4.5 shows the average mode energies $\langle E_r \rangle_{E_{tot}}$ as functions of E_{tot} for a tetratomic molecule with frequencies 200, 300, 500, 800, 1200, and 2000 cm^{-1}. We note that the quantum distribution is very irregular for small E_{tot}, because there are few ways to distribute the energy in the six modes. For $E_{tot} \gtrapprox 2000$ cm^{-1}, as the number of degenerate states is very large, the dependence on E_{tot} becomes more regular. In this regime, the two low-frequency modes (200 and 300 cm^{-1}) share the same average energy, so in a sense they obey the equipartition principle. However, their energies are larger than the classical one, because the other modes have smaller shares that decrease progressively with the mode frequency. Therefore we see that the classical and the quantum microcanonical distributions in general differ for all modes and total energies.

4.4 Static Environmental Effects

In Sect. 2.8 we discussed the environmental effects on the absorption and emission spectra, which are essentially due to modifications of the ground and excited state PESs and wavefunctions caused by the medium. Such effects can be labeled as "static," in the sense that the modifications are not time dependent and concern the stationary states of the system.

A quantitative description of the static effects may be based on a full optimization of the medium coordinates, which can be a reasonable option for a chromophore embedded in a crystal or adsorbed on a solid surface. However, normally such an optimization is only partially representative of the physical reality because of the existence of multiple minima in the energy landscape and because of thermal motions that affect the relative positions and orientations of interacting molecules.

A more comprehensive definition must involve the thermal averaging over the medium coordinates or states. An approximate way to define and compute the static effects of the environment on a molecule of interest is to treat the medium as a continuum characterized by its macroscopic response properties, such as the permittivity ε or the refraction index n. In fact, such properties reflect not only the molecular features of the medium, but also the appropriate statistical averaging. An important consequence is that the potential energy surfaces defined by this approach include the entropic contribution, i.e., are free energy functions of the internal coordinates of the molecule embedded in the dielectric: after averaging over the medium coordinates, the only parameter describing the dielectric is its polarization [4]. The simplest example that illustrates this concept is the interaction energy of a set of point charges in a dielectric fluid:

$$U_{int} = \sum_{i>j} \frac{Q_i Q_j}{4\pi\varepsilon R_{ij}} \,. \tag{4.22}$$

This formula is just the Coulomb law as in vacuo, except that the medium permittivity ε replaces ε_0 in the denominator. It accounts for the much easier ionic dissociation in solvents, especially the polar ones, with respect to gas phase, both in thermal chemistry and in photochemistry. Equation (4.22) does not take into account the polarization free energy of the medium, that would diverge. In fact, according to Born, the interaction free energy of a spherically symmetric ion of charge Q wholly contained in a spherical cavity of radius R with the surrounding polarized dielectric is $\Delta G_{int} = -(\varepsilon - \varepsilon_0)Q^2/(4\pi\varepsilon R)$, while the dielectric polarization free energy is $\Delta G_{pol} = (\varepsilon - \varepsilon_0)Q^2/(8\pi\varepsilon R)$, so the total free energy change for introducing the ion in the cavity is

$$\Delta G_{Born} = -\frac{(\varepsilon - \varepsilon_0)Q^2}{8\pi\varepsilon R} \,. \tag{4.23}$$

This formula shows that smaller ions/cavities and more polar solvents yield larger solvation energies. A further step forward is to consider the polarization of the molecule

embedded in the dielectric. For instance, Onsager found that the free energy of a dipole μ with polarizability α placed at the center of a spherical cavity of radius R is

$$\Delta G_{Onsager} = -\frac{\varepsilon - \varepsilon_0}{4\pi\varepsilon_0(2\varepsilon + \varepsilon_0)} \frac{\mu^2}{R^3 - 2\frac{\varepsilon-\varepsilon_0}{2\varepsilon+\varepsilon_0}\alpha} . \tag{4.24}$$

This formula can be used to analyze the solvation energies of different electronic states (spectral shifts) or conformations.

The concepts applied in these particular cases can be generalized to any charge distribution of the molecule(s) embedded in the medium and to cavities reproducing the molecular shape, by using numerical methods to solve the electrostatic problem. Moreover the electrostatic potential generated by the polarized medium can be added to the molecular Hamiltonian to take fully into account its effect on the electronic wavefunctions by quantum chemistry methods [4–9]. In this way one can define free potential energy functions for the ground and the excited states.

4.5 Dynamic Environmental Effects

Of course, the excited state dynamics is affected by any modification of the PESs, including the "static" environmental effects described in the previous section. Particularly important are the electrostatic interactions with the medium in systems that undergo electron or proton transfer. Especially relevant to photochemistry are changes in the energy gaps between electronic states and in the accessibility of crossing seams [8, 10, 11] (see next chapter).

However, the medium does not equilibrate instantaneously in response to fast geometry changes or electronic transitions of an embedded molecule [6–8]. First of all, the internal motions of an excited molecule can be hindered by repulsive forces due to the proximity of other molecules that do not give way promptly enough. This is especially important for large amplitude motions that characterize (photo)chemical reactions such as bond dissociations and isomerizations. All condensed media affect the excited state dynamics, but the tight packing in crystals and other structured media (for instance reaction sites in biological molecules or hydrogen bonded solvents) are particularly effective in hindering the reaction dynamics. In photochemistry, part of the photon energy can be spent to break the "solvent cage" or similar barriers and also the transfer of momentum to the surrounding molecules can deviate the nuclear trajectory of the reacting molecule. Some examples of caging effects on the quantum yields have been thoroughly analyzed by computational simulations as well as by time-resolved spectroscopy: among others, the photodissociation of nitrosamines [12] and azomethane [12, 13] or the photoisomerization of azobenzene [14] and its derivatives [15].

Even the electrostatic response of the medium is not instantaneous. In solution one can distinguish a fast polarization due to changes in the electronic wavefunctions and

a slow one due to the reorientation and displacement of the solvent molecules. The fast polarization is frequency dependent and can be quantified by the refraction index, while the slow one is most important for polar solvents where it yields the largest contribution to the static permittivity. Fast charge rearrangements of the solute such as electron or proton transfers may be therefore energetically destabilized because the medium does not relax dielectrically in comparably short times, causing a sort of "dielectric friction." See refs. [5, 7, 10] for deeper discussions on this topic.

To the systematic delay effects discussed above one must add the random thermal fluctuations of the environment: together, they result in instantaneous interactions that depart from the mean values corresponding to the statically modified PESs as defined above and can be labeled as "dynamic" effects. In photochemistry, one ubiquitous consequence is the energy transfer from the excited chromophores to the medium or, to a lesser extent, the other way around: only in very rarefied gases or molecular beams the dynamics of a single molecule can be considered as energy conserving. In this context, Langevin-type models play a role analogous to the dielectric continuum ones and are very useful to understand and to predict semiquantitatively the condensed state photodynamics [12, 16, 17]. They mimic the effect of the medium on the nuclear dynamics by a friction term added to the nuclear equations of motion. As friction can only subtract energy to the molecule, a corresponding stochastic force can be added, in order to obtain thermal equilibrium in the long term. We then see that, within the continuum approximations, static and dynamic effects are perfectly separated. However, since basically the same intermolecular interactions (electrostatics, dispersion, repulsion, and so on) are involved both in the static and in the dynamic effects, a rigorous distinction cannot be made without a reference to an arbitrary equilibrium state or to ad hoc approximations.

The vibrational energy transfer between interacting molecules is conceptually similar to IVR. One can extend the model discussed in the previous section by considering two or more molecules as a single one. The vibrational Hamiltonian of the "supermolecule," in the harmonic approximation, provides the zero-order description of the system, and the anharmonic terms couple the normal modes as before. However, some differences must be highlighted. First, the relative translational and rotational motions of the molecules often give place to multiple minima, all accessible at thermal energies, and in a normal mode treatment they usually correspond to low-frequency modes with very anharmonic potentials: such motions are therefore not correctly treated in the one-minimum harmonic approximation. Second, the anharmonic interaction terms between modes localized on different molecules are normally smaller than the intramolecular ones, so the intermolecular vibrational energy transfer is slower, usually requiring times closer to 10 ps than to 1 ps. Third, after a sufficiently long time each molecule will be thermally equilibrated with its environment, i.e., the occupation of each energy level will obey Boltzmann statistics. In the harmonic approximation, for the normal mode Q_r the population of state v_r is

$$P_{v_r} = \mathrm{e}^{-\hbar\omega_r v_r / K_B T} \left(1 - \mathrm{e}^{-\hbar\omega_r / K_B T}\right) . \tag{4.25}$$

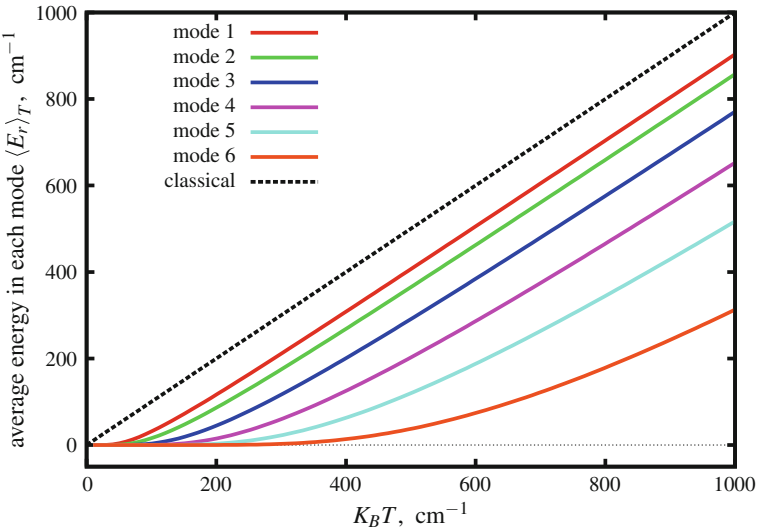

Fig. 4.6 Average energy stored in each vibrational mode as a function of temperature, according to the canonical distribution for a tetratomic molecule with harmonic frequencies of 200, 300, 500, 800, 1200, and 2000 cm^{-1}. The plotted single-mode energies take as reference the ZPE for the quantum distribution and the minimum of the PES for the classical one

As a result, the energy stored in each vibrational mode, averaged over time or over a large molecular sample, is

$$\langle E_r \rangle_T = \frac{\hbar\omega_r}{e^{\hbar\omega_r / K_B T} - 1} \,. \tag{4.26}$$

Note that this energy does not include the ZPE. The $\langle E_r \rangle$ energies as functions of temperature are shown in Fig. 4.6 for the same model molecule of Fig. 4.5, where the microcanonical distribution was plotted. Again, according to classical mechanics the equipartition principle holds, yielding simply $\langle E_r \rangle = K_B T$. For $K_B T \gg \hbar\omega_r$ the quantum distribution approaches the classical one:

$$\langle E_r \rangle_T = K_B T - \frac{\hbar\omega_r}{2} + O\left[\left(\frac{\hbar\omega_r}{K_B T}\right)^3\right] \,. \tag{4.27}$$

We see that the coincidence of the quantum and classical results in this limiting case is much more closely verified if we set the zero of the energy scale at the PES minimum for both, i.e., if we add the ZPE to the quantum average energies shown in Fig. 4.6. The relationship between the microcanonical and the canonical distributions involves the density of states $\rho(E_{tot})$:

$$\langle E_r \rangle_T = \frac{\int_0^\infty \langle E_r \rangle_{E_{tot}} \, \mathrm{e}^{-E_{tot}/K_B T} \rho(E_{tot}) \, \mathrm{d}E_{tot}}{\int_0^\infty \mathrm{e}^{-E_{tot}/K_B T} \rho(E_{tot}) \, \mathrm{d}E_{tot}} \tag{4.28}$$

$\langle E_r \rangle_T$ is an average over all total energies and the large E_{tot} contributions tend to reduce the population difference between high and low frequencies with respect to the microcanonical distribution, as we can see by comparing Figs. 4.5 and 4.6. A qualitative difference is that the microcanonical $\langle E_r \rangle_{E_{tot}}$ for each mode depends on the number and frequencies of the other modes, while the canonical $\langle E_r \rangle_T$ does not.

Thus far, the adiabatic molecular dynamics as described in this chapter can be summarized as follows:

- The light absorption process creates a wavepacket in the excited PES. This wavepacket is normally time dependent. More seldom, it can be stationary if the exciting light is sufficiently monochromatic. In both cases, the wavepacket can be endowed with a certain amount of vibrational energy, depending on the photon energy. This energy excess is distributed in the vibrational modes according to the shapes of the initial and final PESs, in a nonstatistical way.
- If the wavepacket is not stationary, it moves downhill in the excited PES, i.e., the molecular geometry starts changing toward the closest minimum. This phenomenon, often called "geometrical relaxation," can be very fast (down to few femtoseconds), depending on the frequency of the involved vibrations. Oscillations along one or more internal coordinates may follow.
- In isolated polyatomics, the vibrational excitation is redistributed among all modes (IVR) and in few picoseconds it can approach the microcanonical equilibrium distribution. The initial nonstatistical distribution is forgotten.
- In gas phase, collisions will slowly transfer the vibrational excitation to other molecules, at a rate proportional to the total pressure. In the long run, the average amount of vibrational energy and its distribution among the modes will be those expected on the basis of the medium temperature. In condensed phase, the thermal equilibration ("thermalization") times are of the order of 10 ps. The loss of vibrational energy to the medium gradually reduces the ability of the excited molecule to overcome potential energy barriers or to reach bond dissociation limits.

After thermalization the lowest vibrational level is the most populated, almost exclusively for all vibrational modes with $\hbar\omega_r \gg K_B T$. So, even if in the previous steps the excited molecule was able to explore a wide range of conformations thanks to its vibrational energy excess, eventually it settles in a minimum of the PES and the geometrical relaxation is fully accomplished. Activated processes then obey the same kind of kinetics as thermal reactions.

The events described above normally occur in overlapping timescales and can be interrupted by radiationless transitions to lower states. Such transitions can be ultrafast (<1 ps) as described in the next chapter, in which case the excited molecules will not reach neither the microcanonical nor the canonical statistical limit. If, on the contrary, the transitions are slow as discussed in Chap. 3, at least the IVR and often also the thermalization will approach completion. In any case, after switching to a lower PES the system will be again endowed with a vibrational energy excess.

The amount of vibrational energy can be easily larger than after optical excitation, especially when the molecule lands on the ground-state PES that usually presents deep minima. As a consequence, the processes of geometrical relaxation, IVR, and thermalization will take place again in the new PES. Before complete thermal equilibration takes place, in the ground state some processes with large energy barriers may still occur ("hot ground-state" chemistry) thanks to the residual energy excess.

4.6 Computational Note: Quantum Wavepacket Dynamics and Classical Trajectories

As we have seen in the previous sections, the adiabatic excited state dynamics depends on the excitation regime, on the details of the PESs, as well as on static and dynamic environmental effects. Several processes can be distinguished, ideally and also in ad hoc experiments, but normally they overlap in time: for instance, IVR can be studied on its own in rarefied gases, but is intertwined with the vibrational energy loss to the environment in condensed phase. The complexity of excited state dynamics, even when limited to the adiabatic regime, can be tackled by simulation methods that reproduce computationally the time evolution of the excited molecule. Several methods are available to solve the TDSE for nuclear motion and describe the quantum wavepacket dynamics, but classical trajectory approaches are also commonly used because they allow to deal with large systems and long simulation times. More details about computational methods will be given in Sect. 5.5, where the simulation of fast nonadiabatic processes is discussed. In fact, such processes cannot be separated from the nuclear dynamics, so most of the approaches in use for nonadiabatic dynamics are also suitable and were originally developed for the simpler adiabatic case.

It is however worth to comment here how the classical ansatz is appropriate to describe nuclear dynamics. We saw in Sect. 4.2 that certain average properties of a quantum wavepacket (positions, momenta, and their variances) obey the same equations of motion as in classical mechanics. This is the basis for replacing quantum with classical dynamics, which is done by running swarms of classical trajectories with the same initial distributions of coordinates and momenta as in the quantum wavepacket. The above average properties offer a rather complete description of the dynamics as far as the wavepacket is well localized. The stationary vibrational states in molecules are in fact fairly localized, and ultrashort pulses create equally localized wavepackets in the excited PESs. So, in the short time the adiabatic quantum dynamics is well reproduced by a swarm of trajectories. At longer times, the wavepackets tend to delocalize, so their properties are not anymore described satisfactorily by the simple averages and variances of positions and momenta (think for instance of a wavepacket that splits into different reaction channels). Phenomena such as tunneling or the interference of different components of a wavepacket are not properly described by classical mechanics, although ad hoc corrections have been envisaged [18, 19]. The differences in the quantum and classical microcanonical and canonical

energy distributions between vibrational modes at equilibrium have been illustrated in Sects. 4.3 and 4.5. Of particular concern is the role of the zero-point energy in classical dynamics, because due to IVR this amount of energy can be used to reach regions of the PES (transition states or high energy conical intersections) that in quantum dynamics are not accessible. In part, such differences can be reduced by freezing the high-frequency nonreactive modes that contribute most to the problem.

A last observation concerns the excitation process, which deeply affects the photophysical and photochemical dynamics as shown in Sect. 4.2. In the computational simulations of excited state dynamics, this aspect is often drastically simplified, by assuming a certain form of the "initial" excited wavepacket: either the exciting light is supposed to be close to monochromatic and the simulation starts with a vibronic eigenstate in the Born–Oppenheimer approximation; or, more often, a Franck–Condon excitation is postulated and the ground-state $v = 0$ wavefunction is translated to the excited PES. Similar assumptions can be applied to create the initial swarm of trajectories in classical dynamics, by vertical excitation from the ground-state distribution of coordinates and momenta, or by imposing a narrow range of energies in the excited state. Quantum mechanical methods can be complemented with a light–molecule Hamiltonian term, normally in the form of Eq. (3.10), in order to deal correctly with the excitation process. The same can be done in classical trajectory treatments, but some problematic issues arise, mainly because of the unphysical interference between the initial and final state long after a partial transfer of population has taken place. This is due to a general failure of classical (independent) trajectories in multistate systems to reproduce the phenomenon of quantum decoherence (see Sect. 5.5 and Ref. [20]).

Problems

4.1 Calculate the averages and uncertainties of x and $\hat{p}$ for the χ_v eigenfunction of the harmonic oscillator with mass M, frequency ω, and equilibrium position x_e. Verify that for $v = 0$ we have the minimum uncertainty product $\Delta x \Delta p = \hbar/2$. Compare the uncertainty of x in state v with the classical amplitude of the oscillation for the same energy. Make use of the relationships listed in Appendix F.

4.2 Calculate the vibrational energy in the final state for the Franck–Condon excitation between one-dimensional harmonic PESs defined as:

$$U_1 = \frac{1}{2} M\omega_1^2 (R - R_1)^2 \quad \text{and} \quad U_2 = \Delta E_{adia} + \frac{1}{2} M\omega_2^2 (R - R_2)^2$$

Make use of the relationships listed in Appendix F.

4.3 Prove the relationship (4.17).

4.4 Prove the relationship (4.6).

4.5 Prove the relationship (4.21).

4.6 Find all the ways the vibrational energy of 1000 cm^{-1}, in excess of the ZPE, can be distributed among the three normal modes of a triatomic molecule with frequencies 200, 300, and 500 cm^{-1}. What is the microcanonical energy distribution in the three modes for this molecule? Same question if each frequency is sixfold degenerate, as in the case of six weakly interacting identical molecules.

4.7 Quinoline has a much higher fluorescence quantum yield in polar solvents than in the apolar ones, just as 1-pyrenecarboxaldehyde (see Sect. 2.8) and for the same reason. A TD-DFT calculation for the isolated molecule shows that the two lowest excited states are S_1 of $n \rightarrow \pi^*$ type and S_2, $\pi \rightarrow \pi^*$, with an energy difference of 18 kJ/mol. The respective oscillator strengths for transitions from and to the ground state are 0.0019 and 0.0435, so the emission rate of the $\pi \rightarrow \pi^*$ state is about 20 times larger than that of the $n \rightarrow \pi^*$ state. The molecular dipole in the $n \rightarrow \pi^*$ state is 0.79 a.u. and in the $\pi \rightarrow \pi^*$ state, 1.79 a.u. Estimate the free energy difference between the two states in benzene and ethanol, using Onsager's formula, Eq. (4.24) and neglecting the polarizability term. The relative permittivities of benzene and ethanol are $\varepsilon/\varepsilon_0 = 2.3$ and 24.5, respectively. The R^3 parameter can be evaluated from the molecular volume, using the density of quinoline, 1.093 g/cm^3 and its molecular weight, 129.16.

4.8 Compute how many states have an equilibrium population larger than 1%, according to the canonical distribution at $T = 300$ K, Eq. 4.25, with mode frequencies of 100, 400, and 1000 cm^{-1}.

4.9 Watch Animations 4.1 and 4.4 and obtain from them the two oscillation periods, T_h for the harmonic potential and T_m for the Morse one. To which frequencies $\omega = 2\pi/T$ do they correspond? Compare these frequencies with the vibrational frequencies of the two oscillators.

References

1. Zewail, A.H.: Femtochemistry: atomic-scale dynamics of the chemical bond using ultrafast lasers. Angew. Chem. Int. Ed. **39**, 2586–2631 (2000)
2. Ootani, Y., Satoh, K., Nakayama, A., Noro, T., Taketsugu, T.: Ab initio molecular dynamics simulation of photoisomerization in azobenzene in the $n \rightarrow \pi^*$ state. J. Chem. Phys. **131**, 194306/1-10 (2009)
3. Cantatore, V., Granucci, G., Persico, M.: Simulation of the $\pi \rightarrow \pi^*$ photodynamics of azobenzene: decoherence and solvent effects. Comput. Theor. Chem. **1040**, 126–135 (2014)
4. Tomasi, J., Persico, M.: Molecular interactions in solution: an overview of methods based on continuous distributions of the solvent. Chem. Rev. **94** 2027–2094 (1994)
5. Tomasi, J., Mennucci, B., Cammi, R.: Quantum mechanical continuum solvation models. Chem. Rev. **105**, 2999–3094 (2005)
6. Ladanyi, B.M.: Solvation dynamics. In: Cammi, R., Mennucci, B. (eds.) Continuum Solvation Models in Chemical Physics: From Theory to Applications, pp. 366–388. Wiley, Chichester (2007)

7. Newton, M.D.: The role of solvation in electron transfer: theoretical and computational aspects. In: Cammi, R., Mennucci, B. (eds.) Continuum Solvation Models in Chemical Physics: From Theory to Applications, pp. 389–413. Wiley, Chichester (2007)
8. Laage, D., Burghardt, I., Hynes, J.T.: Nonequilibrium solvation and conical intersections. In: Cammi, R., Mennucci, B. (eds.) Continuum Solvation Models in Chemical Physics: From Theory to Applications, pp. 429–449. Wiley, Chichester (2007)
9. Curutchet, C.: Modelling solvent effects in photoinduced energy and electron transfer: the electronic coupling. In: Cammi, R., Mennucci, B. (eds.) Continuum Solvation Models in Chemical Physics: From Theory to Applications, pp. 485–498. Wiley, Chichester (2007)
10. Burghardt, I., Hynes, J.T.: Excited-state charge transfer at a conical intersection: effects of an environment. J. Phys. Chem. A **110**, 11411–11423 (2006)
11. Subotnik, J.E., Cave, R.J., Steele, R.P., Shenvi, N.: The initial and final states of electron and energy transfer processes: diabatization as motivated by system-solvent interactions. J. Chem. Phys. **130**, 234102/1-14 (2009)
12. Cattaneo, P., Granucci, G., Persico, M.: Simulations of condensed phase photochemistry: cage effect and internal conversion in azoalkanes and nitrosamines. J. Phys. Chem. A **103**, 3364–3371 (1999)
13. Cattaneo, P., Persico, M.: Semiclassical simulations of azomethane photochemistry. J. Am. Chem. Soc. **123**, 7638–7645 (2001)
14. Cusati, T., Granucci, G., Persico, M.: Photodynamics and time-resolved fluorescence of azobenzene in solution: a mixed quantum-classical simulation. J. Am. Chem. Soc. **133**, 5109–5123 (2011)
15. Cantatore, V., Granucci, G., Rousseau, G., Padula, G., Persico, M.: Photoisomerization of self-assembled monolayers of azobiphenyls: simulations highlight the role of packing and defects. J. Phys. Chem. Lett. **7**, 4027–4031 (2016)
16. Malhado, J.P., Spezia, R., Hynes, J.T.: Dynamical friction effects on the photoisomerization of a model protonated Schiff base in solution. J. Phys. Chem. A **115**, 3720–3735 (2011)
17. Schwerdtfeger, C.A., Soudackov, A.V., Hammes-Schiffer, S.: Nonadiabatic dynamics of electron transfer in solution: explicit and implicit solvent treatments that include multiple relaxation time scales. J. Chem. Phys. **140**, 034113/1-15 (2014)
18. Makri, N., Miller, W.H.: A semiclassical tunneling model for use in classical trajectory simulations. J. Chem. Phys. **91**, 4026–4036 (1989)
19. Giese, K., Ushiyama, H., Kühn, O.: Tunneling splittings. A classical trajectory approach. Chem. Phys. Lett. **371**, 681–687 (2003)
20. Bajo, J.J., Granucci, G., Persico, M.: Interplay of radiative and nonradiative transitions in surface hopping with radiation-molecule interactions. J. Chem. Phys. **140**, 044113/1-7 (2014)

Chapter 5
Fast Nonadiabatic Dynamics

Abstract In this chapter we present the fast dynamics of a molecular system in regions (avoided crossings, conical intersections) where the Born–Oppenheimer approximation breaks down because the electronic and the nuclear motion are strongly coupled. When a nuclear wavepacket reaches a region where the PESs are close to each other, the nonadiabatic transitions are far from being negligible, and time-dependent perturbation theory cannot be applied. We will show that, in spite of the strong interplay between electronic and nuclear motion, interesting information can be obtained from an approximated mixed quantum/classical model, which leads to the celebrated Landau–Zener formula. Moreover, the main features of conical intersections will be described in some detail.

Keywords Nonadiabatic dynamics · Avoided crossings · Landau-Zener
Conical intersections · Berry's phase · Surface hopping

5.1 Noncrossing Rule and Avoided Crossings

In Sects. 3.10 and 3.11 we argued that large energy gaps imply slow nonadiabatic transitions. Here we want to explore what happens when the PESs get close to each other. Given a pair of electronic adiabatic states $|\varphi_1\rangle$ and $|\varphi_2\rangle$, our first aim is to understand under which circumstances their respective energies U_1 and U_2 can reach a degeneracy point $\mathbf{Q}_x$ where $U_1(\mathbf{Q}_x) = U_2(\mathbf{Q}_x)$. More complicated intersections involving three or more states are not considered in this chapter (however, in some cases $|\varphi_1\rangle$ and $|\varphi_2\rangle$ have to be doubly degenerate; see Sect. 5.4.5). We assume the other states to be far in energy, so that their coupling with $|\varphi_1\rangle$ and $|\varphi_2\rangle$ is small and we can limit ourselves to consider the subspace spanned by these two states. Let $|\eta_1\rangle$, $|\eta_2\rangle$ be an orthogonal basis of that subspace. According to Appendix D we have

$$\begin{aligned} |\varphi_1\rangle &= \cos\theta\, |\eta_1\rangle + \sin\theta\, |\eta_2\rangle \\ |\varphi_2\rangle &= -\sin\theta\, |\eta_1\rangle + \cos\theta\, |\eta_2\rangle \end{aligned} \tag{5.1}$$

which can be written in matrix form as $|\boldsymbol{\varphi}\rangle = |\boldsymbol{\eta}\rangle\, \mathbf{C}$, where

M. Persico and G. Granucci, *Photochemistry*, Theoretical Chemistry
and Computational Modelling, https://doi.org/10.1007/978-3-319-89972-5_5

$$\mathbf{C} = \begin{pmatrix} \cos\theta & -\sin\theta \\ \sin\theta & \cos\theta \end{pmatrix} \tag{5.2}$$

and $\theta \in \mathbb{R}$ given by Eq. (D.4). The eigenenergies U_1, U_2 are (see (D.2))

$$U_{2,1} = \frac{H_{11} + H_{22} \pm \sqrt{\Delta H^2 + 4H_{12}^2}}{2} \tag{5.3}$$

where $\Delta H = H_{22} - H_{11}$ and $H_{ij} = \left\langle \eta_i \left| \hat{H}_{el} \right| \eta_j \right\rangle$. Here and in most of this chapter we are assuming that H_{12} is real. As it will be shown in Sect. 5.4.5, this assumption is justified in many cases. It follows from the above equation that the degeneracy points $\mathbf{Q}_x$ are such that

$$\begin{cases} \Delta H(\mathbf{Q}_x) = 0 \\ H_{12}(\mathbf{Q}_x) = 0 \end{cases} \tag{5.4}$$

We focus here on the case of one internal coordinate ($s = 1$), appropriate for a diatomic molecule. Then, we have two equations to solve and only one unknown, which means the equality $U_1 = U_2$ cannot be satisfied. This is the so-called *noncrossing rule*: two potential energy curves cannot cross, if the two states have the same space and spin symmetry. In fact, as long as the two states have different symmetry, $H_{12}(\mathbf{Q})$ vanishes identically, so we are left with only one equation and the nonintersection rule does not hold. For example, singlet and triplet states can cross, in the electrostatic approximation for $\hat{H}_{el}$.

Of course H_{11} and H_{22} can cross, because $|\eta_1\rangle$ and $|\eta_2\rangle$ are not eigenstates of $\hat{H}_{el}$. When $\Delta H = 0$ one has $U_2 - U_1 = 2\,|H_{12}|$: if the coupling between $|\eta_1\rangle$ and $|\eta_2\rangle$ is small, we may have regions where U_1 and U_2 are very close. These regions are called *avoided crossings*.

An example is offered by the ground and the first excited singlet state of alkali halides. Their wavefunctions will be labeled as φ_1 and φ_2, to keep the numbering of this section. Let us consider in particular NaCl. Approximately, φ_1 and φ_2 are linear combinations of the ionic Na^+Cl^- and of the covalent Na··Cl configurations, and we choose, respectively, η_1 and η_2 to represent these configurations. At short NaCl internuclear distances Q, the ground state φ_1 is mainly described by η_1, while at dissociation $\varphi_1 = \eta_2$. As already discussed in Sect. 2.6.2, the energies of η_1 and η_2 (H_{11} and H_{22}) must cross, and in NaCl the crossing is found at large Q. In fact, at medium/large NaCl distances (say, $Q > 10$ bohr) we have, in atomic units, $H_{11}(Q) = -1/Q + \Delta$, where $\Delta \simeq 0.056$ hartree is the difference between the ionization potential of Na (0.189 hartree) and the electron affinity of Cl (0.133 hartree). Here we have neglected the mutual polarization of the two ions Na^+ and Cl^-, which is however expected to give a small contribution at large Q. In the same energy scale we have $H_{22}(Q) = 0$. Imposing $H_{11}(Q_x) = H_{22}(Q_x)$ we get $Q_x = 1/\Delta \simeq 17.9$ bohr, which is indeed a large internuclear distance, where the above expressions for H_{11} and H_{22} are expected to be sufficiently accurate. Now, φ_1 and φ_2 (hence also η_1 and η_2)

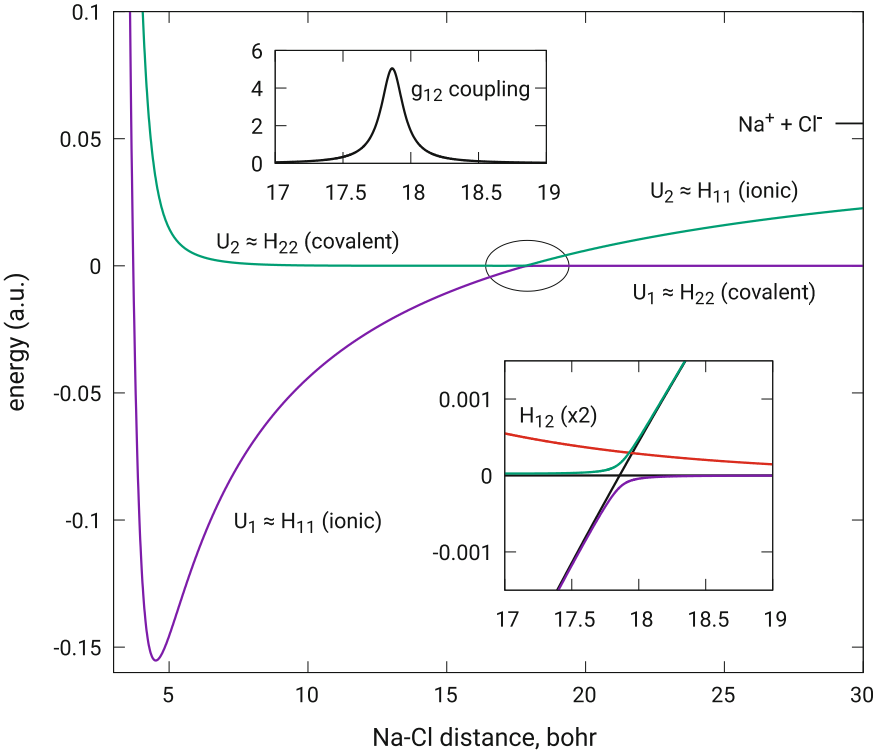

Fig. 5.1 Avoided crossing in NaCl. The adiabatic quantities U_1 and U_2 and g_{12} are represented with full lines, while dashed lines are used for H_{11}, H_{12}, and H_{22}. The crossing region is enlarged in the two insets. All data in atomic units

have the same symmetry, so $H_{12} \neq 0$ and the two adiabatic energies U_1 and U_2 cannot cross. However $H_{12}(Q_x)$ is very small: in fact the two wavefunctions η_1 and η_2 differ for the location of one electron in two different orbitals, belonging respectively to the Cl atom or to the Na atom, and the coupling H_{12} is related to the overlap between the two orbitals (see Appendix E). In particular $H_{12}(Q_x) \simeq 1.5 \cdot 10^{-4}$ hartree for NaCl, so the crossing is very tightly avoided; see Fig. 5.1.

In going through the avoided crossing region, the adiabatic states exchange their description, as it can be appreciated from Fig. 5.1. This is a distinctive feature of an avoided crossing, together with the large value of the nonadiabatic coupling g_{12}.

In terms of the basis set $|\boldsymbol{\eta}\rangle$, indicating with $\nu_{ij} = \langle \eta_i \, | \partial / \partial Q | \, \eta_j \rangle$ the "derivative" or "dynamical" coupling, we have

$$
\begin{aligned}
g_{12} &= \mathbf{C}_1^+ \left\langle \boldsymbol{\eta} \left| \frac{\partial}{\partial Q} \left(\left| \boldsymbol{\eta} \right\rangle \mathbf{C}_2 \right) \right. \right. \\
&= \nu_{12} + \mathbf{C}_1^+ \frac{\partial \mathbf{C}_2}{\partial Q} \\
&= \nu_{12} - \frac{\partial \theta}{\partial Q}
\end{aligned}
\tag{5.5}
$$

where $\mathbf{C}_1$ and $\mathbf{C}_2$ are the first and the second column of matrix $\mathbf{C}$ of Eq. (5.2), and we exploited the antisymmetry of the matrix ν_{ij} for real functions. From the NaCl example referred above it is clear that the term $\partial\theta/\partial Q$ is large only in the crossing region, where $|\Delta H| \sim |H_{12}|$, in agreement with Eq. (2.70). Moreover ν_{12} is expected to be close to zero, as $\eta_1(Q)$ and $\eta_2(Q)$ retain their character at all internuclear distances and do not undergo abrupt changes. This leads to the concept of diabatic states, as discussed in the following section.

In a typical weakly avoided crossing, we consider the area under the function g_{12} between two values Q_a and Q_b placed, respectively, well before and after the crossing:

$$
\left| \int_{Q_a}^{Q_b} g_{12}(Q)\, \mathrm{d}Q \right| \simeq \left| \int_{Q_a}^{Q_b} \frac{\partial \theta}{\partial Q}\, \mathrm{d}Q \right| = |\theta(Q_a) - \theta(Q_b)| \simeq \frac{\pi}{2} \tag{5.6}
$$

The last equality holds because of the state switching that occurs in going from Q_a to Q_b: $\varphi_1 \simeq \eta_1$ and $\varphi_2 \simeq \eta_2$ before the crossing and vice versa after the crossing. Since θ is the switching parameter, it must go from about 0 to $\pm\pi/2$. The above relationship can be used to verify that the state switching is actually complete and that no admixing of other states occurs in the avoided crossing region.

5.2 Diabatic States

When the nonadiabatic coupling is large, it may be convenient to replace the electronic adiabatic states with a set of functions which annihilates, or reduces, the coupling. These electronic functions are called *diabatic states* [1–4]. A good example is offered by the ionic and neutral states of NaCl; see Sect. 5.1 and Fig. 5.1: clearly, one has to perform a large number of calculations in the crossing region in order to reproduce correctly the shape of $U_1(Q)$, $U_2(Q)$, and $g_{12}(Q)$, while the corresponding diabatic quantities H_{11}, H_{22}, and H_{12} change smoothly with Q and can be fitted with simple functions.

Let us define a new orthonormal set $|\boldsymbol{\eta}\rangle$ of electronic basis functions, obtained as linear combinations of the adiabatic set $|\boldsymbol{\varphi}\rangle$

$$
|\boldsymbol{\eta}\rangle = |\boldsymbol{\varphi}\rangle\, \mathbf{T} \tag{5.7}
$$

where $\mathbf{T}$ is unitary. Note that $\mathbf{T}$ is the inverse of matrix $\mathbf{C}$ of Eq. (5.2). The η_k are *strictly* diabatic functions if all the derivative coupling matrices

$$\boldsymbol{\nu}^{(\alpha)} = \left\langle \boldsymbol{\eta} \left| \frac{\partial}{\partial Q_\alpha} \right| \boldsymbol{\eta} \right\rangle = \mathbf{T}^{+}\mathbf{g}^{(\alpha)}\mathbf{T} + \mathbf{T}^{+}\frac{\partial \mathbf{T}}{\partial Q_\alpha} \tag{5.8}$$

vanish $\forall\alpha$. Here $\mathbf{g}^{(\alpha)}$ is the matrix collecting the nonadiabatic couplings $g_{kl}^{(\alpha)}$. From imposing $\boldsymbol{\nu}^{(\alpha)} = 0$ for a complete set of diabatic functions follows that the second derivative couplings also vanish (according to Eq. (2.67)) and that the η_k cannot depend on the nuclear coordinates

$$\frac{\partial \left|\eta_k\right\rangle}{\partial Q_\alpha} = \sum_j \left|\eta_j\right\rangle \left\langle \eta_j \left| \frac{\partial \eta_k}{\partial Q_\alpha} \right\rangle = 0\,. \tag{5.9}$$

Then, a trivial solution for $\boldsymbol{\nu}^{(\alpha)} = 0$ is found by choosing $\eta_k(\mathbf{r}) = \varphi_k(\mathbf{r}; \mathbf{Q}_0)$, where $\mathbf{Q}_0$ is a fixed set of nuclear internal coordinates. The completeness of the basis ensures that Eq. (5.7) is satisfied for any $\mathbf{Q}$, with $\mathbf{T}_{kl}(\mathbf{Q}) = \langle \varphi_k(\mathbf{Q}) \left|\varphi_l(\mathbf{Q}_0)\right\rangle$. This is the so-called *crude* diabatic basis. Of course the trivial solution is not unique.

According to Eq. (5.8), imposing $\boldsymbol{\nu}^{(\alpha)} = 0$ we get

$$\frac{\partial \mathbf{T}}{\partial Q_\alpha} + \mathbf{g}^{(\alpha)}\mathbf{T} = 0 \quad \forall\alpha \tag{5.10}$$

which is the set of differential equations that must be satisfied by the adiabatic-to-diabatic transformation matrix $\mathbf{T}$. The above expression can be made more compact by introducing the vectors of matrices $\mathbf{g} = (\mathbf{g}^{(1)}, \mathbf{g}^{(2)}, \ldots, \mathbf{g}^{(s)})$ and $\mathbf{F} = \mathbf{g}\mathbf{T} = (\mathbf{g}^{(1)}\mathbf{T}, \ldots, \mathbf{g}^{(s)}\mathbf{T})$, obtaining

$$\mathbf{F} = -\nabla \mathbf{T}\,. \tag{5.11}$$

If the electronic functions φ_k are real, $\mathbf{F}$ is a real vector field (actually a matrix of vector fields) and the real function $\mathbf{T}$ (actually a matrix of functions) is the corresponding scalar potential. In other words, $\mathbf{F}$ has to be conservative. A necessary condition for $\mathbf{F}$ to admit a potential is to be irrotational

$$\frac{\partial \mathbf{F}^{(\alpha)}}{\partial Q_\beta} = \frac{\partial \mathbf{F}^{(\beta)}}{\partial Q_\alpha} \tag{5.12}$$

as it follows from the Schwartz theorem on partial derivatives applied to $\mathbf{T}$. Replacing $\mathbf{F} = \mathbf{g}\mathbf{T}$ in Eq. (5.12) and using (5.11) we arrive at the following relation for the nonadiabatic couplings

$$\frac{\partial \mathbf{g}^{(\alpha)}}{\partial Q_\beta} - \frac{\partial \mathbf{g}^{(\beta)}}{\partial Q_\alpha} - \left[\mathbf{g}^{(\alpha)}, \mathbf{g}^{(\beta)}\right] = 0 \quad \forall\alpha, \beta\,. \tag{5.13}$$

Since we know that Eq. (5.11) can be actually solved (by the trivial solutions referred above), the (5.13) has to be fulfilled by the nonadiabatic coupling. In fact

$$\frac{\partial g_{kl}^{(\alpha)}}{\partial Q_\beta} - \frac{\partial g_{kl}^{(\beta)}}{\partial Q_\alpha} = \left\langle \frac{\partial \varphi_k}{\partial Q_\beta} \middle| \frac{\partial \varphi_l}{\partial Q_\alpha} \right\rangle - \left\langle \frac{\partial \varphi_k}{\partial Q_\alpha} \middle| \frac{\partial \varphi_l}{\partial Q_\beta} \right\rangle \tag{5.14}$$

moreover

$$(\mathbf{g}^{(\alpha)}\mathbf{g}^{(\beta)})_{kl} = \sum_m g_{km}^{(\alpha)} g_{ml}^{(\beta)} = -\left\langle \frac{\partial \varphi_k}{\partial Q_\alpha} \middle| \frac{\partial \varphi_l}{\partial Q_\beta} \right\rangle \tag{5.15}$$

where we have exploited the completeness of the adiabatic basis. Equation (5.13) is then easily recovered from (5.14) and (5.15).

In practical problems, the crude diabatic basis is of very limited utility, as one is usually interested in a small number of electronic states (and anyway it is not possible to treat numerically the infinite number of states in a complete Hilbert space for a realistic molecular system). Let us therefore consider a subspace S containing the N_S adiabatic states of interest. The orthogonal subspace is labeled R and normally is infinite-dimensional. We assume that $g_{kl}^{(\alpha)}$, for all Q_α, is vanishingly small when $\varphi_k \in S$ and $\varphi_l \in R$. As a consequence, it can be shown that the same property holds for the second derivative couplings $t_{kl}^{(\alpha)}$, so S is "decoupled" from R. In practice, in the absence of regions of degeneracy or near degeneracy between adiabatic energies belonging to the two orthogonal subspaces, it can be assumed that S and R are decoupled to a good approximation. Within S, the diabatic basis has to depend on $\mathbf{Q}$, as in general the expansion of $\varphi_k(\mathbf{Q}_0)$ in terms of the $\varphi_l(\mathbf{Q})$ is not limited to the functions belonging to S, even if S is decoupled from R. Let us indicate with ${}^S\mathbf{g}$ the restriction to S of $\mathbf{g}$, so that ${}^S\mathbf{g}$ is a vector of $N_S \times N_S$ matrices, and the same for ${}^S\mathbf{F}$. In general, a $N_S \times N_S$ unitary matrix $\mathbf{T}$ solving ${}^S\mathbf{F} = -\nabla\mathbf{T}$ (which is the restriction to S of Eq. (5.10)) cannot be found. In fact, the necessary condition (5.12) for ${}^S\mathbf{F}$ would lead to Eq. (5.13) for ${}^S\mathbf{g}$, which is not, in general, true: taking into account that

$$({}^S\mathbf{g}^{(\alpha)}\,{}^S\mathbf{g}^{(\beta)})_{kl} = \sum_m^{\varphi_m \in S} g_{km}^{(\alpha)} g_{ml}^{(\beta)} = -\left\langle \frac{\partial \varphi_k}{\partial Q_\alpha} \middle| \frac{\partial \varphi_l}{\partial Q_\beta} \right\rangle - \sum_i^{\varphi_i \in R} g_{ki}^{(\alpha)} g_{il}^{(\beta)} \tag{5.16}$$

we get

$$\begin{aligned} &\frac{\partial\, {}^S\mathbf{g}^{(\alpha)}}{\partial Q_\beta} - \frac{\partial\, {}^S\mathbf{g}^{(\beta)}}{\partial Q_\alpha} - \left[{}^S\mathbf{g}^{(\alpha)},\, {}^S\mathbf{g}^{(\beta)}\right] = \mathbf{A} \\ &A_{kl} = \sum_i^{\varphi_i \in R} \left[g_{ki}^{(\alpha)} g_{il}^{(\beta)} - g_{ki}^{(\beta)} g_{il}^{(\alpha)} \right] . \end{aligned} \tag{5.17}$$

Note that, even if $g_{ki}^{(\alpha)}$ with $\varphi_k \in S$ and $\varphi_i \in R$ is assumed to be very small, the elements of the matrix $\mathbf{A}$ are obtained from a sum running on an infinite number of terms which may therefore yield a non-negligible contribution, in general. On

the other hand, the necessary condition (5.12) is always trivially satisfied in one coordinate Q_α (i.e., for $\beta = \alpha$), and in principle Eq. (5.10) restricted to S can be integrated for a single Q_α. Therefore, the strict diabatization can be performed within S for a diatomic molecule, in principle.

To summarize, it is possible to find a unitary matrix $\mathbf{T}$ transforming a truncated adiabatic basis into a strictly diabatic one only for one internal coordinate at a time (or along a given path).

In view of these difficulties, the diabatic states are usually defined using less strict conditions than the exact cancelation of the dynamical couplings. In practice, the ν_{kl} are requested to be minimal, or however negligibly small. The corresponding η_k are then called *quasi-diabatic* states. Obviously the quasi-diabatic basis cannot be uniquely defined, and many different methods have been devised to their evaluation (for a short review see [5]). To cite only a simple example, one could rely on molecular properties: for instance, the transition dipole moment can be used to define dark and bright diabatic states; space localization to define excitonic states, and so on.

The nonadiabatic couplings $g_{kl}^{(\alpha)}$ are expressed in terms of the quasi-diabatic basis in this way

$$g_{kl}^{(\alpha)} = (U_l - U_k)^{-1} \mathbf{C}_k^+ \frac{\partial \mathbf{H}}{\partial Q_\alpha} \mathbf{C}_l + \mathbf{C}_k^+ \boldsymbol{\nu}^{(\alpha)} \mathbf{C}_l \tag{5.18}$$

where $\mathbf{C}_k$ is the kth column of the diabatic-to-adiabatic matrix $\mathbf{C}$ (the inverse of matrix $\mathbf{T}$). The residual derivative coupling between quasi-diabatic functions is usually neglected: anyway, the $g_{kl}^{(\alpha)}$ are large in near-degeneracy regions, where the first term dominates. Equation (5.18) represents a very convenient way to evaluate the nonadiabatic couplings, as the elements $H_{kl} = \left\langle \eta_k \left| \hat{H}_{el} \right| \eta_l \right\rangle$ of matrix $\mathbf{H}$ are, by construction, smooth functions of $\mathbf{Q}$.

Also time evolution is particularly simple in the quasi-diabatic basis. The Born–Huang expansion of the total wavefunction $\Psi(\mathbf{Q}, \mathbf{r}, t)$ becomes

$$\Psi(\mathbf{Q}, \mathbf{r}, t) = \sum_k \Theta_k(\mathbf{Q}, t) \eta_k(\mathbf{r}; \mathbf{Q}) \tag{5.19}$$

where here $\Theta_k(\mathbf{Q}, t)$ are the nuclear wavepackets on the quasi-diabatic states. Their time evolution is given by (compare Eq. (2.78))

$$\mathrm{i}\hbar \frac{\mathrm{d}\Theta_k}{\mathrm{d}t} = \hat{T}_n \Theta_k + \sum_l H_{kl} \Theta_l \tag{5.20}$$

where we have neglected the residual derivative couplings between quasi-diabatic functions, which ought to be small. As noted above, the H_{kl} are smooth functions of $\mathbf{Q}$, while in the adiabatic expression (2.78) both U_k' and $\hat{V}_{kl}^{BO}$ contain terms which diverge at degeneracy points (see Sect. 5.4).

5.3 Landau–Zener Rule

As discussed in Sect. 5.1, in avoided crossing regions the nonadiabatic coupling is large and the energy difference is small; therefore nonradiative transitions between electronic states are very likely. This problem was first tackled by Landau and Zener in 1932, using a classical approximation for the nuclear motion [6, 7]. In particular, it is assumed that the classical description is acceptable for the nuclei, at least as a first approximation, so that the nuclear motion is given by a classical trajectory $\mathbf{Q}(t)$. Then, we consider a time-dependent Schrödinger equation only for the electrons

$$\mathrm{i}\hbar\frac{\mathrm{d}\Psi_{el}(\mathbf{r},t;\mathbf{Q}(t))}{\mathrm{d}t} = \hat{H}_{el}(\mathbf{Q}(t))\Psi_{el}(\mathbf{r},t;\mathbf{Q}(t)) \tag{5.21}$$

where the parametric dependence of the electronic wavefunction Ψ_{el} and Hamiltonian $\hat{H}_{el}$ on the nuclear trajectory $\mathbf{Q}(t)$ has been made explicit. Note in particular that $\hat{H}_{el}$, as well as its eigenfunctions and eigenvalues, depend on time through $\mathbf{Q}(t)$. Therefore, the time evolution operator (2.26) cannot be applied. The Ψ_{el} can be expanded in terms of the adiabatic basis

$$\Psi_{el}(t) = \sum_l a_l(t)\mathrm{e}^{-\mathrm{i}\gamma_l(t)}\varphi_l \qquad \gamma_l(t) = \frac{1}{\hbar}\int_0^t U_l(\mathbf{Q}(t'))\mathrm{d}t' \tag{5.22}$$

where $\mathrm{e}^{-\mathrm{i}\gamma_l(t)}$ is the so-called *dynamical phase*, as opposed to the "static" phase that would be present for a time-independent Hamiltonian (see, for example, Eq. (3.3)). Inserting the above expansion in Eq. (5.21) we obtain

$$\sum_l \dot{a}_l\varphi_l\mathrm{e}^{-\mathrm{i}\gamma_l} = -\sum_l a_l\mathrm{e}^{-\mathrm{i}\gamma_l}\dot{\varphi}_l. \tag{5.23}$$

Multiplying both sides by φ_k^* and integrating on the electronic coordinates we get the differential equation for the adiabatic coefficients a_k

$$\dot{a}_k = -\sum_l a_l(t)\mathrm{e}^{-\mathrm{i}(\gamma_l(t)-\gamma_k(t))}\langle\varphi_k|\dot{\varphi}_l\rangle \tag{5.24}$$

and, according to the chain derivative rule, we have

$$\langle\varphi_k|\dot{\varphi}_l\rangle = \sum_\alpha g_{kl}^{(\alpha)}\dot{Q}_\alpha \tag{5.25}$$

We see that the variation of the coefficients a_k (and thus the probability to make a transition from an adiabatic state to another) depends on the scalar product between the nuclear velocity and the nonadiabatic coupling vectors, which is analogous to the coupling terms $g_{kl}^{(\alpha)}\frac{\partial}{\partial R_\alpha}$ of Eq. (2.62). Note however that in this mixed

quantum/classical approximation the second derivative couplings $t_{kl}^{(\alpha)}$ do not play any role. The phase factor $\exp[-\mathrm{i}(\gamma_l - \gamma_k)]$ is a dephasing term, which oscillates rapidly in time when the energy difference $U_l - U_k$ is large, leading to very small integrated transition probabilities between states well separated in energy.

The electronic wavefunction Ψ_{el} can also be expanded in terms of the diabatic basis

$$\Psi_{el}(t) = \sum_l d_l(t) \mathrm{e}^{-\mathrm{i}\gamma_l^d(t)} \eta_l \qquad \gamma_l^d(t) = \frac{1}{\hbar} \int_0^t H_{ll}(\mathbf{Q}(t'))\mathrm{d}t' \,. \tag{5.26}$$

We assume the dynamical couplings between diabatic wavefunctions to vanish and we proceed as in the adiabatic case to obtain

$$\dot{d}_k = -\frac{\mathrm{i}}{\hbar} \sum_{l(\neq k)} d_l(t) \mathrm{e}^{-\mathrm{i}(\gamma_l^d(t) - \gamma_k^d(t))} H_{kl}(t) \tag{5.27}$$

from which it appears that the transitions between diabatic states are due to the electronic coupling terms $H_{kl} = \left\langle \eta_k \middle| \hat{H}_{el} \middle| \eta_l \right\rangle$. In the following, we will work in the diabatic representation, as the setup of the model is easier and it leads to simpler equations.

Let us consider a two-state system (η_1 and η_2), with one nuclear coordinate Q. The Landau–Zener model is completely defined by setting

$$\begin{aligned} \Delta H(Q) &= H_{22}(Q) - H_{11}(Q) = F\Delta Q \\ H_{12}(Q) &= H_{12} \qquad (real\ constant) \\ Q(t) &= Q_x + vt \end{aligned} \tag{5.28}$$

where $\Delta Q = Q - Q_x$ and F represents the difference in the slopes of $H_{22}(Q)$ and $H_{11}(Q)$, assumed to be linearly dependent on Q. It is also assumed that the nuclei move at constant velocity v. Within this model, the nonadiabatic coupling $g_{12}(Q)$ can be determined by means of the general equation (5.41)

$$g_{12}(Q) = -\frac{\beta/2}{1 + \beta^2 \Delta Q^2} \qquad \beta = \frac{F}{2H_{12}} \,. \tag{5.29}$$

Apart from the global sign, which can be positive or negative according to the sign of β, $g_{12}(Q)$ is a Lorentzian function, centered at $Q = Q_x$, with maximum height $F/4H_{12}$ and FWHM $= |4H_{12}/F|$. Hence, in terms of the adiabatic representation, the strong interaction region, where the nonadiabatic couplings are large and transitions between the electronic adiabatic states are likely, is centered at Q_x and has a width of the order of $4H_{12}/F$.

Note that the Landau–Zener model is adequate to describe a weakly avoided crossing at Q_x. In fact, if the amplitude $\delta Q \approx |H_{12}/F|$ of the crossing region is small enough, one may approximate $\Delta H(Q)$ and $H_{12}(Q)$ taking just the first nonzero term

in their Taylor development at Q_x, as in Eq. (5.28). Moreover, the approximation of constant nuclear velocity v is correct if the time $\delta Q/v \approx |H_{12}/Fv|$ needed to cross the strong interaction region is small enough.

If we apply Eq. (5.26) to the Landau–Zener model we get the following system of coupled differential equations

$$\begin{cases} \dot{d}_1 = -\frac{\mathrm{i}}{\hbar} H_{12} d_2(t) \exp\left\{-\frac{\mathrm{i}}{\hbar}\int_0^t \Delta H \mathrm{d}t'\right\} = -\frac{\mathrm{i}}{\hbar} H_{12} d_2(t) \mathrm{e}^{-\mathrm{i}Fvt^2/2\hbar} \\ \dot{d}_2 = -\frac{\mathrm{i}}{\hbar} H_{12} d_1(t) \mathrm{e}^{\mathrm{i}Fvt^2/2\hbar} \end{cases} \tag{5.30}$$

with the starting condition $d_1(-\infty) = 1$ and $d_2(-\infty) = 0$ (only η_1 is initially populated). As discussed above, the Landau–Zener model is expected to give a realistic description of an avoided crossing if H_{12} is small, which corresponds to a weak diabatic transition probability (see Eq. (5.27)). Therefore, we can apply the time-dependent perturbation theory at first order, which amounts in assuming $d_1 \simeq 1$ at all times. Within this approximation, after the passage through the crossing we have

$$d_2(+\infty) \simeq -\frac{\mathrm{i}}{\hbar} H_{12} \int_{-\infty}^{+\infty} \mathrm{e}^{\mathrm{i}Fvt^2/2\hbar} \mathrm{d}t = -H_{12}\sqrt{\frac{2\pi}{\hbar |vF|}} \mathrm{e}^{\mathrm{i}(\pi/2 \pm \pi/4)} \tag{5.31}$$

where the positive sign has to be chosen if $vF > 0$ and vice versa. Here we have exploited the relation $\int_{-\infty}^{+\infty} \exp(-\alpha x^2)\mathrm{d}x = (\pi/\alpha)^{1/2}$, which is valid for any complex number α with $\mathrm{Re}(\alpha) \geq 0$. The diabatic transition probability P_{dia} in a passage through the crossing is given by $|d_2(+\infty)|^2$

$$P_{dia} \simeq \frac{2\pi H_{12}^2}{\hbar |vF|} \,. \tag{5.32}$$

Note that P_{dia} is proportional to the strength of the electronic coupling and to the time $H_{12}/|vF|$ needed to pass through the crossing. Actually, Eq. (5.30) can be solved exactly in the asymptotic limit, yielding

$$P_{dia} = 1 - \exp\left\{-\frac{2\pi H_{12}^2}{\hbar |vF|}\right\} \,. \tag{5.33}$$

The approximate and the exact solutions tend to coincide for small $H_{12}^2/(\hbar |vF|)$, i.e., when the Landau–Zener model is physically viable. Far from the crossing, the adiabatic states coincide with the diabatic ones and the nonadiabatic coupling vanishes (see Fig. 5.1). In particular, assuming $\beta > 0$, we have $\varphi_1 \simeq \eta_1$ for $Q \ll Q_x$ and $\varphi_2 \simeq \eta_1$ for $Q \gg Q_x$. Therefore, the probability to change adiabatic state corresponds to the probability to stay in the same diabatic state: $P_{adia} = 1 - P_{dia}$. Hence

$$P_{adia} = \exp\left\{-\frac{2\pi H_{12}^2}{\hbar |vF|}\right\} \tag{5.34}$$

which is the celebrated Landau–Zener formula for the adiabatic transition probability. Examples of application of the Landau–Zener formula are given as problems at the end of this chapter.

5.4 Conical Intersections

We get back to the topic of Sect. 5.1, considering now the general case of a polyatomic molecule ($s > 1$). The nonintersection rule is no longer valid with more than one internal coordinate. For example, with two coordinates Q_1 and Q_2 the two-equations system (5.4) in principle can be solved, so we may have one (or several) points where $U_1 = U_2$. With three coordinates we may have $U_2 = U_1$ on a curve. In general, with s internal coordinates the set of points where $U_1 = U_2$, if any, has dimension $s - 2$.

Let us consider the Taylor expansion of the diabatic quantities ΔH and H_{12} at a degeneracy point $\mathbf{Q}_x$ (for later convenience it is useful to consider $2H_{12}$)

$$\begin{aligned} \Delta H(\mathbf{Q}) &= \mathbf{q} \cdot (\mathbf{Q} - \mathbf{Q}_x) + \cdots \\ 2H_{12}(\mathbf{Q}) &= \mathbf{h} \cdot (\mathbf{Q} - \mathbf{Q}_x) + \cdots \end{aligned} \tag{5.35}$$

where

$$\mathbf{q} = \nabla \Delta H(\mathbf{Q}_x) \qquad \text{and} \qquad \mathbf{h} = 2\nabla H_{12}(\mathbf{Q}_x). \tag{5.36}$$

As in the previous sections we assume here $H_{12} \in \mathbb{R}$. We define the two versors $\hat{x} = \mathbf{q}/q$ and $\hat{y} = \mathbf{h}/h$, where q and h are the norms of $\mathbf{q}$ and $\mathbf{h}$, respectively. Then Eq. (5.35) becomes, at first order

$$\Delta H(\mathbf{Q}) = qx \qquad \text{and} \qquad 2H_{12}(\mathbf{Q}) = hy \tag{5.37}$$

where $x = \hat{x} \cdot (\mathbf{Q} - \mathbf{Q}_x)$ and $y = \hat{y} \cdot (\mathbf{Q} - \mathbf{Q}_x)$ are the displacements from the degeneracy point along the two versors. We can always assume, without losing generality, that the two vectors $\mathbf{q}$ and $\mathbf{h}$ are orthogonal. In fact, the diabatic basis is not uniquely defined: in particular, it is determined up to a constant orthogonal transformation, which can be chosen in such a way that $\mathbf{q} \cdot \mathbf{h} = 0$.

The Hamiltonian matrix at the first order in the displacement from $\mathbf{Q}_x$ is

$$\mathbf{H}_{el} = \frac{\mathbf{s}}{2} \cdot (\mathbf{Q} - \mathbf{Q}_x) \begin{pmatrix} 1 & 0 \\ 0 & 1 \end{pmatrix} + \frac{1}{2} \begin{pmatrix} -qx & hy \\ hy & qx \end{pmatrix} \tag{5.38}$$

where $\mathbf{s} = \nabla H_{11}(\mathbf{Q}_x) + \nabla H_{22}(\mathbf{Q}_x)$ and we have set the energy scale so that $H_{11}(\mathbf{Q}_x) = H_{22}(\mathbf{Q}_x) = 0$. The corresponding adiabatic energies are then (see Eq. (5.3))

$$U_{2,1} = \frac{1}{2} \left(\mathbf{s} \cdot (\mathbf{Q} - \mathbf{Q}_x) \pm \sqrt{(qx)^2 + (hy)^2} \right) . \tag{5.39}$$

With $\mathbf{s} = 0$, the above function of x and y is a double cone of which U_1 and U_2 are the upper and the lower part and touch in the vertex. The double cone is circular if $q = h$ and elliptic if $q \neq h$. The term $\mathbf{s} \cdot (\mathbf{Q} - \mathbf{Q}_x)$ can be split into two contributions: one is due to the component of $\mathbf{Q} - \mathbf{Q}_x$ lying in the plane spanned by the vectors $\mathbf{q}$ and $\mathbf{h}$, and the other is due to the orthogonal component. The first contribution is linear in x and y and has the effect to tilt the axis of the double cone, while the second does not depend on x and y and therefore leaves the double cone geometry unaltered.

If $\nabla \Delta H(\mathbf{Q}_x) \neq 0$ and $\nabla H_{12}(\mathbf{Q}_x) \neq 0$ the degeneracy point $\mathbf{Q}_x$ is called *conical intersection* [8]. The set of points of dimension $s - 2$ where $U_1 = U_2$, i.e., the conical intersection points, is called *crossing seam*. Because in the vicinity of a crossing seam nonadiabatic transitions are very likely, the lowest parts of the crossing seam in the upper adiabatic PES act as a *funnel*, i.e., a region of the PES where decay to lower states is fast.

The nonadiabatic coupling vector $\mathbf{g}_{12}$ can be obtained in terms of the diabatic matrix elements exploiting Eqs. (5.5) and (D.5)

$$\mathbf{g}_{12} = -\nabla\theta(\mathbf{Q}) = -\frac{\nabla \operatorname{tg}(2\theta)}{2(1 + \operatorname{tg}^2(2\theta))} \tag{5.40}$$

Then

$$\mathbf{g}_{12} = \frac{\Delta H \nabla H_{12} - H_{12} \nabla \Delta H}{\Delta H^2 + 4H_{12}^2} \tag{5.41}$$

At first order in the displacement from the conical intersection $\mathbf{Q}_x$ we have

$$\mathbf{g}_{12} = \frac{qh}{2(q^2x^2 + h^2y^2)}(-\hat{x}y + \hat{y}x) \tag{5.42}$$

where we have used Eqs. (5.36) and (5.37). In polar coordinates $x = r\cos\phi$ and $y = r\sin\phi$ we obtain

$$\mathbf{g}_{12} = \left(\frac{qh}{q^2\cos^2\phi + h^2\sin^2\phi}\right)\frac{\hat{e}_\phi}{2r} \tag{5.43}$$

where $\hat{e}_\phi = -\hat{x}\sin\phi + \hat{y}\cos\phi$ is a versor in the direction of increasing ϕ. It is clear from the above equations that the coupling $\mathbf{g}_{12}$, for $r \to 0$, lies on the plane spanned by $\mathbf{q}$ and $\mathbf{h}$ and diverges as $1/r$ (see Fig. 5.2). Moreover, is interesting to note that the line integral of $\mathbf{g}_{12}$ along a small circle C in the $\mathbf{q}$—$\mathbf{h}$ plane centered at a conical intersection point gives

$$\oint_C \mathbf{g}_{12} \cdot \mathrm{d}\mathbf{Q} = \pm \int_0^{2\pi} \mathbf{g}_{12} \cdot \hat{e}_\phi r \mathrm{d}\theta = \pm\pi \tag{5.44}$$

where the sign depends on the direction of rotation. This result is due to the presence of the discontinuity at the intersection. In fact, for a two-state system we have, according

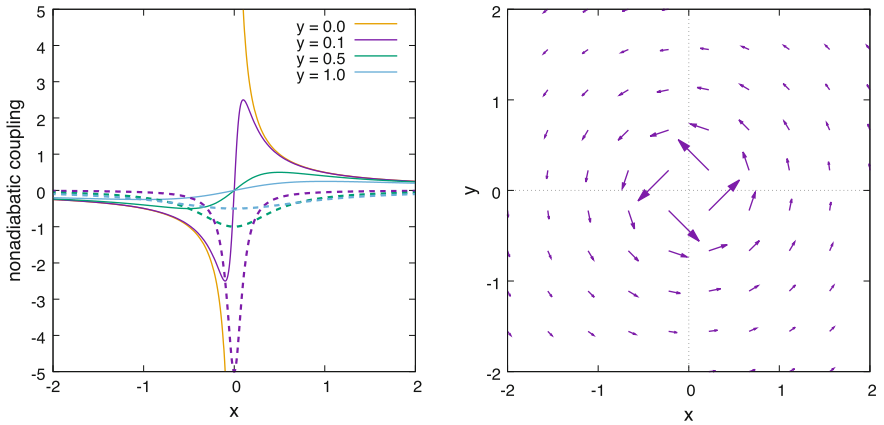

Fig. 5.2 Nonadiabatic coupling vector $\mathbf{g}_{12}$ close to a conical intersection, Eq. 5.42 with $q = h$. In the left panel, $g_{12}^{(x)}(x, y)$ and $g_{12}^{(y)}(x, y)$ are represented as functions of x, for some fixed values of y, with dashed and full lines, respectively. In the right panel $\mathbf{g}_{12}$ is represented by arrows in the x-y plane, having length proportional to the norm of $\mathbf{g}_{12}$

to (5.13), $\partial g_{12}^{(\alpha)}/\partial Q_\beta - \partial g_{12}^{(\beta)}/\partial Q_\alpha = 0$ for all α, β, which ensures the circulation of $\mathbf{g}_{12}$ is equal to zero in a simply connected region where $\mathbf{g}_{12}$ is continuous and derivable.

5.4.1 *Classification of Conical Intersections*

There are several ways to classify conical intersections. Considering the symmetry of the electronic states involved in the intersection, we may have symmetry-required intersections when the two states in $\mathbf{Q}_x$ belong to the same degenerate irreducible representation of a non-Abelian symmetry group. In fact, in that case the Jahn–Teller theorem (see Sect. 5.4.4) ensures that the degeneracy is removed at first order in the displacement from $\mathbf{Q}_x$, which means the degeneracy point has to be a conical intersection. If the two states have different symmetry in $\mathbf{Q}_x$ the conical intersection is called symmetry-allowed, and finally we may have an intersection of two states belonging to the same nondegenerate representation of the molecular point group.

According to another classification scheme a conical intersection is called *peaked* if it represents a local minimum of U_2, and *sloped* otherwise. On the potential energy surface of the upper state U_2, a peaked intersection is normally more easily accessed than a sloped one, so that it usually represents a more efficient funnel to the lower state. Note anyway that in both types of conical intersections, peaked or sloped, the slope of the lower state PES pulls the system away from the intersection region. For this reason, the transitions from upper to lower states tend to be irreversible in polyatomic molecules and/or in condensed phase, where the excess vibrational energy is promptly redistributed among other modes (see Sects. 4.3 and 4.5).

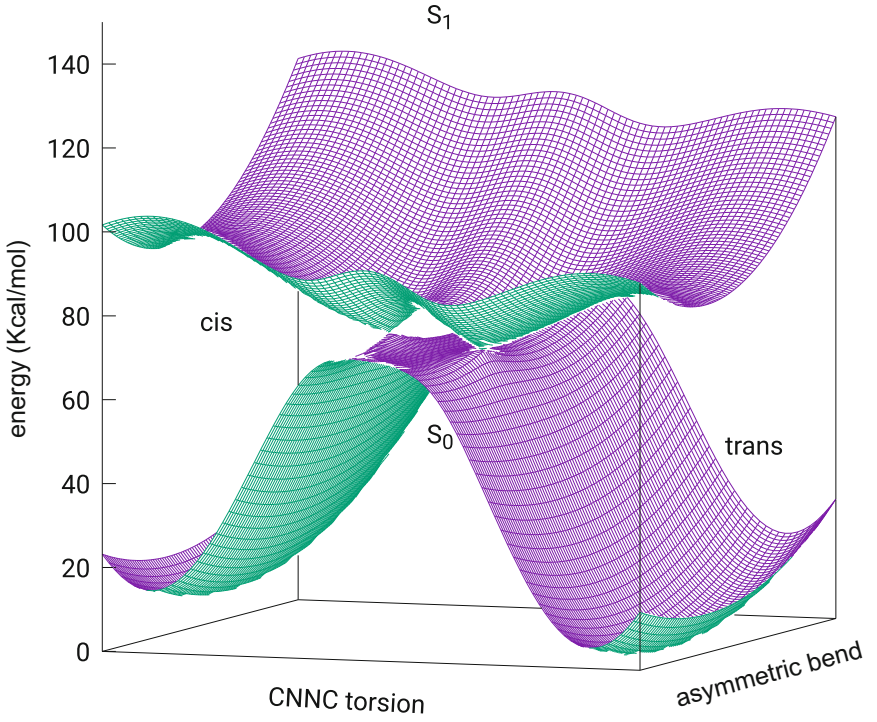

Fig. 5.3 Conical intersections in azomethane

The case of symmetry-allowed conical intersection is particularly easy to visualize. In particular, let Q_S and Q_A be a symmetric and a nonsymmetric coordinate, respectively (i.e., Q_S leaves unaltered the molecular symmetry, while Q_A removes some symmetry element). We consider, for example, S_0 and S_1 in azomethane, CH_3-N=N-CH_3. In the *cis-trans* isomerization pathway the C_2 symmetry is kept, and we can choose the torsion angle CNNC as the Q_S coordinate, and the antisymmetric combination of the two CNN bending angles as the Q_A coordinate. The ground state has A symmetry, while S_1 ($n \rightarrow \pi^*$) has B symmetry. Then, as far as $Q_A = 0$, $H_{12} = 0$, so by varying Q_S with Q_A set to zero we may find a point where $\Delta H = 0$ and the two potential energy curves do cross. Now, fixing Q_A to a (small) nonzero value, the symmetry is removed and, along Q_S, the crossing becomes avoided (the smaller is the value of $|Q_A|$, the more tightly avoided is the crossing). For azomethane, at CNNC $\simeq 90°$ the ground state has a maximum and S_1 a minimum, giving place to two conical intersections in the space of the two coordinates here considered (see Fig. 5.3). Actually, if other coordinates were considered, the two conical intersections might turn out to belong to the same crossing seam.

In azobenzene the maximum of the S_0 PES along the CNNC dihedral, at CNNC $\simeq 90°$, practically coincides with the minimum of the S_1 $n \rightarrow \pi^*$ state: we have therefore a peaked conical intersection, located at about 90° of torsion of the

CNNC angle, which acts as a very efficient funnel. In fact, the S_1 lifetime is well below 1 ps in the gas phase, especially if the *cis* isomer is excited. At CNNC $= 0°$ or $180°$ (i.e., either for the *trans* or for the *cis* isomer) the CNN angles have larger equilibrium values for S_1 than for S_0. For example, the *trans* isomer has CNN $= 115°$ for S_0 and CNN $= 129°$ for S_1. So, opening the CNN angles the S_0 PES rises more steeply with respect to S_1, leading to a sloped conical intersection, which actually belongs to the same crossing seam as the peaked one referred above. Clearly, after $S_0 \rightarrow S_1$ excitation the vibrational coordinate CNN gets excited (see Sect. 3.7), and the sloped conical intersection may be reached, giving rise to "early" decay to S_0 (i.e., at transoid or cisoid geometries), which in turn leads to a decrease of the photoisomerization quantum yield. This phenomenon is more important for the *trans* than for the *cis* isomer, due to the fact that the torsion of the CNNC dihedral after excitation is much faster for the latter. So, in azobenzene the $cis \rightarrow trans$ photoisomerization quantum yield $\Phi_{cis \rightarrow trans}$ is close to 0.6, while $\Phi_{trans \rightarrow cis}$ is considerably lower (about 0.3 after $n \rightarrow \pi^*$ excitation).

In monoalkenes the S_0 and S_1 PES are still quite separated at $90°$ of torsion around the double bond. However, as discussed in Sect. 2.6.4, the two states get closer by pyramidalization of one of the two carbon atoms. In ethylene, this leads to a conical intersection, which is evidently very easily accessed from the Franck–Condon point. As a consequence, the S_1 lifetime in ethylene is very short ($\sim 10^2$ fs).

In acetone a crossing is found between the S_1 and T_1 $n \rightarrow \pi^*$ states by stretching the C-O bond and keeping the C_{2v} geometry of the ground state minimum. Taking into account the spin–orbit coupling, such a crossing is actually a symmetry-allowed conical intersection. In fact, as for the spatial part S_1 and T_1 both belong to the same A_2 irrep, but considering also the symmetry of the spin part, the three components of the triplet actually belong to the B_1, B_2, and A_1 irreps (while the singlet retains A_2 symmetry). The S_1/T_1 spin–orbit coupling is therefore zero at C_{2v} geometry, and the degeneracy is removed along nonsymmetric coordinates. In general, the true crossings of singlet and triplet PESs become avoided crossings or conical intersections when the spin–orbit coupling is introduced in the Hamiltonian. In the approximation of neglecting the coupling among the triplet degenerate states, one can identify a linear combination of them that interacts with the crossing singlet, and two noninteracting orthogonal combinations. So, in this approximation, only one triplet PES gives place to avoided crossings or conical intersections with the singlet one, while the two other degenerate PESs cross the singlet one without constraints. Some consequences for nonadiabatic dynamics are examined in Ref. [9].

5.4.2 Branching Plane (Real Hamiltonian)

The plane spanned by the two vectors $\mathbf{q}$ and $\mathbf{h}$ defined in Eq. (5.36) is called *branching plane*. As far as the first-order approximation is valid, only a displacement from $\mathbf{Q}_x$ in the branching plane is able to produce a value different from zero for ΔH and/or H_{12}, so removing the degeneracy. On the contrary, the degeneracy is kept

if the displacement is orthogonal to $\mathbf{q}$ and $\mathbf{h}$; see Eq. (5.35). The branching plane represents therefore the space, of dimension 2, where the degeneracy of a conical intersection is removed at first order. We stress here that this is just the most common possibility, as conical intersections with branching spaces of dimension 3 or 5 do exist (see Sect. 5.4.5).

Given the arbitrariness in the definition of the diabatic basis, the identification of the branching plane is easier if the two vectors $\mathbf{q}$ and $\mathbf{h}$ are expressed in terms of adiabatic quantities. To this aim, we first observe that, near an intersection point, Eq. (5.18) can be rewritten as

$$(U_l - U_k)\mathbf{g}_{kl} = \mathbf{C}_k^+ \nabla \mathbf{H} \mathbf{C}_l \tag{5.45}$$

Note that, as $U_l - U_k$ tends to zero, $\mathbf{g}_{kl}$ diverges, whereas the term $(U_l - U_k)\mathbf{C}_k^+ \boldsymbol{\nu}^{(\alpha)} \mathbf{C}_l$ vanishes. Moreover, from the Hellmann–Feynman theorem we have

$$\nabla U_k = \mathbf{C}_k^+ \nabla \mathbf{H} \mathbf{C}_k. \tag{5.46}$$

We already know from Eq. (5.42) that $\mathbf{g}_{12}$ lies on the branching plane, and the multiplication of the nonadiabatic coupling by the energy difference is effective in eliminating the divergence at the degeneracy point $\mathbf{Q}_x$. Setting $\Delta U = U_2 - U_1$ and using the columns of $\mathbf{C}$ of Eq. (5.2) for $\mathbf{C}_1$ and $\mathbf{C}_2$ we obtain

$$\begin{aligned} \nabla \Delta U &= \nabla \Delta H \cos(2\theta) - 2\nabla H_{12} \sin(2\theta) \\ 2\Delta U \mathbf{g}_{12} &= \nabla \Delta H \sin(2\theta) + 2\nabla H_{12} \cos(2\theta). \end{aligned} \tag{5.47}$$

Therefore, letting

$$\mathbf{w}_1 = \nabla \Delta U(\mathbf{Q}_x) \qquad \text{and} \qquad \mathbf{w}_2 = 2\Delta U(\mathbf{Q}_x)\mathbf{g}_{12}(\mathbf{Q}_x) \tag{5.48}$$

it is evident that the space spanned by the two vectors $\mathbf{w}_1$ and $\mathbf{w}_2$ is the branching plane.

The knowledge of the branching plane may be useful, for example, to find the minimum energy point of a crossing seam. In fact, starting from any point of the seam, the search for the minimum can be done in a direction orthogonal to $\mathbf{w}_1$ and $\mathbf{w}_2$, so that the degeneracy is maintained. However, the evaluation of the nonadiabatic couplings is quite expensive from the computational point of view, so this procedure is not necessarily the most effective. Finding the minimum energy point of a crossing seam is important in order to assess the energetic accessibility of the seam and therefore its relevance in the photodynamics of the molecular system.

5.4.3 Geometric Phase

When an adiabatic electronic wavefunction is transported around a closed path it acquires a phase, which is called *geometric phase*, or Berry's phase [10–13]. In

particular, the phase factor is just $+1$ and therefore irrelevant, if the loop does not enclose a conical intersection, but is -1 when the loop contains a conical intersection.

Let us consider first an example to illustrate this behavior. The H_3 molecule, in the symmetric D_{3h} conformation, has a degenerate $^2E'$ electronic ground state. According to the Jahn–Teller theorem, this geometry corresponds to a symmetry-required crossing seam. Let us consider a path, enclosing the seam, in which two of the three atoms are cyclically brought closer (see Fig. 5.4). For simplicity we assume that the three atoms are, at all geometries considered here, far apart enough to neglect the overlap between the $1s$ orbitals, as well as the contribution of ionic configurations (with two electrons in the same $1s$ orbital) to the ground-state wavefunction. In this way, a reasonable approximation for the ground-state wavefunction can be obtained from a linear combination of the three Slater determinants

$$\Phi_1 = \overline{\phi}_a \wedge \phi_b \wedge \phi_c \qquad \Phi_2 = \phi_a \wedge \overline{\phi}_b \wedge \phi_c \qquad \Phi_3 = \phi_a \wedge \phi_b \wedge \overline{\phi}_c \tag{5.49}$$

where ϕ_a (respectively, $\overline{\phi}_a$) labels a $1s$ spinorbital centered on atom H_a and with spin part α (respectively, β). Here we limit ourselves to consider the electronic functions with $M_S = 1/2$, which is correct in the electrostatic approximation; see Sect. 5.4.5. At the D_{3h} geometry (labeled "O" in Fig. 5.4), the doubly degenerate $^2E'$ electronic states are

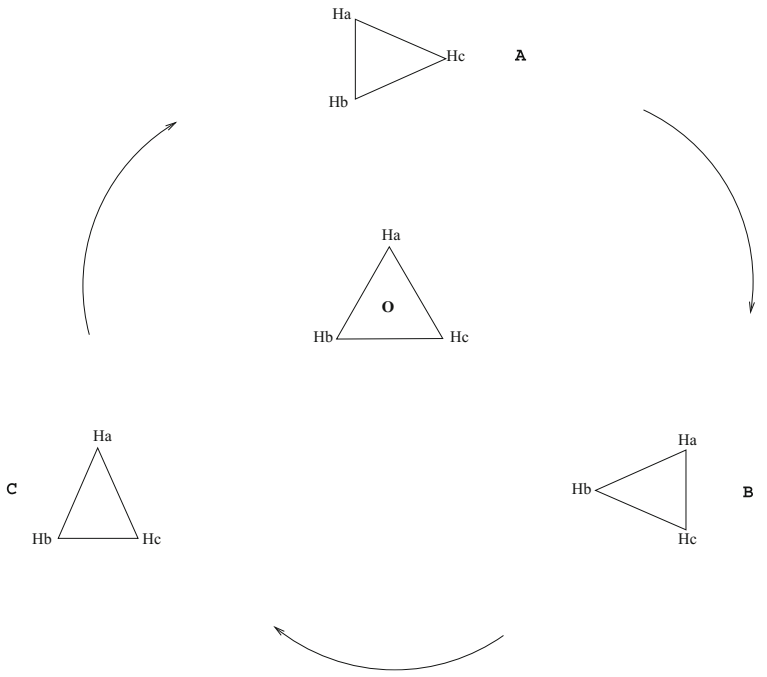

Fig. 5.4 A closed path around the crossing seam in H_3

$$\begin{aligned}\varphi_1(\mathrm{O}) &= \frac{1}{\sqrt{2}}(\Phi_1 - \Phi_2)\\ \varphi_2(\mathrm{O}) &= \frac{1}{\sqrt{6}}(2\Phi_3 - \Phi_1 - \Phi_2)\,.\end{aligned} \tag{5.50}$$

At the C_{2v} geometry "A" (see Fig. 5.4) the ground state φ_1 is obtained by pairing the spin of the two nearest atoms H_a and H_b so as to obtain a singlet, which becomes a doublet adding the third electron

$$\varphi_1(\mathrm{A}) = \frac{1}{\sqrt{2}}(\Phi_1 - \Phi_2)\ . \tag{5.51}$$

Now we want to transport φ_1 from "A" to "B" with continuity, i.e., without abrupt phase changes. To this aim we impose $\langle\varphi_1(\mathrm{A})\,|\varphi_1(\mathrm{B})\rangle > 0$, obtaining

$$\varphi_1(\mathrm{B}) = \frac{1}{\sqrt{2}}(\Phi_1 - \Phi_3)\ . \tag{5.52}$$

We then go from "B" to "C"

$$\varphi_1(\mathrm{C}) = \frac{1}{\sqrt{2}}(\Phi_2 - \Phi_3) \tag{5.53}$$

and from "C" to "A" again

$$\varphi_1'(\mathrm{A}) = \frac{1}{\sqrt{2}}(\Phi_2 - \Phi_1)\,. \tag{5.54}$$

Then, the electronic wavefunction φ_1, transported around a closed loop encircling a conical intersection, has changed its sign.

In general, let us consider one of the adiabatic electronic functions of our two-state system, for example $\varphi_1(\mathbf{Q}) = \eta_1 \cos\theta(\mathbf{Q}) + \eta_2 \sin\theta(\mathbf{Q})$, where the dependence of φ_1 and θ on the nuclear coordinates $\mathbf{Q}$ has been made explicit. The parameter $\theta(\mathbf{Q})$ is determined by Eq. (D.5)

$$\mathrm{tg}(2\theta) = -\frac{2H_{12}}{\Delta H}\ . \tag{5.55}$$

Let then C be an infinitesimal closed path on the branching plane, encircling the conical intersection at $\mathbf{Q}_x$. Note that any infinitesimal displacement orthogonal to the branching plane keeps the degeneracy and cannot turn around the intersection. Given that C is infinitesimal we can use Eq. (5.37) for ΔH and H_{12}. We have therefore, on C

$$\mathrm{tg}(2\theta) = -\frac{hy}{qx} \tag{5.56}$$

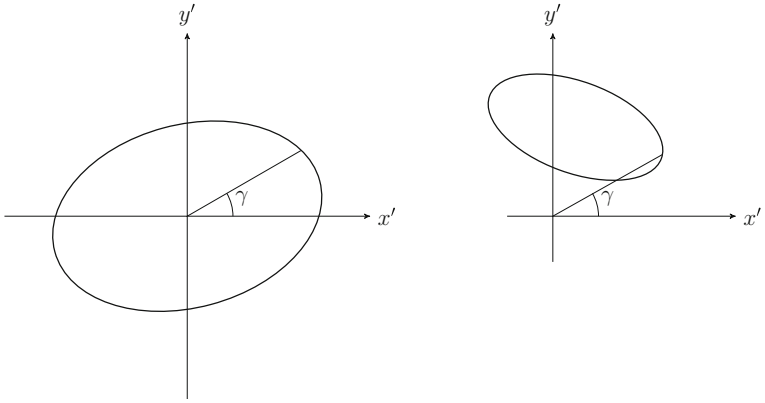

Fig. 5.5 Closed paths in the plane (x', y'), containing (left) or not (right) the conical intersection

where, as in Eq. (5.37), x and y are the displacements from the intersection point along the two (orthogonal) versors $\hat{x}$ and $\hat{y}$. It is convenient to rescale the coordinates as $x' = qx$ and $y' = hy$. At this point we can switch to polar coordinates: $x' = r\cos\gamma$ and $y' = r\sin\gamma$. Then

$$\mathrm{tg}(2\theta) = -\,\mathrm{tg}\,\gamma \tag{5.57}$$

so we can choose $\theta = -\gamma/2$, and $|\varphi_1\rangle$ becomes (see Eq. (5.1))

$$|\varphi_1\rangle = \cos\frac{\gamma}{2}\,|\eta_1\rangle - \sin\frac{\gamma}{2}\,|\eta_2\rangle \ . \tag{5.58}$$

If the closed loop C contains a conical intersection, the angle γ goes from a given starting value γ_i to $\gamma_i \pm 2\pi$, which means the sign of φ_1 has changed (see Fig. 5.5). On the contrary, if C does not contain a conical intersection, the angle γ simply goes from γ_i to γ_i, and the phase of the wavefunction does not change.

With only two nuclear coordinates it is easy to see that what we have shown above for an infinitesimal path can be extended to a closed loop of arbitrary shape, by stretching with continuity the infinitesimal path and exploiting the fact that the geometric phase does not change in a loop not encircling a conical intersection. Note then that we have no sign change as well if the loop contains two conical intersections. In general, when transported around a closed path containing n conical intersections, the electronic wavefunction is multiplied by $(-1)^n$. Things are more complicated if the number s of internal coordinates is larger than 2, as we have to make a clear-cut distinction between a loop encircling or not encircling a conical intersection (which is easier in two dimensions). In that case it is better to reverse the argument: if a sign change is found by transporting the wavefunction around a closed loop of arbitrary shape, the surface bounded by the closed loop has to contain a conical intersection. This fact can be exploited to locate conical intersections in nuclear configurational space.

Because of the geometric phase, in the presence of a conical intersection an adiabatic electronic state φ_k is a multivalued function. Of course, the total wavefunction has to be single-valued, and as a consequence the nuclear part must be multivalued, too. Hence, the presence of the conical intersection induces a coupling between the electronic and the nuclear motion, even when the nonadiabatic effects are negligible. Actually, we could exploit the fact that the adiabatic wavefunctions are defined up to $\mathbf{Q}$-dependent phase factors, by setting

$$\tilde{\varphi}_k(\mathbf{r};\mathbf{Q}) = \mathrm{e}^{\mathrm{i}\Omega_k(\mathbf{Q})}\varphi_k(\mathbf{r};\mathbf{Q}) \tag{5.59}$$

in such a way that $\tilde{\varphi}_k$ is single-valued. The nonadiabatic couplings are not invariant in this "gauge" transformation

$$\tilde{\mathbf{g}}_{kl}(\mathbf{Q}) = \mathrm{e}^{\mathrm{i}(\Omega_l-\Omega_k)}\mathbf{g}_{kl}(\mathbf{Q}) + \mathrm{i}\delta_{kl}\nabla\Omega_l(\mathbf{Q}) \ . \tag{5.60}$$

Note in particular that, while with a real Hamiltonian φ_k can always be chosen real-valued so that $\mathbf{g}_{kk} = 0$, $\tilde{\varphi}_k$ is complex and we have $\tilde{\mathbf{g}}_{kk} = \mathrm{i}\nabla\Omega_k$. We know from (2.64) that $\tilde{\mathbf{g}}_{kk}$ is imaginary; therefore Ω_k is real.

The geometric phase was first discovered by Longuet–Higgins [14] for a two-state system (as the one considered above) and then generalized by Berry [12]. According to Berry, we take $\mathbf{Q}$ as a set of time-dependent external parameters (similarly to Sect. 5.3). Let us consider a closed path C in the $\mathbf{Q}$ space, which is covered in the time interval $[0, T]$, so that $\mathbf{Q}(0) = \mathbf{Q}(T)$. Using the relation $\tilde{\mathbf{g}}_{kk} = \mathrm{i}\nabla\Omega_k$ and the chain derivative rule we obtain

$$\dot{\Omega}_k(t) = \nabla\Omega_k \cdot \dot{\mathbf{Q}} = -\mathrm{i}\tilde{\mathbf{g}}_{kk} \cdot \dot{\mathbf{Q}} \tag{5.61}$$

Then, the accumulated phase $\Omega_k^{(C)}$ in the closed path C is

$$\Omega_k^{(C)} = \Omega_k(T) - \Omega_k(0) = -\mathrm{i}\int_0^T \tilde{\mathbf{g}}_{kk} \cdot \dot{\mathbf{Q}}\mathrm{d}t = -\mathrm{i}\oint_C \tilde{\mathbf{g}}_{kk} \cdot \mathrm{d}\mathbf{Q}. \tag{5.62}$$

Given that $\tilde{\varphi}_k$ is single-valued, it follows from from Eq. (5.59) that the phase factor acquired by φ_k in the closed path C is $\exp(-\mathrm{i}\Omega_k^{(C)})$. Note that $\Omega_k^{(C)}$ has two important properties: it depends on the shape of the path C and not on the velocity at which C is covered, and it is invariant in the gauge transform referred above (see Eq. (5.60)). In fact, for any continuous and derivable f, both $\tilde{\mathbf{g}}_{kk}$ and $\tilde{\mathbf{g}}_{kk} + \mathrm{i}\nabla f$ have the same circulation. It is for these reasons that the phase Ω_k is called *geometric*.

In the two-state case considered above we can choose $\Omega_1 = \Omega_2 = \gamma/2$. Moreover, assuming for simplicity $q = h$, we have $\mathbf{g}_{12} = -\nabla\gamma/2 = -\nabla\Omega_1 = \mathrm{i}\tilde{\mathbf{g}}_{11}$. Then, in a small circle around a conical intersection we get, according to Eq. (5.44): $\exp(-\mathrm{i}\Omega_k^{(C)}) = \mathrm{e}^{\pm\mathrm{i}\pi} = -1$.

In Fig. 5.6 and in the Animation 5.1 we show the time evolution of a wavepacket going through a conical intersection. The two-dimensional model system considered

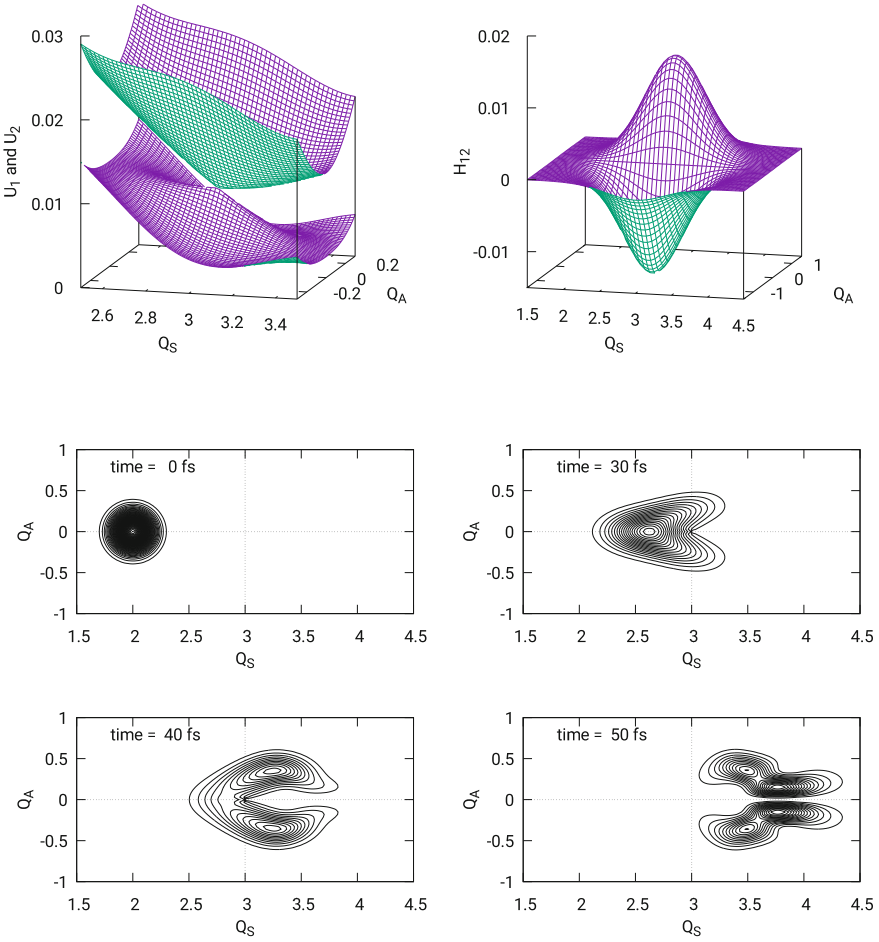

Fig. 5.6 Wavepacket going through a conical intersection. The upper panels show the adiabatic PESs U_1, U_2 (left) and the diabatic coupling H_{12} (right) of the 2D (Q_S and Q_A) model system considered. Energies and coordinates are given in atomic units. The conical intersection is located at $Q_S = 3$ and $Q_A = 0$. Four snapshots of the adiabatic wavepacket Θ_1 at different times are shown as contour plots of the probability density $|\Theta_1(Q_S, Q_A)|^2$

features a symmetry-allowed conical intersection, with the diabatic coupling H_{12} being an odd function of the antisymmetric coordinate Q_A. The dynamics is essentially adiabatic: at time $t = 0$ only the lower state is populated, and the population transfer to the upper state at later times is negligible. The starting wavepacket is Gaussian in both coordinates but, after traversing the conical intersection, it shows a node at $Q_A = 0$, as if it had been sliced by the conical intersection. This can be seen as a manifestation of Berry's phase: the two wings of the wavepacket, that go around

the intersection on opposite sides, gain opposite phases, giving rise to destructive interference.

When performing numerical calculations of wavepacket dynamics using Eq. (2.78), of course one wants to deal with single-valued nuclear wavepackets. Then, the adiabatic Born–Huang expansion of Eq. (2.77) has to be expressed in terms of the single-valued electronic functions $\tilde{\varphi}_k$. In this way, to correctly deal with conical intersections, the geometric phase factors $e^{i\Omega_k}$ have to be explicitly introduced in the wavepacket dynamics. On the contrary, no special care is needed when working in the diabatic basis (Eq. (5.20)), which is not made of eigenfunctions of $\hat{H}_{el}$ and therefore is free from the complexities associated with energy degeneracies.

5.4.4 The Jahn–Teller Effect

We consider a case in which the two states φ_1 and φ_2, in the degeneracy point $\mathbf{Q}_x$, belong to the same degenerate irreducible representation Γ_φ of a non-Abelian point group. Our aim is to establish if $\mathbf{Q}_x$ is a stable conformation against a deformation which reduces the symmetry and removes the degeneracy (i.e., whether $\mathbf{Q}_x$ can be a stationary point for U_1 and U_2). At first order in the displacement $\Delta\mathbf{Q} = \mathbf{Q} - \mathbf{Q}_x$, the matrix elements H_{ij} of $\hat{H}_{el}$ in the diabatic basis are given by

$$H_{ij}(\mathbf{Q}) = H_0\delta_{ij} + \nabla H_{ij}(\mathbf{Q}_x)\cdot\Delta\mathbf{Q} + O(|\Delta\mathbf{Q}|^2) \tag{5.63}$$

where $H_0 = U_1(\mathbf{Q}_x) = U_2(\mathbf{Q}_x)$ represents the degenerate electronic energy at the symmetric configuration $\mathbf{Q}_x$. In a small neighborhood of $\mathbf{Q}_x$, the diabatic states can be identified with the two degenerate electronic states at $\mathbf{Q}_x$. For a given nuclear internal coordinate Q_α

$$\frac{\partial H_{ij}(\mathbf{Q}_x)}{\partial Q_\alpha} = \left\langle \eta_i \left| \frac{\partial \hat{H}_{el}(\mathbf{Q}_x)}{\partial Q_\alpha} \right| \eta_j \right\rangle. \tag{5.64}$$

It is convenient to take as internal coordinates the normal modes, as these can be classified according to the irreducible representation of the point group of the molecule. We are interested in a normal mode Q_α which removes the symmetry and consequently the degeneracy. Therefore, the irreducible representation to which Q_α belongs, Γ_{Q_α}, cannot be the totally symmetric one, Γ_A. Moreover, the integral (5.64) is nonzero only if the direct product of irreducible representations $\Gamma_\varphi \otimes \Gamma_\varphi \otimes \Gamma_{Q_\alpha}$ contains Γ_A. As it is apparent from Eqs. (5.3) and (5.63), if $\partial H_{ij}/\partial Q_\alpha \neq 0$ in $\mathbf{Q}_x$, a displacement along Q_α removes the degeneracy at first order in ΔQ_α. In that case, $\mathbf{Q}_x$ cannot be a stationary point for U_1 and U_2, and in particular it represents a conical intersection. It was first proved by Jahn and Teller [15] that, for a nonlinear polyatomic molecule, it is indeed always possible to find a normal mode Q_α such that $\Gamma_\varphi \otimes \Gamma_\varphi \otimes \Gamma_{Q_\alpha}$ contains Γ_A.

On the contrary, for linear polyatomic molecules in degenerate electronic states (i.e., belonging to one of the bidimensional irreducible representations Π, Δ, etc., of $C_{\infty v}$ or $D_{\infty v}$ symmetry groups) the linear terms (5.64) are zero by symmetry. The degeneracy is removed upon bending at the second order (the Renner–Teller effect). In this case the intersection between U_1 and U_2 is not of the conical type, and in fact the geometric phase effect is absent.

5.4.5 Complex Hamiltonian and Kramers Degeneracy

In the previous section of the present chapter we always assumed that, at least in the vicinity of the crossing, a two-state system can be used as a reasonable approximation, and that H_{12} is a real-valued function. However, in the general case both assumptions must be relaxed. To understand why, it is convenient to consider the time-reversal symmetry.

The symmetry operation called *time reversal* changes the sign of time, so it has the effect to reverse the motion of the system, inverting the sign of linear and angular momentum (see, for example, Sakurai [10] or Merzbacher [16]). As in classical mechanics, an isolated system (or even a system subject to an external conservative field) is symmetric under time reversal. In particular, if $\hat{T}$ is the time-reversal operator, for a system symmetric with respect to time reversal we must obtain the same result if the system is evolved for a time $\mathrm{d}t$ and then $\hat{T}$ is applied, or applying first the time reversal and then evolving for a time $-\mathrm{d}t$. Using the infinitesimal time evolution operator (2.5) we get, for any state $|\Psi\rangle$

$$\left(1 - \frac{\mathrm{i}\mathrm{d}t}{\hbar}\hat{H}\right)\hat{T}\,|\Psi\rangle = \hat{T}\left(1 + \frac{\mathrm{i}\mathrm{d}t}{\hbar}\hat{H}\right)|\Psi\rangle \tag{5.65}$$

so $-\mathrm{i}\hat{H}\hat{T} = \hat{T}\mathrm{i}\hat{H}$. If $\hat{T}$ were a linear operator we would obtain $-\hat{H}\hat{T} = \hat{T}\hat{H}$, which is an absurd result (it would imply that, for any $|\Psi_E\rangle$ eigenstate of $\hat{H}$ with eigenvalue E, $\hat{T}\,|\Psi_E\rangle$ would be eigenstate of $\hat{H}$ with eigenvalue $-E$). Then, we must admit that $\hat{T}\mathrm{i} = -\mathrm{i}\hat{T}$, in such a way that $\hat{H}\hat{T} = \hat{T}\hat{H}$ for our system symmetric under time reversal. Therefore, $\hat{T}$ has to be an *antilinear* operator

$$\hat{T}(a\,|\Psi_1\rangle + b\,|\Psi_2\rangle) = a^*\hat{T}\,|\Psi_1\rangle + b^*\hat{T}\,|\Psi_2\rangle \tag{5.66}$$

where a and b are complex numbers. As time reversal is a symmetry operation, it has to conserve the norm of the wavefunction: $\left\langle \hat{T}\Psi \,\middle|\, \hat{T}\Psi \right\rangle = \langle \Psi\,|\Psi\,\rangle$. However, given that $\hat{T}$ is antilinear, it cannot be unitary. We rather have

$$\left\langle \hat{T}\Psi \,\middle|\, \hat{T}\Phi \right\rangle = \langle \Psi\,|\Phi\,\rangle^* . \tag{5.67}$$

The two Eqs. (5.66) and (5.67) define $\hat{T}$ as an *antiunitary* operator.

As observed above, we expect angular momentum to change sign under time reversal:

$$\hat{T}\hat{\mathbf{J}}\hat{T}^{-1} = -\hat{\mathbf{J}} \tag{5.68}$$

where $\hat{\mathbf{J}}$ represent either spatial or spin (or total) angular momentum. Note in fact that, in this way, $\hat{T}$ commutes with the rotation operator $e^{-\mathrm{i}\hat{\mathbf{J}}\cdot\hat{n}\theta/\hbar}$ (here $\hat{n}$ and θ are the rotation axis versor and the rotation angle), which is indeed a desirable property. Using Eq. (5.68) and the angular momentum commutation relations it is possible to show that

$$\hat{T}\,|j,m\rangle = (-1)^m \mathrm{e}^{\mathrm{i}\gamma_j}\,|j,-m\rangle \tag{5.69}$$

where γ_j is a real number independent on m and $|j,m\rangle$ is an eigenvector of $\hat{J}^2$ and $\hat{J}_z$ with eigenvalues $\hbar^2 j(j+1)$ and $\hbar m$, respectively. The above equation is valid both for integer and half-integer j.

Let us now consider the operator $\hat{T}^2$. Apparently the symmetry operation $\hat{T}^2$ should leave the system unaltered, as much as a rotation of 2π. We obtain

$$\hat{T}^2\,|j,m\rangle = (-1)^m \mathrm{e}^{-\mathrm{i}\gamma_j}\hat{T}\,|j,-m\rangle = (-1)^{2j}\,|j,m\rangle \tag{5.70}$$

which means $\hat{T}^2 = 1$ for j integer and $\hat{T}^2 = -1$ for j half-integer: it appears therefore that $\hat{T}^2$ is actually *equivalent* to a rotation of 2π.

Considering in particular electronic wavefunctions, in which we are interested here, we have

$$\hat{T}^2\varphi = (-1)^{N_e}\varphi \tag{5.71}$$

where N_e is the number of electrons. Note that this result is valid in general, for any electronic wavefunction φ. In fact, the spin part of φ can always be expanded in terms of the eigenstates of $\hat{S}^2$ and $\hat{S}_z$, for which Eq. (5.70) applies (and for the same reason the spatial part is symmetric with respect to $\hat{T}^2$). Now, if φ is eigenstate of $\hat{H}_{el}$ and $\hat{T}$ commutes with $\hat{H}_{el}$, then also $\varphi' = \hat{T}\varphi$ is eigenstate of $\hat{H}_{el}$, with the same eigenvalue. If φ' and φ are actually the same state we have $\varphi' = a\varphi$, where a is a complex number. Then

$$\hat{T}^2\varphi = \hat{T}\hat{T}\varphi = \hat{T}\varphi' = a^*\hat{T}\varphi = |a|^2\,\varphi \tag{5.72}$$

and comparing with (5.71) we obtain $|a|^2 = (-1)^{N_e}$, which can only be valid if N_e is even. Therefore, with an odd number of electrons φ and $\hat{T}\varphi$ are necessarily different. As a consequence, in a system symmetric with respect to time reversal so that $\hat{H}_{el}\hat{T} = \hat{T}\hat{H}_{el}$ and with an odd number of electrons, all the eigenstates of $\hat{H}_{el}$ are at least doubly degenerate. This is the so-called *Kramers degeneracy*.

Because of Kramers degeneracy, a conical intersection may involve four electronic states rather than two. In fact we can distinguish three different cases.

Case A. System symmetric with respect to time reversal ($\hat{H}_{el}\hat{T} = \hat{T}\hat{H}_{el}$) with an even number of electrons. We have $\hat{T}^2 = 1$ and we can always choose a time-reversal adapted basis of electronic functions η_i such that $\hat{T}\eta_i = \eta_i$. Then

$$\left\langle \eta_i \left| \hat{H}_{el} \right| \eta_j \right\rangle = \left\langle \hat{T}\eta_i \left| \hat{H}_{el} \right| \hat{T}\eta_j \right\rangle = \left\langle \hat{T}\eta_i \left| \hat{T}\hat{H}_{el}\eta_j \right\rangle = \left\langle \eta_i \left| \hat{H}_{el} \right| \eta_j \right\rangle^* \tag{5.73}$$

where the last equality follows from (5.67). Therefore, all the matrix elements of $\hat{H}_{el}$ are real, irrespective of the form of $\hat{H}_{el}$ itself. This is the case which has been considered in the previous sections of this chapter.

Case B. System symmetric with respect to time reversal with an odd number of electrons. Because of Kramers degeneracy, a crossing of two potential energy surfaces U_1 and U_2 actually involves not two but four states: φ_1, φ_2, $\hat{T}\varphi_1$, and $\hat{T}\varphi_2$. We consider then the time-reversal adapted basis of electronic functions η_1, η_2, $\hat{T}\eta_1$, and $\hat{T}\eta_2$. The matrix of $\hat{H}_{el}$ in the time-reversal adapted basis can be simplified taking into account that, in the present case, $\hat{T}^2 = -1$ and $\hat{T}$ commutes with $\hat{H}_{el}$

$$\left\langle \hat{T}\eta_i \left| \hat{H}_{el} \right| \hat{T}\eta_j \right\rangle = \left\langle \hat{T}^2\eta_i \left| \hat{T}\hat{H}_{el}\hat{T}\eta_j \right\rangle^* = \left\langle \hat{T}^2\eta_i \left| \hat{H}_{el} \right| \hat{T}^2\eta_j \right\rangle^* = H_{ij}^* \tag{5.74}$$

where, as usual, $\left\langle \eta_i \left| \hat{H}_{el} \right| \eta_j \right\rangle = H_{ij}$ and we also exploited (5.67) in the first equality. Proceeding in the same way we obtain

$$\begin{aligned} \left\langle \hat{T}\eta_i \left| \hat{H}_{el} \right| \eta_i \right\rangle &= 0 \\ \left\langle \hat{T}\eta_i \left| \hat{H}_{el} \right| \eta_j \right\rangle &= -H_{iTj}^* \qquad (i \neq j) \end{aligned} \tag{5.75}$$

were $H_{iTj} = \left\langle \eta_i \left| \hat{H}_{el} \right| \hat{T}\eta_j \right\rangle$. The matrix of $\hat{H}_{el}$ in the basis η_1, η_2, $\hat{T}\eta_1$ and $\hat{T}\eta_2$ is therefore

$$\begin{pmatrix} H_{11} & H_{12} & 0 & H_{1T2} \\ H_{12}^* & H_{22} & -H_{1T2} & 0 \\ 0 & -H_{1T2}^* & H_{11} & H_{12}^* \\ H_{1T2}^* & 0 & H_{12} & H_{22} \end{pmatrix} \tag{5.76}$$

Its diagonalization gives the two doubly degenerate eigenvalues U_1 and U_2

$$U_{2,1} = \frac{1}{2}\left(H_{11} + H_{22} \pm \sqrt{\Delta H^2 + 4\,|H_{12}|^2 + 4\,|H_{1T2}|^2} \right). \tag{5.77}$$

As a consequence, five conditions have to be imposed in order to have $U_1 = U_2$

$$\begin{aligned} \Delta H &= 0 \\ \mathrm{Re}\{H_{12}\} &= 0 \qquad \mathrm{Im}\{H_{12}\} = 0 \\ \mathrm{Re}\{H_{1T2}\} &= 0 \qquad \mathrm{Im}\{H_{1T2}\} = 0 \end{aligned} \tag{5.78}$$

so the branching space actually has dimension 5 in the present case. This has an impact on the geometric phase as well, which shows in this case a more complicated behavior with respect to Sect. 5.4.3.

Note however that, in the absence of spin–orbit coupling (as in the H_3 molecule considered in Sect. 5.4.3), H_{12} is real and $H_{1T2} = 0$: in fact, according to (5.69), the spin of $\hat{T}\eta_2$ is reversed with respect to η_2 (so, either $H_{12} = 0$ or $H_{1T2} = 0$). The 4×4 matrix (5.76) reduces to two identical and uncoupled 2×2 matrices. We are therefore back to the case of branching space of dimension 2.

In general, it can be shown that $H_{1T2} = 0$ if the molecule has C_s symmetry, or higher. In that case, with complex H_{12}, the branching space has dimension 3 (three conditions to impose for $U_1 = U_2$).

Case C. System not symmetric with respect to time reversal ($\hat{H}_{el}\hat{T} \neq \hat{T}\hat{H}_{el}$). This is the case, for example, of a molecule in an external magnetic field. The Kramers degeneracy is removed, but H_{12} is, in general, complex. We have therefore a three-dimensional branching space.

We want now to evaluate the phase $\Omega_k^{(C)}$ (see Eq. (5.62)) in the present context of a complex-valued Hamiltonian [12, 13]. We consider for simplicity a three-dimensional nuclear configurational space so that, due to Stokes' theorem, the circulation of $\tilde{\mathbf{g}}_{kk}$ on C corresponds to the flux of a vector $\mathbf{V}_k = \nabla \times \tilde{\mathbf{g}}_{kk}$ across a surface S_C bounded by C

$$\Omega_k^{(C)} = -\mathrm{i} \oint_C \tilde{\mathbf{g}}_{kk} \cdot \mathrm{d}\mathbf{Q} = -\mathrm{i} \int_{S_C} \mathbf{V}_k \cdot \mathrm{d}\mathbf{S} \,. \tag{5.79}$$

Clearly $\nabla \cdot \mathbf{V}_k = 0$, so the flux of $\mathbf{V}_k$ across a closed surface vanishes (unless the enclosed volume contains a degeneracy point, where $\tilde{\mathbf{g}}_{kk}$ has a singularity). Therefore, the last integral in Eq. (5.79) only depends on the closed path C, and not on the peculiar choice of the surface S_C. We have

$$\mathbf{V}_k = \nabla \times \tilde{\mathbf{g}}_{kk} \tag{5.80}$$

$$= \langle \nabla\tilde{\varphi}_k \,| \times | \, \nabla\tilde{\varphi}_k \rangle \tag{5.81}$$

$$= \sum_{m \neq k} \langle \nabla\tilde{\varphi}_k \,| \tilde{\varphi}_m \rangle \times \langle \tilde{\varphi}_m \,| \nabla\tilde{\varphi}_k \rangle \tag{5.82}$$

$$= \sum_{m \neq k} \frac{\left\langle \varphi_k \left| \nabla \hat{H}_{el} \right| \varphi_m \right\rangle \times \left\langle \varphi_m \left| \nabla \hat{H}_{el} \right| \varphi_k \right\rangle}{(U_k - U_m)^2} \tag{5.83}$$

where we used the relation $\nabla \times (f \nabla g) = \nabla f \times \nabla g$ and Eq. (2.70) for the nonadiabatic couplings. The sum is extended to a complete basis set of adiabatic wavefunctions; the term with $m = k$ is excluded as $\langle \nabla\tilde{\varphi}_k \,| \tilde{\varphi}_k \rangle$ is purely imaginary and the vector product with its complex conjugate vanishes. It is particularly evident from Eq. (5.82) that $\mathbf{V}_k$ is independent on the phases of the electronic functions. It is then not necessary to use the single-valued $\tilde{\varphi}_m$. Moreover, $\mathbf{V}_k$ is imaginary: considering a real Hamiltonian, we can choose φ_m as real so that $\mathbf{V}_k = 0$ and $\Omega_k^{(C)}$ vanishes. This

result for $\Omega_k^{(C)}$ does not contradict what is reported in Sect. 5.4.3. In fact, the Stokes theorem requires the function $\tilde{\mathbf{g}}_{kk}$ to be differentiable on S_C, so Eq. (5.79) is only applicable if the surface S_C does not contain the intersection point, where $\tilde{\mathbf{g}}_{kk}$ has a singularity.

Let us consider now a two-state system. In the vicinity of a conical intersection, at first order in the displacement, the complex-valued Hamiltonian matrix in the diabatic basis can be written in this form (see Eq. (5.38))

$$\mathbf{H}_{el} = \begin{pmatrix} z & x - \mathrm{i}y \\ x + \mathrm{i}y & -z \end{pmatrix} = x\boldsymbol{\sigma}_x + y\boldsymbol{\sigma}_y + z\boldsymbol{\sigma}_z \tag{5.84}$$

apart from a scalar quantity, irrelevant in the present context, and with a suitable scaling for the three nuclear internal coordinates x, y, and z we are considering. The above Hamiltonian is appropriate for cases B or C (note in particular that with only three internal degrees of freedom we have at least C_s symmetry, so H_{1T2} vanishes, and it is not necessary to take into account explicitly Kramers degeneracy). The 2×2 matrices $\boldsymbol{\sigma}_x$, $\boldsymbol{\sigma}_x$, and $\boldsymbol{\sigma}_x$ are the so-called *Pauli spin matrices*

$$\boldsymbol{\sigma}_x = \begin{pmatrix} 0 & 1 \\ 1 & 0 \end{pmatrix} \qquad \boldsymbol{\sigma}_y = \begin{pmatrix} 0 & -\mathrm{i} \\ \mathrm{i} & 0 \end{pmatrix} \qquad \boldsymbol{\sigma}_z = \begin{pmatrix} 1 & 0 \\ 0 & -1 \end{pmatrix} \tag{5.85}$$

as they correspond, apart from a factor $\hbar/2$, to the matrix representations of $\hat{S}_x$, $\hat{S}_y$, and $\hat{S}_z$ for a spin 1/2 system. It is convenient to introduce polar coordinates: $x = r \sin\theta \cos\phi$, $y = r \sin\theta \cos\phi$, and $x = r \cos\theta$. It is then easily verified that the two eigenvectors of (5.84) are

$$\begin{aligned} |\varphi_1\rangle &= -\sin\left(\frac{\theta}{2}\right)|\eta_1\rangle + \mathrm{e}^{\mathrm{i}\phi}\cos\left(\frac{\theta}{2}\right)|\eta_2\rangle \\ |\varphi_2\rangle &= \cos\left(\frac{\theta}{2}\right)|\eta_1\rangle + \mathrm{e}^{\mathrm{i}\phi}\sin\left(\frac{\theta}{2}\right)|\eta_2\rangle \end{aligned} \tag{5.86}$$

with eigenvalues $U_1 = -r$ and $U_2 = r$. From Eq. (5.84) we immediately obtain $\nabla\mathbf{H}_{el} = \boldsymbol{\sigma}$, where $\boldsymbol{\sigma}$ is the vector collecting the Pauli matrices. We are now ready to evaluate the vectors $\mathbf{V}_k$. To this aim, a convenient way to proceed is to recognize that

$$\mathbf{V}_1 = \frac{\left\langle \varphi_1 \middle| \nabla\hat{H}_{el} \middle| \varphi_2 \right\rangle \times \left\langle \varphi_2 \middle| \nabla\hat{H}_{el} \middle| \varphi_1 \right\rangle}{4r^2} = \frac{\left\langle \varphi_1 \middle| \nabla\hat{H}_{el} \times \nabla\hat{H}_{el} \middle| \varphi_1 \right\rangle}{4r^2} \tag{5.87}$$

where the second equality follows from the completeness of the basis and the vanishing vector product of $\left\langle \varphi_1 \middle| \nabla\hat{H}_{el} \middle| \varphi_1 \right\rangle$ with itself. Then, taking advantage of the commutation properties of Pauli matrices ($[\boldsymbol{\sigma}_x, \boldsymbol{\sigma}_y] = 2\mathrm{i}\boldsymbol{\sigma}_z$, etc.), which stem from angular momentum commutation rules, we get

$$\mathbf{V}_1 = \mathrm{i}\frac{\langle\varphi_1\,|\boldsymbol{\sigma}|\,\varphi_1\rangle}{2r^2} = -\mathrm{i}\frac{\hat{r}}{2r^2} \tag{5.88}$$

where $\hat{r}$ is the unit vector in the direction $\mathbf{r} = (x, y, z)$. Analogously, $\mathbf{V}_2 = \mathrm{i}\hat{r}/2r^2$. We have then, from Eq. (5.79)

$$\Omega_1^{(C)} = -\int_{S_C} \frac{\hat{r}}{2r^2} \cdot \mathrm{d}\mathbf{S} = -\frac{1}{2}\int_C \mathrm{d}\omega \tag{5.89}$$

and $\Omega_2^{(C)} = -\Omega_1^{(C)}$. Here $\mathrm{d}\omega$ is the solid angle element: we choose S_C so that the last integral in the above formula represents the solid angle subtended by the closed circuit C at the degeneracy point (remember that the integral is independent on the peculiar choice of the surface S_C). For example, considering a closed loop with constant θ we obtain

$$\Omega_1^{(C)} = -\pi(1 - \cos\theta). \tag{5.90}$$

Note in particular that after a closed loop C in any plane containing the conical intersection, φ_1 acquires a phase factor equal to $\exp(\mathrm{i}\Omega_1^{(C)}) = \mathrm{e}^{-\mathrm{i}\pi} = -1$ if C encloses the degeneracy point (and a factor 1 in the other case). The same for φ_2. This is in agreement with what we obtained for the case of a bidimensional branching space (real Hamiltonian).

We end this section by noting that the relation $\mathbf{V}_k = \nabla \times \tilde{\mathbf{g}}_{kk}$ between $\mathbf{V}_k$ and $\tilde{\mathbf{g}}_{kk}$ is the same as that connecting the magnetic field $\mathbf{B}$ and the vector potential $\mathbf{A}$ in electrodynamics. Actually, the identification of $\tilde{\mathbf{g}}_{kk}$ with a vector potential becomes clearer taking into account that the TDSE (2.78) can be written in the following way, considering only a single state $\tilde{\varphi}_k\Theta_k = \varphi_k \mathrm{e}^{\mathrm{i}\Omega_k}\Theta_k$ (i.e., setting $\mathbf{g}_{kl} = \mathbf{t}_{kl} = 0$ for $l \neq k$)

$$\mathrm{i}\hbar\frac{\mathrm{d}\Theta_k}{\mathrm{d}t} = \left[\frac{1}{2}(\mathbf{P} - \mathrm{i}\hbar\tilde{\mathbf{g}}_{kk})^2 + U_k\right]\Theta_k \tag{5.91}$$

where $\mathbf{P}$ is the vector collecting the nuclear momentum operators $\hat{P}_\alpha = -\mathrm{i}\hbar\partial/\partial Q_\alpha$ conjugated to the mass-weighted nuclear coordinates $Q_\alpha = \sqrt{M_\alpha}R_\alpha$. Here we considered a single-valued electronic state $\tilde{\varphi}_k$, in such a way that the nuclear wavefunction is also single-valued. The above Eq. (5.91) has the same mathematical form as that of a charged particle in an external magnetic field with vector potential proportional to $\mathrm{i}\tilde{\mathbf{g}}_{kk}$. As noted above, with a real Hamiltonian such a field (which is invariant in the gauge transformation $\tilde{\mathbf{g}}_{kk} \to \tilde{\mathbf{g}}_{kk} + \mathrm{i}\nabla f$ with a single-valued f) is zero everywhere except at a conical intersection, where $\mathrm{i}\tilde{\mathbf{g}}_{kk}$ has a singularity. For this reason the vector potential term in Eq. (5.91) cannot be eliminated by a single-valued gauge transformation.

5.5 Computational Note: Methods for Nonadiabatic Dynamics

We consider here some of the most widely used methods for the description of nonadiabatic processes, such as excited state decay, photoisomerizations, photodissociations, energy transfer, and charge transfer, taking place on an ultrafast (sub-picosecond) or fast timescale (say, up to a few tens of ps). Slow nonadiabatic transitions are better tackled by perturbation methods; see Chap. 3.

The numerical integration of the TDSE (2.78), in the form deriving from the adiabatic Born–Huang expansion (2.77), requires the knowledge of the PESs $U_k(\mathbf{Q})$ and of the nonadiabatic couplings $\mathbf{g}_{kl}(\mathbf{Q})$ and $\mathbf{t}_{kl}(\mathbf{Q})$, in the whole region of nuclear coordinates that is accessible to the wavepackets Θ_k. Which electronic states must be included in the expansion and which regions of the PESs will be explored by the wavepackets depend on the initial conditions and particularly on the total energy, but also on the duration of the dynamics of interest. As an alternative, we can express the TDSE in the diabatic representation, Eq. (5.20), and then we need the diabatic quantities $H_{kl}(\mathbf{Q})$) for all the electronic states considered. In principle, this means that the adiabatic or diabatic PESs and couplings must be evaluated a priori for a sufficiently large number of points of the nuclear configuration space and then expressed as analytic functions of the internal coordinates $\mathbf{Q}$. For polyatomic molecules, the fitting or interpolation of the computed electronic quantities is a very cumbersome task, even taking into account the simplifications introduced by the diabatic representation. In part for this reason, approximated approaches in which the nuclear motion is described classically are very popular. In fact, due to the local character of classical mechanics, a "direct" (or "on-the-fly") strategy can be easily adopted, such that the electronic calculations are performed when needed, during the integration of the dynamical equations [17, 18]. In particular, for each time step in a nuclear classical trajectory, one just needs to evaluate the electronic energies and interstate couplings, plus the forces acting on the nuclei, at a single molecular geometry. Of course, the classical approximation is justified on the basis of the relatively large nuclear masses and is valid as far as quantum effects such as zero-point vibrations, tunneling, and interference can be ignored (see Chap. 4).

In the following, we will distinguish between quantum wavepacket dynamics (QWD) and classical trajectory approaches. In some QWD methods an effort is made to keep the nuclear motion as local as possible, for example by using nonspreading and traveling basis functions, such that the direct strategy can be applied. In classical trajectory approaches, the quantum effects that are ignored in the first place can be reintroduced by ad hoc provisions of the method.

5.5.1 Quantum Wavepacket Dynamics

Assuming that the electronic quantities (either the adiabatic U_k, $\mathbf{g}_{kl}(\mathbf{Q})$ and $\mathbf{t}_{kl}(\mathbf{Q})$ or the diabatic $H_{kl}(\mathbf{Q})$) are known, the numerical integration of the TDSE for the nuclear

wavepackets Θ_k is still computationally very demanding. In fact, the computational burden involved in a *brute-force* numerical integration grows exponentially with the number s of vibrational degrees of freedom. For example, we could represent Θ_k on a grid of points, obtained dividing in n parts the interval of values of Q_α of interest, for all α, ending up with a grid of n^s points.

The method that best combines efficiency and accuracy in tackling this difficult problem is the multiconfigurational time-dependent Hartree (MCTDH) [19], in which the wavepackets are expanded in terms of "configurations" Φ_I

$$\Theta_k(\mathbf{Q}, t) = \sum_I A_{I,k}(t)\Phi_I(\mathbf{Q}, t) \ . \tag{5.92}$$

Each configuration is built as a *Hartree product* (i.e., a simple product, as opposed to the antisymmetrized products that are necessary for electrons) of "single-particle functions" (SPFs), in the form

$$\Phi_I(\mathbf{Q}, t) = \prod_\alpha \xi_{I,\alpha}(Q_\alpha, t) \ . \tag{5.93}$$

In a fast nonadiabatic dynamics the nuclear degrees of freedom are normally strongly correlated, so that it is mandatory to adopt a multiconfigurational approach (i.e., to consider more than one configuration per wavepacket). Using more than one configuration allows to represent correctly the splitting of the wavepacket into different pathways, for instance those leading to distinct photodissociation products. If enough configurations are added, the numerical time-dependent wavefunction converges to the exact solution. In the standard version of MCTDH, the SPFs are expanded on a time-independent basis set of one-dimensional functions with time-dependent coefficients. Each SPF is therefore a contraction of the time-independent basis, suitable to represent the wavepacket: the number of SPFs needed to reach convergence is then expected to be small, at least if compared with the number of time-independent basis functions.

The equations of motions for the coefficients $A_{I,k}$ and the SPFs are obtained using the Dirac–Frenkel time-dependent variational principle

$$\left\langle \delta\Psi \left| \mathrm{i}\hbar\frac{\partial}{\partial t} - \hat{H} \right| \Psi \right\rangle = 0 \tag{5.94}$$

where $\delta\Psi$ is an infinitesimal variation of the wavefunction, obtained by changing the parameters it contains (i.e., the coefficients $A_{I,k}$ and those determining the SPFs, in the present case). The resulting equation of motions are complex, but their number is much smaller if compared to the set of equations obtained by using directly the time-independent basis set. We sketch here a derivation of the time-dependent variational principle (5.94), following Raab [20]. We assume that the wavefunction Ψ has a given analytic form and depends on a set of parameters, collected in the vector $\mathbf{a}$. The time derivative of Ψ is then

$$\dot{\Psi} = \sum_j D_j(\mathbf{a})\dot{a}_j \qquad \text{with} \qquad D_j = \frac{\partial \Psi}{\partial a_j} \tag{5.95}$$

For given values $\mathbf{a}$ of the parameters, let us consider the vector space $M(\mathbf{a})$, containing the functions $\sum_j D_j(\mathbf{a})b_j$. In practice, $M(\mathbf{a})$ is a subspace of the Hilbert space to which Ψ belongs, collecting the variations $\delta\Psi$ that are allowed by the assumed analytic form of Ψ. Then, we define an approximate solution of the TDSE by requesting the norm $||\dot{\Psi} - \hat{A}\Psi||$ to be minimum (here we have set $\hat{A} = \hat{H}/\mathrm{i}\hbar$ for simplicity of notation). Assuming the $M(\mathbf{a})$ subspace to be closed, the projection theorem [21] warrants that there is in $M(\mathbf{a})$ only one vector $\dot{\Psi}$ minimizing the distance with $\hat{A}\Psi(\mathbf{a})$, which is obtained by setting $b_j = \dot{a}_j$, and that, for such a vector, $\dot{\Psi} - \hat{A}\Psi$ is orthogonal to $M(\mathbf{a})$. In other words, since $\delta\Psi \in M(\mathbf{a})$, we have $\left\langle \delta\Psi \middle| \dot{\Psi} - \hat{A}\Psi \right\rangle = 0$, which corresponds to Eq. (5.94).

Several variants of the MCTDH method are available [22–24] in which the SPFs are expressed in terms of nonspreading and traveling Gaussian wavepackets

$$\xi_{I,\alpha} = \left(\frac{2a_{I,\alpha}}{\pi}\right)^{1/4} \exp\left[-a_{I,\alpha}(Q_\alpha - \bar{Q}_{I,\alpha})^2 + \mathrm{i}\bar{P}_{I,\alpha}(Q_\alpha - \bar{Q}_{I,\alpha})/\hbar\right] . \tag{5.96}$$

Here $\bar{Q}_{I,\alpha}(t)$ and $\bar{P}_{I,\alpha}(t)$ represent the time-dependent "central" values of the coordinate Q_α and its associated momentum. The advantage in doing this is twofold. First, the expansion in a fixed basis set may become very expensive for large amplitude motions, and this is very effectively avoided resorting to the traveling Gaussians. Moreover, some locality is introduced in the configurations (in fact, each Φ_I is a product of frozen Gaussians peaking at the center $\bar{\mathbf{Q}}_I(t)$). This can be exploited to define approximated on-the-fly strategies. To cite only one example, in the Full Multiple Spawning (FMS) method [25] the configurations centers $\bar{\mathbf{Q}}_I(t)$ and momenta $\bar{\mathbf{P}}_I(t)$ are evolved in time according to classical mechanics, in agreement with Ehrenfest theorem (see Sect. 4.2). The electronic adiabatic basis is considered, and the matrix elements of $U_k(\mathbf{Q})$ and $\hat{V}_{kl}^{BO}$ (see Sect. 2.3) in the configurations, needed for the time evolution of the coefficients $A_{I,k}$, are computed in an approximated way using only local quantities. For example, a first-order approximation for the matrix elements of $U_k(\mathbf{Q})$ is

$$\langle \Phi_I | U_k | \Phi_J \rangle \simeq \langle \Phi_I | \Phi_J \rangle \, U_k(\bar{\mathbf{Q}}_{IJ}) \tag{5.97}$$

and similarly for $\hat{V}_{kl}^{BO}$. Here $\bar{\mathbf{Q}}_{IJ}$ is the centroid of the product $\Phi_I(\mathbf{Q})\Phi_J(\mathbf{Q})$. In this way, the full-time evolution from time t to $t + \Delta t$ only requires the evaluation of the adiabatic energies, their gradients, and the nonadiabatic couplings in the centers $\bar{\mathbf{Q}}_I(t)$ and centroids $\bar{\mathbf{Q}}_{IJ}(t)$. An FMS calculation is normally started with one configuration associated to a given electronic state k. Then, more configurations are added ("spawned") during the time evolution to describe the population transfer to other electronic states or to classically forbidden regions on U_k (tunneling).

5.5.2 Nonadiabatic Classical Trajectories

Many different approaches have been developed in this context; here we focus on the simplest one, in which the nuclear motion is described by a classical trajectory $\mathbf{Q}(t)$, while the electronic wavefunction $\Psi_{el}(\mathbf{r}, t; \mathbf{Q}(t))$ is evolved according to the TDSE (5.21). To reproduce approximately the quantum wavepacket dynamics, a swarm of many trajectories is run, each trajectory being independent of the others. Proceeding as in Sect. 5.3, the Ψ_{el} is expanded in terms of the adiabatic basis functions φ_k, obtaining Eq. (5.24) for the time evolution of the expansion coefficients $a_k(t)$, which can be recast in the equivalent form

$$\dot{\rho}_{kl} = -\mathrm{i}\omega_{kl}\rho_{kl} + \sum_j (\rho_{kj} G_{jl} - \rho_{jl} G_{kj}) \tag{5.98}$$

where $\omega_{kl} = (U_k - U_l)/\hbar$ and $G_{kl} = \langle \varphi_k \, | \dot{\varphi}_l \rangle = \mathbf{g}_{kl} \cdot \dot{\mathbf{Q}}$. Moreover

$$\rho_{kl} = a_k a_l^* \mathrm{e}^{-\mathrm{i}(\gamma_k - \gamma_l)} \tag{5.99}$$

is the electronic density matrix, including the dynamical phase factors of Eq. (5.22). Note that $\rho_{kk}(t) = |a_k|^2$ represents the probability of state k for the given trajectory.

The nuclear trajectory $\mathbf{Q}(t)$ is obtained by integrating the Newton equations of motion. There are two main algorithms according to the form assumed for the potential energy $V(\mathbf{Q})$ driving the nuclear motion. The Ehrenfest or "mean-field" approach is characterized by the following expression

$$V(\mathbf{Q}) = \left\langle \Psi_{el} \left| \hat{H}_{el} \right| \Psi_{el} \right\rangle = \sum_k |a_k|^2 \, U_k \ . \tag{5.100}$$

The forces acting on the nuclei are obtained by requiring the conservation of the total energy $E = \sum_\alpha M_\alpha \dot{Q}_\alpha^2/2 + V(\mathbf{Q})$ (i.e., by setting $\mathrm{d}E/\mathrm{d}t = 0$). Since the nuclear trajectory is determined by an averaged potential, the Ehrenfest method is expected to work correctly in surface crossing situations, but it may evidently give rise to artifacts when the electronic states are well separated in energy.

An alternative strategy with respect to mean-field is adopted in the "Surface Hopping" method [17, 26, 27], where the nuclei always move on the PES of a given state k (the "current" state), i.e., $V(\mathbf{Q}) = U_k(\mathbf{Q})$. During the time evolution, the current state can suddenly change from k to l (an event called a "hop") according to nonadiabatic transition probabilities that depend on how the state probabilities ρ_{ll} change in time. The surface hopping method was proposed and initially developed by Tully [28], to whom is due the most widely used algorithm for the evaluation of transition probabilities, called "fewest switches." In particular, it is assumed that the time evolution of the probability $\rho_{kk}(t)$ is given by a master equation

$$\dot{\rho}_{kk}(t) = \sum_{l \neq k} (\rho_{ll} W_{lk} - \rho_{kk} W_{kl}) \tag{5.101}$$

where the positive quantity W_{lk} represents the transition rate from state l to state k. From Eq. (5.98) we have $\dot{\rho}_{kk}(t) = -2 \sum_{l \neq k} \mathrm{Re}\{\rho_{lk} G_{kl}\}$, which can be put in the above form by defining the transition rates in this way

$$W_{kl} = \frac{\max\{0, B_{kl}\}}{\rho_{kk}} \qquad W_{lk} = \frac{\max\{0, -B_{kl}\}}{\rho_{ll}} \tag{5.102}$$

where

$$B_{kl} = 2\mathrm{Re}\{\rho_{lk} G_{kl}\} \, . \tag{5.103}$$

Therefore, the transition probability $T_{k \to l}$ from the current state k to l in the time interval Δt is

$$T_{k \to l} = \frac{\int_t^{t+\Delta t} \rho_{kk} W_{kl} \mathrm{d}t}{\rho_{kk}(t)} \, . \tag{5.104}$$

With this definition of $T_{k \to l}$ the hops are performed only if there is a net flux of probability from state k to another state in the time interval Δt considered: it is for that reason that the algorithm is called "fewest switches." Of course, $T_{l \to k}$ is just disregarded: if k is the current state, the trajectory cannot hop from l to k. In practice, a surface hopping calculation follows this scheme:

1. Many trajectories are run. The starting conditions (i.e., the initial nuclear coordinates $\mathbf{Q}$ and velocities $\dot{\mathbf{Q}}$) are sampled from a suitable distribution.
2. For each trajectory, the time evolution from t to $t + \Delta t$ is performed integrating numerically the Newton equations of motion for the nuclei on the current state PES U_k and Eq. (5.24) for the electronic wavefunction Ψ_{el}. The transition probability $T_{k \to l}$ is evaluated and used to decide, according to a stochastic algorithm, whether to hop from state k to another state l. If the hop occurs, l becomes the current state and the nuclear trajectory starts evolving on the PES U_l.
3. After a hop from k to l, the velocities of the nuclei are rescaled to compensate for the sudden variation $U_l - U_k$ in the potential energy, so enforcing energy conservation along the trajectory. In the case of an upward hop ($U_l > U_k$), if $U_l - U_k$ is larger than the current nuclear kinetic energy, no adjustment of the velocities is able to ensure energy conservation. In that case, the hop is rejected.
4. Time-dependent or final properties are computed by averaging over the full swarm of trajectories. To this aim, only the current state of each trajectory is considered. For example, the electronic contribution to the energy is given by the current state PES, and the population of a given electronic state l is the fraction of trajectories $\Pi_l(t)$ that are running on that state.

At variance with the mean-field approach, the surface hopping method depends on the representation used (diabatic or adiabatic) and works best if the electronic wavefunction Ψ_{el} is expanded in terms of the adiabatic functions, as assumed here.

In fact, the nuclei are expected to follow the (uniquely determined) adiabatic PESs rather than the diabatic ones, at least far from strong interaction regions (curve or surface crossings). Moreover, it is evident that the picture of sudden hops is physically sound only if the interaction between electronic states is highly localized in space, as is the case for the adiabatic representation (see Fig. 5.1). Otherwise, the mean-field approach would be better suited.

One of the most serious drawbacks in mixed quantum–classical methods like surface hopping or mean-field is the lack of "quantum decoherence". Let us consider the full quantum expression for the electronic density matrix

$$\rho_{kl}^{(q)}(\mathbf{Q}) = \langle \varphi_k \, | \Psi \rangle \, \langle \Psi \, | \varphi_l \rangle = \Theta_k(\mathbf{Q}) \Theta_l^*(\mathbf{Q}) \tag{5.105}$$

where we have used the Born–Huang expansion of Eq. (2.77) for the wavefunction Ψ, and the integration is performed on the electronic coordinates. The superscript q is used to distinguish the above full quantum expression from the semiclassical one of Eq. (5.99). As the wavepackets $\Theta_k(\mathbf{Q})$ and $\Theta_l(\mathbf{Q})$ propagate on the two different PESs U_k and U_l, they evolve toward distinct regions of the phase space, so reducing progressively the interference between them, which is what we call quantum decoherence. In fact, if the two wavepackets are localized far from each other in the $\mathbf{Q}$ coordinates space, $\rho_{kl}^{(q)}$ itself tends to vanish, and with it all coupling matrix elements. If instead $\Theta_k(\mathbf{Q})$ and $\Theta_l(\mathbf{Q})$ still overlap in the $\mathbf{Q}$ space, but are well separated in the momentum space (one is fast and the other is slow or they travel in different directions), the matrix elements of nonadiabatic operators or other couplings will also vanish. In both cases no population transfer will occur any more between them. Even if some coherence remains ($\rho_{kl}^{(q)} \neq 0$), it is important to realize that the phases acquired by the wavepackets along different pathways affect their interference and any further population transfer.

The semiclassical electronic density matrix of Eq. (5.99) behaves in a very different way: for a given trajectory, ρ_{kl} vanishes only if (at least) one of the two coefficients a_k and a_l is zero. In fact, consider, for example, a trajectory roaming through an interaction region where some population transfer takes place. Because the same point of the phase space represents the system in all the electronic states, no decoherence occurs. All the couplings (nonadiabatic, spin–orbit, etc.) will remain effective. Even wandering for a long time in regions where the couplings are negligible would not eliminate the coherences ρ_{kl} (see Eq. (5.98)), so if the trajectory enters again an interaction region it can give place to unphysical interference effects.

Mean-field methods present the additional drawback that all the electronic states contribute to the calculation of the observables, such as quantum yields or transient spectra, but the nuclear trajectories are driven by the average potential. As a result, the trajectories in general do not conform to each potential energy surface and can evolve in quite unphysical ways. Considering surface hopping, the quantum decoherence would be achieved if the electronic wavefunction collapsed smoothly on the current state k, i.e., if in time $a_k \to 1$ and $a_l \to 0$ for $l \neq k$. Since this collapse is not ensured by Eq. (5.98), ad hoc corrections have been introduced to force it [26, 27, 29]. Overall,

apart from cases where interference or tunneling effects play a major role, usually the surface hopping method (with corrections for decoherence) describes correctly the ultrafast nonadiabatic dynamics of molecular systems. Slower processes are more difficult to reproduce because of other drawbacks, in part analyzed in Chap. 4.

Problems

5.1 Consider the ionic/neutral avoided crossing in NaCl (see Fig. 5.1). Evaluate, considering Na and Cl atoms at room temperature ($T = 300$ K), the probability P_{adia} to stay on the neutral state when the avoided crossing is gone through, using the Landau–Zener formula. Use the data given in Sect. 5.1 for H_{12} and F.

5.2 Consider a collision between the two ions Na^+ and Cl^-. Evaluate the probability to have, after the collision, Na^+ and Cl^-. As in the previous problem, use the data given in Sect. 5.1 and neglect any thermal contribution to the kinetic energy in evaluating the nuclear velocity. Note that in a collision the molecule goes twice through the avoided crossing region.

5.3 Find the transformation of the two diabatic states $|\eta_1\rangle$ and $|\eta_2\rangle$ which makes orthogonal the vectors $\mathbf{q}$ and $\mathbf{h}$ of Eq. (5.36). Consider a real Hamiltonian.

5.4 For a system with only two electronic states, express the second derivative couplings $t_{ij}^{(\alpha)}$ $(i, j = 1, 2)$ as functions of $g_{12}^{(\alpha)}$, assuming the adiabatic functions φ_1 and φ_2 to be real-valued. Use this result to find an explicit expression for $\mathbf{t}_{12}$ (i) for the Landau–Zener model and (ii) close to a conical intersection (use Eq. (5.42), considering only the two coordinates x and y, and assuming $q = h$). In the latter case, which kind of singularity have at the conical intersection U_1 and the "corrected" PES U_1' of equation (2.65)?

5.5 Consider a system with two electronic states and two nuclear coordinates x and y, with the following diabatic Hamiltonian

$$\mathbf{H}_{el} = \begin{pmatrix} x^2 & xy \\ xy & y^2 \end{pmatrix} .$$

The two adiabatic PES U_1 and U_2 are degenerate in $(x, y) = (0, 0)$, which is not a conical intersection point. The above Hamiltonian could be appropriate, for example, in a Renner–Teller context. Show that the geometric phase vanishes for any closed path, containing or not the degeneracy point.

References

1. Persico, M.: Electronic diabatic states: definition, computation and application. In: Schleyer, R., Allinger, N. L., Clark, T., Gasteiger, J., Kollman, P.A., Schaefer III, H.F., Schreiner, P.R. (eds.) The Encyclopedia of Computational Chemistry, vol. 2, pp. 852–860. Wiley, Chichester (1998)

2. Cederbaum, L.S.: Born-Oppenheimer approximation and beyond. In: Domcke, W., Yarkony, D.R., Köppel, H. (eds.) Conical Intersections. Electronic Structure, Dynamics & Spectroscopy. World Scientific, Singapore (2004)
3. Köppel, H.: Diabatic representation: methods for the construction of diabatic electronic states. In: Domcke, W., Yarkony, D. R., Köppel, H. (eds.) Conical Intersections. Electronic Structure, Dynamics & Spectroscopy. World Scientific, Singapore (2004)
4. Mead, C.A., Truhlar, D.G.: Conditions for the definition of a strictly diabatic electronic basis for molecular systems. J. Chem. Phys. **77**, 6090–6098 (1982)
5. Eisfeld, W., Vieuxmaire, O., Viel, A.: Full dimensional diabatic potential energy surfaces including dissociation: the $^2E''$ state of NO_3. J. Chem. Phys. **140**, 224109 (2014)
6. Nikitin, E.E.: Nonadiabatic transitions: what we learned from old masters and how much we owe them. Annu. Rev. Phys. Chem. **50**, 1–21 (1999)
7. Nakamura, H.: Nonadiabatic Transition. Concepts, Basic Theories and Applications. World Scientific, Singapore (2012)
8. Yarkony, D.R.: Conical intersections: their description and consequences. In: Domcke, W., Yarkony, D. R., Köppel, H. (eds.) Conical Intersections. Electronic Structure, Dynamics & Spectroscopy. World Scientific, Singapore (2004)
9. Granucci, G., Persico, M., Spighi, G.: Surface hopping trajectory simulations with spin-orbit and dynamical couplings. J. Chem. Phys. **137**, 22A501/1-9 (2012)
10. Sakurai, J.J.: Modern Quantum Mechanics. Addison-Wesley, Reading (1994)
11. Mead, C.A.: The geometric phase in molecular systems. Rev. Mod. Phys. **61**, 51–85 (1984)
12. Berry, M.V.: Quantal phase factors accompanying adiabatic changes. Proc. R. Soc. Lond. A **392**, 45–57 (1984)
13. Child, M.S.: Early perspectives on geometric phase. Adv. Chem. Phys. **124**, 1–38 (2002)
14. Longuet-Higgins, H.C.: Some recent developments in the theory of molecular energy levels. Adv. Spectrosc. **2**, 429–472 (1961)
15. Jahn, H.A., Teller, E.: Stability of polyatomic molecules in degenerate electronic states. I–Orbital degeneracy. Proc. R. Soc. Lond. A **161**, 220-235 (1937)
16. Merzbacher, E.: Quantum Mechanics. Wiley, New York (1998)
17. Persico, M., Granucci, G.: An overview of nonadiabatic dynamics simulations methods, with focus on the direct approach versus the fitting of potential energy surfaces. Theor. Chem. Acc. **133**, 1526 (2014)
18. Tavernelli, I.: Nonadiabatic molecular dynamics simulations: synergies between theory and experiments. Acc. Chem. Res. **48**, 792–800 (2015)
19. Meyer, H.D., Gatti, F., Worth, G.A.: Multidimensional Quantum Dynamics: MCTDH Theory and Applications. Wiley-VCH, Weinheim (2009)
20. Raab, A.: On the Dirac-Frenkel/McLachlan variational principle. Chem. Phys. Lett. **319**, 674–678 (2000)
21. Reed, M., Simon, B.: Methods of Modern Mathematical Physics. I: Functional Analysis. Academic Press, San Diego (1980)
22. Lasorne, B., Worth, G.A., Robb, M.A.: Excited-state dynamics. WIREs Comput. Mol. Sci. **1**, 460–475 (2011)
23. Römer, S., Ruckenbauer, M., Burghardt, I.: Gaussian-based multiconfiguration time-dependent Hartree: a two-layer approach. I. Theory. J. Chem. Phys. **138**, 064106 (2013)
24. Richings, G.W., Polyak, I., Spinlove, K.E., Worth, G.A., Burghardt, I., Lasorne, B.: Quantum dynamics simulations using Gaussian wavepackets: the vMCG method. Int. Rev. Phys. Chem. **34**, 269–308 (2015)
25. Ben-Nun, M., Quenneville, J., Martínez, T.J.: Ab initio multiple spawning: photochemistry from first principles quantum molecular dynamics. J. Phys. Chem. A **104**, 5161–5175 (2000)
26. Wang, L., Akimov, A., Prezhdo, O.V.: Recent progress in surface hopping: 2011–2015. J. Chem. Phys. Lett. **7**, 2100–2112 (2016)
27. Subotnik, J.E., Jain, A., Landry, B., Petit, A., Ouyang, W., Bellonzi, N.: Understanding the surface hopping view of electronic transitions and decoherence. Annu. Rev. Phys. Chem. **67**, 387–417 (2016)

28. Tully, J.C.: Molecular dynamics with electronic transitions. J. Chem. Phys. **93**, 1061–1071 (1990)
29. Granucci, G., Persico, M., Zoccante, A.: Including quantum decoherence in surface hopping. J. Chem. Phys. **133**, 134111/1-9 (2010)

Chapter 6
Charge and Energy Transfer Processes

Abstract In this chapter we shall present the peculiar features of charge and excitation energy transfer processes (CT and ET) that are of basic importance in photosynthesis, photovoltaics, and other areas of biochemistry and technology. The migration of charge or excitation energy between distinct chromophores implies a dramatic change in the electronic wavefunction, so the general nonadiabatic theory we have already discussed also applies to these processes. However, some peculiar features distinguish charge and energy transfer from other nonadiabatic processes. If the two chromophores are placed in two molecules free to move in gas or liquid phase, the transition can only take place during a collision or encounter, so the kinetics of bimolecular processes plays an essential role. However, just because their interaction is a basic requirement for the process to occur, in structured biological or artificial photosystems the single units are fixed at suitable relative positions and orientations. In typical situations, such arrangements also determine easily discernable spectral features. Whenever the interaction between the involved chromophores is not too large, the initial and final electronic states of the CT or ET process constitute a physically sound diabatic representation, which allows to analyze theoretically the main features of the dynamics.

Keywords Charge transfer · Energy transfer · Quenching · Sensitization
Exciton coupling

6.1 Gas-Phase Collisions

The most relevant bimolecular processes in photochemistry are reactions, excitation energy transfers (ET), and charge transfers (CT). For a bimolecular event to occur, the two partners must get close enough; i.e., we need what is called a collision in gas phase or an encounter in liquid phase.

In gas phase, we can take as reference a system made of rigid spheres. The kinetic theory of gases provides the number of collisions per unit time and unit volume between identical spheres:

$$N_{coll} = 8 \left(\frac{\pi K_B T}{M_X} \right)^{1/2} R_X^2 \, C_X^2 \tag{6.1}$$

M. Persico and G. Granucci, *Photochemistry*, Theoretical Chemistry
and Computational Modelling, https://doi.org/10.1007/978-3-319-89972-5_6

where R_X, M_X, and C_X are the radius, mass, and concentration (number density) of the spheres. In a mixture, the number of collisions between spheres of the X and Y types is

$$N_{coll} = \left(\frac{8\pi K_B T}{\mu_{XY}}\right)^{1/2} R_{XY}^2 \; C_X \; C_Y \tag{6.2}$$

where $\mu_{XY} = M_X M_Y/(M_X + M_Y)$ and $R_{XY} = R_X + R_Y$. In general, the rate of a bimolecular process (number of events per unit volume and unit time) can be written as

$$V_{bim} = K \; C_X \; C_Y \tag{6.3}$$

$$K = \left(\frac{8K_B T}{\pi \mu_{XY}}\right)^{1/2} \sigma_{bim} \; (1 + \delta_{XY})^{-1} \; / \; \mathrm{s^{-1} molc^{-1} m^3} \tag{6.4}$$

or, if the concentrations are expressed as molarities

$$K = 1000 \; N_A \left(\frac{8K_B T}{\pi \mu_{XY}}\right)^{1/2} \sigma_{bim} \; (1 + \delta_{XY})^{-1} \; / \; \mathrm{s^{-1} mol^{-1} L} \; . \tag{6.5}$$

Here N_A is Avogadro's number and 1000 is the conversion factor from m^3 to liters. The factor $(1 + \delta_{XY})^{-1}$ takes into account the fact that the colliding pairs for $X \equiv Y$ are half than in the case $X \neq Y$. The quantity σ_{bim} (a surface area) is called the cross section of the bimolecular process. For the collision of rigid spheres, $\sigma_{bim} = \pi(R_X + R_Y)^2$ is a merely geometrical parameter. Its meaning is that the two spheres collide if their centers try to get nearer than the sum of the radii, which is like aiming at a round target with radius $R_X + R_Y$. For real molecules, the cross section depends on the process we are interested in and on the properties of the quantum states of the colliding partners. The cross sections of low probability events are much smaller than the size of the two molecules would imply. A common example is offered by activated processes that can only occur when the kinetic energy in the center of mass system is larger than the activation barrier E^*. This fact is basically taken into account by the Arrhenius factor $\exp(-E^*/K_B T)$ that appears in the expression of the reaction cross sections. The need for particular reciprocal orientations between the colliding partners and the low probability of certain quantum transitions may also concur in reducing the cross section.

Rotational and translational energy transfers take place practically every time two molecules collide. Transitions that change the vibrational energy of one or both partners (transfer of vibrational energy or conversion of vibrational into rotational and translational energies, or vice versa) are normally less probable, because they involve transitions between well-separated quantum levels. The separation of the vibrational motion from the other ones is most effective when only few modes of high frequency are present: for instance, the vibrational thermalization of N_2 in He

is estimated to be 10^7 times slower than the rotational one. In less extreme cases, however, collisions thermally equilibrate all kinds of nuclear motion within $\approx 10^{-8}$ s at standard temperature and pressure.

6.2 Encounters in Solution

The diffusion of a solute in a liquid is slower than that of a component in a gas mixture. On the other hand, when two solute molecules are brought in contact, they normally interact for a longer time than two collision partners: in this sense, an encounter in solution can be much more effective than a gas-phase collision in causing an energy or charge transfer process. Both the rate of encounters and the probability P_{bim} that a given bimolecular event takes place at each encounter concur in determining the rate of the process.

If we assume diffusion to obey Fick's law, the net number of molecules that cross a surface S per unit time is

$$\Phi = -D \frac{\mathrm{d}N}{\mathrm{d}z} S \tag{6.6}$$

where N is the concentration (molecules/m^3), z is a coordinate perpendicular to the surface, and D (m^2/s) is the diffusion coefficient, which depends on the properties of the solute and of the solvent, and on temperature. This law is valid in the absence of forces pushing the molecules in a given direction. We first focus our attention on one molecule Y and investigate how many molecules X per unit time interact with it. Since both X and Y diffuse, the relevant D coefficient in our case is the sum of their diffusion coefficients: $D = D_\mathrm{X} + D_\mathrm{Y}$. If we take a spherical surface of radius R and center in Y, the net flux of X molecules entering the sphere is

$$\Phi = 4\pi D R^2 \frac{\mathrm{d}N_\mathrm{X}}{\mathrm{d}R} . \tag{6.7}$$

Here we are assuming that no potential term attracts X toward Y or repels it, until they get to a sufficiently small "interaction distance" R_{int}. This is not the case with long-range electrostatic forces, for instance when dealing with ions (see the Debye–Huckel theory of electrolytes). Φ is the difference between the ingoing flux Φ_{in} and the outgoing one Φ_{out}: $\Phi = \Phi_{in} - \Phi_{out}$. At $R > R_{int}$, the steady-state concentration of X would be constant, unless a bimolecular process occurring at $R \leq R_{int}$ "annihilates" the X molecules: this sink creates a concentration gradient and a net flux. By "annihilates" we mean that the X molecules are identified by their chemical nature and quantum state, so they cease to exist if any reaction, CT or ET process, converts them into different products (other chemical species and/or different electronic states). The fate of the products is irrelevant to the discussion of the diffusion process (this statement implies the assumption that the products do not affect the diffusion of the reagents). If some X molecules can "survive" the encounter with Y

($P_{bim} < 1$), they will feed an outgoing flux Φ_{out}. The larger the Φ_{out} is, the smaller the net flux Φ and the gradient dN_X/dr. On the contrary, Φ_{in} is not affected by the bimolecular process. Φ cannot depend on R in a steady state, otherwise the number of X molecules in a spherical layer would change in time. Then, we can connect Φ to the asymptotic concentration of X, $N_X(\infty)$, by a simple integral:

$$\begin{aligned} N_X(\infty) &= N_X(R) + \int_R^\infty \frac{dN_X}{dR'}\, dR' = \\ &= N_X(R) + \frac{\Phi}{4\pi D} \int_R^\infty R'^{-2}\, dR' = N_X(R) + \frac{\Phi}{4\pi D R} \,. \end{aligned} \tag{6.8}$$

This equation holds for any R and P_{bim}, but if we take $P_{bim} = 1$ and $R = R_{int}$ it simplifies because within the interaction sphere ($R \le R_{int}$) the concentration $N_X(R)$ vanishes, so the term $N_X(R)$ disappears. Moreover, $P_{bim} = 1$ implies $\Phi_{out}(R_{int}) = 0$ and $\Phi_{in}(R_{int}) = \Phi$. So we get

$$\Phi_{in}(R_{int}) = 4\pi D\ R_{int}\ N_X(\infty) \,. \tag{6.9}$$

If the volume contained in the spheres of radius R_{int} centered on the Y molecules is negligible with respect to that of the whole solution, which is true at low concentrations, we can identify $N_X(\infty)$ with the bulk concentration of X. Then the number of encounters per unit time and per unit volume is

$$R_{enc} = 4\pi\ (D_X + D_Y)\ R_{int}\ N_{X,bulk}\ N_{Y,bulk} \,. \tag{6.10}$$

With $P_{bim} < 1$, Φ_{in} and R_{enc} remain the same, but $\Phi_{out}(R_{int}) = \Phi_{in}(R_{int})\ (1 - P_{bim})$, so $\Phi = \Phi_{in}(R_{int})\ P_{bim}$. By combining Eqs. (6.8) and (6.9) we get

$$N_X(R) = N_X(\infty) - \frac{\Phi_{in}(R_{int})\ P_{bim}}{4\pi D R} = N_X(\infty) \left[1 - \frac{P_{bim} R_{int}}{R}\right] . \tag{6.11}$$

In Fig. 6.1 we show the steady-state concentration of X in two cases, with $P_{bim} = 1$ and with $P_{bim} < 1$.

The rate of the bimolecular process is $R_{enc}\ P_{bim}$. Using molarities for the concentrations:

$$-\frac{d[X]}{dt} = K\ [X]\ [Y] \tag{6.12}$$

with

$$K = 4000\ \pi\ N_A\ (D_X + D_Y)\ R_{int}\ P_{bim} \,. \tag{6.13}$$

The diffusion coefficients depend on the molecular interactions between solvent molecules and with the solutes. They can be approximately parameterized with reference to the solvent viscosity and the solute size. The Stokes–Einstein relationship is valid for spherical particles of radius R:

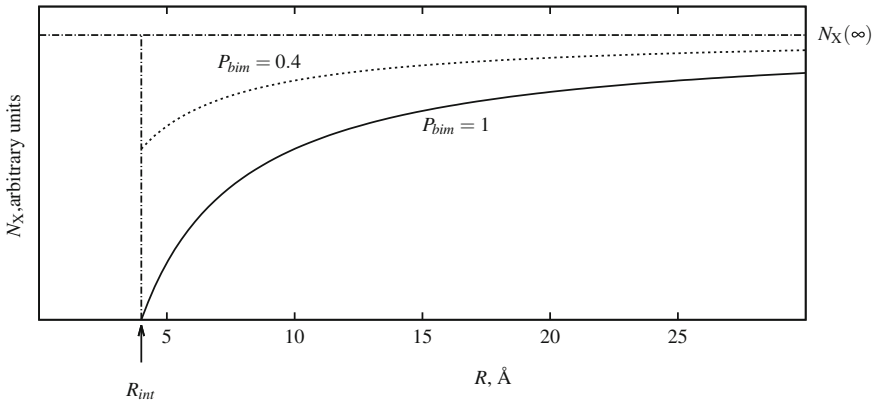

Fig. 6.1 Concentration of the solute X as a function of its distance from Y

Table 6.1 Viscosity of some solvents at 20° C (Pa·s)

Water	0.0010
Organic solvents, not highly structured	$0.0002 \div 0.0020$
Ethylene glycol, $CH_2OH - CH_2OH$	0.0200
Glycerol, $CH_2OH - CHOH - CH_2OH$	1.490

$$D = \frac{K_B T}{6\pi \eta R} \tag{6.14}$$

where η is the viscosity, expressed in Pa·s ($\equiv$ kg $\cdot$ m^{-1}s^{-1}). Then:

$$K = \frac{2000\ R_{gas} T\ R_{int}(R_X + R_Y)}{3\ \eta\ R_X R_Y}\ P_{bim}\ . \tag{6.15}$$

If the solutes are approximately spherical and $R_{int} \simeq (R_X + R_Y)$, we see that the rate constant does not depend too much on the size of the solutes.

The viscosity decreases rapidly with temperature (for liquid water, it is 0.0013 Pa·s at 10° C and 0.00028 at 100° C). Moreover, it increases with the molecular size and with the degree of association of the solvent molecules, for instance with the number of intermolecular hydrogen bonds each molecule can form (see Table 6.1). In the most common solvents, we find $K/P_{bim} \approx 10^9 \div 10^{10}$ l $\cdot$ mol^{-1} $\cdot$ s^{-1}. When $P_{bim} \simeq 1$, we say that the kinetics of the process is "diffusion controlled."

6.3 Electronic Energy Transfers

When a collision in gas phase or an encounter in solution occurs, we can consider the system made up by the two molecules as one "supermolecule" and investigate its dynamics with the same tools we developed in the previous chapters for unimolecular processes. If the supermolecule splits again to yield the same molecules as before the collision/encounter or new ones, the quantum state of the products will depend on the transitions occurred during the interaction time. The supermolecule approach is then suitable to treat energy and charge transfer processes as electronic transitions between well-defined initial and final states. Note that, while the internal degrees of freedom of a molecule (vibrational and electronic) are not or only weakly coupled with the overall translation and rotation, for two interacting molecules the mutual translational and orientational coordinates become internal coordinates of the supermolecule that can exchange energy with the other degrees of freedom (see the discussion at the end of Sect. 6.1 concerning vibrational energy).

Starting from an electronically excited molecule X^*, two kinds of energy transfer processes can occur. In one, the species X^* goes back to the ground state because of the interaction with Y, and the latter, although normally accepting a certain amount of energy, remains in the electronic ground state:

$$X^* + Y \longrightarrow X + Y \, . \tag{6.16}$$

This is a mere quenching of X^*. If instead Y is promoted to an excited state, we talk about electronic excitation transfer or "sensitization":

$$X^* + Y \longrightarrow X + Y^* \, . \tag{6.17}$$

In both cases, as in other nonadiabatic processes, part of the initially available energy is converted into vibrational, rotational, and translational energy shared by the two partners and eventually lost to the medium as depicted in the two Jablonski diagrams of Fig. 6.2. For the excitation transfer to occur, the Y^* state must be lower in energy than X^* or at most slightly higher. In the latter case, Y and/or X^* must possess some extra vibrational energy, possibly supplied by the exciting photon or due to thermal fluctuations.

The nature of the processes (6.16) and (6.17) allows to define a set of diabatic electronic states based on the localization of the excitation and suitable to describe the energy transfer dynamics [1–4]. The initial state is

$$|\eta_i\rangle \equiv |\varphi_{X^*}\varphi_Y\rangle \tag{6.18}$$

where on the RHS we have antisymmetrized products of the wavefunctions representing X in the excited state and Y in the ground state. We are here assuming the orbitals of X and Y to be orthogonal, which is not compatible with perfect localization on either molecule (see Appendix E). An approximate localization of the φ

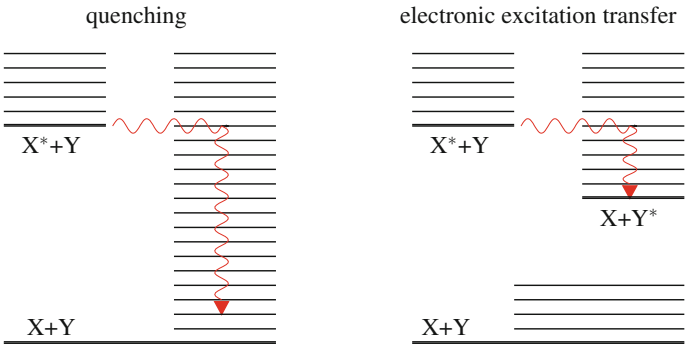

Fig. 6.2 Jablonski diagrams for energy transfer

states is sufficient for qualitative considerations, but small overlaps of nonorthogonal wavefunctions or the partial delocalization of the orthogonal ones can affect quantitative predictions. The final state for quenching is

$$\left|\eta_f\right\rangle \equiv |\varphi_X \varphi_Y\rangle \tag{6.19}$$

and for the electronic excitation transfer

$$\left|\eta_f\right\rangle \equiv |\varphi_X \varphi_{Y^*}\rangle \ . \tag{6.20}$$

The matrix element $H_{i,f} = \left\langle \eta_i \left| \hat{H}_{el} \right| \eta_f \right\rangle$ that determines the transition rate may vanish because the two states differ by symmetry or spin. Symmetry selection rules are fundamental for very simple processes such as atom–atom and atom–diatom collisions, where certain symmetry elements are necessarily present. For polyatomic molecules, which are free to approach each other with arbitrary mutual orientations, symmetry is less important, but in Sect. 6.4.4 we shall examine situations where the interacting molecules are constrained in fixed positions, often in symmetric patterns as in crystals.

Spin selection rules affect all electronic transitions. As we have seen in Sect. 2.4, the spin state of the system can change because of magnetic interactions (ISC), the spin–orbit coupling being usually the most important. In the absence of heavy atoms, ISC is a slow process and hardly occurs during bimolecular interactions. However, when dealing with spin multiplets, i.e., states with nonzero total spin, there exist combinations of the initial states and of the final ones that correspond to the same supermolecule spin. Then, the individual X and Y spins are allowed to change, without changing the spin of the whole system. Two spins S_X and S_Y can sum up as parallel vectors to yield the highest spin multiplet with $S_{X+Y} = S_X + S_Y$ or lower spin multiplets with S_{X+Y} decreased by 1, 2, etc., in $\hbar$ units, down to $S_{X+Y} = |S_X - S_Y|$. These rules, due to Wigner, define the allowed supermolecule spin states in the absence of ISC. The states up to $S_{X+Y} = 2$ are shown in Table 6.2 (note that we omit the cases with $S_X < S_Y$, not to repeat the same line with X and Y exchanged). A

Table 6.2 Spin state combinations that yield up to $S = 2$

molecule X	molecule Y	supermolecule X + Y
$S = 0$ (singlet)	$S = 0$ (singlet)	$S = 0$ (singlet)
$S = 0$ (singlet)	$S = 1/2$ (doublet)	$S = 1/2$ (doublet)
$S = 0$ (singlet)	$S = 1$ (triplet)	$S = 1$ (triplet)
$S = 0$ (singlet)	$S = 3/2$ (quadruplet)	$S = 3/2$ (quadruplet)
$S = 0$ (singlet)	$S = 2$ (quintuplet)	$S = 2$ (quintuplet)
$S = 1/2$ (doublet)	$S = 1/2$ (doublet)	$S = 0$ (singlet) or $S = 1$ (triplet)
$S = 1/2$ (doublet)	$S = 1$ (triplet)	$S = 1/2$ (doublet) or $S = 3/2$ (quadruplet)
$S = 1/2$ (doublet)	$S = 3/2$ (quadruplet)	$S = 1$ (triplet) or $S = 2$ (quintuplet)
$S = 1$ (triplet)	$S = 1$ (triplet)	S =0 (singlet), $S = 1$ (triplet) or $S = 2$ (quintuplet)

typical example in thermal chemistry is the formation of a bond between two radicals (two doublet states) that join to yield a singlet ground-state molecule (if the triplet state is formed, the interaction between the two radicals is substantially repulsive, see Fig. 2.6). In photochemistry, a molecule can dissociate starting from an excited singlet or triplet state, producing two fragments that are doublets (for instance, it has been shown that the photodissociation of the acetone molecule can follow both pathways [5]).

When the supermolecule splits again into X and Y, their spin states can differ from the initial ones. In fact, we see from Table 6.2 that the same spin state of X + Y can correspond to different combinations of states of X and Y. If no charge transfer occurs, the parity of the number of unpaired electrons is conserved, so X and Y cannot switch from integer to semi-integer spin or vice versa. Even with this additional limitation, we see that several kinds of energy transfer processes are possible:

- Quenching of a singlet excited state:

$$\mathrm{X}(S_1) + \mathrm{Y}(S_0) \longrightarrow \mathrm{X}(S_0) + \mathrm{Y}(S_0) \ . \tag{6.21}$$

- Quenching of a doublet excited state:

$$\mathrm{X}(D_1) + \mathrm{Y}(S_0) \longrightarrow \mathrm{X}(D_0) + \mathrm{Y}(S_0) \ . \tag{6.22}$$

- Excitation transfer within the singlet manifold:

$$\mathrm{X}(S_1) + \mathrm{Y}(S_0) \longrightarrow \mathrm{X}(S_0) + \mathrm{Y}(S_1) \ . \tag{6.23}$$

- Excitation transfer within the triplet manifold:

$$\mathrm{X}(T_1) + \mathrm{Y}(S_0) \longrightarrow \mathrm{X}(S_0) + \mathrm{Y}(T_1) \ . \tag{6.24}$$

This process is also called triplet sensitization and is exploited to populate the triplet state of a molecule Y that does not undergo ISC efficiently, by using a "sensitizer" X which has instead a high triplet yield (see Sect. 1.6.2).

- Triplet quenching by oxygen:

$$\mathrm{X}(T_1) + \mathrm{O}_2(^3\Sigma_g^-) \longrightarrow \mathrm{X}(S_0) + \mathrm{O}_2(^1\Delta_g, ^1\Sigma_g^+) \; . \tag{6.25}$$

The ground state of the oxygen molecule is a triplet, but there are two low-lying singlet states, $^1\Delta_g, ^1\Sigma_g^+$, so O_2 can accept energy from most organic molecules in their excited triplet states. Oxygen is therefore an efficient triplet quencher. The singlet oxygen state $^1\Delta_g$ is long-lived and cytotoxic.

- Triplet–triplet annihilation:

$$\mathrm{X}(T_1) + \mathrm{X}(T_1) \longrightarrow \mathrm{X}(S_1) + \mathrm{X}(S_0) \; . \tag{6.26}$$

This is an "energy pooling" process where the energy of two lower-lying triplets is used to populate a higher-lying singlet. The $\mathrm{X}(S_1)$ species may fluoresce, with a lifetime equal to half of that of the triplet [6, 7]. This kind of delayed fluorescence is labeled as "type P" because it was first studied in pyrene.

- Singlet fission:

$$\mathrm{X}(S_1) + \mathrm{X}(S_0) \longrightarrow \mathrm{X}(T_1) + \mathrm{X}(T_1) \; . \tag{6.27}$$

This process is the reverse of the previous one. A singlet with sufficiently high energy donates part of it to a neighboring molecule, so producing two molecules in the triplet state. This process may be used to improve photovoltaics yields, because it can exploit short wavelength photons to produce two electron/hole pairs instead of one.

Besides the interaction matrix element $H_{i,f} = \left\langle \eta_i \left| \hat{H}_{el} \right| \eta_f \right\rangle$, the cross section σ_{bim} and the probability P_{bim} for any of these processes also depend on how close to each other the potential energy surfaces of η_i and η_f can get, during the interaction of the two molecules. If the diabatic PESs do cross, giving place to adiabatically avoided crossings or conical intersections, the transition probability can be large, whereas two PESs that are well separated at all geometries make the radiationless transitions unlikely. For instance, electronic quenching by collisions with rare gas atoms has small cross sections because their interaction with most molecules is repulsive both for the ground and for the excited state and gives place to approximately parallel PESs. This is due to the closed shell configuration of the rare gas atoms and to their lack of low-lying antibonding orbitals that could mix with the molecular orbital hosting the excited electron. A much studied example are the alkali-rare gas interaction potentials, such as those originating from the ^2S and $^2P_{1/2,3/2}$ states of Na, with one electron in the $3s$ or $3p$ orbitals, and the ground state of Xe, as shown in Fig. 6.3 [8]. Rare gases are used as solid matrices or nanodroplets, as well as in gas phase, to cool the translational, rotational, and vibrational degrees of freedom of molecules, without quenching their electronic excitation.

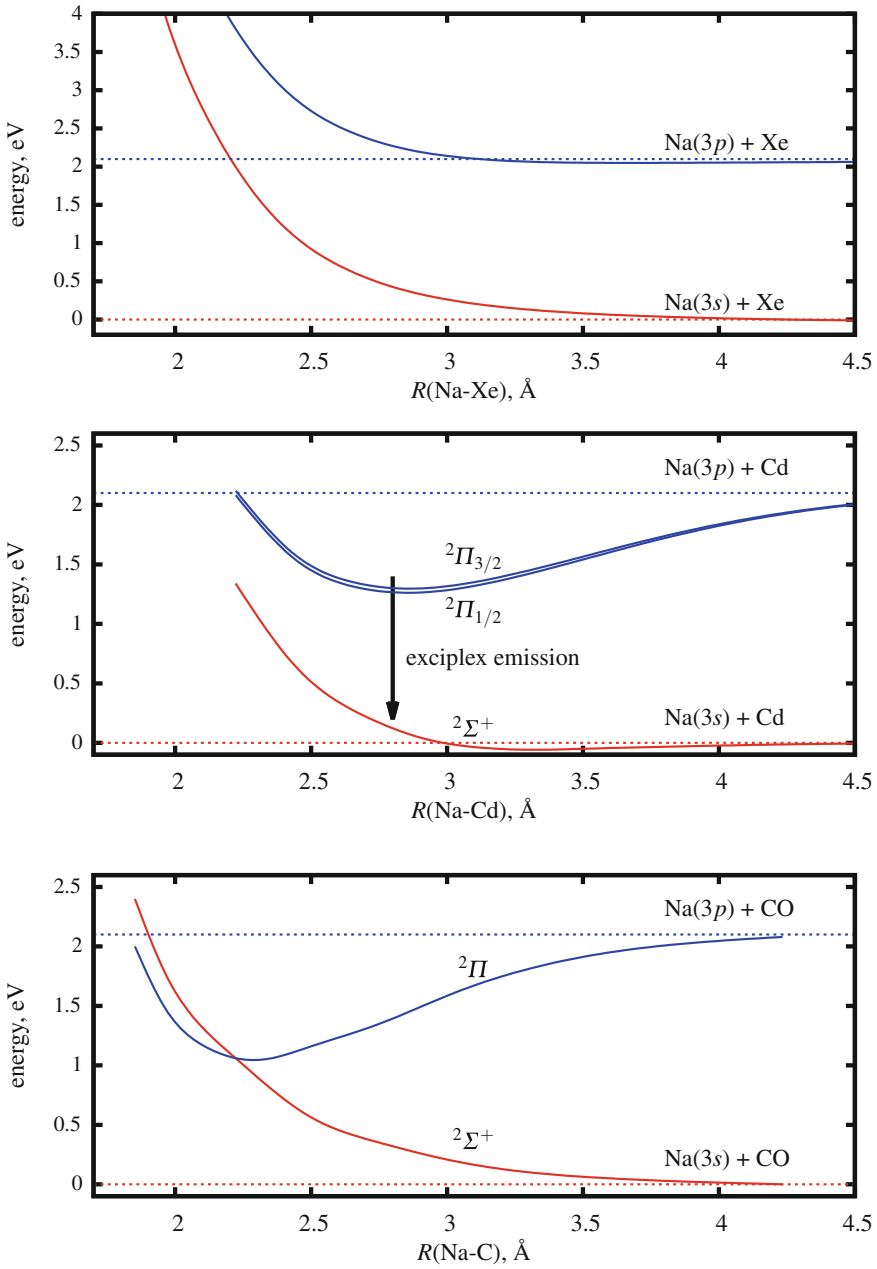

Fig. 6.3 Potential energy curves for the interaction of Na(^2S, $3s$) and Na(^2P, $3p$) with different collision partners. Upper panel: Na+Xe; middle panel: Na+Cd; lower panel: Na+CO, collinear approach

An attractive interaction is instead established between Na($3p$) and atoms with a smaller energy gap between occupied and virtual orbitals, such as Cd (see Fig. 6.3). The lowest potential energy curves in this case are those of $^2\Pi$ states, with a small energy difference due to spin–orbit coupling between the $^2\Pi_{3/2}$ and $^2\Pi_{1/2}$ states (parallel and antiparallel orientation of spin and orbital angular momenta, respectively) [9]. A system which is bound in an excited state but not in the ground state is called an exciplex or excimer. When the excited state is sufficiently long-lived, one can observe light emission at longer wavelengths with respect to the isolated excited species. Similarly, aromatic molecules in solution can form fluorescent excimers. For instance, at low concentrations, pyrene shows a fluorescence band with a clear vibrational structure between 370 and 430 nm, while by increasing the concentration one observes a structureless band between 420 and 550 nm, with $\lambda_{max} = 480$ nm, due to excimer formation.

If the interaction is strongly attractive in the excited state and repulsive in the ground state, the two potential energy curves tend to cross. Such is the case of Na approaching collinearly CO, because binding interactions are established between the electron of Na in a $3p$ orbital perpendicular to the CO axis and the empty π^* orbital of CO, as well as between the empty $3s$ orbital of Na and the lone pairs of CO. The charge transfer configuration Na^+CO^- also contributes to strengthen the attractive interaction in the excited state. On the contrary, in the Na ground state the $3s$ electron and the lone pairs of CO repel each other. In Fig. 6.3 we show the crossing of the $^2\Sigma^+$ and $^2\Pi$ curves for the collinear approach of Na and CO [10]. When considering bent geometries, the $^2\Sigma^+$ state becomes $^2A'$ and the $^2\Pi$ state originates a pair of $^2A'$ and a $^2A''$ states. The two $^2A'$ states therefore give place to a conical intersection, near which the exciplex switches very easily to the ground state and dissociates. The quenching of Na($2p$) by CO molecules is very efficient, with cross sections of the order of 20–50 Å^2, and the same happens with other molecules containing π bonds, such as nitrogen and ethylene.

6.4 Localized Excitations and Energy Transfer Mechanisms

We shall consider two subsystems X and Y, such as two molecules or two distinct chromophores in the same molecule. Each subsystem can be the seat of electronic excitation, but in the adiabatic eigenstates of the whole system the excitation may be delocalized, i.e., distributed over both centers. As already observed in the previous section, the localized description is a good starting point to describe energy transfer phenomena, especially when the initial and final states are definitely localized because of the physical separation of X and Y. The localized states provide a sound physical example of diabatic states, and their interaction matrix elements determine the transition cross sections or probabilities.

6.4.1 Group Functions

In this section we shall tackle the problem of defining localized excitations by introducing the concept of "group functions" with "strong orthogonality" conditions (see McWeeny [11], Sect. 14.1). The advantage is that the matrix elements of the Hamiltonian are given by simple formulas and can be related to properties of the X and Y subsystems, so leading to a better understanding of the energy transfer processes. The group functions are antisymmetric electronic wavefunctions $\Psi_{\mathrm{X},K}$ and $\Psi_{\mathrm{Y},L}$ for the X and Y subsystems, respectively. The space and spin coordinates of the n_X electrons of X will be called x_i and those of the n_Y electrons of Y, y_j. We build $\Psi_{\mathrm{X},K}$ and $\Psi_{\mathrm{Y},L}$ as CI expansions using a set of orthogonal MOs, each of them being localized on either the subsystem X or Y. Such MOs can be obtained for instance by HF or CASSCF calculations for the whole system, followed by a localization procedure based on rotations within each subset of doubly occupied, active or virtual orbitals. Because of the limitations imposed by the preservation of orthogonality, a complete localization will not be achieved unless X and Y are very far apart, but we assume it is possible to attribute each MO to either X or Y (see Appendix E). We define the subspaces S_X and S_Y, each spanned by all the Slater determinants of n_S electrons that only occupy MOs belonging to subsystem S. The $\Psi_{\mathrm{X},J}$ wavefunctions are built with determinants of only one of the two subspaces and therefore belong to either S_X or S_Y. Charge transfer configurations, with the numbers of electrons in X and Y different from n_X and n_Y, are therefore not included in our treatment. We require orthonormalization within each set of group functions:

$$\left\langle \Psi_{\mathrm{X},K} \left| \Psi_{\mathrm{X},K'} \right\rangle = \delta_{K,K'}, \qquad \left\langle \Psi_{\mathrm{Y},L} \left| \Psi_{\mathrm{Y},L'} \right\rangle = \delta_{L,L'} \right. . \tag{6.28}$$

We shall analyze the properties of states $|K, L\rangle$ of the whole system that are represented by antisymmetrized products of group functions $\hat{A}\ \Psi_{\mathrm{X},K}\Psi_{\mathrm{Y},L}$. We must therefore consider transpositions of electrons from $\Psi_{\mathrm{X},K}$ to $\Psi_{\mathrm{Y},L}$, which brings out the strong orthogonality property. This means that the product of two wavefunctions $\Psi_{\mathrm{X},K}$ and $\Psi_{\mathrm{Y},L}$ that happen to share at least one electron vanishes when integrated over the space coordinates of just that electron, because of the MOs orthogonality.

For instance

$$\int \Psi^*_{\mathrm{X},K}(x_1, x_2 \ldots x_{n_\mathrm{X}})\ \Psi_{\mathrm{Y},L}(x_1, y_2 \ldots y_{n_\mathrm{Y}})\ \mathrm{d}r_1^3 = 0 \tag{6.29}$$

(here r_1 stands for the space coordinates contained in x_1).

The electronic Hamiltonian can be partitioned into local (X and Y) terms and interaction terms of zero-, one-, and two-electron type:

$$\hat{H}_{el} = \hat{H}_\mathrm{X} + \hat{H}_\mathrm{Y} + \hat{H}_\mathrm{XY} \tag{6.30}$$

and

$$\hat{H}_\mathrm{XY} = V_{\mathrm{XY},nn} + \hat{H}_{\mathrm{XY},en} + \hat{H}_{\mathrm{YX},en} + \hat{H}_{\mathrm{XY},ee}\ . \tag{6.31}$$

$\hat{H}_{\mathrm{X}}$ and $\hat{H}_{\mathrm{Y}}$ are the electronic Hamiltonians of X and Y, respectively, including the respective nuclear repulsion terms. If α and β number the nuclei of X and Y, respectively:

$$V_{\mathrm{XY},nn} = \sum_{\alpha\in\mathrm{X}}\sum_{\beta\in\mathrm{Y}} \frac{Z_\alpha Z_\beta}{r_{\alpha\beta}} \tag{6.32}$$

$$\hat{H}_{\mathrm{XY},en} = -\sum_{i=1}^{n_{\mathrm{X}}}\sum_{\beta\in\mathrm{Y}} \frac{Z_\beta}{r_{\beta i}} \tag{6.33}$$

$$\hat{H}_{\mathrm{YX},en} = -\sum_{j=1}^{n_{\mathrm{Y}}}\sum_{\alpha\in\mathrm{X}} \frac{Z_\alpha}{r_{\alpha j}} \tag{6.34}$$

$$\hat{H}_{\mathrm{XY},ee} = \sum_{i=1}^{n_{\mathrm{X}}}\sum_{j=1}^{n_{\mathrm{Y}}} \frac{1}{r_{ij}} \tag{6.35}$$

(here and in the following we use atomic units).

The matrix elements between products of group functions can be worked out in the same way as the Slater rules (see McWeeny [11], Sect. 14.1). In our case, with only two factors, a general matrix element is

$$\begin{aligned}\left\langle K, L \left| \hat{H}_{el} \right| K', L' \right\rangle = V_{\mathrm{XY},nn}\, \delta_{K,K'}\, \delta_{L,L'} + \\ + \left\langle \Psi_{\mathrm{X},K} \left| \hat{H}_{\mathrm{X}} + \hat{H}_{\mathrm{XY},en} \right| \Psi_{\mathrm{X},K'} \right\rangle \delta_{L,L'} + \\ + \left\langle \Psi_{\mathrm{Y},L} \left| \hat{H}_{\mathrm{Y}} + \hat{H}_{\mathrm{YX},en} \right| \Psi_{\mathrm{Y},L'} \right\rangle \delta_{K,K'} + \\ + J_{\mathrm{XY},KK'LL'} - K_{\mathrm{XY},KK'LL'}\ .\end{aligned} \tag{6.36}$$

Here

$$\begin{aligned} J_{\mathrm{XY},KK'LL'} &= n_{\mathrm{X}} n_{\mathrm{Y}} \left\langle \Psi_{\mathrm{X},K}\Psi_{\mathrm{Y},L} \left| [r(x_1, y_1)]^{-1} \right| \Psi_{\mathrm{X},K'}\Psi_{\mathrm{Y},L'} \right\rangle \\ K_{\mathrm{XY},KK'LL'} &= n_{\mathrm{X}} n_{\mathrm{Y}} \left\langle \Psi_{\mathrm{X},K}\Psi_{\mathrm{Y},L} \left| [r(x_1, y_1)]^{-1}\ \hat{P}_{\mathrm{XY}} \right| \Psi_{\mathrm{X},K'}\Psi_{\mathrm{Y},L'} \right\rangle \end{aligned} \tag{6.37}$$

and $r(x_1, y_1)$ is the distance between the electrons with coordinates x_1 and y_1, while $\hat{P}_{\mathrm{XY}}$ is the exchange operator between the electrons x_1 and y_1.

We can choose the group functions to be eigenfunctions of $\hat{H}_{\mathrm{X}}$ within the subspace S_{X}, so that $\left\langle \Psi_{\mathrm{X},K} \left| \hat{H}_{\mathrm{X}} \right| \Psi_{\mathrm{X},K'} \right\rangle = E_{\mathrm{X},K}\delta_{K,K'}$. If X and Y do not interact, $E_{\mathrm{X},K}$ is the eigenenergy in the isolated X subsystem, but in general it will depend on the X − Y relationship because the S_{X} and S_{Y} subspaces do change according to how their orthogonality is implemented. Similarly, the matrix elements of $\hat{H}_{\mathrm{Y}}$ can be related to its eigenvalues $E_{\mathrm{Y},L}$. The matrix elements then simplify as shown in Eqs. (6.38) and (6.39). For the K, L state energy we have

$$\left\langle K, L \left| \hat{H}_{el} \right| K, L \right\rangle = E_{\mathrm{X},K} + E_{\mathrm{Y},L} + V_{\mathrm{XY},nn} + \left\langle \Psi_{\mathrm{X},K} \left| \hat{H}_{\mathrm{XY},en} \right| \Psi_{\mathrm{X},K} \right\rangle + \\ + \left\langle \Psi_{\mathrm{Y},L} \left| \hat{H}_{\mathrm{YX},en} \right| \Psi_{\mathrm{Y},L} \right\rangle + J_{\mathrm{XY},KKLL} - K_{\mathrm{XY},KKLL} \, . \tag{6.38}$$

When the electronic transition concerns one of the two subsystems, say X, the relevant off-diagonal matrix element is

$$\left\langle K, L \left| \hat{H}_{el} \right| K', L \right\rangle = \left\langle \Psi_{\mathrm{X},K} \left| \hat{H}_{\mathrm{XY},en} \right| \Psi_{\mathrm{X},K'} \right\rangle + J_{\mathrm{XY},KK'LL} - K_{\mathrm{XY},KK'LL} \, . \tag{6.39}$$

The only interactions that count concern electrons of X with nuclei and electrons of Y. This is the case of pure quenching, as in the processes (6.21) and (6.22) seen in the previous section.

In energy transfer processes where the electronic transition affects both subsystems, we only have two-electron terms:

$$\left\langle K, L \left| \hat{H}_{el} \right| K', L' \right\rangle = J_{\mathrm{XY},KK'LL'} - K_{\mathrm{XY},KK'LL'} \tag{6.40}$$

(this result holds even in the case the group functions are not eigenfunctions of $\hat{H}_{\mathrm{X}}$ and $\hat{H}_{\mathrm{Y}}$). Let us consider first the processes involving triplet states. We shall treat the important case of singlet-to-singlet energy transfer in the next section.

6.4.2 Triplet Sensitization and Singlet Fission

In triplet sensitization, process (6.24), $\Psi_{\mathrm{X},K}$ and $\Psi_{\mathrm{Y},L'}$ are triplets, while $\Psi_{\mathrm{X},K'}$ and $\Psi_{\mathrm{Y},L}$ are ground-state singlets, so $J_{\mathrm{XY},KK'LL'} = 0$ and only $K_{\mathrm{XY},KK'LL'}$ contributes to the interaction matrix element. In the $K_{\mathrm{XY},KK'LL'}$ integral the electron in x_1 appears in the $\Psi_{\mathrm{X},K}$ and $\Psi_{\mathrm{Y},L'}$ wavefunctions, while the electron in y_1 appears in $\Psi_{\mathrm{Y},L}$ and $\Psi_{\mathrm{X},K'}$: in both cases the wavefunctions are approximately localized on the two different subsystems, X and Y, so their products are everywhere small. As the distance between X and Y increases, the localization of MOs and wavefunctions becomes rapidly quite complete because the limitations due to the orthogonality requirement vanish, so the interaction between the initial and final states is only effective in the short range (see again Appendix E). A similar result is obtained using a simplified representation of the group wavefunctions as single two-electron Slater determinants:

$$\hat{A} \, \Psi_{\mathrm{X},K} \Psi_{\mathrm{Y},L} = \hat{A} \, \Psi_{\mathrm{X},T_{1,1}} \Psi_{\mathrm{Y},S_0} = |abc\bar{c}| \tag{6.41}$$

and

$$\hat{A} \, \Psi_{\mathrm{X},K'} \Psi_{\mathrm{Y},K'} = \hat{A} \, \Psi_{\mathrm{X},S_0} \Psi_{\mathrm{Y},T_{1,1}} = |a\bar{a}cd| \tag{6.42}$$

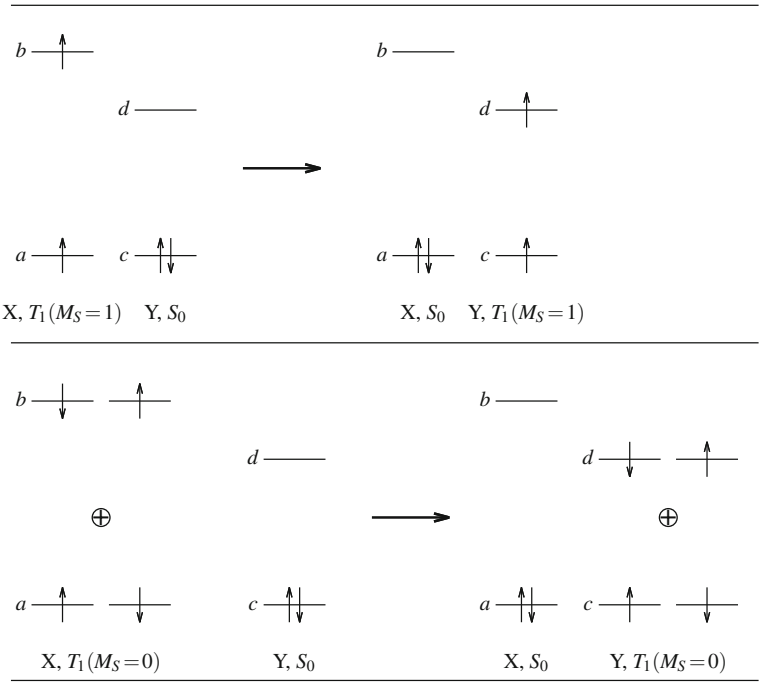

Fig. 6.4 Molecular orbital scheme for triplet sensitization. Upper panel: $M_S = 1$ component of the triplets (the $M_S = -1$ component is quite analogous); lower panel, $M_S = 0$ component. The encircled plus signs indicate the in-phase combination of Slater determinants corresponding to the spin function $(\alpha\beta + \beta\alpha)/\sqrt{2}$

(in the notation we are using for the Slater determinants, ϕ is a spinorbital with α spin, and $\overline{\phi}$ is one with β spin). These are the triplets with $M_S = 1$ (the second index in $T_{1,1}$), but the same conclusions hold for $M_S = 0$ or -1, i.e., $T_{1,0}$ and $T_{1,-1}$ (see scheme 6.4). The initial and final states differ by two spin-orbitals, so

$$\left\langle K, L \left| \hat{H}_{el} \right| K', L' \right\rangle = \left\langle b\bar{c} \left| r_{12}^{-1} \right| \bar{a}d \right\rangle - \left\langle b\bar{c} \left| r_{12}^{-1} \right| d\bar{a} \right\rangle = -\left\langle bc \left| r_{12}^{-1} \right| da \right\rangle \ . \quad (6.43)$$

In the singlet fission process (6.27) the initial state is S_1 in X and S_0 in Y and will be indicated as $|KL\rangle = \left|\Psi_{X,S_1}\Psi_{Y,S_0}\right\rangle$. The general expression of the final state, i.e., the singlet combination of two triplets, is

$$\left|\Psi_{XY,^1(TT)}\right\rangle = 3^{-1/2}\left(\left|\Psi_{X,T_{1,1}}\Psi_{Y,T_{1,-1}}\right\rangle - \left|\Psi_{X,T_{1,0}}\Psi_{Y,T_{1,0}}\right\rangle + \left|\Psi_{X,T_{1,-1}}\Psi_{Y,T_{1,1}}\right\rangle\right) \ . \quad (6.44)$$

We see that the final state is described by a combination of three products of group functions. For each of the three terms in this expression, the matrix element with the initial state contains two products of singlet and triplet states, both for X and for Y,

so here again the only nonvanishing contribution is $-K_{\mathrm{XY},KK'LL'}$. The same holds for the reverse process of triplet–triplet annihilation. So:

$$\left\langle \Psi_{\mathrm{X},S_1}\Psi_{\mathrm{Y},S_0}\left|\hat{H}_{el}\right|\Psi_{\mathrm{XY},^1(TT)}\right\rangle = -n_{\mathrm{X}}n_{\mathrm{Y}} \times\left\langle \Psi_{\mathrm{X},S_1}\Psi_{\mathrm{Y},S_0}\left|[r(x_1,y_1)]^{-1}\ \hat{P}_{\mathrm{XY}}\right|\Psi_{\mathrm{X},T_{1,1}}\Psi_{\mathrm{Y},T_{1,-1}}-\Psi_{\mathrm{X},T_{1,0}}\Psi_{\mathrm{Y},T_{1,0}}+\Psi_{\mathrm{X},T_{1,-1}}\Psi_{\mathrm{Y},T_{1,1}}\right\rangle . \tag{6.45}$$

Even choosing a simplified description based on four MOs, here we need more than two Slater determinants. The singlet excitation localized on X is

$$\hat{A}\ \Psi_{\mathrm{X},S_1}\Psi_{\mathrm{Y},S_0} = 2^{-1/2}\ \left(|a\bar{b}c\bar{c}| - |\bar{a}bc\bar{c}|\right) . \tag{6.46}$$

If the local triplets are approximated by single excitations $a \to b$ and $c \to d$, the expression (6.44) becomes

$$\Psi_{\mathrm{XY},^1(TT)} = 12^{-1/2}\left(2|ab\bar{c}\bar{d}| - |a\bar{b}c\bar{d}| - |\bar{a}bc\bar{d}| - |a\bar{b}\bar{c}d| - |\bar{a}b\bar{c}d| + 2|\bar{a}\bar{b}cd|\right) . \tag{6.47}$$

Then,

$$\left\langle \Psi_{\mathrm{X},S_1}\Psi_{\mathrm{Y},S_0}\left|\hat{H}_{el}\right|\Psi_{\mathrm{XY},^1(TT)}\right\rangle = \left(\frac{3}{2}\right)^{1/2}\left(\left\langle bb\left|r_{12}^{-1}\right|cd\right\rangle - \left\langle aa\left|r_{12}^{-1}\right|cd\right\rangle\right) . \tag{6.48}$$

Other interactions, in particular through charge transfer states, may contribute significantly to coupling the initial and final state [12]. All of them are short-range interactions, as in the case of triplet sensitization.

6.4.3 *Singlet-to-Singlet Excitation Energy Transfer: Dexter and Förster Mechanisms*

In the case of excitation transfer within the singlet manifold, both integrals in Eq. (6.40) are generally nonvanishing. For the same reasons already seen in the previous section when discussing the triplet sensitization and singlet fission processes, the $K_{\mathrm{XY},KK'LL'}$ integral decreases much faster than $J_{\mathrm{XY},KK'LL'}$ when X and Y get far apart. When the exchange interaction is important, i.e., in the short range (a few Å), we say that the "Dexter mechanism" is acting [13]. A different regime, the "Förster mechanism," is reached when the closest atoms of X and Y are ≈10 Å apart or more [14]. Then, the exchange interaction is negligible and

$$\left\langle K,L\left|\hat{H}_{el}\right|K',L'\right\rangle \simeq J_{\mathrm{XY},KK'LL'} = \int \frac{\rho_{\mathrm{X},KK'}(\mathbf{r}_1)\ \rho_{\mathrm{Y},LL'}(\mathbf{r}_2)}{r_{12}}\ \mathrm{d}r_1^3\ \mathrm{d}r_2^3 . \tag{6.49}$$

Here $\mathbf{r}_1$ and $\mathbf{r}_2$ are the positions of the electrons with space and spin coordinates x_1 and y_1, respectively, $r_{12} = |\mathbf{r}_2 - \mathbf{r}_1|$ and

$$\rho_{\mathrm{X},KK'}(r_1) = n_{\mathrm{X}} \sum_{s_1 \ldots s_{n_{\mathrm{X}}}} \int \Psi_{\mathrm{X},K}(x_1 \ldots x_{n_{\mathrm{X}}})\ \Psi_{\mathrm{X},K'}(x_1 \ldots x_{n_{\mathrm{X}}})\ \mathrm{d}r_2^3 \ldots \mathrm{d}r_{n_{\mathrm{X}}}^3 \quad (6.50)$$

is the transition density matrix for the K and K' states. The sum over the spins $s_1 \ldots s_{n_{\mathrm{X}}}$ makes it a spinless density matrix. $\rho_{\mathrm{Y},LL'}(\mathbf{r}_2)$ is defined similarly. We see that the $\left\langle K, L \left| \hat{H}_{el} \right| K', L' \right\rangle$ coupling is formally the Coulomb interaction between two charge distributions, so it is potentially long range.

If the distance between X and Y is larger than the dimensions of the chromophores, we can apply a multipole expansion to evaluate the (6.49) integral (see for instance Bottcher, [15]). We call $\mathbf{R}$ the vector connecting two points within X and Y, respectively (the "centers" of the multipole expansion). Now we redefine $\mathbf{r}_1$ and $\mathbf{r}_2$ as the positions of the electrons of X and Y within two Cartesian frames with the origins in the respective centers.[1] Then, $\mathbf{r}_{12}$ must be rewritten as $|\mathbf{R} + \mathbf{r}_2 - \mathbf{r}_1|$ and

$$\begin{aligned}
&\frac{1}{r_{12}} = \frac{1}{R} + \frac{(\mathbf{r}_1 - \mathbf{r}_2)\cdot\mathbf{R}}{R^3} + \frac{3[(\mathbf{r}_1 - \mathbf{r}_2)\cdot\mathbf{R}]^2}{2R^5} - \frac{(\mathbf{r}_1 - \mathbf{r}_2)^2}{2R^3} + O(R^{-4}) = \\
&= \frac{1}{R} + \frac{(\mathbf{r}_1 - \mathbf{r}_2)\cdot\mathbf{R}}{R^3} + \\
&+ \frac{3\left[(\mathbf{r}_1\cdot\mathbf{R})^2 + (\mathbf{r}_2\cdot\mathbf{R})^2 - 2(\mathbf{r}_1\cdot\mathbf{R})(\mathbf{r}_2\cdot\mathbf{R})\right] - \left[r_1^2 + r_2^2 - 2\mathbf{r}_1\cdot\mathbf{r}_2)\right]\ R^2}{2R^5} + O(R^{-4})\ .
\end{aligned} \quad (6.51)$$

When inserted in Eq. (6.49), the term $1/R$ and all the terms of this development that only depend on $\mathbf{r}_1$ or $\mathbf{r}_2$ do not contribute to the integral because of the orthogonality relationships (6.28). So, neglecting the terms proportional to R^{-4} or higher powers, we remain with

$$\begin{aligned}
&\left\langle K, L \left| \hat{H}_{el} \right| K', L' \right\rangle \simeq \\
&\simeq \int \rho_{\mathrm{X},KK'}(\mathbf{r}_1)\ \rho_{\mathrm{Y},LL'}(\mathbf{r}_2)\ \frac{\mathbf{r}_1\cdot\mathbf{r}_2\ R^2 - 3(\mathbf{r}_1\cdot\mathbf{R})(\mathbf{r}_2\cdot\mathbf{R})}{R^5}\ \mathrm{d}r_1^3\ \mathrm{d}r_2^3 = \\
&= \frac{\boldsymbol{\mu}_{\mathrm{X},KK'}\cdot\boldsymbol{\mu}_{\mathrm{Y},LL'}\ R^2 - 3(\boldsymbol{\mu}_{\mathrm{X},KK'}\cdot\mathbf{R})(\boldsymbol{\mu}_{\mathrm{Y},LL'}\cdot\mathbf{R})}{R^5} = \\
&= \frac{\mu_{\mathrm{X},KK'}\mu_{\mathrm{Y},LL'}}{R^3}\ (\sin\alpha\ \sin\beta\ \cos\phi - 2\cos\alpha\ \cos\beta)\ .
\end{aligned} \quad (6.52)$$

Here $\boldsymbol{\mu}_{\mathrm{X},KK'}$ and $\boldsymbol{\mu}_{\mathrm{Y},LL'}$ are the $K \to K'$ and $L \to L'$ transition dipoles of X and Y, respectively. Moreover, as shown in Fig. 6.5, α is the angle between $\boldsymbol{\mu}_{\mathrm{X},KK'}$ and $\mathbf{R}$, β is the angle between $\boldsymbol{\mu}_{\mathrm{Y},LL'}$ and $\mathbf{R}$, and ϕ is the dihedral angle between the planes $(\boldsymbol{\mu}_{\mathrm{X},KK'}, \mathbf{R})$ and $(\boldsymbol{\mu}_{\mathrm{Y},LL'}, \mathbf{R})$. Equation (6.52) shows how the coupling that causes the energy transfer depends on the mutual orientation of the two chromophores. For

[1] The centers of X and Y can be placed rather arbitrarily, the only requirement being that the distances r_1 and r_2 are much smaller than R. For instance, acceptable choices are the center of mass of each chromophore or the analogous center of charge for the total charge distributions of the orbitals involved in the $K \to K'$ and $L \to L'$ transitions.

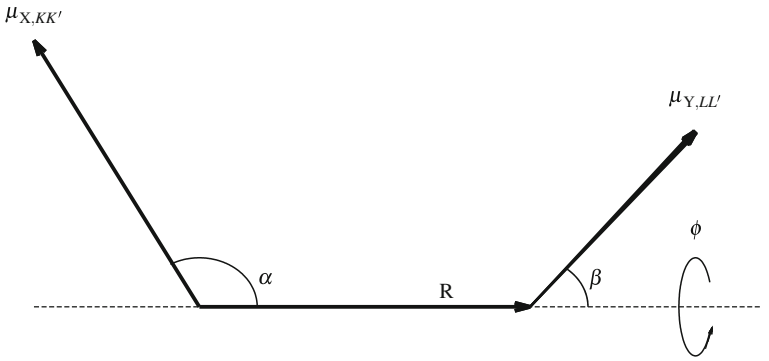

Fig. 6.5 Dipole–dipole coupling

instance, if both dipoles are perpendicular to **R** and to each other, the interaction vanishes. Moreover, the interaction is proportional to R^{-3}.

Once again, we can simplify the wavefunctions to single excitations involving a minimum number of MOs, as shown in scheme Fig. 6.6. The initial state is the same as in singlet fission, see Eq. (6.46). The final state is

$$\hat{A}\ \Psi_{X,S_0}\Psi_{Y,S_1} = 2^{-1/2}\ \left(|a\overline{a}c\overline{d}| - |a\overline{a}\overline{c}d|\right) \tag{6.53}$$

and therefore

$$\left\langle \Psi_{X,S_1}\Psi_{Y,S_0}\left|\hat{H}_{el}\right|\Psi_{X,S_0}\Psi_{Y,S_1}\right\rangle = 2\left\langle ac\left|r_{12}^{-1}\right|bd\right\rangle - \left\langle ac\left|r_{12}^{-1}\right|db\right\rangle\ . \tag{6.54}$$

At large distance, where the exchange integral $\left\langle ac\left|r_{12}^{-1}\right|db\right\rangle$ is negligible, we just have the Coulomb interaction between the two transition densities $\rho_X(r_1) = \sqrt{2}\,a(r_1)b(r_1)$ and $\rho_Y(r_2) = \sqrt{2}\,c(r_2)d(r_2)$.

The energetics of excitation transfer is represented in Fig. 6.2. We shall call $\Delta E_{00,X}$ and $\Delta E_{00,Y}$ the transition energies of X and Y between the lowest vibrational levels ($v = 0$) of S_0 and S_1. If X has undergone thermal equilibration (see Sect. 4.5) before the excitation transfer event, its energy must be close to $\Delta E_{00,X}$. After the excitation transfer, X can be found in any vibrational level of S_0 with energy $E_{vib,X} \leq \Delta E_{XY} = \Delta E_{00,X} - \Delta E_{00,Y}$. The energy loss of X is then $\Delta E_{00,X} - E_{vib,X}$, and it may be equated to a virtual transition energy $h\nu \in [\Delta E_{00,Y}, \Delta E_{00,X}]$ that potentially belongs to the fluorescence spectrum of X (no implication is here meant about the actual probability of emitting a photon of frequency ν). At the same time, Y acquires the same amount of energy $h\nu$ that may be thought as a transition energy belonging to the absorption spectrum of Y, again without reference to the absorption probability. This results in a vibrational energy excess $E_{vib,Y} = \Delta E_{XY} - E_{vib,X} = h\nu - \Delta E_{00,Y}$.

A closer relationship with the emission spectrum of X and the absorption spectrum of Y can be worked out within the dipolar approximation, as in Eq. (6.52). The

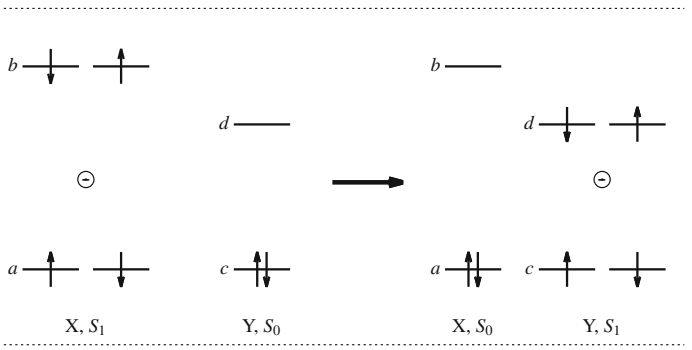

Fig. 6.6 Molecular orbital scheme for singlet-to-singlet energy transfer. The encircled minus signs indicate the out-of-phase combination of Slater determinants corresponding to the spin function $(\alpha\beta - \beta\alpha)/\sqrt{2}$

excitation transfer rate constant $K_{ET} = 1/\tau_{ET}$ can be evaluated by Fermi's Golden Rule, as in Eq. (3.128). The matrix element between the initial and final vibronic states is

$$\begin{aligned} &\left\langle K, 0, L, 0 \left| \hat{H}_{el} \right| K', u, L', v \right\rangle \simeq \\ &\simeq \frac{\mu_{\mathrm{X},K,0,K',u}\ \mu_{\mathrm{Y},L,0,L',v}}{R^3} (\sin\alpha\ \sin\beta\ \cos\phi - 2\cos\alpha\ \cos\beta) \ . \end{aligned} \tag{6.55}$$

Here $K, 0, L, 0$ are the electronic and vibrational indexes of the initial state (we assume both chromophores to be in the ground vibrational state), and K', u, L', v are the indexes of the final state. In particular, the vibrational energy of state u is $E_{vib,\mathrm{X}} = \Delta E_{00,\mathrm{X}} - h\nu$, while that of state v is $E_{vib,\mathrm{Y}} = h\nu - \Delta E_{00,\mathrm{Y}}$. We are also assuming that the direction of the transition dipoles is substantially independent on the molecular geometry, so that the angular factor is not affected by integration over the vibrational coordinates. This assumption is in agreement with the Franck–Condon approximation (see Sect. 4.1), which is usually valid for allowed transitions: note that of course the dipole–dipole interaction is not so important when one or both transitions are forbidden. The density of states of Eq. (3.128) is here the product of the densities of vibrational levels for the final states of X and Y, $\rho_{\mathrm{X}}(E_{vib,\mathrm{X}})\ \rho_{\mathrm{Y}}(E_{vib,\mathrm{Y}})$. To apply Fermi's Golden Rule we must average over the possible final states, i.e., over the virtual photon energy $h\nu$:

$$\begin{aligned} K_{ET} = &\frac{4\pi^2(\sin\alpha\ \sin\beta\ \cos\phi - 2\cos\alpha\ \cos\beta)^2}{R^6} \\ &\times \int_{\Delta E_{00,\mathrm{Y}}}^{\Delta E_{00,\mathrm{X}}} \mu^2_{\mathrm{X},K,0,K',u}\ \rho_{\mathrm{X}}(E_{vib,\mathrm{X}})\ \mu^2_{\mathrm{Y},L,0,L',v}\ \rho_{\mathrm{Y}}(E_{vib,\mathrm{Y}})\ \mathrm{d}\nu \ . \end{aligned} \tag{6.56}$$

We remind that the final vibrational levels u and v and their energies $E_{vib,\mathrm{X}}$ and $E_{vib,\mathrm{Y}}$ are all functions of ν. In the integrand, the factor $\mu^2_{\mathrm{X},K,0,K',u}\ \rho_{\mathrm{X}}(E_{vib,\mathrm{X}})$ is

proportional to the emission probability of X per unit energy (or frequency ν), while $\mu^2_{\mathrm{Y},L,0,L',v}\ \rho_{\mathrm{Y}}(E_{vib,\mathrm{Y}})$ is proportional to the absorption probability of Y, so the rate constant depends on the overlap of the fluorescence spectrum of X with the absorption spectrum of Y. Moreover, K_{ET} decreases with the distance between the two chromophores, proportionally to R^{-6}. Although this is quite a steep decrease, the Förster mechanism acts at longer distances than the Dexter mechanism: in fact, as already seen, the importance of the latter depends on the overlap of the X and Y wavefunctions and therefore its decrease with R is roughly exponential (see Appendix E). The angular factor determines the dependence of K_{ET} on the mutual orientation of the transition dipoles of X and Y. In solution or in any other isotropic medium, it is appropriate to average over the α, β, and ϕ angles: then, the angular factor is replaced by the constant 2/3.

The excitation transfer based on these principles is often called FRET, acronym of "Förster resonance energy transfer" or "fluorescence resonance energy transfer," because it switches off the fluorescence of X and switches on the fluorescence of Y. Note that FRET should not be confused with the emission of a photon by the excited X, followed by absorption of the same photon by a Y molecule. The latter process can occur without any direct interaction of X and Y and is effective to much larger distances. Considering that the irradiance of the light emitted by a pointwise source decreases as the inverse square distance, the probability that a given Y molecule captures the emitted photon is proportional to R^{-2}. However, FRET is much more effective in the intermediate range (tens of Å). More on FRET theory and applications can be found in Govorov et al. [16] and in Medintz and Hildebrandt [17].

6.4.4 Exciton Coupling

In many circumstances the chromophores occupy fixed positions and orientations in space, as in molecular crystals or in metal complexes. The biological evolution and the research in the field of functional materials have created assemblies of similar or identical chromophores that absorb light and transfer the excitation to other chromophores with specific purposes, such as to concentrate the energy in a reactive center. This is called the "antenna effect" and operates for instance in photosynthetic complexes [4]. When the chromophore-to-chromophore interactions are stable in time and the excited states are close in energy, it is easy to observe typical alterations in the spectrum with respect to the isolated molecules.

Let us start with the two chromophores model already presented in the previous section. The adiabatic electronic states can be described as linear combinations of the group functions products:

$$|\Psi_I\rangle = \sum_{K,L} C_{K,L}\ |K, L\rangle\ . \tag{6.57}$$

However, the ground state is usually well represented by the diabatic state with $K = L = 0$, with all other coefficients quite negligible, because its energy separation from other states is much larger than the couplings (6.39) and (6.40). Even a localized excitation $|K, 0\rangle$ or $|0, L\rangle$ with energy well separated from that of other states is a good approximation of an exact eigenstate.

We shall therefore focus on pairs of states $|K, 0\rangle$ and $|0, L\rangle$ that are degenerate or almost so. This is a common situation if the chromophores are identical or differ by small details, such as their chemical environments: for instance, two nucleic acid bases in close positions of the DNA chain but with different neighbors. The two localized states $|K, 0\rangle$ and $|0, L\rangle$, the "excitons," will then give place to a pair of linear combinations that represent (possibly partially) delocalized states. The Hamiltonian matrix elements can be called $H_{KK} = \left\langle K, 0 \left| \hat{H}_{el} \right| K, 0 \right\rangle$, $H_{LL} = \left\langle L, 0 \left| \hat{H}_{el} \right| L, 0 \right\rangle$ and $H_{KL} = H_{LK} = \left\langle K, 0 \left| \hat{H}_{el} \right| L, 0 \right\rangle$. The adiabatic energies and states are (see Appendix D):

$$E_{1,2} = \frac{H_{LL} + H_{KK} \pm \sqrt{\Delta H^2 + 4H_{KL}^2}}{2} \,. \tag{6.58}$$

(here $\Delta H = H_{KK} - H_{LL}$ and the choice of signs is such that $E_1 \leq E_2$) and

$$\begin{aligned} |\psi_1\rangle &= \cos\theta \;\; |0, L\rangle + \sin\theta \;\; |K, 0\rangle \\ |\psi_2\rangle &= -\sin\theta \;\; |0, L\rangle + \cos\theta \;\; |K, 0\rangle \end{aligned} \tag{6.59}$$

with

$$\operatorname{tg}\theta = \frac{\Delta H - \sqrt{\Delta H^2 + 4H_{KL}^2}}{2H_{KL}} \,. \tag{6.60}$$

As we see from Table 6.3, when the coupling is larger than the ΔH energy difference the excitation is delocalized, in state Ψ_1 as well as in Ψ_2. On the contrary, when the coupling is weak (smaller than ΔH), the state Ψ_1 is more similar to the lower in energy among $|K, 0\rangle$ and $|0, L\rangle$, while Ψ_2 resembles the higher of the two. Note that, even if Ψ_2 may be initially populated by optical excitation, normally after a short time the system ends up in Ψ_1 because of internal conversion followed by energy loss to the environment. Therefore, if the excitation is fully or partially localized, it will mostly belong to the chromophore with the lower excitation energy.

The transition dipole moments between the ground state and the two adiabatic states are:

$$\begin{aligned} \boldsymbol{\mu}_{01} &= \cos\theta \;\; \boldsymbol{\mu}_{\mathrm{Y},0L} + \sin\theta \;\; \boldsymbol{\mu}_{\mathrm{X},0K} \\ \boldsymbol{\mu}_{02} &= -\sin\theta \;\; \boldsymbol{\mu}_{\mathrm{Y},0L} + \cos\theta \;\; \boldsymbol{\mu}_{\mathrm{X},0K} \,. \end{aligned} \tag{6.61}$$

We now recall that the photon absorption rates are proportional to the Einstein B coefficients, i.e., to the squares of the transition dipole moments (see Sect. 3.5). It is easy to show that the sum of the excitation rates is the same for the two noninter-

Table 6.3 Localization of the excitation according to the diabatic states energies and coupling

State energies	H_{KL}	ΔH vs H_{KL}	$\theta \simeq$	$\lvert\Psi_1\rangle \simeq$	$\lvert\Psi_2\rangle \simeq$
$H_{KK} > H_{LL}$	—	$\lvert H_{KL}\rvert \ll \lvert\Delta H\rvert$	0	$\lvert 0, L\rangle$	$\lvert K, 0\rangle$
$H_{KK} \simeq H_{LL}$	> 0	$\lvert H_{KL}\rvert \gg \lvert\Delta H\rvert$	$-\pi/4$	$\frac{\lvert 0, L\rangle - \lvert K, 0\rangle}{\sqrt{2}}$	$\frac{\lvert 0, L\rangle + \lvert K, 0\rangle}{\sqrt{2}}$
$H_{KK} \simeq H_{LL}$	< 0	$\lvert H_{KL}\rvert \gg \lvert\Delta H\rvert$	$\pi/4$	$\frac{\lvert 0, L\rangle + \lvert K, 0\rangle}{\sqrt{2}}$	$\frac{\lvert K, 0\rangle - \lvert 0, L\rangle}{\sqrt{2}}$
$H_{KK} < H_{LL}$	—	$\lvert H_{KL}\rvert \ll \lvert\Delta H\rvert$	$\pm\pi/2$	$\pm\lvert K, 0\rangle$	$\mp\lvert 0, L\rangle$

acting subsystems X and Y, as for the two adiabatic states of the whole system with interaction:

$$\mu_{01}^2 + \mu_{02}^2 = \mu_{\mathrm{X},0K}^2 + \mu_{\mathrm{Y},0L}^2 \,. \tag{6.62}$$

So, the overall transition rate is unaffected by the interaction and by the resulting delocalization. However, the individual bands do change when X and Y interact. The resonance frequencies are of course shifted as the transition energies go from H_{LL} and H_{KK} to E_1 and E_2. Moreover, the transition dipoles change according to Eq. (6.61). In our convention (see Appendix D), $\cos\theta$ is positive and the sign of $\sin\theta$ is opposite to that of H_{KL}. So, whether $\boldsymbol{\mu}_{\mathrm{Y},0L}$ and $\boldsymbol{\mu}_{\mathrm{X},0K}$ add or subtract to yield $\boldsymbol{\mu}_{01}$ and $\boldsymbol{\mu}_{02}$ depends on the sign of H_{KL}.[2] In general the stronger band may belong either to the lower or to the higher adiabatic state.

A special and important case is that of two (almost) identical chromophores with Förster interaction, such as biphenyls, binaphthyls, or bilirubins [19]. Their excited states are then (almost) degenerate, $\mu_{\mathrm{X},0K} \simeq \mu_{\mathrm{Y},0L}$ and $\cos\theta \simeq |\sin\theta| \simeq 1/\sqrt{2}$. The interaction is determined by the dipoles themselves according to Eq. (6.55). If, for instance, the transition dipoles are both parallel to $\mathbf{R}$, we have

$$H_{KL} = -\frac{2\mu_{\mathrm{X},0K}\mu_{\mathrm{Y},0L}}{R^3} \simeq -\frac{2\mu^2}{R^3} \tag{6.63}$$

[2] Some of the readers may be used to think that the sign of interaction or transition matrix elements does not matter: in fact, it depends on the arbitrary signs of the wavefunctions, which must not affect the physics. Actually, if more than two states are involved, the relationships between the signs of matrix elements can be important (multiphoton processes are a typical example). Here we have three states, 00, $0L$, and $K0$, and three matrix elements (the fact that two are vectors is irrelevant): H_{KL}, $\boldsymbol{\mu}_{\mathrm{X},0K}$, and $\boldsymbol{\mu}_{\mathrm{Y},0L}$. If we arbitrarily change the sign of the ground state 00, $\boldsymbol{\mu}_{\mathrm{X},0K}$ and $\boldsymbol{\mu}_{\mathrm{Y},0L}$ get reversed, and so do $\boldsymbol{\mu}_{01}$ and $\boldsymbol{\mu}_{02}$, with no effect on the spectral properties. If we change the sign of $0L$, the signs of H_{KL}, $\boldsymbol{\mu}_{\mathrm{Y},0L}$, and $\sin\theta$ also change, so $\boldsymbol{\mu}_{01}$ is reversed and $\boldsymbol{\mu}_{02}$ remains unchanged, and again the physics is not affected. Same considerations for the $K0$ state. A similar situation with interesting dynamical consequences is described in [18].

where μ is the geometrical average of $\mu_{\mathrm{X},0K}$ and $\mu_{\mathrm{Y},0L}$. Then, $\mu_{01} \simeq \sqrt{2}\mu$ and $\mu_{02} \simeq 0$. This means the lower state is bright and the upper state is dark. A more frequent situation is that both dipoles are perpendicular to $\mathbf{R}$. This is the case, e.g., for $\pi \rightarrow \pi^*$ transitions in planar π systems superimposed ("stacked") face-to-face, such configurations being stabilized by dispersion interactions. Then

$$H_{KL} = \frac{\mu_{\mathrm{X},0K}\mu_{\mathrm{Y},0L}}{R^3} \cos\phi \simeq \frac{\mu^2}{R^3} \cos\phi \ . \tag{6.64}$$

It is easy to show that $\mu_{02} \geq \mu_{01}$ for any value of ϕ. The largest difference is found when $\mu_{\mathrm{X},0K}$ and $\mu_{\mathrm{Y},0L}$ are parallel or antiparallel, in which case $\mu_{02} \simeq \sqrt{2}\mu$ and $\mu_{01} \simeq 0$. Again, we have a dark and a bright state, but this time the latter has the higher energy. In such cases, by comparing the absorption band of the two (almost) identical monomers with that of the dimer one observes an hypsochromic shift, i.e., a displacement of the absorption maximum by a frequency $\Delta\nu \simeq \mu^2/(hR^3)$.

As we have seen in Chap. 3, a short coherent pulse of light will excite the system in a bright state, even if this is not an eigenstate of the molecular Hamiltonian. The bright state is a linear combination of excited states that carries all the dipole strength within the frequency bandwidth of the pulse. Consider an assembly of interacting chromophores X_i with close lying locally excited states $|exc_i\rangle$. If their transition dipoles with the ground state are $\langle gs\,|\boldsymbol{\mu}|\,exc_i\rangle = \boldsymbol{\mu}_i$, the bright state is

$$|B\rangle = N \sum_i \mathbf{e}_p \cdot \boldsymbol{\mu}_i \ \ |exc_i\rangle \tag{6.65}$$

where N is the normalization factor and $\mathbf{e}_p$ is the polarization versor of the exciting light. As already observed in Sect. 3.9, if all the $\boldsymbol{\mu}_i$ vectors are parallel, the composition of the bright state does not depend on the light polarization. Any state $|D\rangle$, orthogonal to $|B\rangle$ within the subspace spanned by the $|exc_i\rangle$, is dark:

$$\mathbf{e}_p \cdot \langle gs\,|\boldsymbol{\mu}|\,D\rangle = \sum_i \mathbf{e}_p \cdot \langle gs\,|\boldsymbol{\mu}|\,exc_i\rangle\,\langle exc_i\,|D\rangle = \langle B\,|D\rangle = 0 \ . \tag{6.66}$$

Clearly, the bright state $|B\rangle$ can be quite delocalized over all or some of the chromophores. After a pulse of appropriate central frequency and bandwidth, the initial state $|B\rangle$ will undergo a time evolution that is determined, at least initially, by the localized state energies and couplings, and will entail a migration of the excitation in space, from chromophore to chromophore. However, nonadiabatic transitions and vibrational energy loss to the environment will bring the system into the lowest excited eigenstate at intermediate times, and eventually of course to the ground state.

6.5 Charge or Electron Transfer

Charge transfer (CT) and electron transfer are two synonyms for redox reactions. Those involving excited states are extremely important both in photosynthesis and in solar energy conversion technologies. A general CT process can be summarized as

$$X^{n+} + Y^{m+} \longrightarrow X^{(n+1)+} + Y^{(m-1)+} \tag{6.67}$$

where X acts as electron donor and Y as acceptor. Here n and m can be any integer, usually larger or equal to -1; i.e., X and Y may be anions, cations, or neutral species. Of course, two of the reactants or products have at least one unpaired electron, and often all of the species involved are open shells, for instance transition metal complexes. We shall consider three kinds of processes: the thermal redox reactions for which the basic theory was established by Marcus, the photochemical reactions initiated by a localized excitation, and those following a charge transfer excitation (see Sect. 2.6). The two last processes will be qualified as "photoinitiated" CT and "optical" CT, respectively [20].

In this section we shall also consider the thermal reactions, not only for the sake of comparison with the photochemical CT, but also because their mechanism in many cases involves a sudden change in the electronic configuration and therefore requires a treatment of nonadiabatic dynamics to be correctly described. The orbital schemes for the thermal and the photoinitiated CT are shown in Fig. 6.7, where the reactant X is thought of as a closed shell neutral species and Y^+ as a radical cation (this particular choice of charges, $n = 0$ and $m = 1$ for the reactants, does not limit the generality of the discussion that follows). In the optical CT the charge separation is achieved, at least to a good extent, during the excitation process. Then, during the structural rearrangements that may follow the excitation, no change of the electronic configuration is required to complete the redox reaction. For the thermal process, the initial state indicated in Fig. 6.7 is

$$\hat{A}\, \Psi_{X,S_0} \Psi_{Y,D_0} = |\ldots a\bar{a}c| \,. \tag{6.68}$$

Here we are assuming the orbitals to be orthonormal (and therefore not perfectly localized) as in Sect. 6.4.1. The dots stand for all other doubly occupied orbitals not directly involved in the electron transfer. D_0 indicates the ground-state doublet of the X^+ and Y^+ radical cations. The final state is

$$\hat{A}\, \Psi_{X,D_0} \Psi_{Y,S_0} = |\ldots ac\bar{c}| \,. \tag{6.69}$$

The interaction matrix element is then

$$\left\langle \Psi_{X,S_0} \Psi_{Y,D_0} \left| \hat{H}_{el} \right| \Psi_{X,D_0} \Psi_{Y,S_0} \right\rangle = -h_{ac} - \sum_i \left(2 \left\langle ai \left| r_{12}^{-1} \right| ci \right\rangle - \left\langle ai \left| r_{12}^{-1} \right| ic \right\rangle \right) \,. \tag{6.70}$$

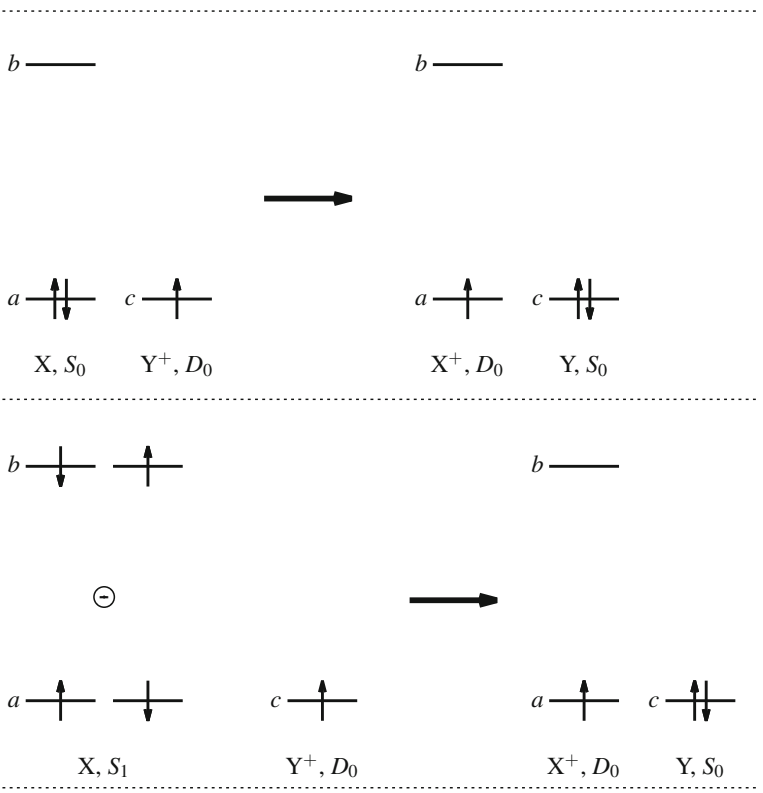

Fig. 6.7 Molecular orbital scheme for electron transfer. Upper panel, thermal ground-state process. Lower panel, photoinitiated process. The encircled minus sign indicates the out of phase combination of Slater determinants corresponding to the spin function $(\alpha\beta - \beta\alpha)/\sqrt{2}$

The sum runs over all the doubly occupied orbitals of both reactants and products. All the contributions contain the products of two orbitals localized in the two different subsystems (a and c in the monoelectronic and in the Coulomb integrals, a and i or c and i in the exchange one). The interaction is therefore short range.

For the photoinitiated process the initial state is

$$\hat{A}\ \Psi_{\mathrm{X},S_n}\Psi_{\mathrm{Y},D_0} = 2^{-1/2}\ \left(|\ldots a\bar{b}c| - |\ldots \bar{a}bc|\right) \tag{6.71}$$

and the final one is the same as before. Then

$$\begin{aligned}&\left\langle \Psi_{\mathrm{X},S_n}\Psi_{\mathrm{Y},D_0}\left|\hat{H}_{el}\right|\Psi_{\mathrm{X},D_0}\Psi_{\mathrm{Y},S_0}\right\rangle = \\ &= -2^{-1/2}\left[h_{bc} + \left\langle ab\left|r_{12}^{-1}\right|ca\right\rangle + \sum_i \left(2\left\langle bi\left|r_{12}^{-1}\right|ci\right\rangle - \left\langle bi\left|r_{12}^{-1}\right|ic\right\rangle\right)\right]\ .\end{aligned} \tag{6.72}$$

Again, all the contributions contain products of orbitals belonging to X and Y, so the interaction is short range. This means that in both cases, when X and Y are not close to each other or connected by conducting bridges, the coupling between the two diabatic states is very small.

In all the electron transfer processes occurring in condensed phase the static effect of the environment is of paramount importance, because the different charge distributions of ground-state reactants, excited and transition states, and products, entail different interactions with the environment. Marcus' theory of thermal CT reactions highlights such effects [21]. For each of the two centers X and Y we focus on a coordinate that affects its interaction with the environment, say R_X and R_Y, respectively. It is particularly easy to identify such coordinates for metal complexes, as the breathing coordinates of the first ligand or solvent shells. For instance, in a complex with only one kind of ligands, often all the ligands are placed at the same distance, R_X or R_Y, from the metal center. If, instead, the distances of the ligands are different, we can take as R_X (or R_Y) an average distance. Normally, as the charge of the metal increases, the equilibrium distance of the ligands decreases. So, if X^{n+} is the donor and Y^{m+} the acceptor, the electron transfer will cause a decrease of the equilibrium value of R_X and an increase of that of R_Y. The model represented in Fig. 6.8 is constructed according to the above considerations. The potential energy surfaces of two diabatic states, $\Psi_{X,S_0}\Psi_{Y,D_0}$ and $\Psi_{X,D_0}\Psi_{Y,S_0}$, are built as sums of Morse functions of R_X and R_Y. To the diabatic PES of the products a constant $\Delta E_r = -12$ kcal/mol is added. The distance between X and Y is assumed to be constant, so the interaction $\left\langle \Psi_{X,S_0}\Psi_{Y,D_0} \left| \hat{H}_{el} \right| \Psi_{X,D_0}\Psi_{Y,S_0} \right\rangle$ has a fixed value of 2 kcal/mol. The products are more stable than the reactants by 12 kcal/mol. The adiabatic potential

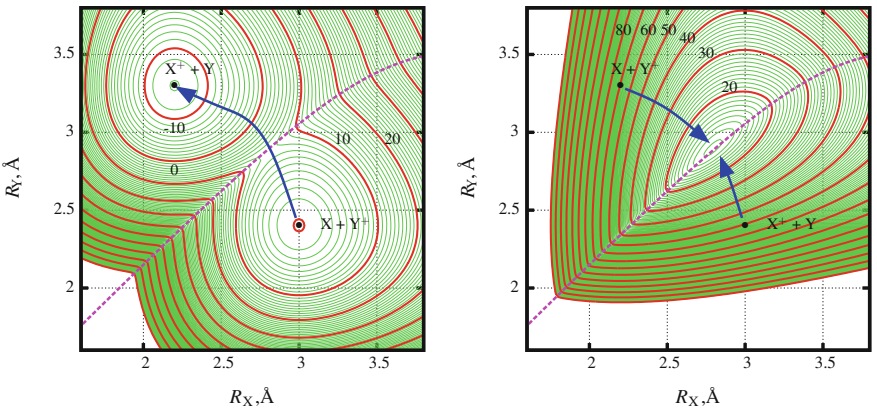

Fig. 6.8 Ideal trajectories in two solvent or ligand coordinates for electron transfer. Left panel: ground-state PES and thermal pathway (blue line). Right panel: excited PES and photochemical pathways (blue lines). The dots indicate minima in the ground-state PES and the corresponding Franck–Condon points. The dashed line shows the crossing seam between diabatic surfaces. The green contour levels are spaced by 1 kcal/mol, the red ones by 10 kcal/mol. Some of the latter are marked with the relative energy in kcal/mol

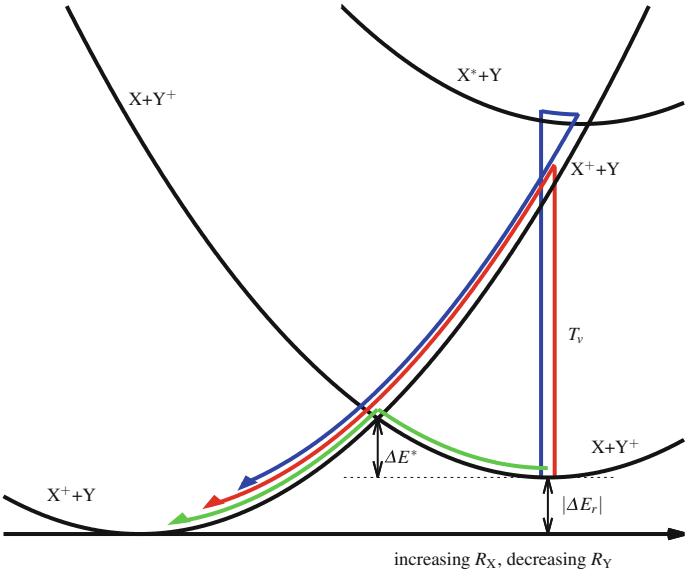

Fig. 6.9 Electron transfer processes seen along the combined R_X, R_Y coordinate

energy surfaces are obtained by diagonalizing the 2×2 Hamiltonian matrix in the diabatic basis. In the plots of the two adiabatic PES, a dashed curve indicates the crossing seam between the diabatic ones (there is no crossing of the adiabatic PESs, because the interaction matrix element is nowhere zero). In the plot, the minimum below the dashed curve represents the adiabatic ground state of the reactants, $X+Y^+$, while the minimum above the seam represents the products, $X^+ + Y$. The excited state has just the opposite character with respect to the ground state. Along the crossing seam the energy gap between the two adiabatic PES is minimum and equal to $2\left\langle \Psi_{X,S_0}\Psi_{Y,D_0}\left|\hat{H}_{el}\right|\Psi_{X,D_0}\Psi_{Y,S_0}\right\rangle$. The charge switch that occurs near the transition state would go from very smooth for larger values of the interaction to quite sudden for an almost vanishing interaction.

The thermal reaction has a transition state that corresponds to the minimum along the crossing seam: in Fig. 6.8 the reaction pathway is drawn as a blue curve. Marcus' evaluation of the activation energy was based on a simplified representation of the PES, where the diabatic potentials are harmonic with the same force constant for both coordinates and both surfaces and the interaction between them is neglected for this purpose. Then the crossing seam is a straight line in the R_X, R_Y plane. The transition state also lies on a straight pathway joining the reactants and products minima. Along such pathway the potential energy curves look as in Fig. 6.9, where the thermal mechanism is shown as the green pathway. With a little algebra one finds that the activation energy is

$$\Delta E^* = \frac{(\Delta E_r + \lambda)^2}{4\lambda} \,. \tag{6.73}$$

Here ΔE_r is the reaction energy, i.e., the energy difference between products and reactants. The λ parameter is the "reorganization energy," i.e., the surplus of energy the products $X^+ + Y$ would have if the ligands or solvent molecules did not readapt to the new charge distribution. In the model it is computed as the energy of $X^+ + Y$ at the equilibrium values of R_X and R_Y for $X + Y^+$, or vice versa. We shall call Δ_X and Δ_Y the differences in the equilibrium values of R_X and R_Y between reactants and products. Then

$$\lambda = \frac{K}{2}\left(\Delta_X^2 + \Delta_Y^2\right) \tag{6.74}$$

where K is the unified force constant of both coordinates. We see that the vertical excitation energy of $X + Y^+$ to the charge transfer state $X^+ + Y$ is $T_v = \lambda + \Delta E_r$ (remember that $\Delta E_r < 0$ in Figs. 6.8 and 6.9). Vice versa, the excitation energy of $X^+ + Y$ to the state $X + Y^+$ is $\lambda - \Delta E_r$, so one can obtain the reorganization energy if both charge transfer bands can be identified in the spectra. The activation energy can also be written

$$\Delta E^* = \frac{T_v^2}{4(T_v - \Delta E_r)} \,. \tag{6.75}$$

It should be noted that, with a proper statistical treatment of all the coordinates (or states) of the chemical environment of the redox pair (ligands, solvent, etc.), all the energies that appear in Eqs. (6.73)–(6.75) would be replaced by free energies, as discussed in Sect. 4.4. In conclusion, the thermal reaction rate will therefore contain an Arrhenius factor $\exp(-\Delta E^*/K_B T)$ that can be related to the reaction energy and to a spectral quantity. However, once the transition state is reached, the $X + Y^+$ state must be converted adiabatically to $X^+ + Y$; i.e., a transition must occur between the two diabatic states. Marcus evaluated the transition probability through the Landau–Zener rule, the key parameter being the matrix element $\left\langle \Psi_{X,S_0}\Psi_{Y,D_0} \middle| \hat{H}_{el} \middle| \Psi_{X,D_0}\Psi_{Y,S_0} \right\rangle$. When this interaction is very small, the probability that an electron jumps from X to Y is low and most molecules will keep going uphill on the initial diabatic PES, until they turn and go back to the reactants minimum. On the contrary, when the interaction is strong, the probability of staying on the ground-state adiabatic PES is high and a pure transition state theory treatment is adequate.

The optical mechanism corresponds to the blue arrows in Fig. 6.8, right panel, and to the red pathway in Fig. 6.9. In this case, the system is directly excited to the charge transfer excited state, i.e., to the other diabatic state. A steep slope, corresponding to the rearrangement of the chemical environment, brings the system to the crossing seam and beyond. Now a weak interaction makes probable to continue on the same diabatic PES and to reach the products minimum, so the quantum yield will be high. However, if the interaction between X and Y is really small, also the charge transfer band in the absorption spectrum will be weak.

Light absorption can also populate a local excited state of X, S_n, higher in energy than the charge transfer one or close to it. This is the beginning of the photoinitiated mechanism (blue pathway in Fig. 6.9). The next step is internal conversion from S_n to the charge transfer state, driven by the coupling $\left\langle \Psi_{\mathrm{X},S_n}\Psi_{\mathrm{Y},D_0} \left| \hat{H}_{el} \right| \Psi_{\mathrm{X},D_0}\Psi_{\mathrm{Y},S_0} \right\rangle$, Eq. (6.72). Again this coupling can be very small if X and Y are too far apart, so this transition may suffer the competition of other quenching mechanisms of X. Once on the X^++Y PES, the dynamics is similar to that of the optical mechanism.

6.6 Computational Note: Diabatic States for ET and CT Studies

As we have seen in this chapter, the diabatic representation based on localization of charge and excitation is a quite natural choice for the analysis of ET and CT phenomena. However, when tackling the computational problem, one finds once again that practically all quantum chemistry methods are devoted to approximate the energies and properties of adiabatic eigenstates. Yet there are also some important technical reasons to switch to a (quasi-)diabatic basis in this context.

A first good reason is that the size of many molecular systems under study, especially the multichromophoric ones, calls for "divide and conquer" strategies [1–4, 20, 22, 23]. So, instead of computing the adiabatic states of the whole system, one determines the state energies of each molecular unit or subunit and the interactions between pairs of such units. More often the DFT and TD-DFT methods are applied, but also wavefunction approaches such as coupled cluster and CASSCF plus perturbation. In so doing, the strategy is intrinsically diabatic. For excitation transfer, the state η_i can be defined as the ground state for all chromophores except for the ith chromophore, which is excited. For charge transfer, the diabatic states differ according to where the exchanged electron is localized. The adiabatic eigenstates are obtained by diagonalizing the Hamiltonian matrix $\mathbf{H}$, the elements of which are $H_{ij} = \left\langle \eta_i \left| \hat{H}_{el} \right| \eta_j \right\rangle$. For spatially well-separated chromophores that interact through Förster's mechanism, the diabatic states can be assumed to be orthogonal. In other cases, as in Dexter's ET and generally in CT, the diabatic basis is nonorthogonal. In this case, the effective interaction between two centers i and j, taking into account the overlap $S_{ij} = \langle \eta_i \, | \eta_j \rangle$, is

$$V_{ij} = \frac{2H_{ij} - S_{ij}(H_{ii} + H_{jj})}{2(1 - S_{ij}^2)} \,. \tag{6.76}$$

Nonorthogonal CI methods can also be applied to the whole system, using the nonorthogonal local orbitals [24].

All the state energies and interaction matrix elements are subject to important environmental effects. Obvious static effects are the different stabilization of ground and excited states of the various chromophores and, even more important, of oxidized/reduced species. Electrostatic interactions between chromophores and between

charged species are screened by polar or polarizable media, especially in the long-range, as is the case with Förster coupling. It is often found that the stabilization of localized excitations or redox states due to the environment, being markedly specific of their peculiar charge distribution, bonding and structure, makes the diabatic representation even more suitable to treat ET and CT [1]. As already mentioned, continuum models of the environment in many cases offer a satisfactory description of these static effects and can also, more schematically, take into account the dynamic polarizability of dielectric media. Specific interactions require to represent all parts of the microenvironment at atomic scale, possibly treating (part of) the environment by force fields (see Curutchet and Mennucci for a thorough discussion of different options [4]).

The diabatic representation may also facilitate the integration of the TDSE to simulate fast nonadiabatic processes. When two or more states are close in energy and are weakly coupled, as is the case with similar molecules loosely interacting, the system finds itself very often close to a crossing seam. Every time a wavepacket or a trajectory goes through the crossing line between two diabatic PESs, since the electronic coupling is weak, the nonadiabatic couplings $\mathbf{g}_{12}$ and $\mathbf{t}_{12}$ present narrow and tall peaks, as in the NaCl avoided crossing of Sect. 5.1. For a trajectory, this means the nonadiabatic coupling changes in time very suddenly, making the numerical integration of the TDSE quite inaccurate unless very small time steps are used. Even if the dynamics is treated in the adiabatic representation, an auxiliary "local diabatization" can avoid this drawback [25]. In principle, the nonlocal nature of quantum wavepackets should prevent the occurrence of such sudden events. However, the evaluation of coupling matrix elements between static or traveling basis functions in MCTDH methods suffers of similar drawbacks. Modeling the dependence of the electronic structure on the internal coordinates by effective Hamiltonian in diabatic representations is a good solution also in this case [26–28].

Several ways to define (quasi)-diabatic representations have been proposed. Most of them consist in an orthogonal transformation ("rotation") of the subset of adiabatic states $\{\ldots \psi_k \ldots\}$ that are energetically accessible during the process under study, to produce the diabatic basis:

$$\{\ldots \eta_i \ldots\} = \{\ldots \psi_k \ldots\}\mathbf{T} \,. \tag{6.77}$$

The adiabatic to diabatic rotation $\mathbf{T}$ can be determined by various ad hoc localization criteria. A general diabatization method consists in constructing (normally nonorthogonal) diabatic templates and in rotating the adiabatic basis to achieve maximum overlap with the templates [29, 30]. If localization is the goal, the templates can be defined as products of X and Y wavefunctions, representing the ground and excited states of the two subsystems. Once the rotation $\mathbf{T}$ has been computed, it can be applied to the diagonal matrix of the adiabatic energies $\mathbf{E}$ to get the Hamiltonian in the diabatic basis:

$$\mathbf{H}^{(dia)} = \mathbf{T}^{\dagger}\, \mathbf{E}\, \mathbf{T} \,. \tag{6.78}$$

The diagonal and off-diagonal elements of $\mathbf{H}$ are the diabatic state energies and the interactions between localized excitations, respectively.

The use of localized molecular orbitals (LMO) is necessary to define group functions and greatly facilitates any diabatization procedure, such as the one just sketched. Nonorthogonal LMOs can be produced by applying quantum chemistry methods (DFT, CASSCF, etc.) separately to single molecules or fragments that compose the whole system, as in the divide and conquer strategies seen above. Orthogonal LMOs can be produced by many localization procedures that are usually applied separately to different subsets of MOs. For instance, the many-electron wavefunction can be kept invariant by applying orthogonal localizing transformations to the occupied and virtual MOs obtained by HF or DFT calculations, and the same can be done with CASSCF by further separating the active MOs. Some localization algorithms were proposed with the aim of improving the efficiency of the configuration interaction method, as for instance the Foster–Boys procedure [31] that minimizes the second moments of the electron densities $|\phi_i|^2$ associated with the LMOs, or the Edmiston–Ruedenberg one [32], that maximize the self-repulsion. These two criteria make no explicit reference to the molecular structure. Other methods tend instead to place the LMOs in particular regions, i.e., near bonds, atoms, or groups of atoms [33–39]. Of particular interest in this context are the procedures put forward by de Silva et al. [40] and by Zhang and Li [38], which allow to choose the groups of atoms in which the user wants to bring the LMOs.

As a last remark, we feel that energy transfer and charge transfer, among other subjects of this textbook, are one of the fields in which the broadest variety of theoretical models and computational methods is being proposed and tested in the last years, probably because of the challenging problems posed by the attempt of understanding fundamental biological processes and of contributing to technological advancements.

Problems

6.1 In a study of the quenching of excited anthraquinone ($C_{14}H_8O_2$) by electron transfer to amines in gas phase [41], the bimolecular rate constant with pyridine (C_5H_5N) was found to be $2.3 \cdot 10^{-19}$ s^{-1} $molc^{-1}$ m^3, at $T = 433$ K. Compute the cross section and compare it with the geometrical cross section, obtained by considering two rigid spheres with volumes equal to the molecular volumes. To evaluate the volumes, use the density of solid anthraquinone (1.308 g/cm^3) and of liquid pyridine (0.982 g/cm^3).

6.2 Compute the average time between two gas-phase collisions and between two encounters in solution, for a given molecule. Make the following "standard" assumptions: hard spheres with radii = 4 Å and molecular masses = 100 a.m.u., $T = 300$ K, $P = 1$ atm, concentration of the other solute 1 mol/L, viscosity of the solvent 10^{-3} kg·m^{-1}s^{-1}.

Table 6.4 Wavelengths (nm) of S_1 and T_1 0–0 bands

	compound	S_1	T_1
A	Anthracene	378	681
B	Perylene	435	795
C	Tetracene	477	954
D	Pentacene	536	1440
E	Rubrene	519	1033

6.3 The wavelengths of the 0–0 bands of the $S_0 - S_1$ and $S_0 - T_1$ transitions are listed in Table 6.4 for five polynuclear aromatic hydrocarbons. Which donor–acceptor pairs satisfy the energy requisites to exhibit FRET? Same question for triplet sensitization. Which compounds are likely to undergo singlet fission? And which triplet–triplet annihilation?

6.4 Prove Eq. (6.62). Can we write a similar relationship for the oscillator strengths?

6.5 Consider an array on n identical chromophores put at the n vertices of a regular polygon, and the n corresponding diabatic states η_i of energy E_{ex} in which the excitation is localized in chromophore i (excitons). Assume their transition dipoles are all parallel and the coupling between the excitons is of Förster type. What is the form of the bright state? We shall apply the approximation that the only important couplings are those between first neighbors, with strength V. How good is this approximation, depending on n? Is the bright state an eigenstate within the subspace spanned by the excitons? What is its energy?

6.6 Three identical chromophores A, B, and C are placed at the vertices of an equilateral triangle. Their absorption transition dipoles have a component μ_r which is

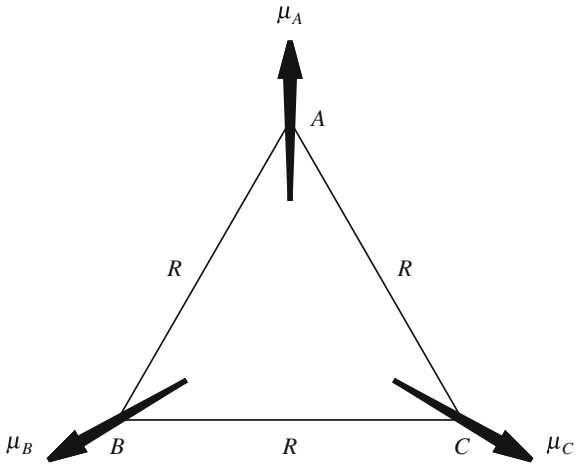

Fig. 6.10 Transition dipole moments for three chromophores symmetrically placed at the vertices of an equilateral triangle

radial with respect to the center of the triangle and a component μ_p perpendicular to the ABC plane, as shown in Fig. 6.10. Note that this could be a model for transitions centered in the equatorial ligands of a trigonal pyramid complex. The distance between the chromophores is R. Show that the excitation transfer dynamics among the four ligands, such as can be observed after a radiation pulse, has a period

$$T = \frac{8\pi\hbar R^3}{12\mu_p^2 + 21\mu_r^2} .$$

Calculate the period with $R = 15$ bohr, $\mu_p = 0.5$ a.u., and $\mu_r = 1$ a.u.

6.7 Same as the previous problem, but with a square arrangement. Four identical chromophores A, B, C, and D are placed at the vertices of a square. Their absorption transition dipoles have a component μ_r which is radial with respect to the center of the square and a component μ_p perpendicular to the $ABCD$ plane. The side of the square has length R. Show that the excitation transfer dynamics among the four ligands, such as can be observed after a radiation pulse, has a period

$$T = \frac{4\pi\hbar R^3}{\left(4+\sqrt{2}\right)\mu_p^2 + 2\left(3+\sqrt{2}\right)\mu_r^2} .$$

Calculate the period with $R = 15$ bohr, $\mu_p = 0.5$ a.u., and $\mu_r = 1$ a.u.

6.8 Prove Marcus' relationship, Eq. (6.73).

References

1. Subotnik, J.E., Cave, R.J., Steele, R.P., Shenvi, N.: The initial and final states of electron and energy transfer processes: diabatization as motivated by system-solvent interactions. J. Chem. Phys. **130**, 234102/1–14 (2009)
2. Voityuk, A.A.: Fragment transition density method to calculate electronic coupling for excitation energy transfer. J. Chem. Phys. **140**, 244117/1–7 (2014)
3. Voityuk, A.A.: Interaction of dark excited states. comparison of computational approaches. J. Phys. Chem. B **119**, 7417–7421 (2015)
4. Curutchet, C., Mennucci, B.: Quantum chemical studies of light harvesting. Chem. Rev. **117**, 294–343 (2017)
5. Favero, L., Granucci, G., Persico, M.: Dynamics of acetone photodissociation: a surface hopping study. Phys. Chem. Chem. Phys. **15**, 20651–20661 (2013)
6. Rohatgi-Mukherjee, K.K.: Fundamentals of Photochemistry. New Age International, New Delhi (2017)
7. Raišys, S., Kazlauskas, K., Juršiėas, S., Simon, Y.C.: The role of triplet exciton diffusion in light-upconverting polymer glasses. ACS Appl. Mater. Interfaces **8**, 15732–15740 (2016)
8. DeVries, P.L., Chang, C., George, T.F., Laskowski, B., Stallcop, J.R.: Computational study of alkali-metal - noble-gas collisions in the presence of nonresonant lasers: Na + Xe + $\hbar\omega_1$ + $\hbar\omega_2$ system. Phys. Rev. **22**, 545–550 (1980)

9. Angeli, C., Persico, M.: Quasi-diabatic and adiabatic states and potential energy curves for Na-Cd collisions and excimer formation. Chem. Phys. **204**, 57–64 (1996)
10. Reiland, W., Tittes, H.-U., Hertel, I.V., Bonačić-Koutecký, V., Persico, M.: Stereochemical effects in the quenching of Na^* ($3\,^2P$) by CO: crossed beam experiment and ab initio CI potential energy surfaces. J. Chem. Phys. **77**, 1908–1920 (1982)
11. McWeeny, R.: Methods of Molecular Quantum Mechanics. Academic Press, London (1992)
12. Smith, M.B., Michl, J.: Singlet fission. Chem. Rev. **110**, 6891–6936 (2010)
13. Dexter, D.L.: A theory of sensitized luminescence in solids. J. Chem. Phys. **21**, 836–850 (1953)
14. Förster, T.: Transfer mechanisms of electronic excitation. Discuss. Faraday Soc. **27**, 7–17 (1959)
15. Bottcher, C.J.: Theory of electric polarization. Elsevier, Amsterdam (1973)
16. Govorov, A., Martínez, P.L.H., Demir, H.V.: Understanding and Modeling Förster-Type Resonance Energy Transfer (FRET). Springer, Singapore (2016)
17. Medintz, I., Hildebrandt, N. (eds.): Förster Resonance Energy Transfer (FRET). From Theory to Applications. Wiley, Weinheim (2014)
18. Romstad, D., Granucci, G., Persico, M.: Nonadiabatic transitions and interference in photodissociation dynamics. Chem. Phys. **219**, 21–30 (1997)
19. Granucci, G., Mazzoni, M., Persico, M., Toniolo, A.: A computational study of the excited states of bilirubin IX. Phys. Chem. Chem. Phys. **7**, 2594–2598 (2005)
20. Newton, M.D.: The role of solvation in electron transfer: theoretical and computational aspects. In: Cammi, R., Mennucci, B. (eds.) Continuum Solvation Models in Chemical Physics: From Theory to Applications, pp. 389–413. Wiley, Chichester (2007)
21. Marcus, R.A.: On the theory of electron transfer reactions VI. unified treatment for homogeneous and electrode reactions. J. Chem. Phys. **43**, 679–701 (1965)
22. Cave, R.J., Edwards, S.T., Kouzelos, J.A., Newton, M.D.: Reduced electronic spaces for modeling donor/acceptor interactions. J. Phys. Chem. B **114**, 14631–14641 (2010)
23. Cave, R.J., Newton, M.D.: Multistate treatments of the electronic coupling in donor-bridge-acceptor systems: insights and caveats from a simple model. J. Phys. Chem. A **118**, 7221–7234 (2014)
24. Wibowo, M., Broer, R., Havenith, R.W.A.: A rigorous nonorthogonal configuration interaction approach for the calculation of electronic couplings between diabatic states applied to singlet fission. Comput. Theor. Chem. **1116**, 190–194 (2017)
25. Plasser, F., Granucci, G., Pittner, J., Barbatti, M., Persico, M., Lischka, H.: Surface hopping dynamics using a locally diabatic formalism: charge transfer in the ethylene dimer cation and excited state dynamics in the 2-pyridone dimer. J. Chem. Phys. **137**, 22A514/1–13 (2012)
26. Burghardt, I., Hynes, J.T.: Excited-state charge transfer at a conical intersection: effects of an environment. J. Phys. Chem. A **110**, 11411–11423 (2006)
27. Worth, G.A., Meyer, H.-D., Köppel, H., Cederbaum, L.S., Burghardt, I.: Using the MCTDH wavepacket propagation method to describe multimode non-adiabatic dynamics. Int. Rev. Phys. Chem. **27**, 569–606 (2008)
28. Malhado, J.P., Spezia, R., Hynes, J.T.: Dynamical friction effects on the photoisomerization of a model protonated Schiff base in solution. J. Phys. Chem. A **115**, 3720–3735 (2011)
29. Cimiraglia, R., Malrieu, J.-P., Persico, M., Spiegelmann, F.: Quasi diabatic states and dynamical couplings from ab initio CI calculations: a new proposal. J. Phys. B **18**, 3073 (1985)
30. Cattaneo, P., Persico, M.: Ab initio determination of quasi-diabatic states for multiple reaction pathways. Chem. Phys. **214**, 49 (1997)
31. Foster, J.M., Boys, S.F.: Canonical configurational interaction procedure. Rev. Mod. Phys. **32**, 300 (1960)
32. Edmiston, C., Ruedenberg, K.: Localized atomic and molecular orbitals. Rev. Mod. Phys. **35**, 457 (1963)
33. Magnasco, V., Perico, A.: Uniform localization of atomic and molecular orbitals I. J. Chem. Phys. **47**, 971–981 (1967)
34. Magnasco, A., Perico, V.: Uniform localization of atomic and molecular orbitals II. J. Chem. Phys. **48**, 800–808 (1968)

35. Pipek, J., Mezey, P.G.: A fast intrinsic localization procedure applicable for ab initio and semiempirical linear combination of atomic orbital wave functions. J. Chem. Phys. **90**, 4916–4926 (1989)
36. Høyvik, I.-M., Jansik, B., Jørgensen, P.: Pipek-Mezey localization of occupied and virtual orbitals. J. Comp. Chem. **34**, 1456–1462 (2013)
37. Lehtola, S., Jónsson, H.: Pipek-Mezey orbital localization using various partial charge estimates. J. Chem. Theory Comput. **10**, 642–649 (2014)
38. Zhang, C., Li, S.: An efficient localization procedure for large systems using a sequential transformation strategy. J. Chem. Phys. **141**, 244106/1–8 (2014)
39. Heßelmann, A.: Local molecular orbitals from a projection onto localized centers. J. Chem. Theory Comput. **12**, 2720–2741 (2016)
40. de Silva, P., Giebułtowski, M., Korchowiec, J.: Fast orbital localization scheme in molecular fragments resolution. Phys. Chem. Chem. Phys. **14**, 546–552 (2012)
41. Zalesskaya, G.A., Sambor, E.G., Bely, N.N.: Photoinduced gas-phase electron transfer reactions. J. Fluor. **14**, 173–180 (2004)

Appendix A
Physical Constants and Conversion Factors

The values of physical constants and conversion factors listed in this appendix are taken from NIST (https://physics.nist.gov/cuu/Constants/). According to the uncertainties quoted by NIST, all the digits here provided are correct.

Physical Constants, International System of Units (SI)

Name	Symbol	Numerical value	Units
Planck constant	h	$6.626070 \cdot 10^{-34}$	J·s
Planck constant/2π	$\hbar$	$1.054572 \cdot 10^{-34}$	J·s
Bohr radius	a_0	$0.529177 \cdot 10^{-10}$	m
Electron mass	m_e	$9.109384 \cdot 10^{-31}$	kg
Neutron mass	m_n	$1.674927 \cdot 10^{-27}$	kg
Proton mass	m_p	$1.672622 \cdot 10^{-27}$	kg
Atomic mass constant	m_u	$1.660539 \cdot 10^{-27}$	kg
Elementary charge	e	$1.602177 \cdot 10^{-19}$	C
Electric constant	ε_0	$8.854188 \cdot 10^{-12}$	F m^{-1}
Speed of light in vacuo	c	$2.99792458 \cdot 10^{8}$	m s^{-1}
Avogadro constant	N_A	$6.022141 \cdot 10^{23}$	
Boltzmann constant	K_B	$1.38065 \cdot 10^{-23}$	J K^{-1}
Molar gas constant	R	8.31446	J mol^{-1} K^{-1}

Energy Conversion Factors

From / to	kJ/mol	kcal/mol	hartree	eV	cm^{-1}
kJ/mol	1	0.239006	$3.80880 \cdot 10^{-4}$	0.0103643	83.5935
kcal/mol	4.184000	1	$1.59360 \cdot 10^{-3}$	0.0433641	349.755
Hartree	2625.50	627.509	1	27.21139	$2.194746 \cdot 10^{5}$
eV	96.4853	23.0605	0.03674932	1	8065.544
cm^{-1}	0.0119627	$2.859144 \cdot 10^{-3}$	$4.556335 \cdot 10^{-6}$	$1.239842 \cdot 10^{-4}$	1

M. Persico and G. Granucci, *Photochemistry*, Theoretical Chemistry and Computational Modelling, https://doi.org/10.1007/978-3-319-89972-5

Atomic Units

Physical constant or observable	a.u. value	SI unit	Conversion factor from	
			a.u. to SI	SI to a.u.
Electron mass, m_e	1			
Elementary charge, e	1			
Planck constant, h	2π			
Planck constant/2π ($\hbar$)	1			
Proton mass, m_p	1836.153			
Atomic mass constant	1822.888			
Bohr radius, a_0	1			
Electric constant, ε_0	$(4\pi)^{-1}$			
Hartree energy, E_h	1			
Rydberg energy, Ry	1/2			
Speed of light	137.035999			
Mass		kg	$9.109384 \cdot 10^{-31}$	$1.097769 \cdot 10^{30}$
Length		Å	0.529177	1.889726
Time		fs	0.02418884	41.341373
Charge		C	$1.602177 \cdot 10^{-19}$	$6.241509 \cdot 10^{18}$
Dipole		C·m	$8.47835 \cdot 10^{-30}$	$1.179475 \cdot 10^{29}$

The atomic unit of energy is also called “hartree” and the unit of length, “bohr.” The Ångström ($1\text{Å} = 10^{-10}$ m) is one of the most used units for length in molecular science.

The debye is a CGS unit, also much used in molecular science, equal to $3.33564 \cdot 10^{-30}$ C·m. The conversion factor from a.u. to debye is 2.541746, and from debye to a.u. is 0.3934303.

The angular frequency ω in atomic units is numerically equal to the corresponding energy $\hbar\omega$.

Appendix B
Dirac's Notation and Operator Algebra

In the notation introduced by Dirac [1, 2], a quantum mechanical state is represented as a ket, for instance $|\psi\rangle$. The set of all the physically meaningful states of a system is a vector space S, because of the linearity of the time-dependent Schrödinger equation. In the vector space S we indicate the scalar product of $|\psi_i\rangle$ and $\left|\psi_j\right\rangle$ as $\left\langle\psi_i \left|\psi_j\right.\right\rangle$. We assume the states to be explicitly represented by wavefunctions ψ that depend on the space (x_i, y_i and z_i) and spin (s_i) coordinates of N particles, collected in the vector

$$\mathbf{x} \equiv \{x_1, y_1, z_1, s_1 \ldots x_i, y_i, z_i, s_i \ldots x_n, y_n, z_n, s_n\} \equiv \{\mathbf{r}_1, s_1 \ldots \mathbf{r}_i, s_i \ldots \mathbf{r}_n, s_n\} \tag{B.1}$$

The "bracket" notation is a useful shorthand for the analytical definition of the scalar product between two wavefunctions, which is

$$\left\langle\psi_i \left|\psi_j\right.\right\rangle = \sum_{s_1 \ldots s_n} \int_{-\infty}^{+\infty} \psi_i^*(\mathbf{x})\psi_j(\mathbf{x})\, \mathrm{d}x_1\, \mathrm{d}y_1\, \mathrm{d}z_1 \ldots \mathrm{d}x_n\, \mathrm{d}y_n\, \mathrm{d}z_n \tag{B.2}$$

Here we sum over all the integer or half-integer values allowed for the z component of the spin of each particle, and we integrate over the three Cartesian coordinates, again for each particle. We see that this definition is consistent with the basic property of scalar products:

$$\left\langle\psi_j \left|\psi_i\right.\right\rangle = \left\langle\psi_i \left|\psi_j\right.\right\rangle^* \tag{B.3}$$

Now suppose $\left|\psi_j\right\rangle$ is a linear combination of other states:

$$\left|\psi_j\right\rangle = \sum_k c_k \left|\phi_k\right\rangle \tag{B.4}$$

Then

$$\left\langle\psi_i \left|\psi_j\right.\right\rangle = \sum_k c_k \left\langle\psi_i \left|\phi_k\right.\right\rangle \tag{B.5}$$

M. Persico and G. Granucci, *Photochemistry*, Theoretical Chemistry and Computational Modelling, https://doi.org/10.1007/978-3-319-89972-5

i.e., the scalar product is linear in the second vector. But, if a similar expansion is done for $|\psi_i\rangle$, i.e.,

$$|\psi_i\rangle = \sum d_k \, |\phi_k\rangle \tag{B.6}$$

we have

$$\langle \psi_i \, | \psi_j \, \rangle = \sum_k d_k^* \, \langle \phi_k \, | \psi_j \, \rangle \tag{B.7}$$

The complex conjugate coefficients in Eq. (B.7) introduce an apparent lack of symmetry between the first and second vector of the scalar product. This asymmetry can be removed by defining a dual space S', the elements of which are in biunivocal relationship with those of S and are indicated by the "bra" symbol $\langle \psi |$. If $|\psi_i\rangle$ is the linear combination (B.6), the corresponding bra is

$$\langle \psi_i | = \sum d_k^* \, \langle \phi_k | \tag{B.8}$$

Then, the scalar product can be seen as a "simple" product of a bra and a ket and is linear in the combination coefficients of both of them.

Operators convert a ket into another ket: $\hat{O} \, |\psi\rangle = |\phi\rangle$. We are interested in linear operators, i.e., operators that obey the rule:

$$\hat{O} \, \sum_k c_k \, |\phi_k\rangle = \sum_k c_k \; \hat{O} \; |\phi_k\rangle \tag{B.9}$$

An operator is defined when we know the result of its application to any ket in the vector space. We shall be mainly concerned with operators that map the vector space S into itself; i.e., if $|\psi\rangle \in S$, then also $\hat{O} \, |\psi\rangle \in S$. The expression $\left\langle \psi_i \left| \hat{O} \right| \psi_j \right\rangle = \langle \psi_i \, | \phi_j \, \rangle$ is then defined as the product of $\langle \psi_i |$ times the ket $|\phi_j\rangle = \hat{O} \, |\psi_j\rangle$. The adjoint of an operator is indicated with a superscript dagger and is defined by

$$\left\langle \psi_i \left| \hat{O}^\dagger \right| \psi_j \right\rangle = \left\langle \psi_j \left| \hat{O} \right| \psi_i \right\rangle^* \quad \forall \;\; |\psi_i\rangle \, , \, |\psi_j\rangle \in S \tag{B.10}$$

If $\hat{O}^\dagger = \hat{O}$, the operator $\hat{O}$ is said to be Hermitian.

The expression $|\psi_i\rangle \, \langle \psi_j|$ is a linear operator. In fact, if we apply it to any ket $|\phi\rangle$, we get the ket $|\psi_i\rangle$ times a constant that is linear in $|\phi\rangle$:

$$\left(|\psi_i\rangle \, \langle \psi_j| \right) \; |\phi\rangle = |\psi_i\rangle \; \langle \psi_j \, | \phi \, \rangle \tag{B.11}$$

If the ket $|\psi_i\rangle$ is normalized, i.e., $\langle \psi_i \, | \psi_i \, \rangle = 1$, we see that $\hat{P}_i = |\psi_i\rangle \, \langle \psi_i|$ is a projector, i.e., an Hermitian operator with the idempotency property $\hat{P}^2 = \hat{P}$. If $\{|\psi_1\rangle \ldots |\psi_n\rangle\}$ are a set of orthonormal vectors, i.e., $\langle \psi_i \, | \psi_j \, \rangle = \delta_{ij}$, then it easy to verify that

$$\hat{P} = \sum_{i=1}^{n} |\psi_i\rangle \langle\psi_i| \tag{B.12}$$

is also a projector.

We say that the vectors $\{|\psi_1\rangle \ldots |\psi_n\rangle\}$ form a basis for space S if any ket $|\phi\rangle \in S$ can be expressed as a linear combination of the basis elements:

$$|\phi\rangle = \sum_{i=1}^{n} c_i \ |\psi_i\rangle \quad \forall \ |\phi\rangle \in S \tag{B.13}$$

If the $|\psi_i\rangle$ are orthonormal, the projector

$$\hat{E} = \sum_{i=1}^{n} |\psi_i\rangle \langle\psi_i| \tag{B.14}$$

is the identity operator; i.e., its application leaves unchanged any vector:

$$\hat{E} |\phi\rangle = |\phi\rangle \quad \forall |\phi\rangle \in S \tag{B.15}$$

In fact, by applying the expression (B.14), often called "the resolution of identity," to the second member of Eq. (B.13) we find

$$\sum_{i=1}^{n} \sum_{j=1}^{n} |\psi_i\rangle \, c_j \, \langle\psi_i | \psi_j\rangle = \sum_{i=1}^{n} \sum_{j=1}^{n} |\psi_i\rangle \, c_j \, \delta_{ij} = \sum_{i=1}^{n} c_i \ |\psi_i\rangle \tag{B.16}$$

which shows the original vector is left unchanged. And, if we apply $\hat{E}$ to the first member we get

$$\hat{E} |\phi\rangle = \sum_{i=1}^{n} |\psi_i\rangle \langle\psi_i | \phi\rangle \tag{B.17}$$

whereby we see that the expansion coefficients are $c_i = \langle\psi_i | \phi\rangle$. The resolution of the identity can be used to express an operator through its representative matrix $\mathbf{O}$:

$$\hat{O} = \hat{E} \ \hat{O} \ \hat{E} = \sum_{i,j=1}^{n} |\psi_i\rangle \left\langle\psi_i \left| \hat{O} \right| \psi_j\right\rangle \langle\psi_j| = \sum_{i,j=1}^{n} |\psi_i\rangle \ O_{ij} \ \langle\psi_j| \tag{B.18}$$

The eigenvectors of Hermitian or unitary operators that map the vector space S into itself constitute a basis and can be chosen to be orthonormal. So, if the $|\psi_i\rangle$ are orthonormal eigenvectors of $\hat{O}$, Eq. (B.18) simplifies to

$$\hat{O} = \sum_{i=1}^{n} |\psi_i\rangle \ \lambda_i \ \langle\psi_i| \tag{B.19}$$

where λ_i is the eigenvalue associated with the eigenvector $|\psi_i\rangle$. The last equation allows us to define functions of operators. Given an ordinary function of complex variable $f(z)$, if every λ_i belongs to the domain of $f(z)$, we define

$$f(\hat{O}) = \sum_{i=1}^{n} |\psi_i\rangle \ f(\lambda_i) \ \langle\psi_i| \tag{B.20}$$

Two operators $\hat{A}$ and $\hat{B}$ are said to commute if

$$[\hat{A}, \hat{B}] \equiv \hat{A}\hat{B} - \hat{B}\hat{A} = 0 \tag{B.21}$$

The expression in square brackets, an operator, is called the commutator of $\hat{A}$ and $\hat{B}$. If two Hermitian operators commute, we can find a basis of orthonormal eigenvectors $|\psi_i\rangle$ of both operators:

$$\begin{aligned} \hat{A}\,|\psi_i\rangle &= \lambda_i\,|\psi_i\rangle \\ \hat{B}\,|\psi_i\rangle &= \mu_i\,|\psi_i\rangle \end{aligned} \tag{B.22}$$

To ascertain in which quantum state the system is, we can measure the physical observable represented by operator $\hat{A}$. Suppose the result of the measure is λ_i. If this is a nondegenerate eigenvalue, i.e., one state is associated with it, we know that the system is in state $|\psi_i\rangle$. But, if λ_i is a degenerate eigenvalue, the system can be in any of the two or more eigenstates associated with it, or in a linear combination of them. Then, to distinguish among these eigenstates, one must measure another property of the system, represented by an operator that has a basis of eigenvectors in common with $\hat{A}$. If we choose $\hat{B}$, the result of the measure may be a nondegenerate eigenvalue μ_i, so the problem of determining the state of the system is solved. Or, μ_i can be degenerate, but all the eigenstates associated with it, except $|\psi_i\rangle$, have eigenvalues of $\hat{A}$ different from λ_i: then, the state of the system is still univocally determined. The last possibility is that two or more eigenstates correspond to the eigenvalues λ_i and μ_i, so that the ambiguity persists. In this case we must look for a third observable that commutes with the first two, and so on. In the end, when every eigenstate is characterized by a unique set of eigenvalues, we say that a "complete set of commuting observables" has been identified. Note that we must avoid to include in the set a function of an operator $\hat{A}$ already selected, because its eigenvalues would have the same degeneracy pattern as those of $\hat{A}$.

For more complete and rigorous treatments, see, for instance, Dirac [1], Dennery and Krzywicki [2], or Merzbacher [3].

References

1. Dirac, P.A.M.: The Principles of Quantum Mechanics. Oxford University Press, Oxford (1947)
2. Dennery, P., Krzywicki, A.: Mathematics for Physicists. Dover, Mineola (1995)
3. Merzbacher, E.: Quantum Mechanics. Wiley, New York (1998)

Appendix C
The Dirac δ Function and the Normalization of Continuum States

The Dirac δ function is a generalized function or distribution. We use its properties in many instances and particularly to treat on the same footing discrete and continuous spectral decompositions. The δ function is defined with reference to the succession

$$d_n(x) = \sqrt{\frac{n}{\pi}}\, \mathrm{e}^{-nx^2} \quad \text{with } n = 1, 2 \ldots \tag{C.1}$$

By definition

$$\int_{-\infty}^{+\infty} \delta(x)\; g(x)\; \mathrm{d}x = g(0) \tag{C.2}$$

for all good functions $g(x)$. Good functions are functions of a real variable for which all derivatives exist and such that

$$\lim_{x \to \pm\infty} x^m\, \frac{\mathrm{d}^n g}{\mathrm{d}x^n} = 0 \quad \forall m, n \geq 0 \tag{C.3}$$

The proper value of $\delta(x)$ is zero for $x \neq 0$, and no proper value exists for $x = 0$.

The main properties of the δ function are:

$$\int_{-\infty}^{+\infty} \delta(x)\; \mathrm{d}x = 1 \tag{C.4}$$

$$\int_{-\infty}^{+\infty} \delta(x)\; f(x)\; \mathrm{d}x = f(0) \tag{C.5}$$

provided $f(x)$ is continuous in the neighborhood of $x = 0$.

$$\int_{-\infty}^{+\infty} \mathrm{e}^{\mathrm{i}\omega x}\; \mathrm{d}x = 2\pi\, \delta(\omega) \tag{C.6}$$

M. Persico and G. Granucci, *Photochemistry*, Theoretical Chemistry and Computational Modelling, https://doi.org/10.1007/978-3-319-89972-5

$$\int_a^b \delta(y(x))\ f(x)\ \mathrm{d}x = \sum_i f(x_i)\ \left|\frac{\mathrm{d}y}{\mathrm{d}x}\right|^{-1}_{x=x_i} \tag{C.7}$$

where the index i runs over all the zeros x_i of the function $y(x)$ with $x_i \in (a, b)$. The zeros must be nondegenerate, i.e., $(\mathrm{d}y/\mathrm{d}x)_{x=x_i} \neq 0$. If a zero falls at one of the integration limits ($x_i = a$ or $x_i = b$), we can apply Eq. (C.7) by counting only half of the contribution relative to x_i.

$$\int_{-\infty}^{x} \delta(x')\ \mathrm{d}x' = H(x) \tag{C.8}$$

where H is the Heaviside function

$$\begin{aligned} H(x) &= 0 \quad \forall x < 0 \\ H(x) &= 1 \quad \forall x > 0 \end{aligned} \tag{C.9}$$

For a more rigorous treatment of distributions and of the δ function, see textbooks of mathematics for physicists such as Dennery and Krzywicki [1] or Arfken, Weber and Harris [2].

In the previous section we introduced Dirac's notation for the elements of a vector space and in particular for the quantum states. The eigenstates of an operator $\hat{O}$ are associated with the respective eigenvalues, although in case of degeneracy the same eigenvalue is associated with more than one eigenstate. The degeneracy ambiguity is solved by identifying a complete set of commuting observables. Another complication is that, in many cases, we have to deal with sets of eigenvalues that are continuous, i.e., can be any real number in a certain interval. For instance, the eigenvalues of the Hamiltonian for a molecular system are in part made of discrete energy levels (those corresponding to bound states) and in part by two kinds of continua: the dissociative continuum, made of the vibrational states above the dissociation threshold reached when two or more groups of atoms get far apart from each other, and the electronic continuum, corresponding to ionization.

When the eigenvalue spectrum is continuous, we see that we cannot number the eigenstates as in Eq. (B.19). Leaving aside for simplicity the degenerate case, we can identify each eigenstate by its eigenvalue:

$$\hat{O}\ |\psi_\lambda\rangle = \lambda\ |\psi_\lambda\rangle \tag{C.10}$$

Now, if we want to generalize the resolution of identity, Eq. (B.14), we can write

$$\hat{E} = \sum_{i=1}^{n} |\psi_i\rangle\ \langle\psi_i| + \int_{\lambda_{min}}^{\lambda_{max}} |\psi_\lambda\rangle\ \langle\psi_\lambda|\ \mathrm{d}\lambda \tag{C.11}$$

Here the index i runs over the states of the discrete spectrum, if any, while the integration range covers the whole continuum spectrum (usually $\lambda_{max} = \infty$). If $|\psi_i\rangle$ and

$|\psi_\lambda\rangle$ are eigenstates of a normal operator, they are or can be chosen to be orthogonal, so $\hat{E}\ \left|\psi_j\right\rangle = \left|\psi_j\right\rangle$ as already seen in Appendix B. For a continuum state we have

$$\hat{E}\ |\psi_{\lambda'}\rangle = \int_{\lambda_{min}}^{\lambda_{max}} |\psi_\lambda\rangle\ \langle\psi_\lambda\,|\psi_{\lambda'}\rangle\ \mathrm{d}\lambda \tag{C.12}$$

Since eigenvectors with different eigenvalues are orthogonal, for $\lambda \neq \lambda'$ we have no contribution to the integral. If we want this expression to yield $|\psi_{\lambda'}\rangle$, we must require

$$\langle\psi_\lambda\,|\psi_{\lambda'}\rangle = \delta(\lambda - \lambda') \tag{C.13}$$

We shall then say that $|\psi_\lambda\rangle$ is "normalized to the δ of λ."

A simple example is provided by the dissociative states of diatomic molecules. The potential has a minimum at the equilibrium distance and then raises gradually (but not always monotonically) to an asymptote for large R. For energies larger than the asymptotic energy U_∞ the spectrum is continuous. In the asymptotic region, starting from a sufficiently large distance R_{asy}, the wavefunction of energy E is $\chi_E(R) = N(E)\,\cos(kR - \phi)$, where $k = \sqrt{2\mu(E - U_\infty)}/\hbar$, μ is the reduced mass, and ϕ is a phase that depends on E and on the shape of the potential for $R < R_{asy}$. We want to determine the normalization factor $N(E)$ so that $\langle\chi_E\,|\chi_{E'}\rangle = \delta(E - E')$. The orthogonality of the χ_E and $\chi_{E'}$ eigenfunctions for $E' \neq E$ is guaranteed. For $E' \to E$ we have an improper integral where the contribution of the finite interval $[0,\, R_{asy}]$ is irrelevant in comparison with the semi-infinite interval $[R_{asy}, \infty]$. So, for the purpose of determining the normalization factor we can replace the wavefunction at $R < R_{asy}$ with the asymptotic form and require:

$$N(E)\ N(E') \int_0^\infty \cos(kR - \phi)\,\cos(k'R - \phi')\,\mathrm{d}R = \delta(E - E') \tag{C.14}$$

where k' and ϕ' are the wavenumber and phase relative to E'. We see that the orthogonality of wavefunctions with $k' \neq k$ is still guaranteed, so we can concentrate on the case $k' \to k$ and $\phi' \to \phi$. After converting the cosine functions to exponentials the first member becomes

$$\begin{aligned}\frac{N(E)\ N(E')}{4} \quad & \left[\mathrm{e}^{-\mathrm{i}(\phi+\phi')}\int_0^\infty \mathrm{e}^{\mathrm{i}(k+k')R}\mathrm{d}R + \mathrm{e}^{\mathrm{i}(\phi+\phi')}\int_0^\infty \mathrm{e}^{-\mathrm{i}(k+k')R}\mathrm{d}R + \right. \\ & \left. + \mathrm{e}^{-\mathrm{i}(\phi-\phi')}\int_0^\infty \mathrm{e}^{\mathrm{i}(k-k')R}\mathrm{d}R + \mathrm{e}^{\mathrm{i}(\phi-\phi')}\int_0^\infty \mathrm{e}^{-\mathrm{i}(k-k')R}\mathrm{d}R\right] = \\ = \frac{N(E)\ N(E')}{4} & \int_{-\infty}^{+\infty} \mathrm{e}^{-\mathrm{i}(k-k')R}\mathrm{d}R = \frac{\pi\ N^2(E)}{2}\ \delta(k - k')\end{aligned} \tag{C.15}$$

We get a normalization to the δ of the wavenumber k if we put $N^2(E) = 2/\pi$, but in order to normalize to the δ of energy we need to convert $\delta(k - k')$ to $\delta(E - E')$:

$$\delta(k-k') = \delta\left[\frac{\sqrt{2\mu}}{\hbar}\left(\sqrt{E-U_\infty}-\sqrt{E'-U_\infty}\right)\right] = \sqrt{\frac{2\hbar^2(E-U_\infty)}{\mu}}\,\delta(E-E') \tag{C.16}$$

The last passage makes use of Eq. (C.7). So, the normalization factor we need is:

$$N(E) = \left[\frac{2\mu}{\pi^2\hbar^2(E-U_\infty)}\right]^{1/4} \tag{C.17}$$

References

1. Dennery, P., Krzywicki, A.: Mathematics for Physicists. Dover, Mineola (1995)
2. Arfken, G.B., Weber, H.J., Harris, F.E.: Mathematical Methods for Physicists. Elsevier, Amsterdam (2012)

Appendix D
Two-State Eigenvector Problem

Although this problem is trivial, it is convenient to write out its solution that is referred to more than once in this book, in order to use the same formulation in all cases. By doing so, we shall remove some arbitrariness which is intrinsic of eigenvector problems (signs or phase factors and ordering of eigenvectors), by setting our conventional choices.

In a basis of two orthonormal states $|1\rangle$ and $|2\rangle$ the Hamiltonian is represented by the matrix elements $H_{ij} = \left\langle i \left| \hat{H} \right| j \right\rangle$. If $H_{12} = H_{21} \in \mathbb{R}$, the eigenvector coefficients can also be chosen real:

$$\begin{aligned} |\psi_1\rangle &= \cos\theta \ |1\rangle + \sin\theta \ |2\rangle \\ |\psi_2\rangle &= -\sin\theta \ |1\rangle + \cos\theta \ |2\rangle \end{aligned} \tag{D.1}$$

where $\theta \in \mathbb{R}$ is the only parameter to be determined, thanks to the orthonormality constraints that are automatically satisfied by Eq. D.1. The solutions of the secular equation are the eigenvalues E_- and E_+:

$$E_\pm = \frac{H_{11} + H_{22} \pm \sqrt{\Delta H^2 + 4H_{12}^2}}{2} \tag{D.2}$$

where $\Delta H = H_{22} - H_{11}$. If we associate the lowest eigenvalue, E_-, to the first eigenstate, $|\psi_1\rangle$, we get

$$\begin{cases} H_{11} \ \cos\theta + H_{12} \ \sin\theta = E_- \ \cos\theta \\ H_{21} \ \cos\theta + H_{22} \ \sin\theta = E_- \ \sin\theta \end{cases} \tag{D.3}$$

Provided $H_{12} \neq 0$, these equations are solved by putting

$$\mathrm{tg}\,\theta = \frac{\Delta H - \sqrt{\Delta H^2 + 4H_{12}^2}}{2H_{12}} \tag{D.4}$$

which can also be written as

M. Persico and G. Granucci, *Photochemistry*, Theoretical Chemistry and Computational Modelling, https://doi.org/10.1007/978-3-319-89972-5

$$\mathrm{tg}(2\theta) = -\frac{2H_{12}}{\Delta H} \tag{D.5}$$

The coefficients are obtained with the usual formulas

$$\cos\theta = \frac{1}{\sqrt{1+\mathrm{tg}^2\,\theta}} \quad \text{and} \quad \sin\theta = \frac{\mathrm{tg}\,\theta}{\sqrt{1+\mathrm{tg}^2\,\theta}} \tag{D.6}$$

Here we have arbitrarily chosen $\cos\theta > 0$, so the sign of $\sin\theta$ is the same as that of $\mathrm{tg}\,\theta$. As we see from Eq. (D.4), $\mathrm{tg}\,\theta$ is opposite in sign to H_{12}. If $H_{12} = 0$, $|\psi_1\rangle$ coincides with either $|1\rangle$ or $|2\rangle$, whichever is the lower in energy. So, if $\Delta H > 0$, $|\cos\theta| = 1$ and $\sin\theta = 0$ and vice versa if $\Delta H < 0$. If the Hamiltonian matrix depends on one or more parameters, as in the case of the electronic Hamiltonian that is a function of the nuclear coordinates, one can use the arbitrariness in the sign of the eigenvectors to ensure continuity as $H_{12} \to 0$.

If H_{12} is complex, say $H_{12} = |H_{12}|\,\mathrm{e}^{\mathrm{i}\gamma}$ and $H_{21} = |H_{12}|\,\mathrm{e}^{-\mathrm{i}\gamma}$ with $\gamma \in \mathbb{R}$, the eigenvector coefficients are in general complex too. It is, however, possible to reduce the problem to the real case, by multiplying the basis states by suitable phase factors. For instance, by replacing $|2\rangle$ with $\mathrm{e}^{-\mathrm{i}\gamma}\,|2\rangle$, the Hamiltonian matrix is real again, with $|H_{12}|$ instead of H_{12} and H_{21}. So, the solutions are

$$E_\pm = \frac{H_{11} + H_{22} \pm \sqrt{\Delta H^2 + 4\,|H_{12}|^2}}{2} \tag{D.7}$$

and

$$\begin{aligned} |\psi_1\rangle &= \cos\theta\ \ |1\rangle + \sin\theta\ \mathrm{e}^{-\mathrm{i}\gamma}\ \ |2\rangle \\ |\psi_2\rangle &= -\sin\theta\ \ |1\rangle + \cos\theta\ \mathrm{e}^{-\mathrm{i}\gamma}\ \ |2\rangle \end{aligned} \tag{D.8}$$

with

$$\mathrm{tg}\,\theta = \frac{\Delta H - \sqrt{\Delta H^2 + 4\,|H_{12}|^2}}{2|H_{12}|}\ . \tag{D.9}$$

Appendix E
Orbital Localization and Orthogonality

Localized molecular orbitals (MOs) are a key concept to discuss phenomena such as charge and excitation transfer (see Chap. 6) and also a useful tool to improve computational efficiency. Theoretical developments, however, may require that all MOs are orthogonal, and this may limit the extent of localization. In this appendix we work out a very simple example that clarifies this aspect.

We consider two equivalent 1s orbitals of two hydrogen atoms, labeled χ_a and χ_b:

$$\chi_\alpha(\mathbf{r}) = \pi^{-1/2}\, \mathrm{e}^{-|\mathbf{r}-\mathbf{R}_\alpha|}\ . \tag{E.1}$$

Here we use atomic units and $\mathbf{R}_\alpha$ is the position of the nucleus, with $\alpha = a$ or b. The overlap integral of the two orbitals is

$$S_{ab} = \langle \chi_a \,|\chi_b \rangle = \mathrm{e}^{-R}\left(1 + R + \frac{1}{3}R^2\right) \tag{E.2}$$

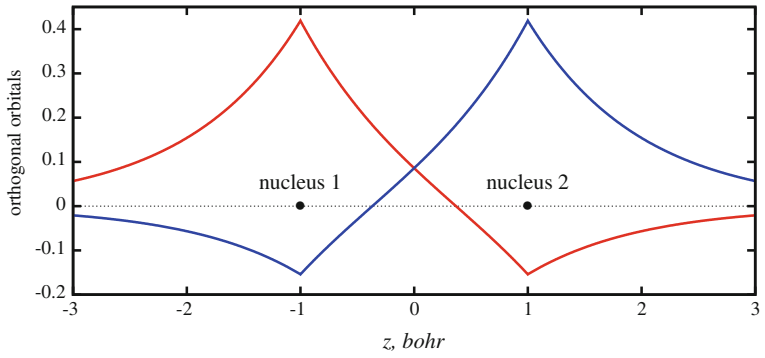

Fig. E.1 Two equivalent and orthogonal combinations of hydrogen 1s orbitals. The two functions are plotted along the internuclear axis, chosen to be the z-axis. The nuclei are 2 bohr apart from each other

M. Persico and G. Granucci, *Photochemistry*, Theoretical Chemistry
and Computational Modelling, https://doi.org/10.1007/978-3-319-89972-5

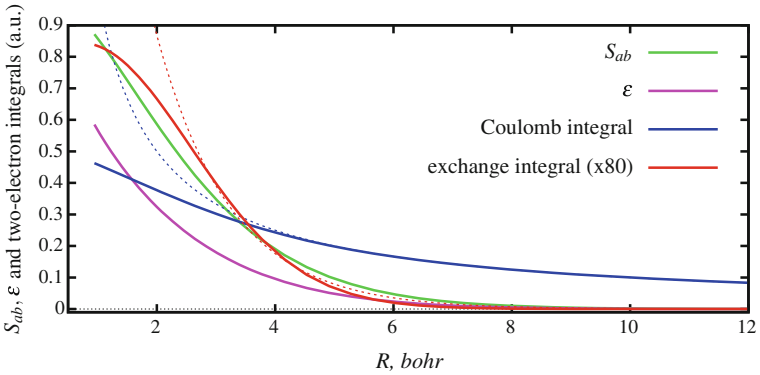

Fig. E.2 Symmetric orthogonalization of two hydrogen 1s orbitals a and b. Overlap S_{ab}, ε coefficient (see Eq. (E.4)), Coulomb and exchange integrals for the orthonormal orbitals, as functions of the internuclear distance R. Dotted lines: $1/R$ function that approximates the Coulomb integral at large distances, and an exponential function fitting the exchange integral for $R > 2.5$ bohr

Here R is the internuclear distance $|\mathbf{R}_a - \mathbf{R}_b|$.

We shall define two equivalent and orthonormal orbitals

$$\begin{aligned} \varphi_a &= \frac{\chi_a - \varepsilon\, \chi_b}{\left(1 - 2\varepsilon S_{ab} + \varepsilon^2\right)^{1/2}} \\ \varphi_b &= \frac{\chi_b - \varepsilon\, \chi_a}{\left(1 - 2\varepsilon S_{ab} + \varepsilon^2\right)^{1/2}} \,. \end{aligned} \tag{E.3}$$

The orthogonality of φ_a and φ_b requires

$$\varepsilon = \frac{1 \pm \sqrt{1 - S_{ab}^2}}{S_{ab}} \,. \tag{E.4}$$

We choose the solution with the minus sign to minimize the "queue" of the φ_a orbital on the b nucleus and vice versa. The orbitals we obtain this way are shown in Fig. E.1. This is the simplest example of Löwdin's symmetric orthogonalization [1], a method to transform a set of nonorthogonal (but normalized) basis functions $\{\ldots \chi_i \ldots\}$ into an orthonormal one $\{\ldots \varphi_i \ldots\}$:

$$\{\ldots \varphi_i \ldots\} = \{\ldots \chi_i \ldots\}\, \mathbf{S}^{-1/2} \tag{E.5}$$

where $\mathbf{S}$ is the overlap matrix ($S_{ij} = \langle \chi_i \,|\, \chi_j \rangle$). It can be shown [2] that this method yields a set of functions that are as close as possible to the original ones in the sense of least squares; i.e., $\sum_i \langle \varphi_i - \chi_i \,|\, \varphi_i - \chi_i \rangle$ is minimized. So, starting from atomic orbitals, one gets the set of orthogonal functions that are most localized.

The interactions between electrons placed in the φ_a and φ_b orbitals are represented by the Coulomb and exchange integrals

$$\left\langle \varphi_a \varphi_b \left| r_{12}^{-1} \right| \varphi_a \varphi_b \right\rangle \qquad \text{and} \qquad \left\langle \varphi_a \varphi_b \left| r_{12}^{-1} \right| \varphi_b \varphi_a \right\rangle \ . \tag{E.6}$$

Figure E.2 shows the dependence of S_{ab}, ε and the two-electron integrals on the internuclear distance. As the internuclear distance increases the overlaps between the χ_α functions and between the charge distributions $\rho_\alpha = -\chi_\alpha^2$ tend to zero. So, the queue of each φ_α orbital on the other nucleus, that is proportional to ε, tends to vanish and $\varphi_\alpha \to \chi_\alpha$. Therefore, when R is large enough the Coulomb integral approaches the interaction of two nonoverlapping spherical charge distributions, i.e., tends to $1/R$ as shown in Fig. E.2 (note that this interaction is perfectly balanced by the nucleus–electron attractions plus the nucleus–nucleus repulsion). At the same time the exchange integral decreases much faster, because the integrand contains two factors $\varphi_a(\mathbf{r}_i)\varphi_b(\mathbf{r}_i)$, with $i = 1, 2$, that are everywhere small when the two orbitals are not overlapping. The dependence of the exchange integral on R beyond an intermediate distance (say 2.5 bohr) can be approximated by an exponential function, as shown in Fig. E.2.

References

1. Lowdin, P.-O.: On the Nonorthogonality problem connected with the use of atomic wavefunctions in the theory of molecules and crystals. J. Chem. Phys. **18**, 365–375 (1950)
2. Mayer, I.: On Löwdin's method of symmetric orthogonalization. Int. J. Quantum Chem. **90**, 63–65 (2002)

Appendix F
The Harmonic Oscillator

The harmonic oscillator is one of the most prominent paradigms in physics, but is also a system with some important peculiarities, in particular at dynamical level [1, 2, 3, 4, 5], as first noted by Galileo. Here we shall review, without deriving them, some of the basic properties of the quantum harmonic oscillator. More complete treatments can be found in almost any textbook on quantum mechanics, for instance Merzbacher [6], Chaps. 5 and 10.

The harmonic oscillator Hamiltonian is

$$\hat{H} = \frac{1}{2m}\ \hat{p}_x^2 + \frac{m\omega^2}{2}(x - x_e)^2 \tag{F.1}$$

where $\hat{p}_x = -\mathrm{i}\hbar \mathrm{d}/\mathrm{d}x$. We replace x and $\hat{p}_x$ by the dimensionless coordinates q and $\hat{p}$:

$$q = \sqrt{\frac{m\omega}{\hbar}}\ (x - x_e) \quad \text{and} \quad \hat{p} = \frac{1}{\sqrt{\hbar m\omega}}\ \hat{p}_x = -\mathrm{i}\frac{\mathrm{d}}{\mathrm{d}q}\ . \tag{F.2}$$

Then $\hat{H}$ takes a more symmetric quadratic form:

$$\hat{H} = \frac{\hbar\omega}{2}\ \left(\hat{p}^2 + q^2\right)\ . \tag{F.3}$$

The eigenvalues of $\hat{H}$ are

$$E_n = \hbar\omega\ \left(n + \frac{1}{2}\right) \quad \text{for } n = 0, 1, 2... \tag{F.4}$$

and the corresponding eigenfunctions are

$$\chi_n(q) = N_n\ H_n(q)\ \mathrm{e}^{-q^2/2} = N_n\ H_n\left(\sqrt{\frac{m\omega}{\hbar}}(x - x_e)\right)\ \mathrm{e}^{-\frac{m\omega}{2\hbar}(x-x_e)^2} \tag{F.5}$$

M. Persico and G. Granucci, *Photochemistry*, Theoretical Chemistry and Computational Modelling, https://doi.org/10.1007/978-3-319-89972-5

Here the H_n are the Hermite orthogonal polynomials that can be derived from Rodriguez' formula

$$H_n(q) = (-1)^n \, \mathrm{e}^{q^2} \, \frac{\mathrm{d}^n}{\mathrm{d}q^n} \mathrm{e}^{-q^2} \tag{F.6}$$

resulting in

$$\begin{aligned} &H_0(q) = 1 \\ &H_1(q) = 2q \\ &H_2(q) = 4q^2 - 2 \\ &H_3(q) = 8q^3 - 12q \\ &H_4(q) = 16q^4 - 48q^2 + 12 \\ &\ldots \end{aligned} \tag{F.7}$$

The normalization factor is

$$N_n = \frac{1}{\sqrt{2^n n!}} \left(\frac{m\omega}{\pi \hbar} \right)^{1/4} . \tag{F.8}$$

The eigenfunction χ_n has n nodes and is an even or odd function of q or $x - x_e$, the parity being that of the quantum number n. The χ_n obey a simple recursion formula that can be expressed as a property of the Hermite polynomials:

$$H_{n+1}(q) = 2q \, H_n(q) - 2n \, H_{n-1}(q) \, . \tag{F.9}$$

Alternatively, one can define the ladder operators

$$\hat{a} = \frac{q + \mathrm{i}\hat{p}}{\sqrt{2}} \quad \text{and} \quad \hat{a}^\dagger = \frac{q - \mathrm{i}\hat{p}}{\sqrt{2}} \tag{F.10}$$

with the following properties:

$$\hat{a} \; \chi_n(q) = \sqrt{n} \; \chi_{n-1}(q) \tag{F.11}$$

$$\hat{a}^\dagger \; \chi_n(q) = \sqrt{n+1} \; \chi_{n+1}(q) \, . \tag{F.12}$$

From Eq. (F.10) one gets

$$q = \frac{\hat{a} + \hat{a}^\dagger}{\sqrt{2}} \quad \text{and} \quad \hat{p} = \frac{\hat{a} - \hat{a}^\dagger}{\sqrt{2}\mathrm{i}} \, . \tag{F.13}$$

These relationships are quite useful to compute matrix elements of q, $\hat{p}$, x, $\hat{p}_x$, as well as their powers and products. For instance

$$\langle \chi_n \, | x | \, \chi_{n'} \rangle = x_e \delta_{n,n'} + \langle \chi_n \, | x - x_e | \, \chi_{n'} \rangle = x_e \delta_{n,n'} + \sqrt{\frac{\hbar}{m\omega}} \, \langle \chi_n \, | q | \, \chi_{n'} \rangle \tag{F.14}$$

and

$$\langle \chi_n \, |q| \, \chi_{n'} \rangle = \frac{1}{\sqrt{2}} \left\langle \chi_n \left| \hat{a} + \hat{a}^\dagger \right| \chi_{n'} \right\rangle = \sqrt{\frac{n+1}{2}} \delta_{n+1,n'} + \sqrt{\frac{n}{2}} \delta_{n-1,n'} \, . \qquad \text{(F.15)}$$

References

1. Heller, E.J.: Time–dependent approach to semiclassical dynamics. J. Chem. Phys. **62**, 1544–1555 (1975)
2. Heller, E.J.: The semiclassical way to molecular spectroscopy Acc. Chem. Res. **14**, 368–375 (1981)
3. Tannor, D.J., Heller, E.J.: Polyatomic Raman scattering for general harmonic potentials. J. Chem. Phys. **77**, 202–218 (1982)
4. Heller, E.J., Sundberg, R.L., Tannor, D.: Simple aspects of Raman scattering. J. Phys. Chem. **86**, 1822–1833 (1982)
5. Tannor, D.J.: Introduction to Quantum Mechanics: A Time-dependent Perspective. University Science Books, Sausalito (2007)
6. Merzbacher, E.: Quantum Mechanics. Wiley, New York (1998)

Appendix G
Animations

This appendix contains the captions for the animations that illustrate some time-dependent properties discussed in Chaps. 3, 4 and 5.

- **Animation 3.1**
  This animation shows the change in time of the function

$$f(\omega, t) = \left[\frac{\sin(\omega\, t/2)}{\omega}\right]^2$$

  which is discussed in Sect. 3.5. During the animation the frequency scale changes twice, to adapt to the shrinking width of the function. The maximum at $\omega = 0$ is kept equal to 1; i.e., we actually plot $f(\omega, t)$ multiplied by the factor $4/t^2$.
  The purpose is to show how the spectral resolution, achieved by exciting with a continuous wave pulse of light, improves with the length of the pulse.
- **Animation 4.1**
  In this animation we show the dynamics of a wavepacket which is created by electronic excitation by a radiation pulse.
  One coordinate is considered, and both the ground and the excited state have harmonic potential energy curves (see Fig. 4.1), namely:

$$U_g(R) = \frac{1}{2} K_g (R - R_g)^2$$

  and

$$U_e(R) = \frac{1}{2} K_e (R - R_e)^2$$

  where $R_g = 4$ bohr, $R_e = 5.5$ bohr, $K_g = 0.075$ a.u., $K_e = 0.0144$ a.u. The reduced mass is 30000 a.u.

M. Persico and G. Granucci, *Photochemistry*, Theoretical Chemistry and Computational Modelling, https://doi.org/10.1007/978-3-319-89972-5

The radiation pulse is Gaussian, with the electric field given by:

$$E(t) = E_{max}\ \mathrm{e}^{-t^2/4\tau^2}\ \sin(\omega\, t)$$

In this simulation, $\tau = 10$ fs. The transition dipole is considered constant and equal to 1 a.u. The electric field amplitude $E_{max} = 0.001$ is sufficiently small as to be in the perturbative regime, but the simulation is numerically exact and does not make use of perturbation theory.
The excited wavepacket is represented as its squared module, $|\Theta_e(R)|^2$.

- **Animation 4.2**
The same as in animation 4.1, but with a longer pulse, $\tau = 60$ fs.
- **Animation 4.3**
The same as in animation 4.1, but with a still longer pulse, $\tau = 250$ fs.
- **Animation 4.4**
In this animation we show the dynamics of a wavepacket which is created by electronic excitation by a radiation pulse, just as in the previous ones, but the two potential energy curves are Morse functions (see Fig. 4.1). Namely:

$$U_g(R) = D_g\left(1 - \mathrm{e}^{-\alpha_g(R-R_g)}\right)^2$$

and

$$U_e(R) = D_e\left(1 - \mathrm{e}^{-\alpha_e(R-R_e)}\right)^2$$

where $R_g = 4$ bohr, $R_e = 5.5$ bohr, $D_g = 0.15$ a.u., $D_e = 0.08$ a.u., $\alpha_g = 0.5$ a.u., and $\alpha_e = 0.3$ a.u. The reduced mass is 30000 a.u.
The radiation pulse is Gaussian, with the electric field given by:

$$E(t) = E_{max}\ \mathrm{e}^{-t^2/4\tau^2}\ \sin(\omega\, t)$$

In this simulation, $\tau = 10$ fs. The transition dipole is considered constant and equal to 1 a.u. The electric field amplitude $E_{max} = 0.001$ is sufficiently small as to be in the perturbative regime, but the simulation is numerically exact and does not make use of perturbation theory.
The excited wavepacket is represented as its squared module, $|\Theta_e(R)|^2$.

- **Animation 4.5**
The same as in animation 4.4, but with a longer pulse, $\tau = 60$ fs.
- **Animation 4.6**
The same as in animation 4.4, but with a still longer pulse, $\tau = 250$ fs.
- **Animation 5.1**
This animation shows a wavepacket going through a conical intersection. The potential energy surfaces are depicted in Fig. 5.6. We simulated the dynamics in two coordinates, Q_S and Q_A, and the conical intersection point is at $Q_S = 3$

and $Q_A = 0$ bohr. Although the numerical calculations are done in the diabatic representation, in practice the wavepacket moves on the lower adiabatic surface only.

The adiabatic wavepacket Θ_1 is shown as contour plots of the probability density $|\Theta_1(Q_S, Q_A, t)|^2$. The purpose is to show the effect of the geometric phase, as discussed in Sect. 5.4.3.

Solutions

Problems of Chap. 1

1.1 If $\lambda^{-1} = 1500\ \text{cm}^{-1} = 1.5 \cdot 10^5\ \text{m}^{-1}$, $E = hc/\lambda = 2.9797 \cdot 10^{-20}$ J. For a mole, and using kJ instead of J, $E = 2.9797 \cdot 10^{-20} \cdot N_A/1000 = 17.94$ kJ/mol. More simply, use the conversion factor from cm^{-1} to kJ/mol, 0.0119627 (see Appendix A).
A wavelength of 500 nm corresponds to $\lambda^{-1} = 10^9/500\ \text{m}^{-1} = 10^7/500\ \text{cm}^{-1} = 20000\ \text{cm}^{-1} = 20000 \cdot 0.0119627$ kJ/mol = 239.25 kJ/mol.

1.2 The He–Ne laser delivers 10^{-3} W on a surface of $\pi \cdot 10^{-6}\ \text{m}^2$, so the irradiance is $10^{-3}/(\pi \cdot 10^{-6}) = 318\ \text{W/m}^2$.
The power of the tungsten lamp emitted in the visible spectrum is 2 W. At a distance of 2 m it is spread on a spherical surface of $4\pi \cdot 2^2 = 50.3\ \text{m}^2$, so the irradiance is $2/50.3 = 0.0398\ \text{W/m}^2$.

1.3 With $\varepsilon = 1000\ \text{mol}^{-1}\ \text{L cm}^{-1}$, a thin layer of thickness l m, with a concentration of 1 mol/L, absorbs a fraction $\ln(10) \cdot 1000 \cdot 100 \cdot l = 2.3 \cdot 10^5 l$ of the impinging light. If the irradiance is 100 W/m^2, a layer of area 1 m^2 absorbs $2.3 \cdot 10^7 l$ W. Since at $\lambda = 500$ nm one photon has the energy of 239.25 kJ/mol (see Problem 1.1), the layer would absorb $2.3 \cdot 10^7 l/239250 = 96.2\ l$ mol of photons per second. In the volume of the layer, l m^3, there are 1000 l mol, so each molecule absorbs in the average $96.2\ l/(1000\ l) = 0.0962$ photons per second, i.e., a photon every 10.4 s.

1.4 If, to excite CCl_3CF_3, we need $\lambda > 220$ nm, the photon energy is $h\nu > 10^7/220 = 45450\ \text{cm}^{-1}$. The C-Cl dissociation energy is 330 kJ/mol = 27600 cm^{-1} (see the conversion factor in Appendix A). Then, the photon energy is well above the bond dissociation energy and the limiting factor for the photodissociation is the absorption spectrum.

1.5 The lifetime of T_1 of benzophenone is determined by the rates of ISC and phosphorescence: $\tau_{T_1} = (1/0.06 + 1/0.007)^{-1} = 0.0063$ s. The rate of ISC starting from S_1 is so much higher than the rate of any other process involving this state

M. Persico and G. Granucci, *Photochemistry*, Theoretical Chemistry and Computational Modelling, https://doi.org/10.1007/978-3-319-89972-5

that it coincides with its lifetime. Since the triplet quantum yield of benzophenone is practically 1, its phosphorescence quantum yield is the emission rate τ_P^{-1} times the triplet lifetime: $\Phi_P = \tau_{T_1}/\tau_P = 0.0063/0.007 = 0.90$.
For naphthalene we have similarly: $\tau_{T_1} = 2.4 \cdot 10^{-6}$ s = 2.4 μs and $\tau_{S_1} = (1/2 + 1 + 1/2)^{-1} = 0.5$ μs. The triplet quantum yield is $(1/2)/((1/2 + 1 + 1/2) = 0.25$, so $\Phi_P = 0.25\ \tau_{T_1}/\tau_P = 0.0017$. The fluorescence quantum yield is $\tau_{S_1}/\tau_F = 0.5$.

1.6 In the experiment of Fig. 1.5, at 150 s we have practically the asymptotic concentrations. If we increase the thermal rate constants to $K'_{A\to B} = 1.8 \cdot K_{A\to B}$ and $K'_{B\to A} = 1.5 \cdot K_{B\to A}$, the asymptote is approached even faster, so a fortiori at 150 s we have

$$\frac{[\mathrm{B}]}{[\mathrm{A}]} \simeq \frac{[\mathrm{B}]_\infty}{[\mathrm{A}]_\infty} = \frac{J_{A\to B}}{K'_{B\to A}} + \frac{K'_{A\to B}}{K'_{B\to A}}$$

The last equality stems from Eq. (1.75). Now, with the old rate constants we had $[\mathrm{B}]_\infty/[\mathrm{A}]_\infty = 3.44$ (data read from Fig. 1.5). At thermal equilibrium, $[\mathrm{B}]/[\mathrm{A}] = K_{A\to B}/K_{B\to A} = 0.111$ (data taken again from Fig. 1.5), so $J_{A\to B}/K_{B\to A} = 3.44 - 0.11 = 3.33$. With the new rate constants, $K'_{A\to B}/K'_{B\to A} = 0.111 \cdot 1.8/1.5 = 0.133$ and $J_{A\to B}/K'_{B\to A} = 3.33/1.5 = 2.22$. Then, $[\mathrm{B}]_\infty/[\mathrm{A}]_\infty = 2.22 + 0.13 = 2.35$ and the fraction of B is 0.70.

Problems of Chap. 2

2.1 In the momentum representation we have $\hat{H}(p) = p^2/2m - \mathrm{i}\hbar F\,\mathrm{d}/\mathrm{d}p$. The stationary states $\psi_E(p)$ are found by solving the time-independent Schrödinger equation

$$\frac{\mathrm{d}\psi_E}{\mathrm{d}p} + \frac{\mathrm{i}}{\hbar F}\left(\frac{p^2}{2m} - E\right)\psi_E = 0$$

which gives

$$\psi_E(p) = \frac{1}{\sqrt{2\pi\hbar F}} \exp\left[\frac{\mathrm{i}}{\hbar F}\left(Ep - \frac{p^3}{6m}\right)\right]$$

with a normalization factor such that $\langle \psi_E \,|\psi_{E'}\rangle = \delta(E - E')$. According to (2.31) we have

$$\begin{aligned}\Psi(p,t) &= \int_{-\infty}^{+\infty} \langle \psi_E \,|\Psi(0)\rangle\, \mathrm{e}^{-\mathrm{i}Et/\hbar}\psi_E \mathrm{d}E \\ &= \left(\frac{2\alpha}{\pi}\right)^{1/4} \frac{\mathrm{e}^{-\mathrm{i}p^3/6\hbar Fm}}{2\pi\hbar F} \int_{-\infty}^{+\infty} \mathrm{e}^{-\alpha x^2} \mathrm{e}^{\mathrm{i}x^3/6\hbar Fm} \int_{-\infty}^{+\infty} \mathrm{e}^{\mathrm{i}(p-Ft-x)E/\hbar F} \mathrm{d}E\mathrm{d}x\ .\end{aligned}$$

According to (C.6) the integral in $\mathrm{d}E$ is proportional to a Dirac δ (in particular it corresponds to $2\pi\hbar F\delta(p - Ft - x)$), so we finally obtain

$$\Psi(p,t) = \left(\frac{2\alpha}{\pi}\right)^{1/4} \exp\left[\mathrm{i}\frac{(p - Ft)^3 - p^3}{6\hbar Fm} - \alpha(p - Ft)^2\right]\ .$$

2.2 For a single Morse oscillator, the number of levels with energy $\leq E_v$ is just $v+1$. Therefore

$$N(E_v) = v + 1 = \frac{2D}{\hbar\omega}\left(1 - \sqrt{1 - E_v/D}\right) + \frac{1}{2}$$

and the density of states $\rho(E)$ is obtained by differentiating $N(E)$ with respect to E: $\rho(E) = (\hbar\omega\sqrt{1 - E/D})^{-1}$. The classical density of states (i.e., without taking into account the quantization of energy) for two noninteracting Morse oscillators $\rho_2^{cl}(E)$ can be obtained from the convolution of two $\rho(E)$

$$\rho_2^{cl}(E) = \int_0^E \rho(E-x)\rho(x)\mathrm{d}x = \frac{2D}{\hbar^2\omega^2}\arcsin\left(\frac{E}{2D-E}\right)$$

for $E < D$.

2.3 We have

$$S_1 \underset{K_{invISC}}{\overset{K_{ISC}}{\rightleftharpoons}} T_1 \qquad \frac{[T_1]}{[S_1]} = \frac{K_{ISC}}{K_{invISC}} .$$

At microcanonical equilibrium, the population ratio $[T_1]/[S_1]$ is given by the corresponding ratio of the vibrational states densities $\rho_{T_1}(E)/\rho_{S_1}(E - \Delta E) = (1/0.75)^{23} = 747$, using Eq. (2.127). Then $K_{invISC} = 4.7\ \mu\mathrm{s}^{-1}$.

2.4 According to Eqs. (2.86), (2.91), and (2.92) we have

$$\begin{aligned}
\varphi_{S_0} &= \phi_1 \wedge \overline{\phi}_1 \\
\varphi_{T_1} &= (\phi_1 \wedge \overline{\phi}_2 + \overline{\phi}_1 \wedge \phi_2)/\sqrt{2} \\
\varphi_{S_1} &= (\phi_1 \wedge \overline{\phi}_2 - \overline{\phi}_1 \wedge \phi_2)/\sqrt{2} .
\end{aligned}$$

Then $U_{S_0} = \left\langle \varphi_{S_0} \middle| \hat{H}_{el} \middle| \varphi_{S_0} \right\rangle = 2\varepsilon_1 + J_{11}, U_{T_1} = \varepsilon_1 + \varepsilon_2 + J_{12} - K_{12}$, and $U_{S_1} = \varepsilon_1 + \varepsilon_2 + J_{12} + K_{12}$. Therefore $U_{T_1} - U_{S_0} = \varepsilon_2 - \varepsilon_1 + J_{12} - J_{11} - K_{12}$ (and of course $U_{S_1} - U_{T_1} = 2K_{12}$). As we assumed $J_{12} < J_{11}$, T_1 is the ground state when $\varepsilon_1 = \varepsilon_2$.

Problems of Chap. 3

3.1 In order to transfer the whole population to the excited level, we need a π pulse, i.e., a pulse of duration $\Delta t = \hbar/W$. Of course the frequency must be tuned to the $1 \rightarrow 2$ transition; i.e., it must be 20000 cm^{-1}. The coupling parameter W is $|\boldsymbol{\mu}_{12} \cdot \mathbf{E}_{00}|$. To be sure that the populations of the nearby states do not exceed 10^{-4}, we consider the maxima of the final state probability according to the Rabi formula (3.31):

$$P_{max} = \frac{W^2}{\hbar^2\Delta\omega^2 + W^2}$$

For small values of P_{max}, $W^2 \ll \hbar^2 \Delta\omega^2$, so to keep $P_{max} < 10^{-4}$ we simply need $|W| < 10^{-2}\hbar|\Delta\omega|$. Since $|\Delta\omega| = 100$ cm^{-1}, in atomic units we have $W < 4.5 \cdot 10^{-6}$, so $\Delta t_{min} = 220000$ a.u. = 5.3 ps.

3.2 With constant V and $\Delta\varepsilon \neq 0$, Eq. (3.35) yields

$$c_2(t) = -\frac{V^*}{\Delta\varepsilon}\left(\mathrm{e}^{\mathrm{i}\Delta\varepsilon\, t/\hbar} - 1\right)$$

and

$$|c_2(t)|^2 = \frac{2|V|^2}{\Delta\varepsilon^2}\left[1 - \cos\left(\frac{\Delta\varepsilon\, t}{2\hbar}\right)\right] = \frac{4|V|^2}{\Delta\varepsilon^2}\sin^2\left(\frac{\Delta\varepsilon\, t}{2\hbar}\right) .$$

The exact Rabi solution, Eq. (3.23), is

$$|c_2(t)|^2 = \frac{4|V|^2}{\Delta\varepsilon^2 + 4|V|^2}\sin^2\left(\frac{\sqrt{\Delta\varepsilon^2 + 4|V|^2}\, t}{2\hbar}\right) .$$

We see that, with $|V| \ll \Delta\varepsilon$, the TDPT solution approximates the exact one, with a slightly larger amplitude and a slightly smaller oscillation frequency:

$$\frac{4|V|^2}{\Delta\varepsilon^2} = \frac{4|V|^2}{\Delta\varepsilon^2 + 4|V|^2}\left(1 + \frac{4|V|^2}{\Delta\varepsilon^2}\right)$$

and

$$\frac{\Delta\varepsilon}{2\hbar} = \frac{\sqrt{\Delta\varepsilon^2 + 4|V|^2}}{2\hbar}\left(1 + \frac{4|V|^2}{\Delta\varepsilon^2}\right)^{-1/2} \simeq \frac{\sqrt{\Delta\varepsilon^2 + 4|V|^2}}{2\hbar}\left(1 - \frac{2|V|^2}{\Delta\varepsilon^2}\right) .$$

With $\Delta\varepsilon = 0$, Eq. (3.35) yields

$$c_2(t) = -\frac{iV^*t}{\hbar}$$

and

$$|c_2(t)|^2 = \frac{|V|^2t^2}{\hbar^2} .$$

The exact Rabi solution, Eq. (3.23), in this case is simply

$$|c_2(t)|^2 = \sin^2\left(\frac{|V|\, t}{\hbar}\right) = \left[\frac{|V|\, t}{\hbar} - \frac{1}{6}\left(\frac{|V|\, t}{\hbar}\right)^3 + O(t^5)\right]^2 = \frac{|V|^2t^2}{\hbar^2}\left[1 - \frac{|V|^2t^2}{3\hbar^2} + O(t^4)\right] .$$

This solution is acceptably accurate if $t \ll \hbar/|V|$.

3.3 The Fourier transform of $A(t)$ as given by Eq. (3.89) is

$$\tilde{A}(\omega) = (2\pi)^{-1/2} \int_{-\infty}^{+\infty} \mathrm{d}t \int_{E_{min}}^{\infty} |c(E)|^2 \, \mathrm{e}^{\mathrm{i}Et/\hbar} \, \mathrm{e}^{-\mathrm{i}\omega t} \, \mathrm{d}E =$$
$$= (2\pi)^{1/2} \int_{E_{min}}^{\infty} |c(E)|^2 \, \delta(E/\hbar - \omega) \, \mathrm{d}E = (2\pi)^{1/2} \, \hbar \, |c(\hbar\omega)|^2 = (2\pi)^{1/2} \, S(\omega) \, .$$

Equation (3.85) is therefore satisfied and, of course the same is true for Eq. (3.86):

$$\tilde{S}(t) = (2\pi)^{-1/2} \int_{-\infty}^{+\infty} \hbar \, |c(\hbar\omega)|^2 \, \mathrm{e}^{-\mathrm{i}\omega t} \, \mathrm{d}\omega =$$
$$= (2\pi)^{-1/2} \int_{-\infty}^{+\infty} \hbar \, |c(E)|^2 \, \mathrm{e}^{-\mathrm{i}Et/\hbar} \, \mathrm{d}E = (2\pi)^{-1/2} \, A(-t) \, .$$

3.4 The autocorrelation function of the bright state is

$$A(t) = \int_{-\infty}^{+\infty} S(\omega) \, \mathrm{e}^{\mathrm{i}\omega t} \, \mathrm{d}\omega =$$
$$= \cos^2\theta \int_{-\infty}^{+\infty} \delta(\omega - E_-/\hbar) \, \mathrm{e}^{\mathrm{i}\omega t} \, \mathrm{d}\omega + \sin^2\theta \int_{-\infty}^{+\infty} \delta(\omega - E_+/\hbar) \, \mathrm{e}^{\mathrm{i}\omega t} \, \mathrm{d}\omega =$$
$$= \cos^2\theta \, \mathrm{e}^{\mathrm{i}E_- t/\hbar} + \sin^2\theta \, \mathrm{e}^{\mathrm{i}E_+ t/\hbar} \, .$$

The population of the bright state is then

$$|A(t)|^2 = \cos^4\theta + \sin^4\theta + \cos^2\theta \, \sin^2\theta \left[\mathrm{e}^{\mathrm{i}(E_+ - E_-)t/\hbar} + \mathrm{e}^{-\mathrm{i}(E_+ - E_-)t/\hbar}\right] =$$
$$= \cos^4\theta + \sin^4\theta + 2\cos^2\theta \, \sin^2\theta \, - 2\cos^2\theta \, \sin^2\theta \left[1 - \cos\left(\frac{\sqrt{(\varepsilon_B - \varepsilon_D)^2 + 4|V|^2}}{\hbar}\right)\right] =$$
$$= 1 - \frac{4 \, \mathrm{tg}^2\theta}{(1 + \mathrm{tg}^2\theta)^2} \, \sin^2\left(\frac{\Omega_R t}{2}\right) \, .$$

If we put $\alpha = (\varepsilon_B - \varepsilon_D)/|2V|$ and use Eq. (3.94) for $\mathrm{tg}\theta$, the amplitude of the oscillation is

$$\frac{4 \, \mathrm{tg}^2\theta}{(1 + \mathrm{tg}^2\theta)^2} = 4\left[\frac{\alpha - \sqrt{1+\alpha^2}}{1 + (\alpha - \sqrt{1+\alpha^2})^2}\right]^2 =$$
$$= 4\left[\left(\alpha - \sqrt{1+\alpha^2}\right)^{-1} + \alpha - \sqrt{1+\alpha^2}\right]^{-2} = \frac{1}{1+\alpha^2} \, .$$

We see that both the oscillation frequency and its amplitude are the expected ones, in agreement with Eq. (3.98).

3.5 In atomic units, Eq. (3.130) reads

$$f(\nu_a, \nu_b) \simeq \frac{2}{3} \, \Delta E_{vert} \, \left\langle \chi_{l0} \left| \mu_{lk}^2 \right| \chi_{l0} \right\rangle \, .$$

From the truncated development (3.132), the squared electronic transition dipole is

$$\mu_{lk}^2(\mathbf{Q}) \simeq \mu_{lk}^2(0) + 2\boldsymbol{\mu}_{lk}(0) \cdot \sum_r \left(\frac{\partial \boldsymbol{\mu}_{lk}}{\partial Q_r}\right)_{\mathbf{Q}=0} Q_r + \sum_{r,s} \left(\frac{\partial \boldsymbol{\mu}_{lk}}{\partial Q_r}\right)_{\mathbf{Q}=0} \cdot \left(\frac{\partial \boldsymbol{\mu}_{lk}}{\partial Q_s}\right)_{\mathbf{Q}=0} Q_r Q_s \ .$$

We remember that

$$\chi_{l0} = \prod_t \chi_0^{(t)}(Q_t)$$

where $\chi_0^{(t)}$ is the $v_t = 0$ eigenfunction of the harmonic oscillator for the normal mode Q_t in the initial electronic state l. When we insert the above expression of $\mu_{lk}^2(\mathbf{Q})$ in the matrix element $\langle \chi_{l0} \left| \mu_{lk}^2 \right| \chi_{l0} \rangle$ we obtain three contributions. The first is

$$\langle \chi_{l0} \left| \mu_{lk}^2(0) \right| \chi_{l0} \rangle = \mu_{lk}^2(0) \ .$$

This is the dominant contribution for symmetry-allowed transitions, and if we limit ourselves to this term, we get the equivalent of Eq. (3.131):

$$f(v_a, v_b) \simeq \frac{2}{3} \, \Delta E_{vert} \, \mu_{lk}^2(0) \ .$$

The second contribution vanishes. In fact, it is a sum term, one for each mode, where the only variable is Q_r, and $\left\langle \chi_0^{(r)} \left| Q_r \right| \chi_0^{(r)} \right\rangle = 0$ because $[\chi_0^{(r)}]^2$ is an even function of Q_r, so the integrand is odd.

The third contribution contains off-diagonal terms with products $Q_r Q_s$, with $r \neq s$, which also vanish because the integrand is an odd function of both coordinates. Only the terms with $r = s$ are nonzero. Making use of the ladder operators $\hat{a}_r$ and $\hat{a}_r^\dagger$ (see Appendix F), their contribution turns out to be

$$\begin{aligned}
&\frac{2}{3} \, \Delta E_{vert} \sum_r \left(\frac{\partial \boldsymbol{\mu}_{lk}}{\partial Q_r}\right)_{\mathbf{Q}=0}^2 \left\langle \chi_0^{(r)} \left| Q_r^2 \right| \chi_0^{(r)} \right\rangle = \\
&= \frac{1}{3} \, \Delta E_{vert} \sum_r \omega_r^{-1} \left(\frac{\partial \boldsymbol{\mu}_{lk}}{\partial Q_r}\right)_{\mathbf{Q}=0}^2 \left\langle \chi_0^{(r)} \left| (\hat{a} + \hat{a}^\dagger)^2 \right| \chi_0^{(r)} \right\rangle = \\
&= \frac{1}{3} \, \Delta E_{vert} \sum_r \omega_r^{-1} \left(\frac{\partial \boldsymbol{\mu}_{lk}}{\partial Q_r}\right)_{\mathbf{Q}=0}^2 \ .
\end{aligned}$$

This is normally the dominant term for symmetry-forbidden transitions.

Problems of Chap. 4

4.1 From Eq. (F.14) we get:

$$\langle \chi_v \left| x \right| \chi_v \rangle = x_e$$

The momentum matrix element can be expressed in terms of the ladder operators:

$$\langle \chi_v \left| \hat{p}_x \right| \chi_v \rangle = -\mathrm{i}\sqrt{\frac{\hbar M\omega}{2}} \langle \chi_v \left| \hat{a} - \hat{a}^\dagger \right| \chi_v \rangle = 0$$

Actually there is a more general proof, not based on the properties of the harmonic oscillator, that the mean value of $\hat{p}$ is zero for real wavefunctions that vanish at $x \to \pm\infty$. In fact:

$$\int_{-\infty}^{+\infty} \psi(x) \, \frac{\mathrm{d}\psi(x)}{\mathrm{d}x} \, \mathrm{d}x = \left[\psi^2(x)\right]_{-\infty}^{\infty} - \int_{-\infty}^{+\infty} \frac{\mathrm{d}\psi(x)}{\mathrm{d}x} \, \psi(x) \, \mathrm{d}x$$

The integral in the LHS is equal to minus itself, so it must vanish.

We now consider the variances:

$$\Delta x^2 = \langle \chi_v \left| (x - x_e)^2 \right| \chi_v \rangle = \frac{\hbar}{2M\omega} \langle \chi_v \left| (\hat{a} + \hat{a}^\dagger)^2 \right| \chi_v \rangle = \frac{\hbar(2v+1)}{2M\omega}$$

$$\Delta p^2 = \langle \chi_v \left| p^2 \right| \chi_v \rangle = -\frac{\hbar M\omega}{2} \langle \chi_v \left| (\hat{a} - \hat{a}^\dagger)^2 \right| \chi_v \rangle = \frac{\hbar M\omega(2v+1)}{2}$$

The indetermination product is

$$\Delta x \; \Delta p = \frac{\hbar(2v+1)}{2}$$

which takes the minimum value $\hbar/2$ for $v = 0$.

The classical amplitude of oscillation is obtained by equating the total energy with the potential energy:

$$\hbar\omega \left(v + \frac{1}{2} \right) = \frac{1}{2} M\omega^2 \Delta x_{cl}^2$$

We get $\Delta x_{cl} = \left(\dfrac{\hbar(2v+1)}{M\omega} \right)^{1/2}$. This result differs from the quantum mechanical uncertainty Δx by just a factor $\sqrt{2}$, which is quite reasonable since Δx_{cl} is the maximum elongation whereas Δx is the "root-mean-square" elongation.

4.2 The total energy is made of potential + kinetic energy. With respect to the minimum of the excited state, ΔE_{adia}, the average potential energy is:

$$\langle U \rangle = \frac{1}{2} M\omega_2^2 \langle \chi_{1,0} \left| (R - R_2)^2 \right| \chi_{1,0} \rangle$$

The eigenfunction $\chi_{1,0}(R)$ belongs to the initial electronic state 1, so we shall use the associated ladder operators that allow to write

$$R = R_1 + \sqrt{\frac{\hbar}{2M\omega_1}} \, (\hat{a} + \hat{a}^\dagger)$$

Then

$$\langle U\rangle = \frac{1}{2}M\omega_2^2\left\langle \chi_{1,0}\left|\left[R_1 - R_2 + \sqrt{\frac{\hbar}{2M\omega_1}}\,(\hat{a}+\hat{a}^\dagger)\right]^2\right|\chi_{1,0}\right\rangle$$

When developing the square, the linear terms in $\hat{a}$ and $\hat{a}^\dagger$ do not contribute, so we are left with:

$$\langle U\rangle = \frac{1}{2}M\omega_2^2(R_1 - R_2)^2 + \frac{\hbar\omega_2^2}{4\omega_1}$$

The first term in the RHS is the potential energy of the center of the wavepacket (the same one would calculate for vertical excitation in classical terms). The second term is the contribution due to the curvature of the U_2 potential: if $\omega_2 = \omega_1$, it would be just the potential energy of the $\chi_{1,0}$ eigenfunction in the initial state. Finally, we need the kinetic energy contribution:

$$\langle T\rangle = \frac{1}{2M}\left\langle \chi_{1,0}\left|\hat{P}_R^2\right|\chi_{1,0}\right\rangle = -\frac{\hbar\omega_1}{4}\left\langle \chi_{1,0}\left|(\hat{a}-\hat{a}^\dagger)^2\right|\chi_{1,0}\right\rangle = \frac{\hbar\omega_1}{4}$$

which is, of course, the same average kinetic energy as in the initial state. In total, the vibrational energy is

$$E_{vib} = \frac{1}{2}M\omega_2^2(R_1 - R_2)^2 + \frac{\hbar\omega_2^2}{4\omega_1} + \frac{\hbar\omega_1}{4}$$

With respect to the ZPE in the final state:

$$E_{vib} - \mathrm{ZPE} = \frac{1}{2}M\omega_2^2(R_1 - R_2)^2 + \frac{\hbar(\omega_1-\omega_2)^2}{4\omega_1}$$

4.3

$$\begin{aligned}
&\frac{\mathrm{d}}{\mathrm{d}t}\left\langle\psi\left|(\hat{p}_i - \langle\hat{p}_i\rangle)^2\right|\psi\right\rangle = \\
&= \frac{\mathrm{i}}{\hbar}\left\langle\psi\left|\left[\hat{H},(\hat{p}_i - \langle\hat{p}_i\rangle)^2\right]\right|\psi\right\rangle = \\
&= \frac{\mathrm{i}}{\hbar}\left\langle\psi\left|(\hat{p}_i - \langle\hat{p}_i\rangle)\left[V(\mathbf{x}),\hat{p}_i\right] + \left[V(\mathbf{x}),\hat{p}_i\right](\hat{p}_i - \langle\hat{p}_i\rangle)\right|\psi\right\rangle = \\
&= \left\langle\psi\left|(\hat{p}_i - \langle\hat{p}_i\rangle)\left[V(\mathbf{x}),\frac{\partial}{\partial x_i}\right] + \left[V(\mathbf{x}),\frac{\partial}{\partial x_i}\right](\hat{p}_i - \langle\hat{p}_i\rangle)\right|\psi\right\rangle = \\
&= -\left\langle\psi\left|(\hat{p}_i - \langle\hat{p}_i\rangle)\frac{\partial V}{\partial x_i} + \frac{\partial V}{\partial x_i}(\hat{p}_i - \langle\hat{p}_i\rangle)\right|\psi\right\rangle = \\
&= -\left\langle\psi\left|(\hat{p}_i - \langle\hat{p}_i\rangle)\left(\frac{\partial V}{\partial x_i} - \left\langle\frac{\partial V}{\partial x_i}\right\rangle\right) + \left(\frac{\partial V}{\partial x_i} - \left\langle\frac{\partial V}{\partial x_i}\right\rangle\right)(\hat{p}_i - \langle\hat{p}_i\rangle)\right|\psi\right\rangle
\end{aligned}$$

The last equality stems from the fact that $\hat{p}_i - \langle \hat{p}_i \rangle$ multiplied by a constant averages to zero.

4.4

$$\frac{\mathrm{d}\langle x_i \rangle}{\mathrm{d}t} = \frac{\mathrm{i}}{\hbar}\left\langle \psi \left| \left[\hat{T}, x_i\right] \right| \psi \right\rangle = \frac{\mathrm{i}}{2\hbar m_i}\left\langle \psi \left| \left[\hat{p}_i^2, x_i\right] \right| \psi \right\rangle =$$
$$= \frac{\mathrm{i}}{2\hbar m_i}\left\langle \psi \left| \hat{p}_i \left[\hat{p}_i, x_i\right] + \left[\hat{p}_i, x_i\right] \hat{p}_i \right| \psi \right\rangle = \frac{\langle p_i \rangle}{m_i}$$

4.5 The variable Q_r can be replaced by $\sqrt{\hbar/(2\omega_r)}(\hat{a}_r + \hat{a}_r^\dagger)$ and similarly for Q_s and Q_t. Then:

$$\begin{aligned}
&\langle v_r, v_s, v_t \,|Q_r Q_s Q_t| v_r', v_s', v_t' \rangle = \\
&= \left(\frac{\hbar^3}{8\omega_r\omega_s\omega_t}\right)^{1/2} \left\langle v_r, v_s, v_t \left| (\hat{a}_r + \hat{a}_r^\dagger)(\hat{a}_s + \hat{a}_s^\dagger)(\hat{a}_t + \hat{a}_t^\dagger) \right| v_r', v_s', v_t' \right\rangle = \\
&= \left(\frac{\hbar^3}{8\omega_r\omega_s\omega_t}\right)^{1/2} \langle v_r \left| \hat{a}_r + \hat{a}_r^\dagger \right| v_r' \rangle \langle v_s \left| \hat{a}_s + \hat{a}_s^\dagger \right| v_s' \rangle \left\langle v_t \left| \hat{a}_t + \hat{a}_t^\dagger \right| v_t' \right\rangle = \\
&= \left\{ \frac{\hbar^3[(v_r+1)\delta_{v_{r+1},v_r'} + v_r\delta_{v_{r-1},v_r'}][(v_s+1)\delta_{v_{s+1},v_s'} + v_s\delta_{v_{s-1},v_s'}][(v_t+1)\delta_{v_{t+1},v_t'} + v_t\delta_{v_{t-1},v_t'}]}{8\omega_r\omega_s\omega_t} \right\}^{1/2}
\end{aligned}$$

This result is expressed more compactly in Eq. (4.21).

4.6 There are four ways to distribute 1000 cm^{-1} in the three modes with frequencies 200, 300, and 500 cm^{-1}. The numbers of quanta per mode are in the first three columns of Table G.1. The next three columns show the energies E_1, E_2, and E_3 stored in the modes for each choice of vibrational quantum numbers. Below are the averages obtained with the same weight (1/4) for each set of quantum numbers: $\langle E_1 \rangle = 400$ cm^{-1}, $\langle E_2 \rangle = 225$ cm^{-1}, and $\langle E_3 \rangle = 375$ cm^{-1}. The distribution is irregular (the middle frequency has got the lowest energy) because it depends on the (very few) combinations of three energies multiplied by integer numbers that sum up to 1000 cm^{-1}.

If every mode is n-fold degenerate, the number of states which can be obtained by putting v_i quanta in that mode is

$$g_i = \frac{(n + v_i - 1)!}{v_i!(n-1)!}$$

(see Sect. 2.5.2). For the set of quantum numbers v_1, v_2, v_3 the total degeneracy is $g_1 g_2 g_3$ (last column of Table G.1). The last line of the table shows the average mode energies in the degenerate case, obtained using as weights the products $g_1 g_2 g_3$, normalized to their sum. We see that, because we now consider many more states (930), the average energy decreases regularly from the first to the third mode.

4.7 The simplified Onsager formula, expressed in atomic units, is

$$\Delta G_{Onsager} = -\frac{\kappa - 1}{2\kappa + 1}\frac{\mu^2}{R^3}$$

Table G.1 Microcanonical distribution in three modes. Energies in cm^{-1}

No degeneration						Sixfold degeneracy			
v_1	v_2	v_3	E_1	E_2	E_3	g_1	g_2	g_3	$g_1 g_2 g_3$
5	0	0	1000	0	0	252	1	1	252
2	2	0	400	600	0	21	21	1	441
1	1	1	200	300	500	6	6	6	216
0	0	2	0	0	1000	1	1	21	21
Average, no deg.			400	225	375				
Average, deg.= 6			507	354	139				

The molecular volume is the ratio of the molecular mass to the density:

$$V_M = \frac{M_M}{N_A \rho} \text{ cm}^3 = \frac{M_M}{N_A \rho} \ 10^{24} \text{ Å}^3$$

Then

$$R^3 = \frac{3V_M}{4\pi} = 46.8 \text{ Å}^3 = 316 \text{ bohr}^3$$

With $\kappa = 2.3$ (benzene) we get $\Delta G_{Onsager} = -1.2$ kJ/mol for the $n \rightarrow \pi^*$ state and -6.2 kJ/mol for the $\pi \rightarrow \pi^*$ state. With $\kappa = 24.5$ (ethanol) we get $\Delta G_{Onsager} = -2.5$ kJ/mol and -12.5 kJ/mol, respectively. So, in benzene the difference in ΔG between the two states is reduced by 5 kJ/mol: $18 - 6.2 + 1.2 = 13$ kJ/mol, while in ethanol it is reduced by twice as much: $18 - 12.5 + 2.5 = 8.0$ kJ/mol. Remember that all these values are only rough estimates and more accurate calculations may confirm that the $\pi \rightarrow \pi^*$ state in polar solvents is almost degenerate or lower that the $n \rightarrow \pi^*$ one, so explaining the more intense fluorescence obtained in the latter environment.

4.8 If the quantum number v_r in Eq. (4.25) could assume any real value, one might solve the equation for the unknown v_r to obtain a given probability P_{v_r}:

$$v_r = \frac{K_B T}{\hbar \omega_r} \ln \left(\frac{1 - \text{e}^{-\hbar \omega_r / K_B T}}{P_{v_r}} \right)$$

Since P_{v_r} is a decreasing function of v_r, the result we are looking for is the largest integer that is smaller than the value computed by this formula. With $T = 300$ K, $K_B T = 208.5$ cm^{-1}. With $P_{v_r} = 10^{-2}$ and a frequency of 100 cm^{-1}, the above formula yields $v_r = 7.6$, with 400 cm^{-1} it yields $v_r = 2.3$, and with 1000 cm^{-1} it yields $v_r = 0.96$. So, the last v_r with a population larger than 10^{-2} is 7, 2, and 0, respectively. The number of states significantly populated, according to this standard, is 8, 3, and 1, respectively.

4.9 The two periods are approximately $T_h = 220$ fs and $T_m = 270$ fs. They correspond to the frequencies $\omega_h = 6.9 \cdot 10^{-4}$ a.u. and $\omega_m = 5.6 \cdot 10^{-4}$ a.u. The vibrational frequency of the harmonic oscillator is $\sqrt{K/M} = 6.93 \cdot 10^{-4}$ a.u., in good agreement with the oscillation period.

The vibrational levels of a Morse oscillator obey a simple formula (see Problem 2.2). The basic vibrational frequency is $6.9 \cdot 10^{-4}$ a.u., somewhat higher than that desumed from the oscillation period. However, as discussed in Sect. 4.2, the excited wavepacket is a superposition of stationary states with the largest coefficients for vibrational quantum numbers close to 40. According to the above-mentioned formula, the levels around $v = 40$ are separated by about $5.7 \cdot 10^{-4}$ a.u., in much better agreement with the "measured" period.

Problems of Chap. 5

5.1 From the equipartition theorem $Mv^2 = K_B T$, where M is the reduced mass of the diatomic molecule and v is the velocity on the neutral potential energy curve (i.e., the velocity at which the ionic/neutral crossing is traversed). We have then $v = 1.93 \cdot 10^{-4}$ a.u. Using atomic units $|F| = Q_x^{-2} = \Delta^2$, where Δ is the difference between the ionization potential of Na and the electron affinity of Cl. Taking the numerical values for H_{12} and Δ from Sect. 5.1 we obtain $P_{adia} = 0.792$.

5.2 Let us first evaluate the Landau–Zener probability P_{adia}. In this respect, the only difference with the previous problem is the kinetic energy in the crossing region, which in the present case corresponds to Δ. Then, $v = \sqrt{2\Delta/M} = 2.10 \cdot 10^{-3}$ a.u. and $P_{adia} = 0.979$. After the first passage through the crossing the populations of the ionic and the covalent state are, respectively, $P \equiv P_{adia}$ and $1 - P$. After the second passage the population of the ionic state is made of two contributions: $(1 - P)(1 - P)$ and P^2, coming, respectively, from the covalent and the ionic state. The probability of the ionic state after the collision is therefore $1 + 2P(P - 1) = 0.959$.

5.3 With a real Hamiltonian the wavefunctions can be taken as real. We consider an orthogonal transformation not dependent on the nuclear coordinates, leading to the new diabatic basis $|\eta_1'\rangle$ $|\eta_2'\rangle$

$$
\begin{aligned}
|\eta_1'\rangle &= |\eta_1\rangle \cos\theta + |\eta_2\rangle \sin\theta \\
|\eta_2'\rangle &= -|\eta_1\rangle \sin\theta + |\eta_2\rangle \cos\theta \ .
\end{aligned}
$$

We have then to determine θ as a function of $\mathbf{q}$ and $\mathbf{h}$. The two vectors $\mathbf{q}$ and $\mathbf{h}$ in the new basis are

$$
\begin{aligned}
\mathbf{q}' &= \mathbf{C}_2^t \nabla \mathbf{H}(\mathbf{Q}_x)\mathbf{C}_2 - \mathbf{C}_1^t \nabla \mathbf{H}(\mathbf{Q}_x)\mathbf{C}_1 \\
\mathbf{h}' &= 2\mathbf{C}_1^t \nabla \mathbf{H}(\mathbf{Q}_x)\mathbf{C}_1
\end{aligned}
$$

where $\mathbf{C}_1^t = (\cos\theta,\ \sin\theta)$ and $\mathbf{C}_2^t = (-\sin\theta,\ \cos\theta)$. We have therefore

$$
\begin{aligned}
\mathbf{q}' &= \mathbf{q}\cos(2\theta) - \mathbf{h}\sin(2\theta) \\
\mathbf{h}' &= \mathbf{q}\sin(2\theta) + \mathbf{h}\cos(2\theta) \ .
\end{aligned}
$$

The condition to impose is $\mathbf{q}' \cdot \mathbf{h}' = 0$. We obtain

$$q^2 \cos(2\theta) \sin(2\theta) - h^2 \cos(2\theta) \sin(2\theta) + \mathbf{q} \cdot \mathbf{h}(\cos^2(2\theta) - \sin^2(2\theta)) = 0$$

which gives

$$\mathrm{tg}(4\theta) = \frac{2\mathbf{q} \cdot \mathbf{h}}{h^2 - q^2}$$

where q and h are the norms of $\mathbf{q}$ and $\mathbf{h}$, respectively.

5.4 Using Eq. (2.66) and taking into account that $g_{ii}^{(\alpha)} = 0$ for real wavefunctions, we obtain immediately

$$t_{11}^{(\alpha)} = t_{22}^{(\alpha)} = -\left(g_{12}^{(\alpha)}\right)^2 \qquad \text{and} \qquad t_{12}^{(\alpha)} = \frac{\partial g_{12}^{(\alpha)}}{\partial Q_\alpha} \, .$$

For the Landau–Zener model we have, using Eq. (5.29)

$$t_{12}(Q) = -\frac{\beta^3 \Delta Q}{(1 + \beta^2 \Delta Q^2)^2} \, .$$

Close to a conical intersection, using Eq. (5.42) with $q = h$ we obtain

$$\mathbf{t}_{12} = \frac{xy}{(x^2 + y^2)^2}(\hat{x} - \hat{y}) \, .$$

According to (5.39) U_1 has a cusp at the conical intersection. For U_1' we have

$$U_1' = U_1 - \frac{\hbar^2}{2} \sum_\alpha \frac{t_{11}^{(\alpha)}}{M_\alpha} = U_1 + \frac{\hbar^2}{2} \sum_\alpha \frac{\left(g_{12}^{(\alpha)}\right)^2}{M_\alpha}$$

so that U_1' is discontinuous (it diverges) at the intersection.

5.5 Equation (5.1) gives the adiabatic states in terms of the diabatic ones, with $\mathrm{tg}(2\theta) = -2H_{12}/\Delta H$, according to (D.5). We have then

$$\mathrm{tg}(2\theta) = -\frac{2xy}{y^2 - x^2} = -\mathrm{tg}(2\gamma) \, .$$

In the last equation we switched to polar coordinates $x = r \cos\gamma$ and $y = r \sin\gamma$. We can therefore choose $\theta = -\gamma$, obtaining

$$\begin{aligned} |\varphi_1\rangle &= |\eta_1\rangle \cos\gamma - |\eta_2\rangle \sin\gamma \\ |\varphi_2\rangle &= |\eta_1\rangle \sin\gamma + |\eta_2\rangle \cos\gamma \, . \end{aligned}$$

Traveling along a closed path C, γ returns to its initial value γ_i if C does not contain the degeneracy point, while it goes from γ_i to $\gamma_i \pm 2\pi$ if C contains the degeneracy point (see Fig. 5.5). In either case both $|\varphi_1\rangle$ and $|\varphi_2\rangle$ retain their sign.

Problems of Chap. 6

6.1 We calculate the cross section from Eq. (6.4):

$$\sigma_{bim} = \left(\frac{\pi\mu}{8K_BT}\right)^{1/2} K = \left(\frac{\pi N_A \mu}{8RT}\right)^{1/2} K = 5.8 \cdot 10^{-22}\ \mathrm{m}^2 = 0.058\ \text{Å}^2\ .$$

The reduced mass μ was computed from the molecular masses:

$$\mu = \frac{208.22 \cdot 79.10}{208.22 + 79.10} \frac{10^{-3}}{N_A}\ \mathrm{kg} = \frac{0.0573}{N_A}\ \mathrm{kg}\ .$$

The hard sphere cross section can be evaluated from the molecular volumes. For anthraquinone $V_{mol} = 208.22 \cdot 10^{24}/(N_A\rho) = 264$ Å^2. For pyridine $V_{mol} = 79.10 \cdot 10^{24}/(N_A\rho) = 133$ Å^2. The respective radii are then $R_{mol} = (3V_{mol}/4\pi)^{1/3} = 4.0$ Å and 3.2 Å, respectively. Then, $\sigma = 160$ Å^2, about 3000 times the real one. This means it takes an average of about 3000 collisions with pyridine molecules to quench an excited anthraquinone molecule.

6.2 In gas phase the overall rate of collisions is given by Eq. (6.2). The number of collisions a single X molecule undergoes per unit time is computed putting the number density $C_X = 1$. In the formula we have: $\mu_{XY} = 100\ /(2 \cdot 10^3\ N_A) = 0.05/N_A$ kg and $C_Y = N_A P/(RT) = 2.45 \cdot 10^{25}$. So the collision rate is $4.35 \cdot 10^8\ \mathrm{s}^{-1}$ and the average time between two collisions is its inverse, i.e., 2.3 ns.

In solution the rate for hard sphere encounters is given by Eq. (6.10). The number density of Y is $1000\ N_A$ molec/m^3, and the concentration of X is put equal to 1. The diffusion coefficients, multiplied by Avogadro's number, are $N_A D = R_{gas}T/(6\pi\eta R) = 3.31 \cdot 10^{14}$ m^2/s. If $R_{int} = R_X + R_Y$, the rate of encounters is $6.7 \cdot 10^9\ \mathrm{s}^{-1}$ and the average time between two encounters is 0.15 ns.

6.3 FRET requires the fluorescence spectrum of the donor, at $\lambda \geq \lambda_{00}(S_1)$, to overlap with the absorption spectrum of the acceptor, $\lambda \leq \lambda_{00}(S_1)$. So $\lambda_{00}(S_1)$ must be shorter for the donor than for the acceptor. Viable donor–acceptor pairs are: A-B, A-C, A-D, A-E, B-C, B-D, B-E, C-D, C-E, E-D.

For triplet sensitization the same rule holds for $\lambda_{00}(T_1)$ and the viable pairs happen to be the same.

For singlet fission we want $2(E_{T_1} - E_{S_0}) \leq E_{S_1} - E_{S_0}$, which translates into $2\lambda_{00}(S_1) \leq \lambda_{00}(T_1)$. This relationship is obeyed by C and D. Actually C and E are very close to the limit. Triplet–triplet annihilation requires just the opposite, i.e., $2(E_{T_1} - E_{S_0}) \geq E_{S_1} - E_{S_0}$, so in principle A and B should do it, while low yields may be obtained for C and E.

6.4

$$\mu_{01}^2 + \mu_{02}^2 = \left|\cos\theta\ \boldsymbol{\mu}_{\mathrm{Y},0L} + \sin\theta\ \boldsymbol{\mu}_{\mathrm{X},0K}\right|^2 + \left|-\sin\theta\ \boldsymbol{\mu}_{\mathrm{Y},0L} + \cos\theta\ \boldsymbol{\mu}_{\mathrm{X},0K}\right|^2 =$$
$$= \cos^2\theta\mu_{\mathrm{Y},0L}^2 + \sin^2\theta\mu_{\mathrm{X},0K}^2 + 2\sin\theta\cos\theta\boldsymbol{\mu}_{\mathrm{Y},0L}\cdot\boldsymbol{\mu}_{\mathrm{X},0K} +$$
$$+ \sin^2\theta\mu_{\mathrm{Y},0L}^2 + \cos^2\theta\mu_{\mathrm{X},0K}^2 - 2\sin\theta\cos\theta\boldsymbol{\mu}_{\mathrm{Y},0L}\cdot\boldsymbol{\mu}_{\mathrm{X},0K} =$$
$$= \mu_{\mathrm{X},0K}^2 + \mu_{\mathrm{Y},0L}^2\ .$$

The oscillator strengths contain energy or frequency factors as in Eqs. (3.59) and (3.131), so in principle the simplifications that lead to the above rule for the squared transition dipoles cannot be applied. However, since in Sect. 6.4.4 we are considering transitions with about the same frequency, both before and after exciton coupling, a similar relationship approximately holds also for the oscillator strengths.

6.5 Since the transition dipoles are parallel, according to Eq. (6.65) all the coefficients of the bright state $|B\rangle$ are equal. So, if we want it normalized:

$$|B\rangle = n^{-1/2} \sum_{i=1}^{n} |\eta_i\rangle\ .$$

As to the approximation of neglecting the couplings with other chromophores beyond first neighbors, with $n = 3$ it is not an approximation, since there are only first neighbors. With a square of side L in length, the distance between second neighbors is the diagonal, which is $\sqrt{2}L$ long. The dipole–dipole coupling decreases with R^{-3}, so the coupling we are neglecting is $2^{-3/2}\ V \simeq 0.35\ V$. In general the distance between second neighbors is $2L\cos(\pi/n)$, so for large n the coupling tends to $V/8$.

The Hamiltonian of the system is:

$$\hat{H} = E_{ex} \sum_{j=1}^{n} |\eta_j\rangle\langle\eta_j| + V \sum_{j=1}^{n-1} \left(|\eta_j\rangle\langle\eta_{j+1}| + |\eta_{j+1}\rangle\langle\eta_j|\right) + |\eta_n\rangle\ V\ \langle\eta_1| + |\eta_1\rangle\ V\ \langle\eta_n|\ .$$

It is easy to see that

$$\hat{H}\,|B\rangle = n^{-1/2}\ E_{ex} \sum_{i=1}^{n} |\eta_i\rangle + n^{-1/2}\ 2V \sum_{i=1}^{n} |\eta_i\rangle = (E_{ex} + 2V)\,|B\rangle\ .$$

We see that the bright state is an eigenstate with energy $E_{ex} + 2V$.

6.6 Using Eq. (6.52) we find that the interaction between any two transition dipoles is:

$$V = \frac{1}{R^3}\left[\mu_p^2 + \mu_r^2\sin(\pi/6)\ \sin(5\pi/6) - 2\mu_r^2\cos(\pi/6)\ \cos(5\pi/6)\right] = \frac{4\mu_p^2 + 7\mu_r^2}{4R^3}\ .$$

The Hamiltonian matrix in the basis of the three localized excitations $|A\rangle$, $|B\rangle$, and $|C\rangle$ is therefore:

$$\mathbf{H} = \begin{pmatrix} E_l & V & V \\ V & E_l & V \\ V & V & E_l \end{pmatrix}$$

where E_l is the transition energy for the single chromophore. The eigenvalues of this matrix are given by the secular equation:

$$(E_l - E)^3 + 2V^3 - 3V^2(E_l - E) = 0 \, .$$

There are two eigenvalues, $E_1 = E_l - V$ and $E_2 = E_l + 2V$. The eigenvalue E_1 is degenerate and corresponds to the eigenstates

$$|1\rangle = 6^{-1/2} \left(2\,|A\rangle - |B\rangle - |C\rangle\right)$$

and

$$\left|1'\right\rangle = 2^{-1/2} \left(|B\rangle - |C\rangle\right) \, .$$

The eigenvalue E_2 corresponds to the eigenstate

$$|2\rangle = 3^{-1/2} \left(|A\rangle + |B\rangle + |C\rangle\right)$$

Any excitation that populates states associated with both eigenvalues generates a non–stationary state. If C_1, $C_{1'}$, and C_2 are the initial coefficients of the three states, the excited state will evolve in time as

$$\begin{aligned} |\psi(t)\rangle &= C_1 \, \mathrm{e}^{-\mathrm{i}E_1 t/\hbar} \, |1\rangle + C_{1'} \, \mathrm{e}^{-\mathrm{i}E_1 t/\hbar} \left|1'\right\rangle + C_2 \, \mathrm{e}^{-\mathrm{i}E_2 t/\hbar} \, |2\rangle = \\ &= \mathrm{e}^{-\mathrm{i}(E_l - V)t/\hbar} \left(C_1 \, |1\rangle + C_{1'} \left|1'\right\rangle + C_2 \, \mathrm{e}^{-3\mathrm{i}Vt/\hbar} \, |2\rangle\right) \, . \end{aligned}$$

We see that, apart from the irrelevant phase factor that is common to all terms, this expression contains the periodic factor $\exp(-3\mathrm{i}Vt/\hbar)$, with frequency $\omega = 3V$ in a.u., and period

$$T = \frac{2\pi}{\omega} = \frac{8\pi R^3}{4\mu_p^2 + 21\mu_r^2} \;\; \text{a.u.}$$

With $R = 15$ bohr, $\mu_p = 0.5$ a.u., and $\mu_r = 1$ a.u., $T \simeq 3500$ a.u. $\simeq 85$ fs.

6.7 Using Eq. (6.52) we find that the interaction between the transition dipoles of two adjacent chromophores is:

$$V_{12} = \frac{\mu_p^2 + \mu_r^2 \sin^2(\pi/4) + 2\mu_r^2 \cos^2(\pi/4)}{R^3} = \frac{2\mu_p^2 + 3\mu_r^2}{2R^3} \, .$$

The coupling between dipoles at opposite vertices is instead:

$$V_{13} = \frac{\mu_p^2 + 2\mu_r^2}{2\sqrt{2}R^3} \ .$$

The Hamiltonian matrix in the basis of the four localized excitations $|A\rangle$, $|B\rangle$, $|C\rangle$, and $|D\rangle$ is therefore:

$$\mathbf{H} = \begin{pmatrix} E_l & V_{12} & V_{13} & V_{12} \\ V_{12} & E_l & V_{12} & V_{13} \\ V_{13} & V_{12} & E_l & V_{12} \\ V_{12} & V_{13} & V_{12} & E_l \end{pmatrix}$$

where E_l is the transition energy for the single chromophore. On the basis of symmetry, the eigenstates are

$$\begin{aligned} |\phi_1\rangle &= \frac{1}{2}\left(|A\rangle - |B\rangle + |C\rangle - |D\rangle\right) \\ |\phi_2\rangle &= \frac{1}{2}\left(|A\rangle + |B\rangle - |C\rangle - |D\rangle\right) \\ |\phi_{2'}\rangle &= \frac{1}{2}\left(|A\rangle - |B\rangle - |C\rangle + |D\rangle\right) \\ |\phi_1\rangle &= \frac{1}{2}\left(|A\rangle + |B\rangle + |C\rangle + |D\rangle\right) \ . \end{aligned}$$

It is easy to see that the associated eigenvalues are

$$E_1 = E_l - 2V_{12} + V_{13}, \quad E_2 = E_{2'} = E_l - V_{13}, \quad E_3 = E_l + 2V_{12} + V_{13} \ .$$

These three levels are not equispaced, so in principle one would not expect a periodic behavior. However, it is easy to see that the first eigenstate is dark. Calling $|gs\rangle$ the ground state:

$$\langle gs\,|\boldsymbol{\mu}|\,\phi_1\rangle = \boldsymbol{\mu}_A - \boldsymbol{\mu}_B + \boldsymbol{\mu}_C - \boldsymbol{\mu}_D = 0 \ .$$

Then, optical excitation leaves us with three states on two levels:

$$\begin{aligned} &|\psi(t)\rangle = \mathrm{e}^{-\mathrm{i}E_2 t/\hbar}\left(C_2\ |2\rangle + C_{2'}\ \left|2'\right\rangle\right) + C_3\ \mathrm{e}^{-\mathrm{i}E_3 t/\hbar}\,|3\rangle = \\ &= \mathrm{e}^{-\mathrm{i}(E_l - 2V_{12} + V_{13})t/\hbar}\left(C_2\,|2\rangle + C_{2'}\left|2'\right\rangle + C_3\ \mathrm{e}^{-2\mathrm{i}(V_{12}+V_{13})t/\hbar}\,|3\rangle\right) \ . \end{aligned}$$

We see that, apart from the irrelevant phase factor that is common to all terms, this expression contains the periodic factor $\exp(-2\mathrm{i}(V_{12} + V_{13})t/\hbar)$, with frequency $\omega = 2(V_{12} + V_{13})$ in a.u., and period

$$T = \frac{2\pi}{\omega} = \frac{4\pi R^3}{(4+\sqrt{2})\mu_p^2 + 2(3+\sqrt{2})\mu_r^2} \ \text{a.u.}$$

With $R = 15$ bohr, $\mu_p = 0.5$ a.u., and $\mu_r = 1$ a.u., $T \simeq 4200$ a.u. $\simeq 100$ fs.

6.8 The two potentials for reactants and products can be written, respectively, as

$$U_r(\Delta R_X, \Delta R_Y) = \frac{K}{2}\,(\Delta R_X^2 + \Delta R_Y^2)$$
$$U_p(\Delta R_X, \Delta R_Y) = \Delta E_r + \frac{K}{2}\,\left[(\Delta R_X - \Delta_X)^2 + (\Delta R_Y - \Delta_Y)^2)\right]$$

where ΔR_X and ΔR_Y are the displacements of R_X and R_Y from the equilibrium position of the reactants, while Δ_X and Δ_Y are the displacements needed to go from reactants to products. We first locate the crossing seam between the two diabatic surfaces and then minimize the energy to find the transition state. The crossing seam is given by $(\Delta R_X, \Delta R_Y)$ that satisfy the constraint $U_r = U_p$:

$$\frac{K}{2}\,(\Delta R_X^2 + \Delta R_Y^2) = \Delta E_r + \frac{K}{2}\,\left[(\Delta R_X - \Delta_X)^2 + (\Delta R_Y - \Delta_Y)^2)\right] \Longrightarrow$$
$$\Delta E_r + \frac{K}{2}\,\left[\Delta_X^2 - 2\Delta_X \Delta R_X + \Delta_Y^2 - 2\Delta_Y \Delta R_Y\right] = 0 \Longrightarrow$$
$$\Delta R_Y = \Delta_Y^{-1}\left(\frac{\Delta E_r}{K} + \frac{\Delta_X^2 + \Delta_Y^2}{2} - \Delta_X \Delta R_X\right).$$

So, in correspondence of the crossing seam, we have

$$U_r = U_p = \frac{K}{2}\,\left[\Delta R_X^2 + \Delta_Y^{-2}\left(\frac{\Delta E_r}{K} + \frac{\Delta_X^2 + \Delta_Y^2}{2} - \Delta_X \Delta R_X\right)^2\right].$$

The minimum of this function of ΔR_X is found for

$$\Delta R_X = \Delta_X \frac{\Delta E_r + K(\Delta_X^2 + \Delta_Y^2)/2}{K(\Delta_X^2 + \Delta_Y^2)} = \Delta_X \frac{\Delta E_r + \lambda}{2\lambda}$$

(remember that $\lambda = K(\Delta_X^2 + \Delta_Y^2)/2$). Also ΔR_Y takes a similar form:

$$\Delta R_Y = \Delta_Y \frac{\Delta E_r + \lambda}{2\lambda}$$

and the transition energy is

$$\Delta E^* = \frac{K}{2}(\Delta_X^2 + \Delta_Y^2)\frac{(\Delta E_r + \lambda)^2}{4\lambda^2} = \frac{(\Delta E_r + \lambda)^2}{4\lambda}.$$

Index

M. Persico and G. Granucci, *Photochemistry*, Theoretical Chemistry and Computational Modelling, https://doi.org/10.1007/978-3-319-89972-5